

# Novel Multifunctional Polymers from Aromatic Diamines by Oxidative Polymerizations

Xin-Gui Li,\* Mei-Rong Huang, and Wei Duan

*Department of Polymer Materials Science and Engineering, State Key Laboratory of Concrete Materials Research, College of Materials Science and Engineering, Tongji University, 1239 Siping Road, Shanghai 200092, P. R. China*

Yu-Liang Yang

*Department of Macromolecular Science, Key Laboratory of Molecular Engineering of Polymers, Fudan University, Shanghai 200433, P. R. China*

Received January 29, 2002

## Contents

I. Introduction	2926	2. Cyclic Voltammograms of Other Aromatic Diamines	2961
II. Oxidation Potential of Aromatic Diamines	2929	3. Effect of Electrolyte Solutions on the Cyclic Voltammograms	2962
III. Comparison of Four Oxidative Polymerizations of Aromatic Diamines	2932	4. Cyclic Voltammograms during the Copolymerization with Aniline	2964
IV. Chemically Oxidative Polymerization and Polymers of Aromatic Diamines	2934	C. Constant Potential Electropolymerization	2966
A. General Procedure	2934	D. Constant Current Electropolymerization	2967
B. Effect of Polymerization Conditions	2936	E. Effect of Reaction Conditions on the Electropolymerization	2967
C. Molecular Structure and Spectroscopy	2937	F. Electroco-polymerization	2969
1. FT-IR Spectroscopy	2941	G. Spectroscopic Characteristics and Molecular Structure	2970
2. NMR Spectroscopy	2942	1. IR and <sup>1</sup> H NMR Spectroscopy	2970
3. UV–vis Spectroscopy	2943	2. Raman Spectroscopy	2972
4. XPS Spectroscopy	2943	3. UV–vis Spectroscopy	2974
5. Elemental Analysis	2944	4. XPS Spectroscopy	2976
6. Circular Dichroic Spectroscopy	2945	5. EPR Spectroscopy	2978
7. ESR Spectroscopy	2946	6. Electrochemical Impedance and Admittance Spectroscopy	2978
8. Effect of Reaction Conditions on the Molecular Structure	2946	H. Solubility and Molecular Weight	2980
D. Wide-Angle X-ray Diffractograms	2947	I. Morphological and Supramolecular Structures	2981
E. Solubility and Molecular Weight	2948	J. Properties	2984
F. Electrical Conductivity	2949	K. Relationship between the Structures of Monomers and Polymers	2986
G. Miscellaneous Properties	2951	VIII. Oxidation Polymerization Mechanisms	2986
V. Enzyme-Catalyzed Oxidative Polymerization and Polymers of Aromatic Diamines	2953	IX. Multifunctionality and Potential Applications of the Aromatic Diamine Polymers	2989
A. Enzyme-Catalyzed Oxidative Polymerization	2953	A. Electroactivity	2989
B. Enzyme-Catalyzed Oxidative Oligomerization	2954	B. Permselectivity	2994
C. Structure and Properties of Enzyme-Catalyzed Oxidative Polymers	2954	C. Electrochromic Film	2995
VI. Photocatalyzed Oxidative Polymerization of Aromatic Diamines	2956	D. Amperometric Biosensors	2997
A. Photocatalyzed Oxidative Polymerization	2956	1. Technique of Enzyme Immobilization Involving Aromatic Diamine Polymers	2998
B. Effect of Reaction Conditions on Photocatalyzed Oxidative Polymerization	2957	2. Biosensor Applications	2999
VII. Electrochemically Oxidative Polymerization and Polymers from Aromatic Diamines	2958	3. Factors Affecting the Characteristics of the Biosensors	3008
A. Electrooxidative Polymerization Procedure	2960	4. Bifunctional Biosensor	3011
B. Cyclic Voltammograms of Aromatic Diamines	2961	5. Summary	3011
1. Cyclic Voltammograms of Phenylenediamines	2961	E. Miscellaneous Sensors and Detectors	3011
		1. Acoustic Wave Sensor	3011
		2. Capacitive Sensor	3012
		3. Piezoelectric Immunosensor	3012
		4. Amperometric Ion Detector	3012

\* To whom correspondence should be addressed. Phone: +86 21 65980524 or +86 21 65799455. Fax: +86 21 65980530. E-mail: lixingui@tongji.edu.cn.

5. pH Sensor	3013
6. Humidity Sensor	3013
7. Chemiluminescence Biodetector	3014
8. Summary	3014
F. Electrocatalyst of Redox Reactions	3014
G. Heavy Metal Ion Complex and Detection	3016
H. Electric and Electronic Materials	3018
1. Switch	3018
2. Electrochemical Capacitor	3018
3. Modifying Film of Cell Electrodes	3018
I. Anticorrosion Coating for Metals	3019
J. Micropatterning Films	3019
K. Additives in Lubricating Oil	3020
L. Applications of the Oxidation of Aromatic Diamines	3020
1. Immunosorbent Assay	3020
2. Detection of Hemoglobin, H <sub>2</sub> O <sub>2</sub> , and Laccase	3021
3. Detection of Traces of Metal Ions	3021
4. Determination of the Surface Area of Noble Metal Catalysts	3022
5. Determination of Phenol, Catechol, and Ascorbic Acid	3022
X. Conclusions and Prospects	3023
XI. Nomenclature	3024
XII. Acknowledgments	3025
XIII. References	3025

## I. Introduction

Since discovered in the late 19th century,<sup>1,2</sup> increasing research interest has focused on the electrically conductive nature of the aromatic polymer family such as polyaniline (PAN),<sup>3–25</sup> aniline (AN), with its derivative copolymers,<sup>26–30</sup> polyaminopyridine<sup>31,32</sup> and its copolymers,<sup>33,34</sup> polyaminoquinoline,<sup>35</sup> polymethylquinoline,<sup>36</sup> polypyrrole (PPY),<sup>37–55</sup> and its copolymers,<sup>56–58</sup> and polythiophene.<sup>59–61</sup> In recent years, the polymer family is considered as being composed of organic conductive materials with very promising properties, such as good environmental stability,<sup>7,19,38,40,62</sup> moderately high conductivity upon doping suitable ions,<sup>3,7,41,42</sup> and higher gas separation efficiencies.<sup>63–68</sup> Furthermore, the polymers exhibit widely potential applications in rechargeable battery, electrochromic display, electrocatalyst, anti-static and anticorrosive materials, electrode materials, sensor, detector, and gas separation membranes.<sup>16,18,19,22,25,37,45,47,49,50,53</sup>

There are extensive studies in the literature concerning the synthesis, characterization, and application of conductive polymers of this family.<sup>56–74</sup> Thus far, various nitrogenous polymers of the family have been prepared by different methods, as shown in Table 1. PAN has been successfully prepared by several techniques including chemically oxidative polymerization,<sup>7,75</sup> electrochemically oxidative polymerization,<sup>76,77</sup> plasma polymerization,<sup>78</sup> and photoinduced electron-transfer photooxidative polymerization.<sup>87</sup> It is found from Table 1 that the PAN and PPY prepared by chemically and electrochemically oxidative polymerization, respectively, have high electrical conductivity. However, some problems such as low molecular weight, low solubility in common organic



Xin-Gui Li is a Professor at Tongji University in China. Professor Li's research interests have been focused on new polymeric materials for advanced technologies for the past 16 years and on the molecular design and synthesis of the polymers with liquid crystallinity, electrical conductivity, and gas-separating ability. He was born in Jiang-Xi province, China, in 1963. He was matriculated at the age of 15 in 1978 by Donghua University (former name China Textile University) at Shanghai and received his B.Sc. degree (1982) at the age of 19 and his M.Sc. (1986) and Ph.D. (1988) degrees in Chemical Fiber at Donghua University under the direction of Professor Dr. Tong Sun. He was Assistant Professor in 1989, Associate Professor in 1991, and Professor since 1993 at Tianjin Institute of Textile Science and Technology. In 1997 he has become a Professor at Tongji University. From 1999 to 2000 he was a visiting professor at the Institute of Technical Chemistry in Technical University of Berlin, Germany. He was selected in Cheung Kong (Chang-Jiang) Scholars Program of the Ministry of Education China in 1999, a very famous and important program for outstanding young scientists in China. Prof. Li received the "Citation Classic Award" by the Institute of Scientific Information, USA, in 2000. He published an academic book *Advanced Materials Engineering of Liquid Crystalline Polymers* in 2000 and has authored 120 articles in 22 international journals.



Mei-Rong Huang was born in Nan-Chang, Jiang-Xi, China, in 1963. She graduated from Donghua University, where she received her B.Sc. degree in 1985 and M.Sc. degree in 1988 in Chemical Fiber under the guidance of Professor Dr. Bai-Rong Fang. She has been a lecturer since 1990 and an associate professor since 1998. Her research interests are focused on multifunctional aromatic polymers. She is a key teacher of the Ministry of Education, China. She received the "Citation Classic Award" of the Institute of Scientific Information, USA. She has published a technical book and authored 80 articles in international journals.

solvents,<sup>19</sup> and poor mechanical property<sup>36,69,85</sup> cause difficulties in the determination of the molecular structures and restrict them to widely practical use. To combine the electrical, chemical, and physical properties of the corresponding homopolymers and then improve them further, the aromatic polymers containing two components have been prepared as copolymers, composites, bilayers, or blends. Some



Wei Duan is a Ph.D. candidate in Tongji University in China. He was born in Hunan, China, in 1973. His M.Sc. degree (1999) was earned in Materials Science at Central South University under the direction of Professor Si-Qi Zhang. From 1996 to 1999 he investigated thermal battery anode materials and received the reward of the "Chinese Bureau of Non-Ferrous Metal Industry". His research interest is conducting polymers.



Yu-Liang Yang was born in Zhe-Jiang, China, in 1952. He graduated from Fudan University, Shanghai, China, where he received his M.Sc. and Ph.D. degrees in 1982 and 1984 in Polymer Chemistry and Physics, respectively, under the supervisor of Professor Dr. Tong-Yin Yu. He was a member of Professor H. W. Spiess' research group at the Max-Planck Institute for Polymerforschung, Germany, as a postdoctoral associate from 1986 to 1988. He became an associate professor in 1986 and a professor in 1991 of Macromolecular Science at Fudan University. He was chosen in the Cheung Kong Scholars Program of China. Prof. Yang received the Prize of Chinese Youth Chemists by Chinese Chemical Society (1986), Guanghua Award of Science Technology by the Ministry of Electronic Industry of China (1994), the Foundation of Distinguished Young Scientist of China (1996), 1st Prize for the Development of Science Technology by the State Commission of Education of China (1998), and 1st Prize for the Natural Science of Chinese University (2001). He has published an academic book *Monte Carlo Method in Polymer Science* and authored more than 150 articles and 9 patents.

peculiar characteristics have been combined.<sup>8,14,15,35,36,88</sup> PAN, which has long been known to exhibit an interesting electrical conductivity and was recently rediscovered as a novel conducting polymer, should be an attractive conductive polymer due to its environmental stability, easy reversibility of protonation, excellent redox recyclability,<sup>69</sup> ease of synthesis, and low price.<sup>5,8,15,19,20</sup> In particular, its very large variable range of conductivity with doping process, humidity, and electrical field, nonlinear conducting characteristics and better filtering properties of undoped PAN, better microwave absorbing ability, and electromagnetic shielding efficiency of HCl-doped PAN allow the type of PAN to be adapted according to the specific

applications in electrical and electronic industrial fields.<sup>89</sup> PAN has been deeply investigated and is now produced industrially on a small scale.<sup>90</sup> The possible commercial applications of PAN and its blend in antielectrostatic transparent coating, corrosion protection, printed circuit board, electromagnetic interference shielding, electrochromic and chemochromic windows, sensor, and indicator have been reviewed.<sup>91</sup> The success of PAN has attracted many investigators to study the synthesis and properties of the polymers from AN derivatives. One way to make derivatives of PAN is to polymerize substituted ANs such as alkyl,<sup>92-94</sup> alkoxy,<sup>95</sup> amino,<sup>69-73</sup> as well as *N*-alkyl-substituted AN.<sup>96-98</sup> These polymers from AN derivatives exhibit an enhanced solubility in organic solvents, an improved processibility, but usually decreased conductivity and molecular weight as compared with the PAN.

One of the latest advances in conducting polymers is the creation of aromatic diamine polymers by oxidative polymerizations. The polymers of aromatic diamines including PDs, DANs, DAAQs, benzidine, naphthidine, and diaminopyridine have received increasing attention. These monomers are very susceptible to oxidative polymerization via oxidation of one or both amino groups to give linear polyaminoniline, linear polyaminonaphthylamine, ladder polyphenazine, and phenazine unit containing polymers. It is believed that investigations on the aromatic diamine polymers are more attractive since they exhibit more novel multifunctionality than PAN and PPY. The polymers have shown apparently different characteristics versus widely researched conducting polymers such as PAN and PPY in the application of electrocatalysis, electrochromics, sensors, electrode materials, heavy metal ion complex, and detection,<sup>99,100</sup> although the polymerization mechanism and properties of the polymers have not been definitely reported. It should be appreciated that the aromatic diamine polymers possess good multifunctionality partially due to one free amino group per repetitive unit on the polymers. The novel multifunctional oxidative polymers of three PD isomers, three DAN isomers, two DAAQ isomers, benzidine, diaminophenazine, hydroxy-PD (diaminophenol), and hydroxylaniline, as well as their copolymers with AN, alkyylaniline, alkoxyaniline, and pyrimidylamine have been extensively investigated all over the world. Most of the polymers of the aromatic diamines have been prepared by electrochemical polymerization, but only a small number of polymers were obtained through chemically oxidative polymerization. Investigations on enzyme- and photocatalyzed oxidative polymerizations are very few.

The earliest investigation was in 1911, when it was predicted that the univalent oxidation products of the *p*PD and its derivatives are free radicals that may polymerize in a sufficiently concentrated solution at low temperature or in the solid state.<sup>101,102</sup> In 1943, Michaelis and Granick discussed the formation of polymers of the *p*PD and its derivatives oxidized by halogen and perchlorate in acidic aqueous solution.<sup>103</sup> Polarographic investigations of *o*PD were reported with gold, graphite, and platinum electrodes in HCl

**Table 1. Preparation and Properties of Conductive Films of Nitrogen-Containing Aromatic Polymers**

polymers	polymerization method	electrical conductivity at doped state (S/cm)	mechanical properties	refs
PAN	chemically oxidative polymerization	1–10	tensile strength 110 MPa Young's modulus 2.2 GPa elongation at break 8%	7,75
PAN	electrochemically oxidative polymerization	8.4	tensile strength 0.84 MPa elongation at break 7.5%	76,77
PAN	plasma polymerization	$10^{-7}$ – $10^{-4}$		78,79
PPY	interfacial polymerization	1–10	not good	64,80
PPY	chemical oxidative polymerization	0.05–10.7	tensile strength 46 MPa Young's modulus 862 MPa elongation at break 7%	81
PPY	electropolymerization	15–105	tensile strength 70 MPa Young's modulus 4 GPa elongation at break 8%	82,83
PPY	plasma polymerization	$4 \times 10^{-9}$		84
poly(methylpyrrole)	electropolymerization	4.1	fragile	85
poly(methylquinoline)	electropolymerization	$10^{-5}$	tensile strength 25 MPa Young's modulus 2 GPa elongation at break 8%	36
poly( <i>N</i> -seleno- <i>p</i> -phenylenediamine)	polycondensation	$3.1 \times 10^{-7}$		86

and buffer (pH = 1–4) solutions, and the oxidation potential, critical oxidation potential, and polarographic half-wave potential of *o*PD were given first by Lord and Rogers in 1954.<sup>104</sup> Porcher and Adams examined the anodic polarography of three PDs on a rotating Pt electrode using a current-scanning technique in 1956.<sup>105</sup> They observed a linear relationship between limiting current and *p*PD concentration. The electropolymerization mechanism of three PDs was first suggested by Elving and Krivis in 1958.<sup>106</sup> They proposed that the oxidation mechanism of three PDs depends on the PD monomer structure and solution pH value.<sup>107</sup> The electrochemical characteristics including capacities and electrode efficiencies of PDs and their derivatives such as methyl-*p*PD, chloro-*p*PD, 2,6-dichloro-*p*PD, 4-hydroxy-*m*PD, amino-*p*PD, and 12DAN in basic electrolyte (1.44 M NaOH solution) were systematically studied for the first time by Glicksman in 1961.<sup>108</sup> In 1963, Mark and Anson first reported the effect of acid strength on the electrooxidation of PDs and their *N*-substituted derivatives including *N,N*-dimethyl-*p*PD and *N*-phenyl-*p*PD on Pt electrode by chronopotentiometry.<sup>109</sup> The electrode filming phenomenon of PDs was first found by Prater in 1973.<sup>110</sup> A polarogram for 3-methyl-*o*PD solution was studied for the polarographic reduction of Ni<sup>2+</sup> in 2001.<sup>111</sup> However, *Po*PD was first prepared as a stable film on an electrode by electropolymerization of *o*PD in acidic solution by Yacynych and Mark in 1976.<sup>112</sup> The electrical conductivity of the *Po*PD film prepared by electrooxidation was reported for the first time by Yano et al. in 1985.<sup>113</sup> Since 1986, increasing investigations on the electropolymerization of aromatic diamines have appeared.

As compared with the electropolymerization of aromatic diamines, studies on the chemically oxidative polymerization of the aromatic diamines occurred later and were of decreased intensity. Bach pioneered the chemically oxidative polymerization of *p*PD with metal chelate and oxygen as oxidant in 1966.<sup>114</sup> The chemically oxidative polymerization of *p*PD was first reported as an additive of AN polymerization in order to increase the rate and yield of polymerization.<sup>115</sup> Chemically oxidative polymerization of four aromatic

diamines with persulfate as the oxidant in acidic aqueous solution from 0 °C to room temperature was developed for the first time by Chan, Rawat, and co-workers in 1991.<sup>69,116</sup> The enzymatic oxidative polymerization of *o*PD was first carried out by using HRP and H<sub>2</sub>O<sub>2</sub> as catalyst and oxidant, respectively, at room temperature by Kobayashi et al. in 1992.<sup>117</sup> In 1995, the chemically oxidative polymerization of *o*PD was found to form ladder-like poly(aminophenazine) if the polymerization was performed in glacial acetic acid at 118 °C.<sup>70</sup> From then on, the oxidative polymerization and polymers from aromatic diamines have been being extensively investigated because the polymers exhibit a number of advantages including the choice of monomer, diversity and facility of polymerization, variety of macromolecular structure, variability of electroconductivity, multifunctionality, and potentially wide applicability. In recent years the oxidative polymers of the aromatic diamines have undergone a very rapid development in academic research and industrial application. Significant progress has been made in the successful synthetic techniques, the characterization of structure and properties, and the design of functional materials of the polymers.

Several reviews concerning electroconductive PAN,<sup>118–127</sup> PPY,<sup>121,128–131</sup> polythiophene,<sup>121,122,131–135</sup> and poly(1,6-heptadiyne)<sup>136</sup> and conducting PAN blends and composites<sup>137</sup> have appeared recently. The coordinating ability of PDs has been reviewed.<sup>138</sup> However, there have been no previous reviews on the polymers and copolymers prepared from the PDs and other aromatic diamines by an oxidative polymerization per se. In this review, comprehensive research results of the preparation, polymerization mechanism, macromolecular and morphological structures, properties, multifunctionality, and widely potential applications of the polymers and copolymers are the focus for the first time based on the literature reported mainly since 1943. Some comments and guidelines for further academic research, materials performance optimization, and commercially industrial applications required to make a major impact are offered.

**Table 2. Oxidation Potential ( $E_{ox}$ ) of *o*-Phenylenediamine under Different Conditions by Cyclic Voltammetry**

electrode/ area (cm <sup>2</sup> )	scanning rate (mV s <sup>-1</sup> )	oxidation solution	oxidation potential $E_{ox}$	refs
Au/0.8	5	5 mM <i>o</i> PD, 0.1 M borate buffer, pH = 9	0.31 V vs SCE	140
Pt/–	3	3 mM <i>o</i> PD, deaerated phosphate buffer (pH = 7), 3 mM Ni(NO <sub>3</sub> ) <sub>2</sub>	0.33 V vs Ag/AgCl	112
Pt/–	3	3 mM <i>o</i> PD, phosphate buffer (pH = 7)	0.35 V vs Ag/AgCl	112
GC/0.13	50	10 mM <i>o</i> PD, 0.1 M KCl/water (pH = 7)	0.35, 0.55 V vs SCE	141
Au/0.0003	50	10 mM <i>o</i> PD, 0.1 M KCl in nonionic lyotropic liquid crystalline phase/water (50/50 wt) (pH = 7)	0.38, 0.55 V vs SCE	141
graphite/–	1.2	0.25 mM <i>o</i> PD, buffer pH = 4	0.40 V vs SCE	104
Pt/–	50	5 mM <i>o</i> PD, phosphate buffer (pH = 7)	0.40 V vs Ag/AgCl	142
OCS/0.07		10 mM <i>o</i> PD, GOx 500 U/mL, deaerated phosphate buffer (pH = 7)	0.40, 0.61 V vs Ag/AgCl	143
GC/0.1	200	10 mM <i>o</i> PD, deaerated phosphate buffer (pH = 7)	0.42, 0.64 V vs Ag/AgCl	144
Pt/0.6	100	10 mM <i>o</i> PD, 0.1 M NaClO <sub>4</sub> + 20 mM pyridine/CH <sub>3</sub> CN	0.42, 0.68 V vs Ag/AgCl	145
Au/0.8	5	5 mM <i>o</i> PD, 0.1 M acetate buffer, pH = 4	0.48 V vs SCE	140
Pt/–	50	5 mM <i>o</i> PD, acetate buffer, pH = 5.2	0.48 V vs Ag/AgCl/KCl	146
Au/0.01	50	5 mM <i>o</i> PD, acetate buffer pH = 5.2	0.5 V vs Ag/AgCl	147
Au/–	50	10 mM <i>o</i> PD, 0.1 M acetate buffer, pH = 6	0.5 V vs SCE	148
Au/1	50	5 mM <i>o</i> PD, buffer, pH = 7.4	0.5 V vs Ag/AgCl	149
ITO/4	100	100 mM <i>o</i> PD, 0.1 M H <sub>2</sub> SO <sub>4</sub>	0.5 V vs Ag/AgCl	150
Au/0.32	10	50 mM <i>o</i> PD, 0.5 M H <sub>2</sub> SO <sub>4</sub>	0.5 V vs SCE	151
Pt/–	50	5 mM <i>o</i> PD, phosphate buffer pH = 7.0	0.51 V vs SCE	152
GC/0.07	50	50 mM <i>o</i> PD, 0.2 M Na <sub>2</sub> SO <sub>4</sub> /0.1 M H <sub>2</sub> SO <sub>4</sub>	0.53 V vs SCE	153
Pt/0.5	50	5 mM <i>o</i> PD, 0.5 M Na <sub>2</sub> SO <sub>4</sub> /H <sub>2</sub> SO <sub>4</sub> , pH = 1	0.6 V vs Ag/AgCl/KCl	154
graphite/–	1.2	0.25 mM <i>o</i> PD, 0.1 M HCl	0.61 V vs SCE	104
Pt/0.16	50	1 mM <i>o</i> PD, 15 M HCl in N <sub>2</sub>	0.63, 0.85 V vs SCE	155
Au/0.28	50	50 mM <i>o</i> PD, 0.5 M H <sub>2</sub> SO <sub>4</sub>	0.68 V vs SSCE	156
Au/0.03	20	100 mM <i>o</i> PD, 1 M H <sub>2</sub> SO <sub>4</sub>	0.69 V vs SCE	157
Au/0.2	50	50 mM <i>o</i> PD, 0.1 M H <sub>2</sub> SO <sub>4</sub>	0.7 V vs SCE	158
ITO/4	100	50 mM <i>o</i> PD, 1 M H <sub>2</sub> SO <sub>4</sub> , 0.5 M KHSO <sub>4</sub>	0.7 V vs SCE	159,160
Au/0.2	50	50 mM <i>o</i> PD, 0.5 M H <sub>2</sub> SO <sub>4</sub>	0.72 V vs SCE	161
Pt/2	50	50 mM <i>o</i> PD, 1 M H <sub>2</sub> SO <sub>4</sub>	>0.75 V vs RHE	162
Au/0.2	50	50 mM <i>o</i> PD, 0.1 M H <sub>2</sub> SO <sub>4</sub>	0.76 V vs SCE	161
Au/0.02	50	50 mM <i>o</i> PD, 0.1 M KCl/H <sub>2</sub> O in N <sub>2</sub>	0.78 V vs Ag/AgCl	163
PB/ITO/4	100	50 mM <i>o</i> PD, 1 M H <sub>2</sub> SO <sub>4</sub> , 0.5 M KHSO <sub>4</sub>	0.9 V vs SCE	159,160
ITO/3.28	100	50 mM <i>o</i> PD, 0.1 M H <sub>2</sub> SO <sub>4</sub>	1.1 V vs SCE	164

This review will mainly discuss the oxidative polymerizations and polymers of four series of aromatic diamines including PD, DAN, DAAQ, and diaminopyridine. *o*PD, *m*PD, *p*PD, benzidine, dithio-dianiline, diaminodiphenyl ether, and their derivatives as well as 15DAN, 18DAN, 23DAN, naphthidine, 14DAAQ, 15DAAQ, 23DAPy, and 26DAPy have been primarily discussed.

## II. Oxidation Potential of Aromatic Diamines

The oxidation potential of aromatic diamines, a basic and important parameter for the oxidative polymerization, can be determined easily on the basis of the first scan of cyclic voltammograms during the electropolymerization. A lower oxidation potential means there is a stronger ability for the aromatic diamines to lose an electron with further higher initial activity and rate of oxidative polymerization. On the other hand, the oxidation potential is also an electrochemical parameter illustrating the electrochemical behaviors of aromatic diamines. The earliest reports on the electrochemical behavior of aromatic diamines were focused on the polarographic studies. It is found that the polarographic half-wave potentials depend on the structure and concentration of the aromatic diamines and the pH value of the acidic aqueous solution. Generally, *m*PD at 0.25 mM exhibits a higher half-wave potential in a range of 0.81–0.86 V vs SCE and *o*PD and *p*PD exhibit a lower half-wave potential of 0.50–0.54 V vs SCE.<sup>104</sup>

With increasing PD concentration, the half-wave potential decreases significantly. For example, if *p*PD concentration increases from 0.05 to 1.02 mM, its half-wave potential decreases from 0.58 to 0.20 V vs SCE.<sup>105,106</sup> Lord and Rogers also reported the critical oxidation potential of *o*PD, *m*PD, and *p*PD as 0.79, 1.09, and 0.71 V vs SCE, respectively.<sup>104</sup> The half-wave potential of *o*PD steadily decreases with increasing pH.<sup>112</sup> It is seen that the value of the critical oxidation potential for the same PD is higher than that of polarographic half-wave potential. However, there is no direct relationship between the polarographic half-wave potential/critical oxidation potential and the electrooxidative behavior. Therefore, recent investigations on the electrooxidative characteristics of aromatic diamines concentrate on the oxidation potential by cyclic voltammetry.

Almost all aromatic diamines can be electrooxidized irreversibly, and their oxidation appears as broad peaks in the potential region of 0.15–1.7 V during the first scan of CVs. These irreversible anodic peaks are considered to correspond to the oxidation of the parent amino group to the corresponding cation radical and of this cation radical to the corresponding dication.<sup>139</sup> The potential corresponding to the irreversible peak is defined as the oxidation potential of the aromatic diamine monomer for the oxidative polymerization. Tables 2–4 compare the oxidation potentials ( $E_{ox}$ ) of three PD monomers and their derivatives as well as other aromatic diamines with

**Table 3. Oxidation Potential ( $E_{ox}$ ) of *m*- and *p*-Phenylenediamines (*m*PD and *p*PD) and 1,5- and 1,8-Diaminonaphthalenes (15DAN and 18DAN) under Different Conditions by Cyclic Voltammetry**

monomers	electrode/ area (cm <sup>2</sup> )	scanning rate (mV s <sup>-1</sup> )	oxidation solution	oxidation potential, $E_{ox}$	refs	
<i>m</i> PD	Au/0.03	5	5 mM <i>m</i> PD, phosphate buffer pH = 8.1	0.58 V vs SCE	165	
	graphite/-	1.2	0.25 mM <i>m</i> PD, buffer pH = 4	0.65 V vs SCE	104	
	Au/0.02	50	100 mM <i>m</i> PD, 0.1 M KCl/H <sub>2</sub> O	0.80 V vs Ag/AgCl	166	
	Pt/-	50	100 mM <i>m</i> PD, 0.1 M KCl/H <sub>2</sub> O	0.81 V vs Ag/AgCl	167	
	Au/0.28	40	48 mM <i>m</i> PD, 1.2 M H <sub>2</sub> SO <sub>4</sub>	0.90 V vs SCE	168	
<i>p</i> PD	graphite/-	1.2	0.25 mM <i>p</i> PD, 0.1 M HCl	0.94 V vs SCE	104	
	Pt/0.6	100	10 mM <i>p</i> PD, 0.1 M NaClO <sub>4</sub> + 20 mM pyridine/CH <sub>3</sub> CN	0.19, 0.42, 0.76 V vs Ag/AgCl	145	
	graphite/-	1.2	0.25 mM <i>p</i> PD, buffer pH = 4	0.38 V vs SCE	104	
	graphite/-	1.2	0.25 mM <i>p</i> PD, 0.1 M HCl	0.58 V vs SCE	104	
	IrO <sub>2</sub> -Ti/4	50	100 mM <i>p</i> PD, 0.5 M H <sub>2</sub> SO <sub>4</sub>	0.61 V vs Ag/AgCl	169	
	Pt/3	25	2 mM <i>p</i> PD, 1 M HCl	0.62 V vs SCE	115	
	Pt/0.02	50	20 mM <i>p</i> PD, 0.1 M KCl	0.75 V vs Ag/AgCl	170	
	Pt/-	500	<i>p</i> PD, pH = 6.2–6.5	0.81 V vs SHE	171	
	Au/0.01	160	20 mM 15DAN, 0.1 M LiClO <sub>4</sub> /CH <sub>3</sub> CN	0.18 V vs Ag/Ag <sup>+</sup>	172	
	Pt/0.2	20	1.5 mM 15DAN, 0.1 M LiClO <sub>4</sub> /CH <sub>3</sub> CN	0.4 V vs SCE	173	
15DAN	Au/0.2	40	20 mM 15DAN, 0.1 M LiClO <sub>4</sub> /CH <sub>3</sub> CN	0.43 V vs SCE	174	
	Pt/0.2	20	1.5 mM 15DAN, 0.1 M LiClO <sub>4</sub> CH <sub>3</sub> CN	0.48 V vs SCE	175	
	GC/0.28	50	1 mM 15DAN, 0.1 or 2 M HCl	0.62 V vs SCE	176	
	Pt/0.2	20	1 mM 15DAN, 0.2 M NaClO <sub>4</sub> /0.1 M HClO <sub>4</sub>	0.66 V vs SCE	175,177	
	GC/0.28	50	1.1 mM 15DAN, 0.1 M HCl	0.68 V vs Ag/AgCl	178	
	rotating Au/0.03	40	20 mM 15DAN, 0.1 M LiClO <sub>4</sub> /CH <sub>3</sub> CN	0.74 V vs SCE	174	
	mild steel/-	50	1 mM 15DAN, 1 M HClO <sub>4</sub>	0.74 V vs SCE	179	
	GC/0.28	50	20 mM 15DAN, 0.2 M HClO <sub>4</sub> , 0.1 M N(C <sub>4</sub> H <sub>9</sub> ) <sub>4</sub> ClO <sub>4</sub> /CH <sub>3</sub> OH	0.83 V vs SCE	176	
	Pt/0.19	20	100 mM 15DAN, 0.2 M HClO <sub>4</sub> , 0.1 M N(C <sub>4</sub> H <sub>9</sub> ) <sub>4</sub> ClO <sub>4</sub> /CH <sub>3</sub> CN	0.88 V vs SCE	176	
	18DAN	Au/0.01	160	10 mM 18DAN, 0.1 M LiClO <sub>4</sub> /CH <sub>3</sub> CN	0.15 V vs Ag/Ag <sup>+</sup>	172
		quartz crystal/0.21	50	10 mM 18DAN, 0.1 M LiClO <sub>4</sub> /CH <sub>3</sub> CN	0.44 V vs SCE	180
		BPG/-	50	10 mM 18DAN, 0.1 M NaClO <sub>4</sub> /H <sub>2</sub> O, pH = 1	0.62 V vs SSCE	139
		Pt/0.38	100	10 mM 18DAN, 0.1 M N(C <sub>2</sub> H <sub>5</sub> ) <sub>4</sub> ClO <sub>4</sub> /CH <sub>3</sub> CN	0.62 V vs Ag/AgCl	181

AN in various media. It is seen from Table 2 that the oxidation potential of *o*PD varies dramatically from 0.31 to 1.1 V, depending on the measuring conditions. Similarly, the oxidation potentials of *m*PD, *p*PD, 15DAN, and 18DAN also vary significantly with measuring conditions, as listed in Table 3. Unfortunately, there is no regular relationship between the oxidation potential and measuring conditions. This indicates that the oxidation potential is an easily variable parameter.

However, there are dependencies of the oxidation potential on the electrolyte pH and potential scan rate. It is found that the oxidation potential of *o*PD decreases from 0.6, 0.48, and 0.43 V to 0.45 V vs Ag/AgCl with increasing electropolymerization pH from 1, 3, and 5 to 7.<sup>154</sup> It is interesting that the second oxidation potential of *o*PD appears at a pH no lower than 3 and decreases from 0.75 to 0.72 with increasing pH value from 3 to 5–7. The second oxidation peak also exhibits an increased intensity with pH value. Two oxidation peaks at 0.63 and 0.85 V vs SCE of *o*PD were also observed in 1.5 M HCl aqueous solution.<sup>155</sup> This may indicate that both -NH<sub>2</sub> groups on *o*PD are oxidized and participate in the polymerization. On the other hand, with increasing scan rate from 60, 90, 140, 200, and 240 mV s<sup>-1</sup> during the electrooxidation of 18DAN (10 mM) on a rotating Au disk electrode (0.03 cm<sup>2</sup>) at a constant rotation rate of 25 rad s<sup>-1</sup> in 0.1 M LiClO<sub>4</sub>/acetonitrile, the oxidation potential of the 18DAN decreases from 0.57, 0.55, 0.31, 0.25, and 0.22 V vs Ag/Ag<sup>+</sup>.<sup>172</sup> At low scan rates broad peak-shaped current-potential curves are observed. The shape of the curves changes from

a peaked to an S-shaped profile with a well-formed limiting current at scan rates higher than 180 mV s<sup>-1</sup>. Both curves are not similar to sharp peaked ones for the oxidation of 18DAN on stationary Au electrode at 160 mV s<sup>-1</sup>. In addition, the oxidation potential of 18DAN exhibits an increasing tendency with increasing rotation speeds of Au disk from 38 to 130 rad s<sup>-1</sup> at a constant scan rate of 240 mV s<sup>-1</sup>. On the basis of the Levich-Koutecky analysis, the diffusion coefficients and heterogeneous rate constants of the electrooxidation of 15DAN (5 mM) and 18DAN (10 mM) in LiClO<sub>4</sub>/acetonitrile using a rotating Au disk electrode were determined. It is suggested by chronoamperometric experiments that the rate constants of electrooxidation of both monomers are strongly potential dependent and the diffusion coefficients are 2.4 × 10<sup>-6</sup> cm<sup>2</sup> s<sup>-1</sup> for 15DAN and 6.8 × 10<sup>-6</sup> cm<sup>2</sup> s<sup>-1</sup> for 18DAN, which are slightly higher than the diffusion coefficient (5 × 10<sup>-6</sup> cm<sup>2</sup> s<sup>-1</sup>) for 18DAN at the stationary Au electrode. The heterogeneous rate constant is about 5.7 × 10<sup>-3</sup> cm s<sup>-1</sup> for both monomers. The diffusion coefficients and heterogeneous rate constants determined by voltammetric experiments at high scan rates are different from those by chronoamperometric experiments. The diffusion coefficients are 3.9 × 10<sup>-6</sup> cm<sup>2</sup> s<sup>-1</sup> for 15DAN and 5.4 × 10<sup>-6</sup> cm<sup>2</sup> s<sup>-1</sup> for 18DAN, and the heterogeneous rate constants are 3.6 × 10<sup>-3</sup> and 7.5 × 10<sup>-3</sup> cm s<sup>-1</sup> for 15DAN and 18DAN, respectively. This indicates that the kinetics for the initial oxidation of both monomers differ only slightly, and the differences in properties of P15DAN and P18DAN formed finally could be due to the different consecutive coupling reaction of

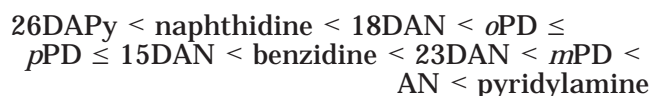
**Table 4. Oxidation Potential ( $E_{ox}$ ) of Various Aromatic Diamines by Cyclic Voltammetry**

monomers	electrode/ area (cm <sup>2</sup> )	scanning rate (mV s <sup>-1</sup> )	oxidation solution	oxidation potential, $E_{ox}$	refs
<i>o</i> PD	Au/0.02	50	50 mM <i>o</i> PD, 0.1 M KCl/H <sub>2</sub> O in N <sub>2</sub>	0.78 V vs Ag/AgCl	163
3-hydroxy <i>o</i> PD	Pt/0.07	100	50 mM 3-hydroxy <i>o</i> PD, 0.1 M Na <sub>2</sub> SO <sub>4</sub> (pH = 1)	0.5 V vs SCE	182
3-hydroxy <i>o</i> PD	Pt/0.07	100	50 mM 3-hydroxy <i>o</i> PD, 0.1 M N(C <sub>4</sub> H <sub>9</sub> ) <sub>4</sub> BF <sub>4</sub> /CH <sub>3</sub> CN	0.7 V vs SCE	182
<i>m</i> PD	Au/0.28	40	48 mM <i>m</i> PD, 1.2 M H <sub>2</sub> SO <sub>4</sub>	0.90 V vs SCE	168
4-methoxy benzene azo- <i>m</i> PD	Pt/0.125	100	50 mM 4-methoxy benzene azo- <i>m</i> PD, 0.1 M HCl in 50% ethanol/H <sub>2</sub> O	0.72 V vs SCE	183
<i>p</i> PD	IrO <sub>2</sub> -Ti/4	50	100 mM <i>p</i> PD, 0.5 M H <sub>2</sub> SO <sub>4</sub>	0.61 V vs Ag/AgCl	169
<i>N</i> -phenyl- <i>p</i> PD	Pt/3	25	1 M HCl	0.50 V vs SCE	184
sulfonated <i>p</i> PD	IrO <sub>2</sub> -Ti/4	50	100 mM sulfonated <i>p</i> PD, 1 M HCl	0.58 V vs Ag/AgCl	185
sulfonated <i>p</i> PD	Pt/-	20	sulfonated <i>p</i> PD, pH 6 in N <sub>2</sub>	0.58 V vs Ag/AgCl	186
26DAPy	Pt/0.2	50(100)	10 mM 26DAPy, 0.1 M LiClO <sub>4</sub> /CH <sub>3</sub> CN	0.52(0.4) V vs Ag/Ag <sup>+</sup>	187
15DAN	rotating Au/0.03	40	20 mM 15DAN, 0.1 M LiClO <sub>4</sub> /CH <sub>3</sub> CN	0.74 V vs SCE	174
18DAN	Pt/0.38	100	10 mM 18DAN, 0.1 M N(C <sub>2</sub> H <sub>5</sub> ) <sub>4</sub> ClO <sub>4</sub> /CH <sub>3</sub> CN	0.62 V vs Ag/AgCl	181
23DAN	BPG/-	50	20 mM 23DAN, 0.2 M NaClO <sub>4</sub> /H <sub>2</sub> O, pH = 1	0.82 V vs SSCE	139
23DAN	GC/0.27	50	20 mM 23DAN, 0.2 M NaClO <sub>4</sub> /HClO <sub>4</sub> , pH = 1	0.82 V vs SCE	188
benzidine	Pt(GC)/1.28	100(50)	0.5(1.0) mM benzidine, 0.3(0.5) M NaClO <sub>4</sub> /0.1(0.5) M HClO <sub>4</sub>	0.65(0.68) V vs SCE (Ag/AgCl)	189
benzidine	Pt/3	25	1 M HCl	0.67 V vs SCE	184
naphthidine	Pt/0.13	100	1 mM naphthidine, 0.4 M NaClO <sub>4</sub> /CH <sub>3</sub> CN	0.49 V vs SCE	190
8-(3-acetylimino-6- methyl-2,4-dioxopyran)- 1-aminonaphthalenephenol	Pt/2	100	1 mM 8-(3-acetylimino-6-methyl-2,4- dioxopyran)-1-aminonaphthalene- phenol, 0.1 M LiClO <sub>4</sub> /CH <sub>3</sub> CN	0.6 V vs Ag/AgCl	191
15DAN/AN	mild steel/-	50	1 mM 15DAN, 100 mM AN, 1 M HClO <sub>4</sub>	0.74, 1.0 V vs SCE	179
AN	Pt/0.3-3	25-50	200-500 mM AN, 0.5-1 M HCl	1.03-1.07 V vs SCE	169,192
AN	mild steel/-	50	100 mM AN, 1 M HClO <sub>4</sub>	1.05 V vs SCE	179
HAN	ITO/4	100	100 mM HAN, 0.1 M H <sub>2</sub> SO <sub>4</sub>	0.7 V vs Ag/AgCl	150
ANO	ITO/-	50	1 mM ANO, 1 M HCl	0.82 V vs Ag/AgCl	193

oxidized monomer units rather than the initial oxidation kinetics. One of two amino groups of each 18DAN probably does not participate in the oxidative polymerization, resulting in a unique property of P18DAN of extracting some heavy metal ions from the solution. P15DAN does not exhibit such property, since both amino groups on 15DAN are oxidized and take part in coupling for polymerization.

Compton et al. calculated theoretically the oxidation potential of *p*PD using a combination of ab initio methods and molecular dynamic simulations.<sup>171</sup> The theoretical potential 0.837 V is found to be slightly higher than experimental value 0.812 V vs SHE. The error margin is not significantly greater than the statistical error in the simulations. It is found that all of three PDs have basically lower oxidation potentials than AN and alkyl- or alkoxy-substituted AN monomers.<sup>115,192</sup> Therefore, the polymers of three PDs can be oxidatively formed at a lower potential, while the oxidation of *p*PD and *o*PD proceeds much more slowly than that of AN.<sup>70,194-196</sup> Furthermore, substituted PDs and substituted AN, such as hydroxy, 4-methoxy benzene azo, and sulfonated, exhibit lower oxidation potentials than unsubstituted PDs and unsubstituted AN, see Table 4.<sup>174,177,185</sup> Also, the mixture monomer of 5-aminoquinoline with AN shows a high oxidation potential of 1.24 V vs SHE.<sup>35</sup> Furthermore, 2-pyridylamine,<sup>197</sup> 3-pyridylamine,<sup>198</sup> and 4-pyridylamine<sup>199</sup> exhibit higher oxidation potentials of 1.32, 1.7, and 1.3 V in acidic/neutral media, respectively. The oxidation potential of 4-pyridyl-

amine in basic medium is 1.2 V.<sup>199</sup> It appears that 3-pyridylamine exhibits the highest oxidation potential in the aromatic amines.<sup>198</sup> However, 2,6-diaminopyridine (26DAPy)<sup>187</sup> and naphthidine<sup>190</sup> exhibit the lowest and the second lowest oxidation potentials. Therefore, on the basis of the average value of the oxidation potential listed in Tables 2-4, the oxidation potentials of several typical aromatic diamines are ranked as follows



Aromatic diamines can be oxidized at low applied potentials and form cation radicals as mediators in electron-transfer processes to initiate the polymerization, whereas the applied potential has to be high enough (ca. 0.7 V) to oxidize AN monomer, generate initiator species, and achieve a comparable rate. In view of the oxidation course, the oxidized aromatic diamines can undergo electrophilic substitution reactions with AN monomer at the *para* position to result in polymer growth, which effectively bypasses the rate-determining step.<sup>200</sup> It follows that the addition of small amounts of aromatic diamines (0.05-2 mol % with respect to AN), *p*PD, benzidine, *N*-phenyl-*p*PD, has been used to effectively increase the rate and yield of the chemically and electrochemically oxidative polymerization of AN and toluidine with (NH<sub>4</sub>)<sub>2</sub>S<sub>2</sub>O<sub>8</sub>, Na<sub>2</sub>Cr<sub>2</sub>O<sub>7</sub>, and KIO<sub>3</sub> as oxidant or by

**Table 5. Comparison of Four Oxidative Polymerizations of Aromatic Diamines**

method	polymerization						polymer			literature number
	monomer number	temp (°C)	time	yield	productivity	procedure	form	molecular weight	mechanical property	
chemically oxidative	medium	25–118	long (> 12 h)	high	large	medium	particle	lower	good	medium
enzyme-catalyzed oxidative	few	30	medium	high	small	complicated	particle	lower (higher)	general	few
photocatalyzed oxidative	very few	25	short (< 2 h)	medium	large	complicated	particle or film	lower	not good	few
electrochemically oxidative	large	25	short (< 1 h)	low	small	simple	film	higher	medium	large

cyclic voltammetry in the potential sweep ranges from  $-0.2$  to  $0.8$  V vs SCE, respectively.<sup>115,184,200,201</sup> The addition of small amounts of aromatic diamines can significantly narrow the molecular weight distribution of the PAN.<sup>184,202</sup> The *p*PD also had the best catalytic effect on the AN electropolymerization at about 0.78 mol % with respect to AN,<sup>203</sup> although the addition of 0.02 mol % *p*PD affected little the electropolymerization rate of AN. For instance, the time corresponding to the onset of blue-to-green transition occurring during the polymerization of 0.2 M AN and 1 mM additive in 0.1 M HCl with 2 wt %  $(\text{NH}_4)_2\text{S}_2\text{O}_8$  as oxidant and indicating consumption of the oxidant is 14 min (additive *p*PD), 18 min (additive *N*-phenyl-*p*PD), 32 min (additive *o*PD), and 44–49 min (without additive).<sup>196</sup> However, the *m*PD will retard AN polymerization, since the time corresponding to the onset of blue-to-green transition occurring during the AN polymerization will be largely prolonged to 305 min upon addition of 1 mM *m*PD. On the other hand, the addition of 0.5% *N*-phenyl-*p*PD or *p*PD with respect to the polymerizable AN decreases the initiation time at  $-25$  °C from 4.5 to 3.5 or 1.5 min and the polymerization time from 60 to 35 or 28 min.<sup>204</sup> The conversion of AN/aromatic diamine(160/1 mol) polymerization at 5 min increases in the order 5 wt % without aromatic diamine, 13 wt % for *N*-phenyl-*p*PD, 14 wt % for *p*PD, and 20 wt % for benzidine and polymer yield at 20 min 9 wt % without aromatic diamine, 18 wt % for *p*PD, and 23 wt % for both *N*-phenyl-*p*PD and benzidine.<sup>184</sup> Moreover, PAN was produced with an up-limit switch potential at 0.6 V in the presence of *p*PD, while no polymer formed at 0.6 V in the absence of the *p*PD within a reasonable period up to 10 h.<sup>201</sup> Therefore, the rate of oxidative polymerization of AN in the presence of the aromatic diamine additives generally increases in the order of *N*-phenyl-*p*PD < benzidine < *p*PD, which is not the same as the order of their oxidation potential.<sup>184</sup> For the same additive of aromatic diamine, a higher concentration of aromatic diamine gives a faster rate of the polymerization. Apparently, another advantage of adding aromatic diamines with lower oxidation potentials is that a lower applied potential or a mild oxidant such as  $\text{H}_2\text{O}_2$ ,  $\text{O}_2$  together with CuO, CuCl,  $\text{V}_2\text{O}_5$  can be used for the polymerization of AN and its derivatives without sacrificing the rate of polymerization, where side reactions could not occur.

Note that this increase of polymerization rate is associated with the decrease in the molecular weight and electroconductivity. For example, the inherent viscosity of the PAN decreases from 1.82 (without

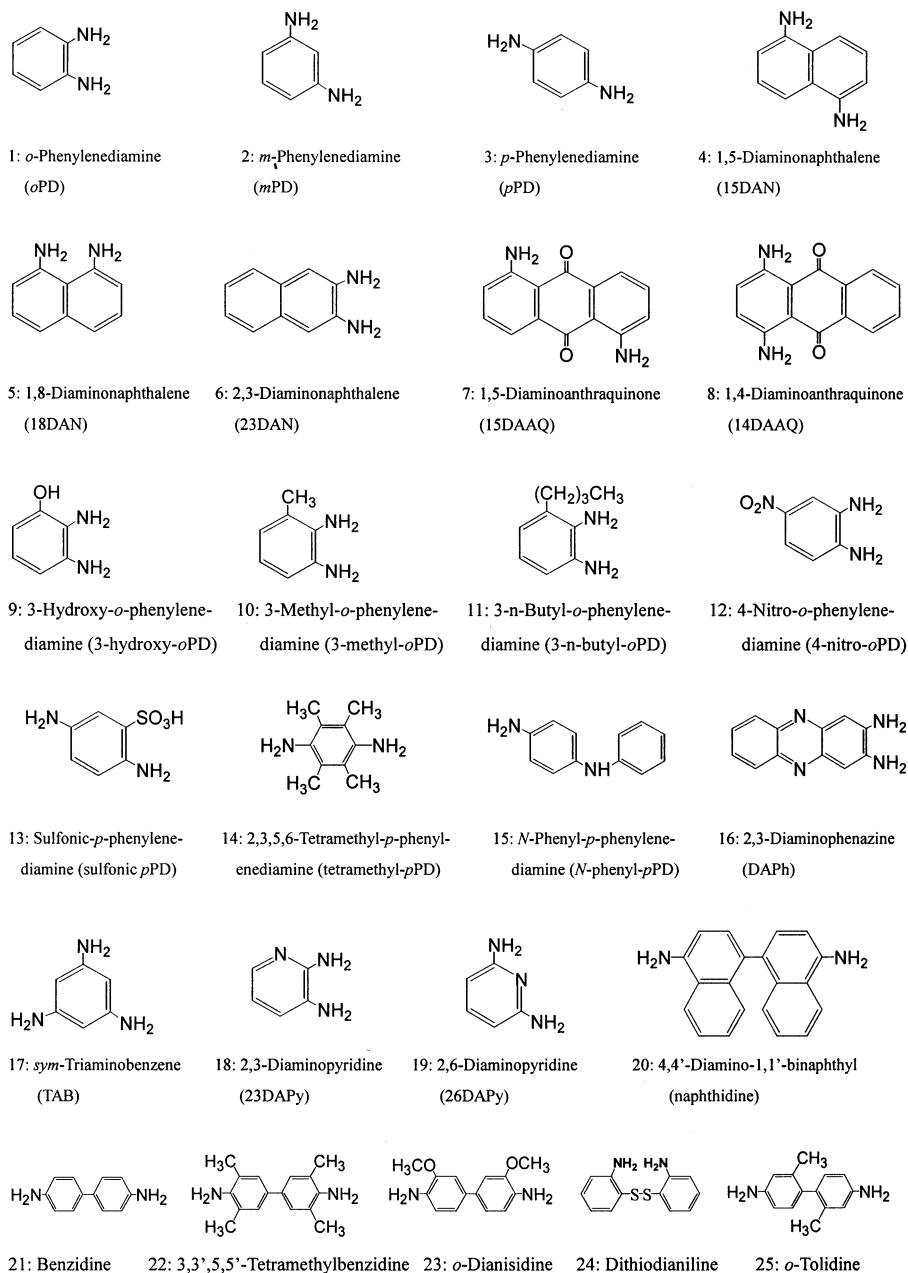
addition) to 1.14 dL/g (with addition of 0.5 mol % *N*-phenyl-*p*PD).<sup>204</sup> With increasing *N*-phenyl-*p*PD concentration from 0, 2, 5, 8, 15, to 20 mol %, the number-average molecular weight of the AN/*N*-phenyl-*p*PD polymer obtained in aqueous HCl solution with  $(\text{NH}_4)_2\text{S}_2\text{O}_8$  as oxidant at  $-5$  °C decreases from 25 100, 14 500, 6100, 4100, 3000, to 2600 g/mol.<sup>202</sup> Its polydispersity in molecular weight also decreases from 3.8, 3.6, 1.85, 1.8, 1.75, to 1.55. Similarly, in the polymer system with *p*PD as the initiator, both the molecular weight and polydispersity also decrease with the increase in the *p*PD concentration. With either *p*PD or *N*-phenyl-*p*PD as the initiator at 2–5 mol % or higher, the GPC curve changes from a bimodal pattern for pure PAN to a single narrow peak for the AN/*p*PD or AN/*N*-phenyl-*p*PD copolymer. Although the molecular weight distribution of electropolymerized PAN also gets narrowed by adding *N*-phenyl-*p*PD, the addition of *p*PD and benzidine might widen the molecular weight distribution.<sup>184</sup> It appears that the molecular weight and its distribution of PAN could be regulated to some extent by varying the amount of the aromatic diamine initiator. In summary, the *p*PD, *N*-phenyl-*p*PD, and benzidine can markedly accelerate the oxidative polymerization of AN and toluidine, *o*PD has little effect on AN polymerization, while *m*PD with a relatively high oxidation potential caused its retardation.

### III. Comparison of Four Oxidative Polymerizations of Aromatic Diamines

Among the four techniques reported for the synthesis of the polymers from aromatic diamines, chemically oxidative polymerization and electrochemically oxidative polymerization have been widely used but the enzyme-catalyzed and photocatalyzed oxidative polymerizations have been scarcely used. Some important characteristics of the four oxidative polymerization techniques have been summarized in Table 5. A principal advantage of chemically oxidative polymerization concerns the possibility of mass production of powdered products at a reasonable cost. This is often difficult to achieve with electrochemical techniques. However, chemically oxidative polymerization was not very convenient because the process is slightly complicated and the polymerization time is much longer than the electropolymerization and photooxidative polymerization. As a multicomponent system, the chemically oxidative polymerization is composed of the monomer, oxidant, acid, and water.



## Scheme 1. Applicable Aromatic Diamine Monomers for Oxidative Polymerizations



In principle, all of the aromatic diamines can be oxidized into polymers. However, only a few monomers, typically *o*PD, *m*PD, *p*PD, and 15DAN, shown in Scheme 1, have been successfully polymerized using the chemically oxidative polymerization. The main role of the oxidant is to oxidize the monomer and determine the number of growing polymer chains to some extent. Generally, the higher the feed concentration of the oxidant, the larger the number of growing polymer chains is. Therefore, with increasing the oxidant concentration, the theoretical molecular weight or degree of polymerization decreases when other conditions are the same. Ammonium, sodium, and potassium persulfates are representatively used as oxidants. Iodine,  $\text{Fe}^{3+}$  chelate, ceric ammonium nitrate, and  $\text{Cu}(\text{NO}_3)_2$  are occasionally employed. HCl aqueous solution is the most frequently applied as polymerization medium.

It seems that the monomers of chemically oxidative polymerization are all suitable to the enzyme-catalyzed oxidative polymerization. However, the enzyme as catalyst is requisite for a successful enzyme-catalyzed oxidative polymerization. Therefore, enzyme-catalyzed oxidative polymerization is complicated and expensive due to the addition of enzyme. Until now, the oxidant and enzyme used are  $\text{H}_2\text{O}_2$  and HRP, respectively, even though cytochrome *c* is sometimes used but only an oligomer could be obtained. In contrast to the chemically oxidative polymerization, organic additive such as 1,4-dioxane is essential in order to prepare high molecular weight polymer by the enzyme-catalyzed oxidative polymerization.

The photocatalyzed oxidative polymerization is quite different from the other three oxidative polymerizations on all sides. Only two aromatic diamine

monomers, *N*-phenyl-*p*-phenylenediamine (*N*-phenyl-*p*PD, the dimer of AN) and 2,3,5,6-tetramethyl-*p*-phenylenediamine (tetramethyl-*p*PD), have been reported to polymerize into PAN<sup>87</sup> and poly (tetramethyl-*p*PD)<sup>205</sup> by the photocatalyzed oxidative polymerization. Photoinduced electron transfer such as tris(2,2'-bipyridyl)ruthenium and methyl viologen as well as illumination of the visible light or sunlight irradiation is needed also. Therefore, photocatalyzed oxidative polymerization was difficult because it can be induced only by the photoinduced electron transfer between tris(2,2'-bipyridyl)ruthenium complex and electroactive materials, i.e., electron acceptors and donors.<sup>87</sup> The most wondrous feature of the photooxidative polymerization is that this polymerization can be successfully carried out when the monomer *N*-phenyl-*p*PD exists in the solid state as compared with the other three oxidative polymerizations.<sup>206</sup> Note that the PAN obtained has a lower polymerization yield and lower molecular weight than that by the chemically oxidative polymerization from *N*-phenyl-*p*PD and/or AN.<sup>207</sup>

One of the greatest advantages of electropolymerization is that almost all aromatic diamines listed in Scheme 1 and Tables 3 and 4 are applicable for polymerization. The oxidant is not needed, but a suitable DC potential or current must be applied through the monomer solutions for a successful electropolymerization. The polymerization medium must be an electrolyte solution including three types: (1) H<sub>2</sub>SO<sub>4</sub>, HCl, HClO<sub>4</sub>, KCl, KHSO<sub>4</sub>, Na<sub>2</sub>SO<sub>4</sub>, NaNO<sub>3</sub>, LiClO<sub>4</sub>, NaClO<sub>4</sub>, and N(C<sub>2</sub>H<sub>5</sub>)<sub>4</sub>ClO<sub>4</sub> aqueous solutions; (2) phosphate, acetate, and borate buffer solutions with a constant pH value; (3) LiClO<sub>4</sub>, NaClO<sub>4</sub>, N(C<sub>2</sub>H<sub>5</sub>)<sub>4</sub>ClO<sub>4</sub>, N(C<sub>4</sub>H<sub>9</sub>)<sub>4</sub>ClO<sub>4</sub>, N(C<sub>4</sub>H<sub>9</sub>)<sub>4</sub>BF<sub>4</sub>, and N(C<sub>4</sub>H<sub>9</sub>)<sub>4</sub>ClO<sub>4</sub> organic solutions in acetonitrile, methanol, and *sym*-dichloroethane. The molecular weight of aromatic diamine polymers prepared by electropolymerization is usually higher than that prepared by chemically oxidative polymerization, but the mechanical property of film prepared by the products of electropolymerization is not good as that of chemically oxidative polymerization. It is estimated that if the film prepared by electropolymerization is dissolved in suitable solvent and then cast film from the solution saturated with PPDs, the resulting film may have better properties than the film synthesized directly by interfacial chemically oxidative polymerization or electropolymerization. Electropolymerization, which has been used to polymerize most aromatic polymers, has a number of attractive features.<sup>118</sup> (1) The most salient feature is that polymerization, doping, and processing take place simultaneously, which is virtually impossible by the other three methods. (2) Applicable aromatic diamine monomers are the most extensive. (3) A much wider choice of cations and anions as "dopant" is available. (4) Polymer films can be easily produced on a metallic object of any desired shape, and a uniform doping of film can be simply accomplished. (5) Both free-standing and supported ultrathin conducting films applicable in electronic devices can be directly obtained. (6) The thickness of the resulting films can be controlled by varying time at either

constant potential or constant current or varying the number of potential cycles at cyclic voltammetry. (7) With suitable control over experimental parameters, it is possible to produce homogeneous and dense films. (8) Electrochemical polymerization reactions (in most case) can be carried out at room temperature.

Thus, in the last two decades, electropolymerization has attracted more attention than the other three oxidative polymerizations. An introduction to and some historical background of electropolymerization were reviewed earlier.<sup>118</sup> This review article gives an account of the four oxidative polymerizations of various aromatic diamines as well as the macromolecular and supramolecular structures, properties, and applications of resulting polymers. Until now, the amount of research literature concerning the chemically oxidative polymerization of the aromatic diamines has been much less than that concerning their electrochemically oxidative polymerization, whereas their enzyme-catalyzed and photocatalyzed oxidative polymerizations have been scarcely reported.

Although there are so many monomers of aromatic diamines, such as 3 PD isomers, 12 DAN isomers, and 12 DAAQ isomers, and their derivatives, not all monomers are suitable to polymerize via the four oxidative polymerizations. In addition, each monomer has its own unique and optimal technique of oxidative polymerization.<sup>140–185</sup> For instance, the optimal technique of oxidative polymerization for 15DAN, 18DAN, and 23DAN seems to be the electrooxidative polymerization only,<sup>139,173–181</sup> while the optimal technique of oxidative polymerization for 14DAAQ and 15DAAQ is both chemically and electrochemically oxidative polymerizations.<sup>208,209</sup> On the other hand, oxidative polymerization has its individual optimum scope of monomers. Among four oxidative polymerizations, the electrooxidative polymerization apparently allows the formation of the polymers from most of the aromatic diamine monomers. The range of aromatic diamine monomers suitable to chemically oxidative polymerization is slightly wider than that by enzyme-catalyzed oxidative polymerization. On the contrary, the aromatic diamine monomers polymerizable photocatalyzed oxidatively are the least.

#### IV. Chemically Oxidative Polymerization and Polymers of Aromatic Diamines

Thus far, only a few reports have described the formation of polymeric products by chemical oxidation of aromatic diamines. However, relatively few reports have appeared on the synthesis and structure of the polymers from aromatic diamines prepared by chemically oxidative polymerization. Table 6 lists the synthetic conditions, polymerization yield, and conductivity of PPDs, P15DAN, PBZ, poly(4,4'-diaminodiphenyl ether), 14DAAQ, and 15DAAQ complexes and three PD copolymers.

##### A. General Procedure

The oxidative polymerization was generally accomplished as follows: first, PD monomers and

**Table 6. Preparation of the Polymer Powders from Aromatic Diamines by Chemically and Enzyme-Catalyzed Oxidative Polymerizations under Various Conditions**

polymer	powder color	solvent	temp (°C)	time (h)	oxidant/catalyst	polymn. yield (wt %)	conductivity (S/cm)	refs
<i>Po</i> PD	orange	HCl/H <sub>2</sub> O	0–2	> 72	(NH <sub>4</sub> ) <sub>2</sub> S <sub>2</sub> O <sub>8</sub>		4 × 10 <sup>-12</sup>	194
<i>Pm</i> PD	brown	HCl/H <sub>2</sub> O	0–2	> 72	(NH <sub>4</sub> ) <sub>2</sub> S <sub>2</sub> O <sub>8</sub>		2 × 10 <sup>-11</sup>	194
<i>Pp</i> PD	brown	HCl/H <sub>2</sub> O	0–2	> 72	(NH <sub>4</sub> ) <sub>2</sub> S <sub>2</sub> O <sub>8</sub>		8 × 10 <sup>-10</sup>	194
<i>Po</i> PD	black	glacial CH <sub>3</sub> COOH	118	72	(NH <sub>4</sub> ) <sub>2</sub> S <sub>2</sub> O <sub>8</sub>	38	< 10 <sup>-6</sup>	70
<i>Po</i> PD		CH <sub>3</sub> COOH/H <sub>2</sub> O	100	8	none	0		210
<i>Pm</i> PD	dark	CH <sub>3</sub> COOH/H <sub>2</sub> O	100	8	none	15	2.3 × 10 <sup>-8</sup>	210
<i>Pp</i> PD	dark	CH <sub>3</sub> COOH/H <sub>2</sub> O	100	8	none	60	1.2 × 10 <sup>-8</sup>	210
<i>Po</i> PD	dark	H <sub>2</sub> O	100	8	iodine	83	1.7 × 10 <sup>-8</sup>	210
<i>Pm</i> PD	dark	H <sub>2</sub> O	100	8	iodine	150		210
<i>Pp</i> PD	dark	H <sub>2</sub> O	100	8	iodine	83	1.7 × 10 <sup>-8</sup>	210
<i>Po</i> PD	dark	H <sub>2</sub> O	100	8	(NH <sub>4</sub> ) <sub>2</sub> S <sub>2</sub> O <sub>8</sub>	60	4.7 × 10 <sup>-8</sup>	210
<i>Pm</i> PD	dark	H <sub>2</sub> O	100	8	(NH <sub>4</sub> ) <sub>2</sub> S <sub>2</sub> O <sub>8</sub>	75		210
<i>Pp</i> PD	dark	H <sub>2</sub> O	100	8	(NH <sub>4</sub> ) <sub>2</sub> S <sub>2</sub> O <sub>8</sub>	90	8.3 × 10 <sup>-9</sup>	210
PBZ	black	HCl/H <sub>2</sub> O	0–5	> 2	(NH <sub>4</sub> ) <sub>2</sub> S <sub>2</sub> O <sub>8</sub> /FeSO <sub>4</sub>		1.7 × 10 <sup>-7</sup>	116
poly(4,4'-diamino-diphenyl ether)	black	HCl/H <sub>2</sub> O	0–5	> 2	(NH <sub>4</sub> ) <sub>2</sub> S <sub>2</sub> O <sub>8</sub> /FeSO <sub>4</sub>		1.4 × 10 <sup>-9</sup>	116
<i>Pp</i> PD	black	HCl/H <sub>2</sub> O	0–5	> 2	(NH <sub>4</sub> ) <sub>2</sub> S <sub>2</sub> O <sub>8</sub> /FeSO <sub>4</sub>		6.9 × 10 <sup>-6</sup>	116
<i>Pm</i> PD	black	HCl/H <sub>2</sub> O	25	24	Na <sub>2</sub> S <sub>2</sub> O <sub>8</sub>		6.4 × 10 <sup>-2</sup>	69
<i>Pp</i> PD	bluish-black	HCl/H <sub>2</sub> O		> 12	K <sub>2</sub> S <sub>2</sub> O <sub>8</sub>	82.5	6.3 × 10 <sup>-6</sup>	62
<i>Pp</i> PD	black	H <sub>2</sub> O	21	7	Fe <sup>3+</sup> chelate/EDTA/O <sub>2</sub>	99.8	10 <sup>-10</sup>	211,212
<i>o</i> PD/AN(1/1) copolymer	black	HCl/H <sub>2</sub> O	0–2	> 72	(NH <sub>4</sub> ) <sub>2</sub> S <sub>2</sub> O <sub>8</sub>	> 50	1	194
<i>m</i> PD/AN(1/1) copolymer	black	HCl/H <sub>2</sub> O	0–2	> 72	(NH <sub>4</sub> ) <sub>2</sub> S <sub>2</sub> O <sub>8</sub>	> 50	2 × 10 <sup>-11</sup>	194
<i>p</i> PD/AN(1/1) copolymer	black	HCl/H <sub>2</sub> O	0–2	> 72	(NH <sub>4</sub> ) <sub>2</sub> S <sub>2</sub> O <sub>8</sub>	> 50	10 <sup>-4</sup>	194
14DAAQ complex	reddish-brown	DMF		1	(NH <sub>4</sub> ) <sub>2</sub> [Ce(NO <sub>3</sub> ) <sub>6</sub> ]	58	0.186	208
15DAAQ complex	black	DMF		0.5	Cu(NO <sub>3</sub> ) <sub>2</sub> /N(C <sub>2</sub> H <sub>5</sub> ) <sub>3</sub>	53	5.2	209
three PPDs	black	1,4-dioxane and/or HEPES pH 7.1	30	24	H <sub>2</sub> O <sub>2</sub> /HRP	30–90		71,72
PPD	colored	SESS + isooctane + HEPES pH 7.1	30	> 12	H <sub>2</sub> O <sub>2</sub> /HRP	0–80		73

oxidant were separately dissolved in acidic aqueous solutions. Then the polymerization reaction was initiated by steadily adding oxidant solution dropwise into the monomer solution at 25–30 °C for *m*PD and *p*PD in common inorganic or organic acidic aqueous solutions and 118 °C for *o*PD only in glacial acetic acid. The dropwise addition of oxidant solution is beneficial for obtaining polymers with a relatively high molecular weight and narrow molecular weight distribution because the oxidation polymerization of the aromatic diamines is highly exothermic. Finally, the reaction continued for at least 12 h. The resulting powder product was filtered and dried at temperatures lower than 60 °C. A drying temperature of higher than 60 °C might lead to cross-linking of the polymers. As shown in Table 6, the acids used for the preparation of aromatic diamine polymers mainly include HCl and glacial acetic acid. The effective oxidants are persulfate, iodine, H<sub>2</sub>O<sub>2</sub>, ceric ammonium nitrate, and Cu(NO<sub>3</sub>)<sub>2</sub>. Among them, the persulfates including Na<sup>+</sup>, K<sup>+</sup>, and NH<sub>4</sub><sup>+</sup> persulfates are commonly employed as oxidizing agents. Note that the oxidant is not necessary to the chemical oxidative polymerization of *m*PD and *p*PD. For example, *m*PD and *p*PD in oxidant-free acetic acid aqueous solution can polymerize into polymers with the characteristics of semiconductors at polymerization yields of 15% and 60%, respectively. However, the oxidant is required for the chemically oxidative polymerization of *o*PD because no oxidative polymer of *o*PD can be obtained even if reaction at flux temperature in acetic acid aqueous solution is allowed

to proceed for 8 h. Moreover, the oxidative polymerization yield of *o*PD is usually the lowest and the yield of *p*PD the highest, as seen in Tables 6 and 7.<sup>213</sup>

The effect of the feed procedure on the copolymerization and copolymer structure of aromatic diamines has been examined. The chemical oxidative polymerization was also initiated by adding monomer solution dropwise into oxidant solution, but the molecular weight of the resulting polymers may be low.

Very recently, oxidative oligomerization of *p*PD with *cis*-bisglycinato Cu<sup>2+</sup> monohydrate and Co<sup>2+</sup> dionemoxime complex and H<sub>2</sub>O<sub>2</sub> mixture as oxidants in water was reported.<sup>214</sup> Black powders were obtained with the polymerization yield from 45% to 65%. They are stable in neutral media but degrade in acidic media based on the UV–vis spectra.

The oxidative polymerization of 14DAAQ and 15DAAQ using ceric ammonium nitrate, Cu(NO<sub>3</sub>)<sub>2</sub>, CuCl, Ni(NO<sub>3</sub>)<sub>2</sub>, AgNO<sub>3</sub>, PdCl<sub>2</sub>, FeCl<sub>3</sub>, K<sub>2</sub>S<sub>2</sub>O<sub>8</sub>, and KIO<sub>4</sub> as oxidants in organic solvents such as DMF, pyridine, and acetonitrile and sometimes containing triethylamine as a catalyst at room temperature for 0.5–24 h has been reported.<sup>208,209</sup> It was found that the polymerization gives different colored powdered precipitates depending on the oxidants. The oxidative polymers of 14DAAQ using ceric ammonium nitrate and 15DAAQ using PdCl<sub>2</sub> are reddish-brown, the oxidative polymers of 15DAAQ using Cu(NO<sub>3</sub>)<sub>2</sub> and CuCl are black, and the oxidative polymers of 15DAAQ using ceric ammonium nitrate and K<sub>2</sub>S<sub>2</sub>O<sub>8</sub> are brown. These precipitates are believed to be semiconducting coordination polymers consisting of

**Table 7. Preparation of Polyphenylenediamines with 0.5 M (NH<sub>4</sub>)<sub>2</sub>S<sub>2</sub>O<sub>8</sub> as Oxidant at Ambient Temperature as Well as the Diameter (nm) and Polydispersity of the Polyphenylenediamine Particles Stabilized with Water-Soluble Polymers<sup>213</sup>**

monomer	polymn. yield (%)	pellet conductivity (S/cm)	density (g/cm <sup>3</sup> )	particle diameter (nm)/polydispersity		
				PVP	PVA	HPC
(a) oxidation of PD base of 0.2 M in acid-free aqueous solution						
<i>o</i> PD	61	$5.3 \times 10^{-13}$	1.43	420/0.21	>2000(unstable)/-	>2000(unstable)/-
<i>m</i> PD	72	$6.0 \times 10^{-10}$	1.51	310/0.08	320/0.10	1280/0.29
<i>p</i> PD	73	$2.4 \times 10^{-10}$	1.41	846/0.49	>2000(unstable)/-	precipitate
AN	85	0.013	1.34	precipitate	precipitate	precipitate
(b) oxidation of PD•2HCl salt of 0.2 M						
<i>o</i> PD	32	$6.8 \times 10^{-13}$	1.40	1210/0.68	precipitate	>2000(unstable)/-
<i>m</i> PD	39	$6.0 \times 10^{-14}$	1.55	200/0.24	450/0.10	1180/0.37
<i>p</i> PD	43	$2.5 \times 10^{-13}$	1.44	660/0.43	precipitate	>2000(unstable)/-
AN	79	7.2	1.34	473/0.19	264/0.17	995/0.44
(c) oxidation of PD hydrochlorides in excess of 1 M HCl						
<i>o</i> PD	41	$9.7 \times 10^{-12}$	1.41	precipitate	precipitate	>2000(unstable)/-
<i>m</i> PD	22	$2.1 \times 10^{-11}$	1.36	290/0.10	220/0.04	660/0.23
<i>p</i> PD	43	$2.4 \times 10^{-10}$	1.43	precipitate	precipitate	>2000(unstable)/-
AN	70	13	1.33	490/0.23	300/0.25	780/0.50

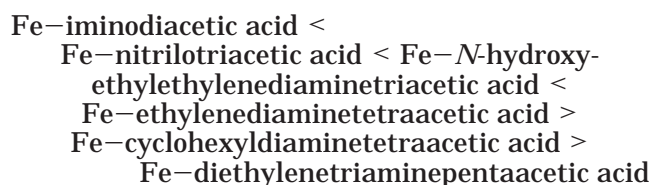
difunctional ligand molecules linked by metal atoms with degrees of polymerization lower than 20.

## B. Effect of Polymerization Conditions

The polymerization reaction is markedly affected by the reaction conditions including monomer, solvent composition, oxidant, temperature, and time.<sup>215</sup> The influence of monomer structure on the oxidation polymerization of aromatic diamines was first investigated by Michaelis and Granick.<sup>103</sup> It is suggested that all yellow or red semiquinone radicals from *p*PD, 2-methyl-*p*PD, 2,3,4,5-tetramethyl-*p*PD, 2-sulfonic-*p*PD, 2-chloro-*p*PD, *N*-methyl-*p*PD, *N,N*-dimethyl-*p*PD, *N,N*-dimethyl-*p*PD, and *N,N,N*-trimethyl-*p*PD oxidized by bromine at rather concentrated monomer/HCl/NaCl/acetate buffer (pH 4.6) solution can polymerize at low temperatures such as -12 to 0 °C and rapidly and irreversibly to become green, greenish-brown, or brownish-violet polymers. However, the radical derived from *N,N,N,N*-tetramethyl-*p*PD does not polymerize and remains a very stable monomeric free radical even in the solid state because all four hydrogen atoms are substituted by methyl groups and no bond could be established for the polymerization. The polymers of *p*PD, *N,N*-dimethyl-*p*PD, and 2,3,4,5-tetramethyl-*p*PD oxidized by bromine and NaClO<sub>4</sub> at -10 °C exhibit molecular formulas of [H<sub>2</sub>-NC<sub>6</sub>H<sub>4</sub>NH<sub>2</sub>•Br]<sub>*n*</sub>, [H<sub>3</sub>C-HNC<sub>6</sub>H<sub>4</sub>NH-CH<sub>3</sub>•ClO<sub>4</sub>]<sub>*n*</sub>, and {H<sub>2</sub>N[(H<sub>3</sub>C)<sub>2</sub>C<sub>6</sub>(CH<sub>3</sub>)<sub>2</sub>]NH<sub>2</sub>•ClO<sub>4</sub>]<sub>*n*</sub>, respectively. It is interesting that these polymers are too intensely colored crystals to permit observation of their optical properties. The fresh [H<sub>3</sub>C-HNC<sub>6</sub>H<sub>4</sub>NH-CH<sub>3</sub>•ClO<sub>4</sub>]<sub>*n*</sub> crystal is dichroitic, blue and yellow. After 5 days in a vacuum the intensely colored crystals could turn to a reddish-brown resin. {H<sub>2</sub>N[(H<sub>3</sub>C)<sub>2</sub>C<sub>6</sub>(CH<sub>3</sub>)<sub>2</sub>]NH<sub>2</sub>•ClO<sub>4</sub>]<sub>*n*</sub> is a dark blue crystal exhibiting symmetrical extinction that is deep blue-green along one optic axis and yellow along the other. It is apparent that the polymers are completely different from the amorphous and black oxidative polymers obtained with Fe<sup>3+</sup> chelate/O<sub>2</sub> and (NH<sub>4</sub>)<sub>2</sub>S<sub>2</sub>O<sub>8</sub> as oxidant.

Tsuchida et al. investigated the oxidative coupling polymerization of *p*PD in aqueous solution of Fe<sup>3+</sup> chelates of ethylenediaminetetraacetic acid, *N*-hy-

droxyethylethylenediaminetriacetic acid, and nitrilotriacetic acid in the presence of oxygen at 21–23 °C.<sup>216</sup> It is found that the polymerization yield is linearly proportional to the amount of oxygen, which strongly depends on the oxidant used.<sup>212</sup> In the absence of oxidant, the rate of oxygen absorption is slow and no *p*PD polymer precipitates. In the presence of iron salt with a molar ratio of iron salt/*p*PD of 1/10, the rate is still slow but a polymer with a yield of 22.6% for 7 h was obtained. If the iron chelate with a molar ratio of iron chelate/*p*PD of 1/10 was used, the *p*PD solution soon turned black with high polymerization yield of 96.3% accompanied by rapid oxygen absorption. Apparently the catalytic oxidative effect of the iron chelate is obvious in the presence of oxygen, because in the absence of oxygen ferric chelate can give only a small amount of polymer with a yield of 5.3%, whereas Fe<sup>2+</sup> chelate does not exhibit a catalytic effect. These indicate that oxygen participates in the oxidative polymerization. The *p*PD polymerization also depended on the pH of polymerization system, *p*PD/Fe<sup>3+</sup>-chelate molar ratio, and chelate type. The polymerization rate appears to increase gradually with increasing pH from 4 to 7 and reaches a maximum value at pH 7–8. The equimolar complex of *p*PD with Fe<sup>3+</sup>-chelate exhibits the highest polymerization activity. Perhaps Fe-ethylenediaminetetraacetic acid could be the best oxidant giving the fastest oxidative polymerization rate of *p*PD. The oxidative polymerization rate of *p*PD changes with the Fe<sup>3+</sup>-chelate oxidant in the following order



To control the electrical conductivity of polymer on a submolecular level, the copolymers of various PDs with AN have been prepared.<sup>185,192,194</sup> Prokes and coworkers prepared PD/AN copolymers by using PD- and AN-HCl salts as monomers.<sup>194</sup> The copolymerization yield is high (>50%), but the structure of the

copolymers has not been well elucidated. They deduced that the chemical composition and properties of the copolymers would change with the oxidant/monomer ratio and reaction conditions.

Prasad et al. investigated the effect of 100 mM acidic aqueous solution on the chemical oxidative polymerization of 100 mM *o*PD with 120 mM  $K_2S_2O_8$  as oxidant at 20 °C for 4–5 h under nitrogen.<sup>155</sup> It is found that the polymerization production increases from 430, 725, 740, to 750 mg on changing the acid from  $H_2SO_4$ ,  $H_2C_2O_4$ ,  $HClO_4$ , to  $CH_3COOH$ . Reddish-brown *Po*PD was obtained from the polymerization medium.

Sulimenko et al. investigated the effect of the HCl concentration on the oxidative polymerization of three PDs listed in Table 7.<sup>213</sup> It is found that the oxidative polymerization products of three PDs are usually obtained in good yields, especially when PD bases are used as a starting monomer in acid-free aqueous solution. Therefore, it is concluded that acid is not necessary for the chemically oxidative polymerization of aromatic amines.

The oxidative polymerization activity of aromatic diamines depends significantly on the monomeric structure, leading to quite different molecular weights. The induction period is very short or missing for *p*PD, while the oxidation behavior of *m*PD resembles that of AN, but *m*PD exhibits the strongest exotherm. When a higher *m*PD concentration and large volumes of reaction mixtures are employed, the overheating of the oxidation system can lead to an explosive course of the polymerization, whereas *o*PD shows the longest induction period and an exotherm similar to that of *p*PD. It appears that the chemical oxidation of *o*PD, at most, leads to an oligomeric product of good solubility in organic solvents, although its electrooxidation has been reported to form polymer.<sup>140–164</sup> *p*PD forms soluble oxidative polymer, but *m*PD yields polymeric materials of limited solubility in organic solvents. The variation of the electroconductivity with polymerization was followed in Table 7.<sup>213</sup> It is found that the *Pp*PD and *Pm*PD usually exhibit higher electroconductivity than *Po*PD, implying that *Pp*PD and *Pm*PD have a longer  $\pi$ -conjugated structure possibly due to the higher molecular weight, as discussed in part E of this section.

The influence of monomer structure and HCl concentration on the colloid characteristics of the final three PD polymers stabilized with water-soluble polymers is listed in Table 7.<sup>213</sup> *Pm*PD colloids of a good quality, having small particle size and low polydispersity, are obtained for all three steric stabilizers. Among them, PVP is the most efficient stabilizer. The colloidal stability of *Pm*PD and PAN is good, and no change in particle size and uniformity has been observed after months and even years. On the contrary, limited stability has been found in *Pp*PD dispersions. Additionally, a strong influence of a very small amount of *p*PD on the PAN particle shape was observed when HPC was used as a steric stabilizer in the AN dispersion polymerization in aqueous medium.<sup>217</sup> The spherical shape of particles prepared at 0 °C in the absence of *p*PD changes to the rice-grain morphology when the rate of PAN

formation has been moderately increased by the addition of 20 mM *p*PD (*p*PD/AN molar ratio = 1/10000). The coral-like cylindrical morphology having a diameter of about 200 nm was produced under similar conditions at a higher reaction rate in the presence of 200 mM *p*PD. The granular surface of cylinders is composed of small primary particles with attached HPC. The branched dendritic structure based on cylindrical elements developed when the polymerization rate was still faster at 2 mM *p*PD. A macroscopic precipitate of indescribable fractal appearance was obtained at 20 mM *p*PD (*p*PD/AN molar ratio = 1/10), indicating that the particle morphology is controlled by the rate of PAN formation, which is efficiently increased by introduction of a small amount of *p*PD.

In addition to the aromatic diamines, an aromatic triamine, i.e., *sym*-triaminobenzene (TAB) (No. 17 in Scheme 1), with iodine as oxidant in a variety of solvents including acetic acid and in the vapor phase can polymerize and form an electron-rich network black polymer, of special interest as a potential organic ferromagnet or conducting polymer.<sup>218,219</sup> Iodine may play a role in oxidizing the formed polymer.<sup>219</sup> However, the polymerization of TAB can also occur even in the absence of iodine. A strong influence of temperature on the polymerization rate of TAB is found. At 25 °C, the polymerization took about 48 h before any polymer could be seen. At 50 °C under an inert atmosphere, a yellow/orange precipitate formed after 4 h. At 110 °C, the precipitate forms after 5 min. The yellow polymer obtained at 50 °C can be neutralized with triethylamine or by simply washing with acetonitrile, giving an almost colorless product. The polymerization activation energy is about 75 kJ/mol. The polymerization exhibits a strong dependence on the acid strength. Without acid or with only catalytic amounts of acid, no polymerization would be observed even when heating. If an excess amount of strong acid such as formic acid is used, no polymer is obtained either, even with heating because di- and triprotonated TAB on the amino groups (not the ring carbons) is formed, since triprotonated TAB on the amino groups does not give a polymer. It is believed that the acidity of acetic acid perfectly matches the basicity of the TAB. Note that the acetate ion itself is not critical for the polymerization of the TAB because heating a neat mixture of the monoacid ( $HBF_4$ ) salt of TAB and TAB itself also results in the formation of poly(TAB). However, heating  $TABH^+BF_4^-$  alone in acetonitrile gives no polymer. The polymerization mechanism of TAB has been speculated. The first step is protonation of TAB to give a ring-protonated nonaromatic intermediate containing a  $=NH_2^+$ -group; the second step is that the monoprotinated TAB is attacked nucleophilically by a TAB to form addition product; this then eliminates ammonium ions to give  $=NH^+$  groups; the third step is nucleophilic attack by another TAB, until the network poly(TAB) is formed.

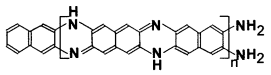
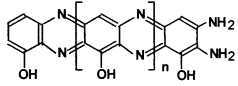
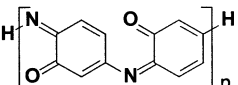
### C. Molecular Structure and Spectroscopy

The molecular structure of PPD polymers has been characterized by means of FT-IR, NMR, XPS, and

**Table 8. Macromolecular Structure and IR Characteristics (wavenumber  $\text{cm}^{-1}$ ) of the Aromatic Diamine Polymers by Oxidative Polymerizations<sup>a</sup>**

No	Polymers and their polymerization condition	Macromolecular structure	Stretching vibrations							Refs.		
			N-H	NH <sub>2</sub>	C-H	C=N	C=C	C-N-C	C-C		C-H	
<b>1</b>	<b>Poly(aminophenazine)</b> Oxidative polymerization (NH <sub>4</sub> ) <sub>2</sub> S <sub>2</sub> O <sub>8</sub> in acetic acid at 118°C		3433sh 3367b	3150b		1500~ 1700b				839m 756s 595m	70	
<b>2</b>	<b>Poly(o-phenylenediamine)</b> Oxidative polymerization (NH <sub>4</sub> ) <sub>2</sub> S <sub>2</sub> O <sub>8</sub> in acetic acid at 118°C		3388b	3180b 1117s	3060vw	1616s	1474s	1352sh 1232sh	1189w	858w 764sh 614sh	220 221	
<b>3</b>	<b>Poly(o-phenylenediamine)</b> Electropolymerization on ITO between -0.5 and +1.3V vs. SCE in 0.1 M H <sub>2</sub> SO <sub>4</sub>		3430b	3173s		1672w 1625w	1532s	1368w 1252w	1145w	838vw 755w	164	
<b>4</b>	<b>Poly(o-phenylenediamine)</b> Electropolymerization on Pt between -0.2 and +0.8V vs. SCE in 0.1 M H <sub>2</sub> SO <sub>4</sub>		3402b	3170s		1629w	1531s	1241w	1134s	629w	222	
<b>5</b>	<b>Poly(m-phenylenediamine)</b> Oxidative polymerization K <sub>2</sub> S <sub>2</sub> O <sub>8</sub> in HCl at room temp.		3435s 3256			1627s		1384w 1263w	1129w	874w 567m	223	
<b>6</b>	<b>Poly(m-phenylenediamine)</b> Enzyme oxidative polymerization H <sub>2</sub> O <sub>2</sub> in buffer pH 7.1 at 30°C		3359b 3266b	3152b		1592s	1435m		1190w	560w	71	
<b>7</b>	<b>Poly(p-phenylenediamine)</b> Enzyme oxidative polymerization H <sub>2</sub> O <sub>2</sub> in buffer pH 7.1 at 30°C		3402b 3283b			1640m	1535s	1266w	1205w	833w 752w	72	
<b>8</b>	<b>Poly(p-phenylenediamine)</b> Oxidative polymerization K <sub>2</sub> S <sub>2</sub> O <sub>8</sub> in HCl at room temp.		3392b 3216			1573s	1500s	1300m		830 752	62	
<b>9</b>	<b>Poly(p-phenylenediamine)</b> Oxidative polymerization K <sub>2</sub> S <sub>2</sub> O <sub>8</sub> in HCl at room temp.		3218b			3031vw	1570s	1511s	1346w 1293m 1286m	1169m	899vw 825m	224
<b>10</b>	<b>p-Phenylenediamine</b> oligomer, Oxidative polymerization Cu <sup>2+</sup> or Co <sup>2+</sup> in H <sub>2</sub> O <sub>2</sub> at 30°C		3432 3333			2665s		1545s			214	
<b>11</b>	<b>Poly(1,5-diaminonaphthalene)</b> Oxidative polymerization by FeCl <sub>3</sub> /CH <sub>3</sub> OH		3340b			3040	1624		1247	1145w	770	225
<b>12</b>	<b>Poly(1,5-diaminonaphthalene)</b> Electropolymerization in 0.1M N(C <sub>4</sub> H <sub>9</sub> ) <sub>4</sub> ClO <sub>4</sub> /0.2 M HClO <sub>4</sub> /CH <sub>3</sub> OH		3224b	3150b	3080b	1655w	1600m 1579m 1529b	1292w	1084s (ClO <sub>4</sub> )	773w 757w 827w	176	
<b>13</b>	<b>Poly(1,5-diaminonaphthalene)</b> Electropolymerization in 0.1M N(C <sub>4</sub> H <sub>9</sub> ) <sub>4</sub> ClO <sub>4</sub> /0.2 M HClO <sub>4</sub> /CH <sub>3</sub> CN		3350m 3232s	3142b	3080b	1648w	1602m	1250w	1098s (ClO <sub>4</sub> )	797w 752w 820w	176	
<b>14</b>	<b>Poly(1,5-diaminonaphthalene)</b> Electropolymerization in 0.1M LiClO <sub>4</sub> /CH <sub>3</sub> CN		3340b 3430b 3230b			3020w	1624 1595	1560 1520	1295 1247	1145s 1088s (ClO <sub>4</sub> )	760w 815w	174
<b>15</b>	<b>Poly(1,5-diaminonaphthalene)</b> Electropolymerization in 0.1M LiClO <sub>4</sub> /CH <sub>3</sub> CN		3342m 3225m			3035w	1650	1580m 1556m 1531m	1243m	1090s (ClO <sub>4</sub> )	773s 620s 814m	173
<b>16</b>	<b>Poly(1,8-diaminonaphthalene)</b> Electropolymerization in 0.1M N(C <sub>2</sub> H <sub>5</sub> ) <sub>4</sub> ClO <sub>4</sub> /CH <sub>3</sub> CN		3340b 3200b			3060w	1600b,s	1470w	1247	1120m	780w	181
<b>17</b>	<b>Poly(1,8-diaminonaphthalene)</b> Electropolymerization in 0.1M LiClO <sub>4</sub> /0.1M HClO <sub>4</sub>		3385b				1626b	1460w	1282b	1130m	765w	226
								1420w		1090s(ClO <sub>4</sub> )	826m	

**Table 8 (Continued)**

No	Polymers and their polymerization condition	Macromolecular structure	Stretching vibrations							Refs.	
			N-H	NH <sub>2</sub>	C-H	C=N	C=C	C-N-C	C-C		C-H
<b>18</b>	<b>Poly(1,8-diaminonaphthalene)</b> Electropolymerization in 0.2M NaClO <sub>4</sub> / H <sub>2</sub> O		3400b			1645		1265		770 820	139
<b>19</b>	<b>Poly(2,3-diaminonaphthalene)</b> Electropolymerization in 0.2M NaClO <sub>4</sub> / H <sub>2</sub> O		3350			1645		1265	1200	750	139
<b>20</b>	<b>Poly(1,5-diaminoanthraquinone)</b> Electropolymerization in 0.1M N(C <sub>2</sub> H <sub>5</sub> ) <sub>4</sub> ClO <sub>4</sub> + 0.5 M CF <sub>3</sub> COOH		3430b	3170w		1580s	1500s	1250s		830b 710-820	227
<b>21</b>	<b>Poly(2,3-diaminophenol)</b> Electropolymerization		3450b 3200b(O-H)			1620b	1600b				182
<b>22</b>	<b>Poly(o-hydroxyaniline)</b> Electropolymerization in 0.5 M Na <sub>2</sub> SO <sub>4</sub>		3420b		3060	1645	1580-1590	1310		935 760-850	228

<sup>a</sup> b = broad; m = medium; s = strong; sh = sharp; vw = very weak; w = weak.

**Table 9. Assignments for IR Absorption Bands (wavenumber, cm<sup>-1</sup>) for the Copolymers of Phenylenediamine with Aromatic Monoamines by Chemically Oxidative Polymerization<sup>a</sup>**

polymers	-N-H-	-NH <sub>2</sub>	aromatic C-H	aliphatic C-H	quinoid C-C	benzenoid C-C	quinoid C-N	benzenoid C-N	refs
<b>PoPD</b>	3388b,s	3180b	1117s,sh 858w 764sh 614sh	2910vw 2850vw	1616s,sh	1474s	1352sh 1189w	1232sh	220
<b>oPD/XY</b> (70/30) copolymer	3401b,s	3200b	1111s,sh 868w 765sh 619sh	2910w 2850w	1613s,sh 1695m	1481s 1187m	1339sh	1238w	220
<b>oPD/MA</b> (70/30) copolymer	3394b,s 3222b		1114s,sh 862w 764sh 612sh		1622s,sh	1483s	1352sh 1188m	1236w	221
<b>PmPD</b>	3435s		874w 567m	2925w 2854vw	1627s	1129w 1457vw	1384w 1263w	1264w	223
<b>mPD/XY</b> (90/10) copolymer	3435b,s		2967vw 874w,sh 569b	2926w 2854vw	1627s,sh	1129s	1384sh	1275w	215
<b>mPD/XY</b> (70/30) copolymer	3350b,s 3217b		828m 689w 615w	2927w	1620b 1492b	1528b	1384b	1282b	215
<b>mPD/XY</b> (50/50) copolymer	3391b,s 3229sh		874m 828w 600m	2920w	1621b 1485b	1524w	1384b	1284b	215
<b>mPD/MA</b> (90/10) copolymer	3435b,s 3217b		875w 569w	2925m,sh 2854w	1628s	1128m 1456w	1384b	1255w	215
<b>PpPD</b>	3218b,s		899s,sh 825s		1570s,sh 1169m	1511s 1286m	1346sh	1293m	224
<b>pPD/XY</b> (90/10) copolymer	3338b,s 3220b,s		3031vw 899s,sh 827s	2929vw 2857vw	1569s,sh	1511s 1173m	1349sh	1273m	224
<b>pPD/PHT</b> (90/10) copolymer	3434b 3368b 3309b	3170b	3055vw 892w 841m	2933vw	1640m 1497s 1474m	1528s 1147w	1341w	1234m	229

<sup>a</sup> Abbreviations: b = broad; m = medium; s = strong; sh = sharp; vw = very weak; w = weak.

UV-vis spectroscopies. Some important characteristics of FT-IR, NMR, and UV-vis spectroscopies are summarized in Tables 8–11. Among the three isomers of PPD, the structure of PoPD has been substantially defined by researchers, while the structure of PmPD has not been fully elucidated because the

PmPD obtained by chemical oxidative polymerization is almost insoluble in most solvents. PmPD structure can be characterized only by solid-state techniques such as FT-IR, XPS, and solid-state <sup>13</sup>C NMR.<sup>69,223</sup> It is believed that the polymerization procedure has some effect on the structure of PPDs.

**Table 10. NMR Characteristics of the Polymers Prepared from Aromatic Diamines by a Chemically Oxidative Polymerization**

no. <sup>a</sup>	polymer	chemical shift (ppm) and assignments		refs
		<sup>1</sup> H NMR	<sup>13</sup> C NMR	
1	poly(aminophenazines) acetate	6.90, 7.08, 7.25sh, -NH- and -NH <sub>2</sub> protons 7.87b, the protons at C1 and C4 positions 7.57b, the protons at C5 C7, and C8 positions	99.0, 115.0, 128.0b, 140.0b, 143.0b	70
2	poly(aminophenazine) acetate	6.92, 7.09, 7.26sh, -NH- and -NH <sub>2</sub> protons 8.00b, aromatic protons on phenazine rings		220
1	poly(aminophenazine)	6.90–6.40m ABX; 7.10–6.80m, 9.00–7.10br	114.0, 116.0, 128.0b; 140.0b	70
3	poly( <i>o</i> -phenylenediamine)	4–6b, -NH- protons	102, hydrogen-bonded carbons next to two C–N bonds	72
		6–8b, aromatic protons	126–128, hydrogen-bonded carbons next to one C–N bond	117
	poly( <i>o</i> -phenylenediamine)	8.0s, 7.7s, 6.9s, aromatic protons 7.1w, 7.25w, 7.4w, the protons on terminal units	143–145, nitrogen-bonded carbons no analyzable signals	164
	poly( <i>m</i> -phenylenediamine)	4–6b, -NH- protons; 6–8b, aromatic protons	No analyzable signals	72
	poly( <i>m</i> -phenylenediamine)		117.6s, hydrogen-bonded carbons in benzenoid 136.9s, nitrogen-bonded carbons in benzenoid 172.3w, carbons (C=N) in quinoid unit	223
7	poly( <i>p</i> -phenylenediamine)	4.7–5.8b, -NH- protons 6.6(5.8–9.0)b, <i>p</i> -disubstituted aromatic protons	no analyzable signals	72
8	poly( <i>p</i> -phenylenediamine)	4.5b, -NH- and -NH <sub>2</sub> protons 6.8m, benzenoid protons; 7.9m, quinoid protons	no analyzable signals	62
9	poly( <i>p</i> -phenylenediamine)	5.55sh, -NH <sub>2</sub> protons 6.58m, 6.61m, 6.81s, 6.83s, 6.99w, 7.02w, 7.14sh, 7.17sh, -NH- protons 7.35b, 7.44b, 9.17m, 9.62w, aromatic protons	-	224
10	<i>p</i> PD oligomer(Cu <sup>2+</sup> oxidant)	5.0s, 3H -NH <sub>2</sub> protons; 5.7s, 1H -NH-NH- protons 6.0s, 3H =N-NH- protons	153.3, 148.3, 144.9, 140.0, quinoid carbons 122.2, 114.3, 90.6, benzenoid carbons	214
10	<i>p</i> PD oligomer (Co <sup>2+</sup> oxidant)	6.6s, 8H; 7.5s, 0.1H aromatic protons 5.0bs, -NH <sub>2</sub> protons; 5.75s, -NH-NH- protons 6.0s, =N-NH- protons; 6.7s, aromatic protons	153.3, 148.3, 144.9, 140.0, quinoid carbons 122.2, 114.3, 90.6, benzenoid carbons	214
15	poly(1,5-diaminonaphthalene)	6.0b (4H), -NH <sub>2</sub> protons 6.65m, 6.80m, 7.11s, 7.28s, 7.51b (8H), benzenoid protons 7.72b, 8.3m, 8.5s, 8.66m, 9.1w, 9.2m, 9.4b (8H) quinoid protons		173
	polybenzidine	3.5(sh), -NH- protons 6.85, 7.6(coupled doublets); benzenoid protons 7.85, 8.0(coupled doublets); quinoid protons		230
	poly( <i>N,N</i> -diphenylbenzidine)	3.5(doublet), -NH- protons 6.9–7.9(multiple peaks), aromatic protons		230
	<i>o</i> PD/XY (70/30) copolymer	6.5–9.0b, aromatic protons on phenazine rings		220
	<i>o</i> PD/MA (70/30) copolymer	2.88w, -CH <sub>3</sub> protons; 6.84, 7.10, 7.35sh, -NH- and -NH <sub>2</sub> protons		221
	<i>m</i> PD/PHT (70/30) copolymer	6.92, 7.09, 7.26sh, -NH- and -NH <sub>2</sub> protons 8.01b, 8.23b, aromatic protons on phenazine and pyrimidyl rings		229
	<i>p</i> PD/XY(90/10) copolymer	5.03w, 5.07w, 5.14w, -NH <sub>2</sub> protons 5.71w, 5.8w, 5.87w, 6.0, 6.19w, 6.26w, -NH- protons 6.7m, 7.0m, 7.15m, aromatic protons 1.285s, -CH <sub>3</sub> protons; 3.97m, 4.06m, -OCH <sub>2</sub> - protons		224
	poly( <i>sym</i> -triaminobenzene)	2.40~2.59m, -CH <sub>3</sub> protons; 6.2~7.1w, -NH- protons 7.29m, aromatic protons on 2,3-xylylidine units 7.56m, 7.74s, aromatic protons on the quinoxaline units	140s, C–N; 100s, C–H	218

<sup>a</sup> No. corresponds to the no. of the polymer listed in Table 8: b = broad; m = medium; s = strong; sh = sharp; w = weak.



**Table 11. UV-vis Characteristics of the Polymers and Copolymers from Aromatic Diamines by Oxidative Polymerizations**

polymer	wavelength of the absorption bands (nm)			refs
	phenazine	quinonediimine	other structure	
poly(aminophenazine)	392m	677w		70
poly( <i>o</i> -phenylenediamine)	459m			72
poly( <i>o</i> -phenylenediamine)	465b, 490b			158
poly( <i>o</i> -phenylenediamine)	462w		270m	222
<i>o</i> -phenylenediamine/ <i>o</i> -phenetidine (90/10) copolymer	434m		270s, 281s	229
poly( <i>m</i> -phenylenediamine)	459w			72
<i>m</i> -phenylenediamine/ <i>o</i> -phenetidine (90/10) copolymer	459w		258s, 279m, 338b	229
poly( <i>p</i> -phenylenediamine)	404b	543w	275s, 344w	62
poly( <i>p</i> -phenylenediamine) without acetic acid			337s, 497m	72
poly( <i>p</i> -phenylenediamine) with acetic acid	405m	636b	308m, 360m, 543m	72
<i>p</i> -phenylenediamine oligomer	473		332	214
<i>p</i> -phenylenediamine/ <i>o</i> -phenetidine (90/10) copolymer	424w	530w	257s, 272m, 308b	229
poly(1,5-diaminonaphthalene)		650b		225
poly(1,5-diaminonaphthalene)		580b	277s, 350m	178
poly(1,8-diaminonaphthalene)			500	226
poly(3-hydroxy- <i>o</i> PD)	467w		300b	182
poly( <i>N,N</i> -diphenylbenzidine) (undoped)			345s	230
poly( <i>N,N</i> -diphenylbenzidine) (doped)		660m	250s	
polydithiodianiline		640b		231
dithiodianiline/AN(2/175) copolymer (undoped)		620m	325s	232
dithiodianiline/AN(2/175) copolymer (doped)		780b	353b	

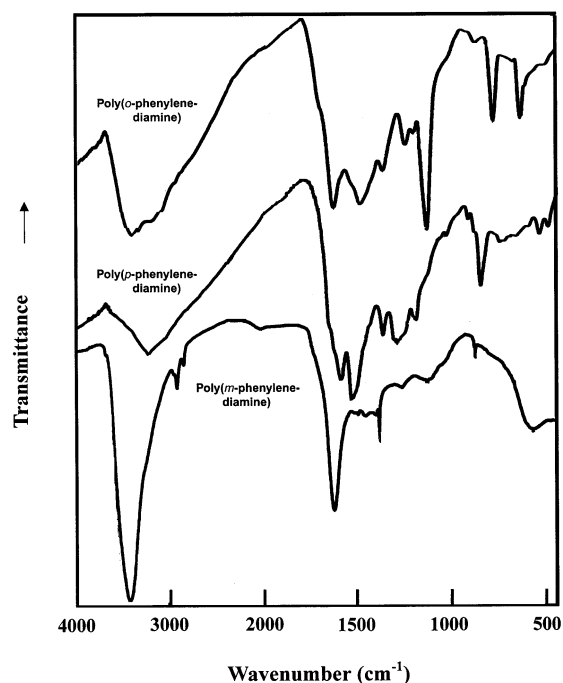


**Figure 1.** FT-IR spectra of poly(*o*-phenylenediamine) (PoPD),<sup>220,221</sup> poly(*p*-phenylenediamine) (PpPD),<sup>224</sup> and poly(*m*-phenylenediamine) (PmPD)<sup>223</sup> prepared by chemically oxidative polymerization.

### 1. FT-IR Spectroscopy

FT-IR spectroscopy has conveniently provided valuable information regarding the linkage of aromatic diamines for oxidative polymerization. In the IR spectra of PD, DAN, and DAAQ polymers, shown in Table 8 and Figure 1, a large broad adsorption peak is observed from 3700 to 1800  $\text{cm}^{-1}$ . This type of absorption is frequently encountered in electrically conductive polymers due to electronic transitions from the valence band to the conduction band.<sup>208</sup> Almost all polymers from the three PDs exhibit two or three broad peaks at 3435–3213 and 3180–3150  $\text{cm}^{-1}$ , suggesting N–H stretching vibrations of –NH–

and –NH<sub>2</sub> groups, respectively. The peaks between 935 and 820  $\text{cm}^{-1}$  are attributed to the out-of-plane bending motions of C–H of 1,2,4,5-tetrasubstituted benzene nuclei of phenazine units, implying that the polymers have the basic phenazine skeleton. In the region between 1570 and 1640  $\text{cm}^{-1}$  as well as between 1435 and 1535  $\text{cm}^{-1}$ , the polymers show strong peaks associated with the C=N and C=C stretching vibrations in the phenazine ring. This is further testified by observation of the out-of-plane C–H bending vibration of 1,2,4-trisubstituted benzene nuclei in the phenazine skeleton at the medium or weak peaks at 752–764 and 560–629  $\text{cm}^{-1}$ , indicating that the PPDs are not fully ladder polymers. It can be concluded that the oxidative polymerization and electropolymerization of three PDs do not give very large differences in the IR spectra of the final polymers. The IR and <sup>1</sup>H NMR spectra and element analysis results suggest that the *o*PD polymer synthesized by electropolymerization has a 1,4-substituted benzenoid–quinoid backbone structure containing one –NH<sub>2</sub> group on each 1,4-substituted benzenoid or quinoid unit.<sup>164</sup> It is reported that application of different levels of oxidizing agents does not cause a very big difference in IR spectra of the *p*PD polymers obtained but leads to some differences in the intensity of some bands.<sup>62</sup> Other polymers listed in Table 8 exhibit similar IR spectral characteristics with PD polymers except for an additional C=O stretching vibration at 1610 and 1670  $\text{cm}^{-1}$  corresponding to P15DAAQ and PHAN, respectively. Table 9 summarizes the assignments for the IR absorption bands for the copolymers of PDs with four aromatic amines by oxidative polymerization. It is seen that introduction of no more than 30 mol % of comonomers containing a single amino group hardly ever causes a significant change of the IR spectra,<sup>220,221,223,224</sup> implying that the phenazine-like structure remains. Abnormal IR effects of in-situ IR spectra of PoPD on electrodes of nanometer thin films of Pt, Pd, and Rh have been investigated.<sup>233</sup>

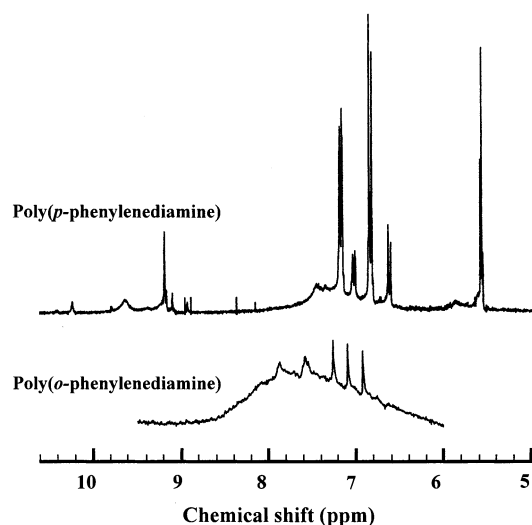


**Figure 2.** Typical  $^1\text{H}$  NMR spectra in  $\text{DMSO}-d_6$  at 300 MHz of poly(*o*-phenylenediamine)(PoPD)<sup>70</sup> and poly(*p*-phenylenediamine)(PpPD)<sup>224</sup> prepared by chemically oxidative polymerization.

## 2. NMR Spectroscopy

As mentioned above, three polymers of *o*PD, *m*PD, and *p*PD exhibit similar N–H stretching bands but exhibit different  $^1\text{H}$  NMR characteristics of –NH– and –NH<sub>2</sub> protons, as summarized in Table 10 and Figure 2. No  $^1\text{H}$  NMR spectra of P*m*PD and TAB polymer were reported because of their insolubility in deuterated solvents.<sup>218,223</sup> PoPD, i.e., PDAPh, obtained in glacial acetic acid at 118 °C, exhibits three sharp peaks at 6.90, 7.08, and 7.25 ppm for –NH– and –NH<sub>2</sub> protons, whereas the polymers formed in aqueous solution at room temperature exhibit weak or broad peaks at 4.0–7.17 ppm for –NH– and –NH<sub>2</sub> protons. Broad peaks suggest a mixture of different chemical environments of –NH– and –NH<sub>2</sub> protons. Note that there is a significant influence of oxidant and testing solvent on the  $^1\text{H}$  NMR characteristics of the same PpPD and PoPD, as shown in Figures 3 and 4.

As seen in the bottom spectrum in Figure 3, PpPD obtained with  $\text{K}_2\text{S}_2\text{O}_8$  as the oxidant exhibits a very strong sharp doublet at ca. 5.58 ppm due to –NH<sub>2</sub> proton and a very strong sharp quadruplet at 6.6–7.2 ppm due to aromatic protons.<sup>224</sup> The middle spectrum exhibits a strong broad peak centered at 4.5 ppm due to –NH<sub>2</sub> protons.<sup>62</sup> On the other hand, both PpPDs obtained with  $\text{K}_2\text{S}_2\text{O}_8$  as the oxidant exhibit several weak peaks at 8.9–10.2 ppm, but the PpPD prepared by enzyme-catalyzed oxidative polymerization with  $\text{H}_2\text{O}_2/\text{HRP}$  as the oxidant/catalyst does not. These significant differences may result from different molecular structure and molecular weight. For example, the top PpPD may have the higher molecular weight, while the middle PpPD should contain more amino groups in its macromolecular chain.

As shown in Figure 4, three strong and sharp –NH<sub>2</sub>–NH– proton peaks with high resolution in  $\text{DMSO}-d_6$  will become an overlapped multiple peak in deuterated TFA, because of the different interactions between –NH<sub>2</sub>–NH– protons and solvents.

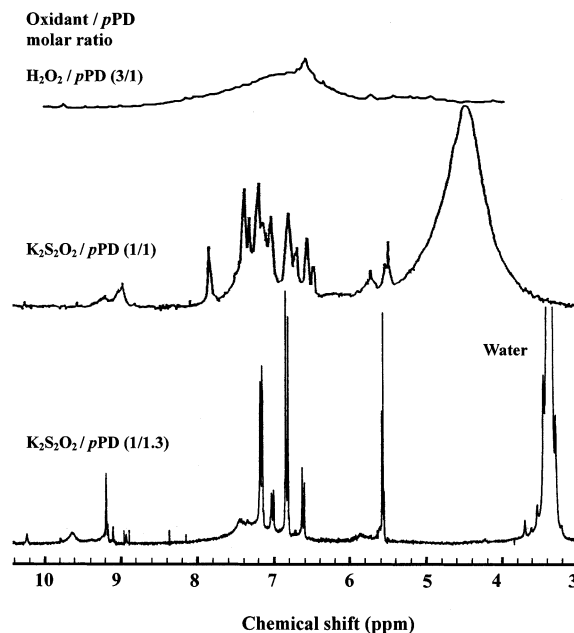


**Figure 3.**  $^1\text{H}$  NMR spectra in  $\text{DMSO}-d_6$  of poly(*p*-phenylenediamine)(PpPD) prepared by chemically oxidative polymerization with the oxidants/*p*PD molar ratio of  $\text{H}_2\text{O}_2$ –HRP/*p*PD (3/1) at 500 MHz (top),<sup>72</sup>  $\text{K}_2\text{S}_2\text{O}_8$ /*p*PD (1/1) at 200 MHz<sup>62</sup> (middle), and  $\text{K}_2\text{S}_2\text{O}_8$ /*p*PD (10/13) at 300 MHz<sup>224</sup> (bottom).

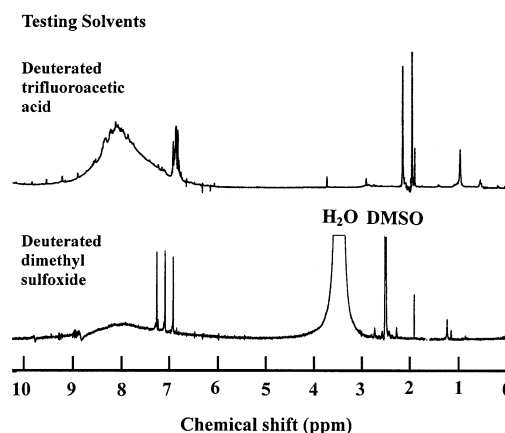


**Figure 4.**  $^1\text{H}$  NMR spectra in two testing deuterated solvents of poly(*o*-phenylenediamine)(PoPD) prepared by chemically oxidative polymerization at 300 MHz.<sup>220,221</sup>

The resonance peak due to aromatic protons also varies with testing solvents.

Four copolymers of PDs with aromatic monoamines exhibit nearly the same  $^1\text{H}$  NMR characteristics of –NH– and –NH<sub>2</sub> protons as the corresponding homopolymers except for additional –CH<sub>3</sub> and –OCH<sub>2</sub>CH<sub>3</sub> resonance peaks. Representative  $^1\text{H}$  NMR spectra of *o*PD/PHT, *m*PD/PHT, and *p*PD/PHT (50/50) copolymers are shown in Figure 5. *o*PD/PHT copolymer exhibits quite different strong and sharp quadruple peaks with high resolution ascribed to the aromatic protons as compared with *m*PD/PHT and *p*PD/PHT copolymers, because the molecular weight of *o*PD/PHT copolymer is lower than that of the other two copolymers.

Although  $^1\text{H}$  NMR spectroscopy is very useful to characterize the macromolecular chain structure of soluble polymers from aromatic diamines, the solu-

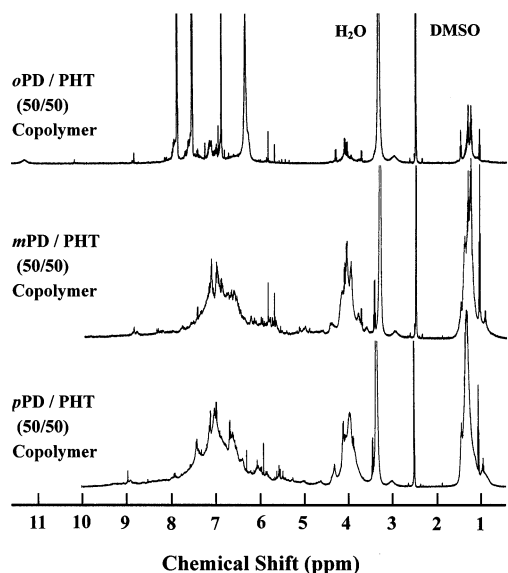


**Figure 5.** Typical  $^1\text{H}$  NMR spectra for the three copolymers of *o*PD/PHT, *m*PD/PHT, and *p*PD/PHT with the molar ratio of 50/50 in  $\text{DMSO}-d_6$  at 500 MHz.<sup>229</sup>

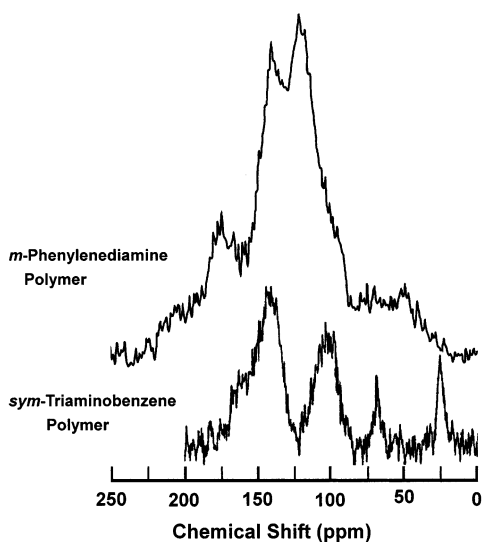


**Figure 6.** High-resolution solid-state  $^{13}\text{C}$  NMR spectra of poly(*m*-phenylenediamine) (P*m*PD)<sup>223</sup> at 75.6 MHz and poly(*sym*-triaminobenzene) (Poly(TAB))<sup>218</sup> synthesized by chemically oxidative polymerization.

tion  $^{13}\text{C}$  NMR spectra of PD polymers are generally broad, and no signals were especially useful to analyze their molecular structure, probably due to low PD polymer content in the solution.<sup>70,72,164</sup> However, the solid-state  $^{13}\text{C}$  NMR spectra of *m*PD and TAB polymers seem to exhibit some valuable information for the analysis of their molecular structure, as shown in Figure 6. For *m*PD polymer, the strongest signal at 117.6 ppm should be assigned to the hydrogen-bonded carbon (C–H) in the benzenoid unit and the second strongest signal at 136.9 ppm is assigned to the nitrogen-bonded carbon (C–NH) in the benzenoid unit.<sup>223</sup> The weak signal at 172.3 ppm is assigned to C=N in the quinoid unit, indicating low content of quinoid unit in the *m*PD homopolymer. The weakest signal in a chemical shift range from 90 to 40 ppm might be due to primary amine-bonded carbon (C–NH<sub>2</sub>) in the end group and/or noncyclized units, suggesting higher molecular weight and/or the

presence of a small amount of the open ring-containing –NH<sub>2</sub> group.

The solid-state  $^{13}\text{C}$  NMR spectrum of the TAB polymer gives the strongest peak at 140 ppm and the second strongest peak at 102 ppm, which are attributed to the carbons in C–N and C–H bonds, respectively.<sup>218</sup> A shoulder peak at ca. 165 ppm could be due to C=O in the dopant (CH<sub>3</sub>COOH) or C=N in the quinoid unit in the polymers, whereas another weak peak at 22 ppm should be due to the dopant (CH<sub>3</sub>COOH) and the weakest peak at ca. 68 ppm to the CH<sub>2</sub> unit in the ring-protonated subunits. These results show that there are predominantly two types of carbons (C–N and C–H) and a small amount of quinoid unit containing C=N in the TAB polymer.

### 3. UV-vis Spectroscopy

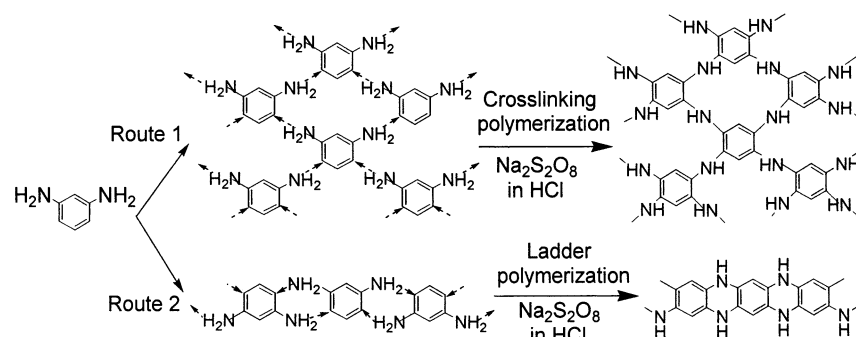
UV-vis spectroscopy has been extensively used to evaluate the electronic structure of electrically conducting polymers. UV-vis spectral characteristics of the polymers and copolymers from aromatic diamines are summarized in Tables 11 and 12. Although three copolymers with *o*PD/PHT, *m*PD/PHT, and *p*PD/PHT with a molar ratio of 90/10 exhibit different UV-vis spectral characteristics, most of the polymers and copolymers from PDs show two major absorbances at the wavelength of 392–467 and 636–677 nm. The band between 392 and 467 nm is attributed to a  $\pi$ – $\pi^*$  transition associated with the phenazine unit conjugated to long pairs of bridging nitrogens.<sup>70</sup> A lower energy band between 636 and 677 nm should be assigned to the quinonediimine-like structure. The other bands may be due to a  $\pi$ – $\pi^*$  transition between conjugated adjacent benzenoid units (320 nm),<sup>62</sup> azobenzene (337 nm), and quinoneimine (497 nm).<sup>72</sup> Other aromatic diamine and aminoquinoline polymers showed a broad UV-vis absorption band between 640 and 675 nm due to the typically oxidized structure for conductive polymers as well as other bands at 300, 330, 430, 467, and 520 nm. Usually the absorption at a longer wavelength, >500 nm, is mainly due to the oxidized form whereas that at ca. 330 nm includes contributions of both the reduced and oxidized forms.<sup>35</sup>

### 4. XPS Spectroscopy

Because of the low solubility, the structure of some aromatic diamine polymers such as P*m*PD has not been completely elaborated. XPS technique has been especially applied to investigate the electronic and chemical structure of the insoluble polymer as well as the interaction between the dopant and polymer.<sup>69</sup> For the P*m*PD polymerized by the oxidant of Na<sub>2</sub>S<sub>2</sub>O<sub>8</sub> in HCl aqueous solution, XPS studies indicated the existence of nitrogen atoms in four different environments of various degrees of oxidation, which is the same as those in doped PAN.<sup>69</sup> It is reported that the N<sub>1s</sub> spectrum of P*m*PD can be resolved into four components.<sup>69</sup> The lowest binding energy component at 399.2 eV is attributed to the neutral imine nitrogen (–N<sup>••</sup>=) followed by the amine nitrogen (–N<sup>•</sup>H–) at 400.2 eV with the strongest intensity. Another two components at 401.2 (the second strongest) and 402.5 eV correspond to the protonated imine (–N<sup>+</sup>(HCl)=) and amine (–N<sup>+</sup>H(HCl)–) ni-

**Table 12. Effect of Applied Potential on UV-vis Characteristics (wavelength, nm) of the Polymers Prepared from Aromatic Diamines**

polymer	applied potential V vs Ag/AgCl	wavelength of the absorption bands (nm)			refs
		phenazine	quinonediimine	other structure	
poly( <i>o</i> -phenylenediamine)	total-ox	450b	735w	300m, 530m	97
	semi-ox	430w		300m, 500m	
<i>N,N</i> -diphenyl- <i>p</i> -phenylenediamine polymer	0			881w, 997w	234
	0.2		675b	384s, 881w, 997w	
	0.4		570b	881w, 997w	
poly(1,5-diaminoanthraquinone)	-1.4-0		670b	515w	227
	0-1		640b	520w	
polybenzidine cast film	-1.0-0.0	400w			230
	+0.26	400w	620w		
polybenzidine virgin film	+0.63	400m	550w		230
	-0.25	400w	610w		
	0	400w	590w		
	+0.21	400w	530w		
	+0.63	400m	500w		
poly( <i>N,N</i> -diphenylbenzidine) cast film	-1.0		530w	330s	230
	+0.5	420w		328s, 300s	
	+2.0		650w	328m, 300s	
poly( <i>N,N</i> -diphenylbenzidine) virgin film	-1.0		530w	300s, 330m	230
	+0.5		550w	300s, 330m	
	+2.0		640w	300s, 330m	

**Figure 7.** Possible coupling orientations in poly(*m*-phenylenediamine) (*PmPD*).<sup>69</sup>

trogens, respectively. Furthermore, most of the protonation occurs at the imine nitrogen rather than the amine nitrogen, with a ratio of doped amine to doped imine of 0.34. The  $C_{1S}$  spectrum of *PmPD* can also be resolved into four components, the first component at 285.0 eV due to the hydrocarbon C-H and carbon-carbon C-C, the second component at 286.1 eV with the largest intensity attributed to the carbon bonded with the neutral nitrogen atoms, the third and the weakest fourth components at 287.1 and 288.3 eV corresponding to the carbons bonded to doped imine and amine nitrogen, respectively. It is calculated that the area ratio of the (C-C + C-H) to (C-N + C=N) components is 0.6. Additionally, the XPS  $Cl_{2P}$  spectrum of *PmPD* has also been analyzed.<sup>69</sup> Therefore, the surface elemental stoichiometry of *PmPD* is  $C_{7.4}N_2Cl_{0.69}$ . Furthermore, two possible structures—network or ladder-like structures with tetrasubstituted benzene nuclei—depending on the orientation as shown in Figure 7, have been proposed according to the results of XPS.<sup>69</sup>

### 5. Elemental Analysis

Another very powerful technique for investigating the molecular structure of aromatic diamine polymers is elemental analysis. Elemental analysis is often used to study the molecular structure of aromatic diamine polymers,<sup>214</sup> in particular the insoluble

*mPD* polymer<sup>69</sup> and low soluble DAAQ complexes,<sup>208,209</sup> because conventional solution characterization of the insoluble polymers is impossible. Elemental analysis is also a powerful technique of measuring metal content in the metal cation-oxidized DAAQ complex.<sup>208,209,214</sup> It is found in Table 13 that the empirical formula of *PmPD* varied with the oxidant used. The nitrogen content in the *PmPD* is slightly lower if using  $K_2S_2O_8$  rather than  $Na_2S_2O_8$ . The empirical formulas of the *PmPD* are different from that of the *PoPD*, indicating a difference between the macromolecular structures of the *PmPD* and *PoPD*. It seems that the bulk carbon content for the same *PmPD* obtained with  $Na_2S_2O_8$  as oxidant determined by elemental analysis is lower than the surface carbon content determined by XPS.<sup>69</sup>

For the oxidative oligomer of *pPD* by *cis*-bisglycinato  $Cu^{2+}$  monohydrate, the C, H, N, and Cu contents listed in Table 13 are close to the calculated four elemental contents of 60.54, 3.5, 22.83, and 8.15 wt %, respectively, based on the molecular formula  $[(C_6H_4ON)(-C_6H_4N_2-)]_{12}(C_6H_6N_2)_2Cu(OH)_2$ .<sup>214</sup> When the oxidant was changed to  $Co^{2+}$  dionemoxime complex, the C, H, N, and Co weight contents for oxidative oligomer of *pPD* change very slightly. It is seen from Table 13 that C, H, N, and metal contents in the oxidative oligomer of *pPD* are almost the same regardless of the variation of oxidants, indicating that

**Table 13. Elemental Assay and Empirical Formula for the Oxidative Products of Aromatic Diamines**

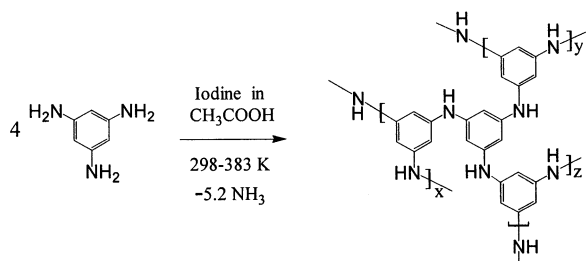
polymers/oxidant	C wt %	H wt %	N wt %	O wt %	metal wt %	empirical formula	refs
poly( <i>o</i> -phenylenediamine)/(NH <sub>4</sub> ) <sub>2</sub> S <sub>2</sub> O <sub>8</sub>	61.2	2.79	19.3			C <sub>6</sub> H <sub>3.3</sub> N <sub>1.6</sub>	70
poly( <i>o</i> -phenylenediamine)/electropolymerization						C <sub>6</sub> H <sub>5.3</sub> N <sub>1.9</sub>	164
poly( <i>m</i> -phenylenediamine)/Na <sub>2</sub> S <sub>2</sub> O <sub>8</sub>	60.9	2.8	22.6	0	0	C <sub>6</sub> H <sub>3.2</sub> N <sub>1.8</sub>	69
poly( <i>m</i> -phenylenediamine)/K <sub>2</sub> S <sub>2</sub> O <sub>8</sub>	49.2	4.18	15.9			C <sub>6</sub> H <sub>6.1</sub> N <sub>1.7</sub>	229
poly( <i>p</i> -phenylenediamine)/Fe <sup>3+</sup> chelate/oxygen	71.8	4.22	4.45			C <sub>6</sub> H <sub>4.2</sub> N <sub>1.8</sub>	211
polybenzidine	78.2	4.34	15.2	1.9(F)		C <sub>12</sub> H <sub>8</sub> N <sub>2</sub> F <sub>0.39</sub>	230
poly( <i>N,N</i> -diphenylbenzidine)	84.8	5.1	8.45	1.0(F)		C <sub>24</sub> H <sub>17</sub> N <sub>2</sub> F <sub>0.36</sub>	230
oligo( <i>p</i> -phenylenediamine)/bisglycinatocopper(II)	59.8	5.16	21.6		7.2	C <sub>6</sub> H <sub>6.2</sub> N <sub>1.8</sub> Cu <sub>0.14</sub>	214
oligo( <i>p</i> -phenylenediamine)/Co <sup>2+</sup> dionemonoxime	61.0	5.11	21.4		7.4	C <sub>6</sub> H <sub>6.1</sub> N <sub>1.8</sub> Co <sub>0.15</sub>	214
1,4-diaminoanthraquinone complex/(NH <sub>4</sub> ) <sub>2</sub> [Ce(NO <sub>3</sub> ) <sub>6</sub> ]	59.6	3.91	12.4	24.1	0	C <sub>14</sub> H <sub>11</sub> N <sub>2.47</sub> O <sub>4.3</sub>	208
1,5-diaminoanthraquinone complex/(NH <sub>4</sub> ) <sub>2</sub> [Ce(NO <sub>3</sub> ) <sub>6</sub> ]	40.3	3.88	17.2	38.6	0	C <sub>14</sub> H <sub>15.9</sub> N <sub>5.1</sub> O <sub>10.0</sub>	209
1,5-diaminoanthraquinone complex/KIO <sub>4</sub>	64.3	3.35	10.1	22.2	0	C <sub>14</sub> H <sub>8.7</sub> N <sub>1.9</sub> O <sub>3.6</sub>	209
1,5-diaminoanthraquinone complex/Cu(NO <sub>3</sub> ) <sub>2</sub>	48.5	2.69	9.31	25.2	14.3	C <sub>14</sub> H <sub>9.2</sub> N <sub>2.3</sub> O <sub>5.5</sub> Cu <sub>0.8</sub>	209
1,5-diaminoanthraquinone complex/CuCl-acetone	48.5	2.79	7.12	26.2	15.4	C <sub>14</sub> H <sub>9.6</sub> N <sub>1.8</sub> O <sub>5.7</sub> Cu <sub>0.8</sub>	209
1,5-diaminoanthraquinone complex/CuCl-pyridine	49.8	2.69	7.80	24.8	14.9	C <sub>14</sub> H <sub>9.0</sub> N <sub>1.9</sub> O <sub>5.2</sub> Cu <sub>0.8</sub>	209
1,5-diaminoanthraquinone complex/Ni(NO <sub>3</sub> ) <sub>2</sub>	52.1	3.00	8.10	25.3	11.6	C <sub>14</sub> H <sub>9.6</sub> N <sub>1.9</sub> O <sub>5.1</sub> Ni <sub>0.7</sub>	209
1,5-diaminoanthraquinone complex/AgNO <sub>3</sub>	41.0	2.32	7.41	34.6	14.7	C <sub>14</sub> H <sub>9.4</sub> N <sub>2.2</sub> O <sub>8.8</sub> Ag <sub>0.6</sub>	209
1,5-diaminoanthraquinone complex/CoCl <sub>2</sub>	49.8	3.11	7.92	6.21	33.0	C <sub>14</sub> H <sub>10.4</sub> N <sub>1.9</sub> O <sub>1.3</sub> Co <sub>1.9</sub>	209
1,5-diaminoanthraquinone complex/PdCl <sub>2</sub>	46.6	3.10	7.96	19.8	22.6	C <sub>14</sub> H <sub>11.1</sub> N <sub>2.1</sub> O <sub>4.5</sub> Pd <sub>0.8</sub>	209
1,5-diaminoanthraquinone complex/FeCl <sub>3</sub>	58.4	4.41	9.59			C <sub>14</sub> H <sub>12.7</sub> N <sub>2.0</sub>	209
poly( <i>sym</i> -triaminobenzene)/-	68.8	5.15	22.1			C <sub>6</sub> H <sub>5.1</sub> N <sub>1.7</sub>	218

the molecular formula may be the same. In addition, as listed in Table 13, the oxidative oligomer of *p*PD exhibits nearly the same carbon/nitrogen ratio but a much higher hydrogen content compared with the *Pm*PD obtained with Na<sub>2</sub>S<sub>2</sub>O<sub>8</sub> as oxidant, possibly implying different oxidizing levels.<sup>69</sup>

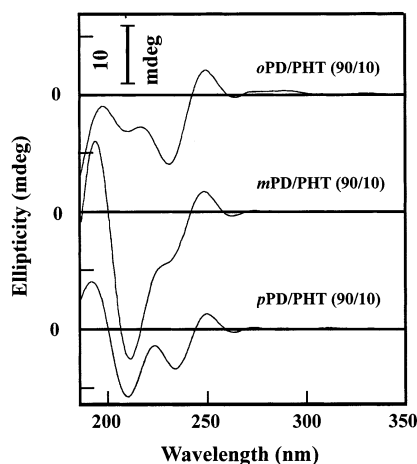
When the same oxidant of (NH<sub>4</sub>)<sub>2</sub>[Ce(NO<sub>3</sub>)<sub>6</sub>] was used, the 15DAAQ complex obtained exhibits much higher nitrogen and oxygen contents than the 14DAAQ complex. Note that the C/N molar ratio in the 15DAAQ complex varies in a very small range from 14/1.8 to 14/2.3 with the eight oxidants except for (NH<sub>4</sub>)<sub>2</sub>[Ce(NO<sub>3</sub>)<sub>6</sub>]. The metal molar content in the complex is almost constant despite the changing oxidant except for CoCl<sub>2</sub>. However, hydrogen and oxygen contents vary significantly with the oxidants.

Elemental analysis indicates that the molecular formulas of TAB polymer protonated by acetic acid and deprotonated polymer are C<sub>6</sub>H<sub>5.1</sub>N<sub>1.7</sub>(CH<sub>3</sub>-COOH)<sub>0.43</sub> and C<sub>6</sub>H<sub>5.1</sub>N<sub>1.7</sub>(CH<sub>3</sub>COO)<sub>0.13</sub>, respectively.<sup>218,219</sup> In addition, the loss of nitrogen and hydrogen corresponding to net elimination of 1.3 NH<sub>3</sub> units per benzene ring occurs during the polymerization. Therefore, the real molecular structure of the TAB polymer should lie between two extreme cases: with extensive internal cross-linking (C<sub>6</sub>H<sub>4.5</sub>N<sub>1.5</sub>) and numerous free amino groups (C<sub>6</sub>H<sub>6</sub>N<sub>2</sub>), azo group (C<sub>6</sub>H<sub>3</sub>N<sub>3</sub>), or hydrazine group (C<sub>6</sub>H<sub>6</sub>N<sub>3</sub>). It can be concluded from a combination of <sup>13</sup>C NMR and

#### Scheme 2



17

26: Poly(*sym*-triaminobenzene)

**Figure 8.** Circular dichroic (CD) spectra (short wavelength) in DMSO at 30 °C of the three copolymers of *o*PD/PHT, *m*PD/PHT, and *p*PD/PHT with the molar ratio of 90/10 synthesized by chemically oxidative polymerization.<sup>229</sup>

elemental analysis results that the TAB polymer is a network polymer having the molecular structure in Scheme 2.

#### 6. Circular Dichroic Spectroscopy

CD spectroscopy has been used to characterize the chiroptical properties of the polymers in the solution. Very few studies have been done on the CD spectroscopy of aromatic diamine polymers. CD spectra of only the copolymer solutions of *o*PD, *m*PD, and *p*PD (90 mol %) with PHT (10 mol %) in DMSO have been compared in Figures 8 and 9 because of the insolubility of *m*PD homopolymer.<sup>223,229</sup> Apparently three copolymers exhibit different big ellipticity in the wavelength range of 185–240 nm, almost the same medium ellipticity in 240–300 nm, and very small ellipticity in 300–500 nm, indicating that three copolymers are chiroptically active and different from each other because of the different macromolecular chain structure suggested above. The chiroptical activity may be attributed to the extended rigid

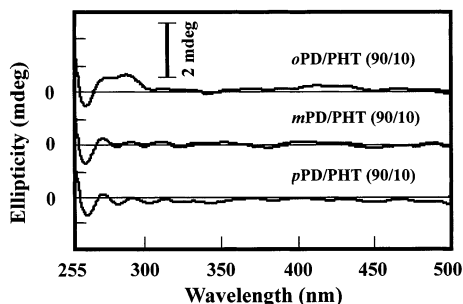


**Figure 9.** Circular dichroic (CD) spectra (long wavelength) in DMSO at 30 °C of the three copolymers of *o*PD/PHT, *m*PD/PHT, and *p*PD/PHT with the molar ratio of 90/10 synthesized by chemically oxidative polymerization.<sup>229</sup>

rodlike chain configuration of the copolymers. One practical problem often encountered in the application of CD spectroscopy is that several good solvents of aromatic diamine polymers exhibit CD interference at relatively long wavelength whereas the almost interference-free solvents such as water and ethanol cannot generally dissolve the polymers. Consequently, CD spectroscopy in DMSO in a short wavelength range such as 185–240 nm might not be absolutely reliable. To eliminate the solvent interference, solid ultrathin film of several nanometers should be the best sample for measurement of CD spectroscopy.

### 7. ESR Spectroscopy

ESR spectroscopy is a useful technique for investigating the electron and radical in the conducting polymers. However, there are only a few reports on the ESR spectroscopy of the aromatic diamine polymers prepared by oxidative polymerization. It is suggested that PD polymers exhibit a single ESR peak with a  $g$  value of 2.004–2.006 and a maximum peak width of 13–36 G.<sup>210</sup> Tsuchida et al. suggested that the ESR spectrum of polyazophenylene from *p*PD has a single absorption with a peak width at the maximum slope between 7 and 12 G.<sup>211</sup> The solid-state *p*PD oligomer by copper oxidant exhibits a sharp ESR signal at 3180 G due to a free radical inside the oligomer and a broad ESR absorption at 3165 G due to  $\text{Cu}^{2+}$  ion in the oligomer.<sup>214</sup> These signals are not affected significantly on heating, but a slight dependence on the position of the signals on changing the central field was observed. The *p*PD oligomer oxidized by cobalt complex exhibits only one signal at 3200 G due to a radical. In addition, the radical in the end group of the oligomer could be stabilized by metal ions. The solid ESR spectra of *p*PD oligomer vary significantly with the oxidants used for the oxidative oligomerization.

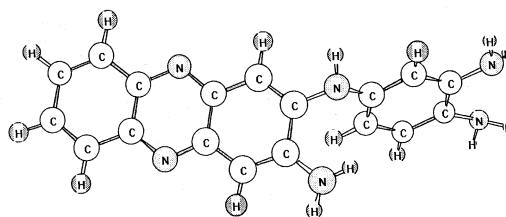
The ESR spectra of  $(\text{NH}_4)_2[\text{Ce}(\text{NO}_3)_6]$ -oxidized 14DAAQ complex and  $\text{Cu}(\text{NO}_3)_2$ -oxidized 15DAAQ complex exhibit a similar dependence on the temperature.<sup>208,209</sup> Relatively sharp strong signals at 3252 and 2926 G for 14DAAQ and 15DAAQ complex, respectively, were observed at 77 K. At 300 K, broad signals at 3253 and 2868 G for 14DAAQ and 15DAAQ complex, respectively, were observed with a weaker intensity probably due to stronger electron exchange and delocalization. The strong signal at 77 K centered

at  $g = 1.982$  was an indication of some hyperfine interaction. A close  $g$  value of 2.079 was found for 15DAAQ complex at 300 K. 15DAAQ complexes, oxidized by other oxidants such as  $\text{CuCl}$ ,  $\text{CuCl}$  with precoordinated oxygen,  $\text{Ni}(\text{NO}_3)_2$ ,  $\text{AgNO}_3$ ,  $\text{CoCl}_2$ ,  $\text{PdCl}_2$ ,  $\text{FeCl}_3$ ,  $(\text{NH}_4)_2[\text{Ce}(\text{NO}_3)_6]$ ,  $\text{KIO}_4$ , and  $\text{K}_2\text{S}_2\text{O}_8$ , all have  $g$  values in a range from 1.993 to 2.086 at 300 K.<sup>209</sup> The small deviation of the  $g$  value from 2.00 indicates that these metals may not be involved in the final materials. In fact, elemental analysis suggests that there is a small amount of Cu, Ni, Ag, and Co in the respective complexes, even though the elemental analysis of the complexes formed by oxidizing 14DAAQ and 15DAAQ with  $(\text{NH}_4)_2[\text{Ce}(\text{NO}_3)_6]$  and  $\text{KIO}_4$  does not indicate the presence of cerium and potassium. Therefore,  $(\text{NH}_4)_2[\text{Ce}(\text{NO}_3)_6]$  and  $\text{KIO}_4$  are unique because they oxidize 14DAAQ and 15DAAQ without coordinating with the respective products. In addition, there is an apparent difference between the ESR spectra of  $\text{Ce}^{4+}$ -oxidized 14DAAQ complex and  $\text{Cu}^{2+}$ -oxidized 15DAAQ complex at both 77 and 300 K. An additional weak signal at ca. 3258 G appeared for 14DAAQ complex. It is seen that the study on the CD and ESR spectroscopies of the oxidative polymers from aromatic diamines is very fragmentary, and more efforts are needed in coming years.

### 8. Effect of Reaction Conditions on the Molecular Structure

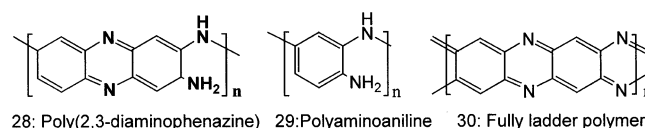
The molecular structure of the polymers from aromatic diamines usually varies significantly with the polymerization conditions. For *P*oPD, the oxidation of *o*PD by  $(\text{NH}_4)_2\text{S}_2\text{O}_8$  is very sensitive to the reaction conditions. When the oxidation reaction proceeds at lower temperature such as room temperature, a dimer, DAPh, is formed and shown in No. 16 of Scheme 1. At higher temperature a crystalline trimer, [3-amino-2-(3,4-diaminophenylamino)]phenazine, is found (Scheme 3). Only reaction temperatures higher than 100 °C give the polymers shown in Scheme 4.<sup>70</sup>

#### Scheme 3



27: [3-Amino-2-(3,4-diaminophenylamino)]phenazine

#### Scheme 4



28: Poly(2,3-diaminophenazine) 29: Polyaminoaniline 30: Fully ladder polymer

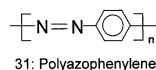
Note that the oxidation of *o*PD with persulfate leads to an intermediate structure between polyaminoaniline and fully ladder polymer. The product with the intermediate structure is a poly(2,3-diaminophenazine) (PDAPh), as shown in Scheme 4.<sup>70</sup> Oxidation

polymerization of *o*PD with  $K_2S_2O_8$  in acidic solutions afforded head-to-tail polymers with trisubstituted benzene nuclei.<sup>155</sup> When *o*PD is subjected to oxidation there exist two limiting cases. If a two-electron oxidation process takes place, an amine-substituted PAN-like structure (polyaminoaniline) could result (No. 29 in Scheme 4).<sup>70</sup> On the other hand, if a six-electron oxidation process takes place, a fully ladder polymer (No. 30 in Scheme 4) should be obtained.<sup>70</sup>

The above analysis is based on the formation of N–C couplings of *o*PD monomers. For comparison, when enzyme-catalyzed polymerized with  $H_2O_2$  as an oxidant and HRP as a catalyst in 1,4-dioxane/phosphate buffer solutions,<sup>72,117</sup> a linear structure was proposed for the polymer by  $^1H$  NMR, IR, and UV–vis spectral data. Yano and co-workers proposed a structure consisting of 1,4-substituted benzenoid and quinoid moieties for P*o*PD obtained electrochemically.<sup>164</sup> A detailed discussion will be given in the following corresponding sections.

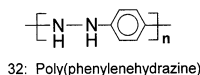
For P*p*PD, linear polymers with azo linkages were obtained by polymerization with oxygen by the catalysis with copper complexes.<sup>114,216</sup> The oxidation polymerization of *p*PD with  $Fe^{3+}$  chelate/oxygen and  $Cu^{2+}$ –pyridine complex as oxidants gives polyazophenylene (Scheme 5).<sup>211,212</sup>

#### Scheme 5



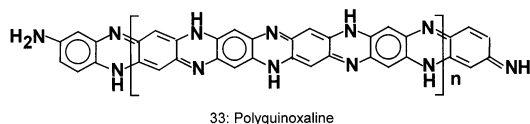
When  $(NH_4)_2S_2O_8$  serves as oxidant in acid-free water, it appears that *p*PD is oxidized into the hydrazine polymer, see Scheme 6.<sup>210</sup>

#### Scheme 6



On the other hand, the oxidative polymerization of *p*PD with  $K_2S_2O_8$  yields a polyquinoxaline, a material having a ladder structure and fully oxidized state (Scheme 7).<sup>62</sup>

#### Scheme 7



Very recently it was reported that the chemically oxidative polymerization of *N*-phenyl-*p*PD gives a linear PAN with a high polymerization yield.<sup>207</sup> Apparently both the oxidant used and the *N*-substituted group will affect the macromolecular structure of *p*PD polymers significantly.

### D. Wide-Angle X-ray Diffractograms

There are not as many investigations of WAXD diffractograms of the oxidative polymers from aromatic diamines. There are three different crystalline characteristics for the polymers. The ammonium persulfate-oxidized benzidine polymers (PBZ),<sup>235</sup> me-

tallic salt-oxidized DAAQ complexes,<sup>208</sup> as well as  $Br_2^-$  and  $NaClO_4^-$ -oxidized *p*PD and its derivative polymers<sup>215</sup> are crystalline, but persulfate-oxidized PD polymers are noncrystalline. In complete contrast, crystalline characteristics should be due to the diversity of the macromolecular chain regularity and sometimes molecular weight when the molecular weight is low enough. PBZ, DAAQ complexes, and bromine-/perchlorate-oxidized *p*PD and its derivative polymers should have regular chain structure, whereas persulfate-oxidized PD polymers might exhibit varying chain structure. This is further verified by an amorphous TAB polymer exhibiting complicated three-dimensional network structure.<sup>218</sup> Unfortunately, no research report on the wide-angle X-ray diffraction of DAN polymers is found.

It is reported that both PBZ and benzidine powders are polycrystalline in nature, but they exhibit different diffraction characteristics.<sup>235</sup> The most intense peaks of the PBZ correspond to *d* spacings of 1.36, 0.46, 0.37, and 0.28 nm, together with several medium peaks at *d* spacings of 2.0, 0.8, 0.48, 0.43, 0.39, 0.35, 0.32, and 0.31 nm, whereas the *d* spacings of the benzidine monomer are 0.44 (the strongest), 0.49, 0.40, 0.35, 0.33, and 0.20 nm. Note that the crystalline feature of as-prepared PBZ is not affected by doping with  $H_2SO_4$  and  $HNO_3$ , though the polymer changes its color from blue to deep brownish-black upon protonation. The powder of  $Ce^{4+}$ -oxidized 14DAAQ complex is crystalline, and the most intense peak corresponds to a *d* spacing of 1.04 nm together with the crystallite size ranging from 20 to 27.5 nm, whereas the *d* spacing of the 14DAAQ monomer is 1.3 nm.<sup>208</sup> There is also a series of small sharp peaks at diffraction angles (*d* spacing) of  $15.5^\circ$  (0.572 nm),  $21.2^\circ$  (0.419 nm),  $23.1^\circ$  (0.385 nm),  $27.1^\circ$  (0.329 nm),  $33.0^\circ$  (0.271 nm), and  $44.4^\circ$  (0.204 nm). Powder wide-angle X-ray diffractograms of a series of 15DAAQ complexes suggest that they are polycrystalline in nature. They have various crystallite sizes and various numbers of repeating units which depend strongly on the oxidants used.<sup>209</sup> The 15DAAQ complex oxidized by  $Ni(NO_3)_2$  exhibits the smallest crystallite of 3.2–4.9 nm and the smallest numbers of repeating units of 3–5. The 15DAAQ complex oxidized by  $K_2S_2O_8$  exhibits the largest crystallite of 29.3–35.1 nm and the largest number of repeating units of 29–25.

Three PD polymers obtained by oxidizing with  $(NH_4)_2S_2O_8$  and  $K_2S_2O_8$  exhibit amorphous structure, as shown in Figure 10. P*m*PD seems to be the most amorphous possibly, due to its complicated three-dimensional network structure,<sup>223</sup> whereas P*p*PD with a relatively ordered ladder structure is the most crystalline, although the absolute crystallinity of P*p*PD is very low.<sup>224</sup> Furthermore, P*p*PD and P*o*PD polymers exhibit a diffraction peak with stronger intensity at ca.  $3^\circ$  than at  $15\text{--}30^\circ$ , indicating the presence of larger crystallite sizes.<sup>220,221,224</sup> On the contrary, the diffraction intensity of P*m*PD at ca.  $3^\circ$  is basically 0. Therefore, it can be concluded that three PD polymers possess different crystalline structures,<sup>223</sup> which result from quite different macromolecular chain structures, as shown in Table 8 and

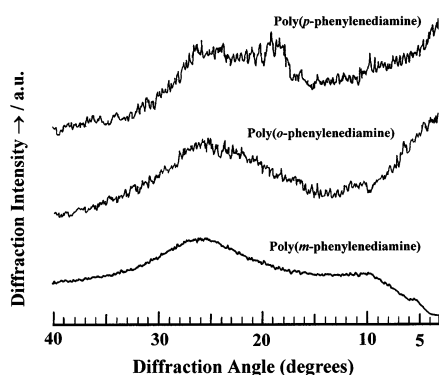


**Figure 10.** WAXD diffractograms of poly(*p*-phenylenediamine) (PpPD),<sup>224</sup> poly(*o*-phenylenediamine) (PoPD),<sup>220,221</sup> and poly(*m*-phenylenediamine) (PmPD)<sup>223</sup> prepared by chemically oxidative polymerization.

Figure 7. Note that the strong diffraction peak at ca. 3° will become significantly weaker upon copolymerization of *o*PD with 10 mol % MA and XY.<sup>220,221</sup> When the content of MA is up to 30 mol %, the *o*PD/MA copolymer obtained exhibits a very weak diffraction peak at 3°.

On the contrary, with incorporating 10 mol % AS or XY unit into *m*PD polymer, the *m*PD/AS and *m*PD/XY copolymers obtained possess almost the same WAXD characteristics as *m*PD homopolymer.<sup>215,223</sup> When 50 mol % AS or XY unit is introduced, a weak diffraction peak at ca. 10° for *m*PD homopolymer will become more intense. Two terpolymers with *m*PD/AS/XY ratios of 70/25/5 and 53/39/8 also exhibit enhanced peak intensity at ca. 10° as compared with *m*PD homopolymer.<sup>223</sup> This indicates that the crystalline structure of *m*PD polymer is influenced strongly by copolymerization, because the copolymerization of *m*PD with AS and XY obviously interrupts the cross-linking structure of *m*PD polymer, increasing the spacing and randomness of intermolecular and intramolecular chains as well as amorphism.

## E. Solubility and Molecular Weight

The solubility of aromatic diamine polymers exhibits a significant dependence on their macromo-

lecular structures. The P*o*PD and P*p*PD polymers basically with linear and/or ladder structures were soluble in DMSO, DMF, and NMP and partly soluble in THF and acetone; P*m*PD obtained by chemical oxidative polymerization with (NH<sub>4</sub>)<sub>2</sub>S<sub>2</sub>O<sub>8</sub> as oxidant in HCl solution is insoluble in most solvents, as summarized in Tables 14 and 15. TAB polymer is also completely insoluble in common solvents including concentrated H<sub>2</sub>SO<sub>4</sub>.<sup>218</sup> The insolubility of P*m*PD and TAB polymer should be due to their three-dimensional network structures shown in Figure 7<sup>69</sup> and Scheme 2.<sup>218</sup> The solubility and molecular weight of polymers depended on the monomer and solution composition that was used for the polymerization. From Table 14 it can be seen that in different polymerization conditions the molecular weight is different without any regularity, since the chain structures of PPDs are changed with the polymerization conditions as mentioned earlier. However, the solubility of polymers was nearly independent of the reaction time of polymer synthesis.<sup>72</sup>

For the partly soluble polymers, it is interesting to find differences between the soluble and insoluble parts. Tsuchida et al. found that the soluble and insoluble part of the P*p*PD oxidized by Fe<sup>3+</sup> chelate/oxygen is 20.6 and 79.4 wt %, respectively.<sup>211</sup> The soluble part has a melting temperature of 180–200 °C and a molecular weight of 439, corresponding to a degree of polymerization of 4. These values imply that the soluble part is an oligomer whereas the insoluble part should have a relatively high molecular weight since it does not melt even at 300 °C. All the results listed in Table 14 suggest that the solubility is primarily determined by molecular structure rather than molecular weight of the polymers as long as the molecular weight is not low enough. Note that the semiconducting polymer complexes from 14DAAQ and 15DAAQ are highly insoluble in common solvents except in DMSO,<sup>208,209</sup> maybe due to their reaction with DMSO to regenerate the starting 14DAAQ and 15DAAQ. Therefore, this dissolution accompanies degradation.

It is reported that a high molecular weight, conjugated main chain azopolymer prepared from *p*PD

**Table 14. Solubility in Organic Solvents and Molecular Weight of the Polymers Prepared from Aromatic Diamines by Oxidative Polymerizations**

polymers	NMP <sup>a</sup> wt %	DMF <sup>a</sup> wt %	THF <sup>a</sup> wt %	$\bar{M}_n$	oxidative polymerization conditions	refs
P <i>o</i> PD	100		SS <sup>b</sup>	( $\bar{M}_w = 2000$ ) <sup>c</sup>	PD·2HCl/1 M HCl/H <sub>2</sub> O, (NH <sub>4</sub> ) <sub>2</sub> S <sub>2</sub> O <sub>8</sub> at 0–2 °C for several days	194
P <i>m</i> PD	0	0	0			
P <i>p</i> PD	100		SS <sup>b</sup>	( $\bar{M}_w = 10\,000$ ) <sup>c</sup>		
P <i>o</i> PD	100		MS <sup>b</sup>	4000 <sup>d</sup>	acetic acid/(NH <sub>4</sub> ) <sub>2</sub> S <sub>2</sub> O <sub>8</sub> at 118 °C for 72 h	70
P <i>o</i> PD	100	100	PS <sup>b</sup>	3500 <sup>e</sup>	HRP and H <sub>2</sub> O <sub>2</sub> in SESS/isooctane/HEPES at 30 °C for 12 h	73
P <i>m</i> PD		MS <sup>b</sup>	PS <sup>b</sup>	4100 <sup>e</sup>		
P <i>p</i> PD		MS <sup>b</sup>	PS <sup>b</sup>	3900 <sup>e</sup>		
P <i>o</i> PD	100	100	15	3700 <sup>e</sup> (1.9) <sup>f</sup>	HRP and H <sub>2</sub> O <sub>2</sub> in 1,4-dioxane/water(15/85 v/v) at 30 °C for 6 h	72
P <i>m</i> PD	100	90	2	4200 <sup>e</sup> (1.7) <sup>f</sup>		
P <i>p</i> PD	34	12	15	4900 <sup>e</sup> (1.7) <sup>f</sup>		
P <i>o</i> PD	100	100	PS <sup>b</sup>	20 000 (800) <sup>g</sup>	HRP and H <sub>2</sub> O <sub>2</sub> in 1,4-dioxane/phosphate buffer, pH = 7 at room temperature for 24 h, polymerization yield = 33% electropolymerization in 0.1 M LiClO <sub>4</sub> in CH <sub>3</sub> CN	117
P15DAN	100	100	100	844		173

<sup>a</sup> Weight percent of soluble parts of polymers. <sup>b</sup> MS, mainly soluble; PS, partially soluble; SS, slightly soluble. <sup>c</sup> The examining solvent is DMSO. <sup>d</sup> The molecular weight of the soluble part of P*o*PD in DMSO. <sup>e</sup> Molecular weight of THF-soluble part of polymers determined by GPC. <sup>f</sup> The molecular weight distribution index  $\bar{M}_w/\bar{M}_n$  of the polymers. <sup>g</sup> The molecular weight of the P*o*PD obtained in the absence of HRP at the same other conditions.



**Table 15. Solubility and Intrinsic Viscosity of the Copolymers from Phenylenediamines (PDs) and Aromatic Amines in Organic Solvents<sup>a</sup>**

copolymer	feed monomer molar ratio	intrinsic viscosity in DMSO dL/g	NMP wt %	DMSO wt %	TFA	acetic acid	benzene	THF	CHCl <sub>3</sub>	ethylene chloride	refs
<i>o</i> PD/XY	100/0	0.12	100	100	MS	PS	PS	SS	SS	IS	220
	90/10	0.13	100	100	S	MS	PS	SS	PS	PS	
	70/30	0.12	100	100	S	MS	MS	MS	PS	MS	
<i>o</i> PD/MA	90/10	0.26	100	100	S	PS	PS	MS	PS	SS	221
	70/30	0.22	100	100	S	SS	MS	SS	PS	SS	
<i>m</i> PD/XY	100/0		0	0		IS	IS	IS	IS	IS	215,223
	90/10		10	33		IS	IS	IS	IS	IS	
	70/30		41	36		IS	IS	IS	IS	IS	
	50/50		41	38		SS	SS	SS	SS	SS	
<i>m</i> PD/MT	90/10		35	13		IS	IS	IS	IS	IS	215
	70/30	0.1	71	33		IS	IS	IS	IS	IS	
<i>m</i> PD/AS	50/50	0.13	86	100		IS	IS	IS	IS	IS	215,223
	90/10		12	3		IS	IS	IS	IS	IS	
	70/30		29	51		IS	IS	IS	IS	IS	
<i>p</i> PD/XY	50/50	0.03	61	64		SS	SS	SS	SS	SS	224
	100/0	0.45	100	MS	PS	SS	SS	SS	SS	IS	
	90/10	0.16	100	100	MS	SS	SS	SS	SS	IS	
	70/30	0.13	100	100	S	PS	IS	MS	IS	IS	
	60/40	0.11	100	100	S	PS	SS	S	PS	PS	

<sup>a</sup> IS, insoluble; MS, mainly soluble; PS, partially soluble; S, soluble; SS, slightly soluble.

sulfonic acid is highly soluble in water over a wide pH range and also soluble in common polar organic solvents such as DMF, DMSO, and NMP completely because of the presence of sulfonic acid groups.<sup>236</sup>

The molecular weights of three PD polymers prepared with the same conditions increase in the order of *Po*PD < *Pm*PD < *Pp*PD. Therefore, on the basis of the order of polymerization yield (Tables 6 and 7) and molecular weight (Table 14), it appears that the activity of chemical oxidative polymerization of three PD isomers in HCl solution increases in the order



The very significant influence of the molar ratio of oxidant over aromatic diamines on the molecular weight of the polymers is not investigated systematically. Generally, a small amount of oxidant could be preferable for obtaining polymers with relatively high molecular weight. However, too little oxidant might lead to too low a polymerization yield. If more oxidant is added, a higher polymerization yield should be obtained but compromised with a lower molecular weight, because too many active cation radicals formed will terminate each other at a very early stage. Thus, detailed studies with a series of oxidant/aromatic diamine ratios are needed to optimize the relationship between the oxidant/monomer ratio and molecular weight.

To increase the solubility of the PPDs, some copolymers have been developed. Abe et al. produced a conducting copolymer film containing a quinone-diimine structural unit and PD structural unit in the repeating unit by doping with a protonic acid<sup>237</sup> and found that the copolymer is soluble in an organic solvent in the undoped state and has an intrinsic viscosity of higher than 0.4 dL/g measured in NMP at 30 °C. The copolymers of PDs with AN derivatives by introducing alkyl and alkoxy side groups in the rigid PPD main chain<sup>168,169,220,221,223,224</sup> show better solubility than three pure PPDs in Table 15. Li and Huang and colleagues prepared a series of copoly-

mers of *o*PD/XY, *o*PD/MA, *m*PD/XY, *m*PD/MT, *m*PD/AS, and *p*PD/XY and found that the solubility and intrinsic viscosity of the copolymers exhibited an apparent composition dependency.<sup>220,221,223,224</sup> In particular, the solubility of *m*PD copolymers in DMSO and NMP is much better than that of pure *Pm*PD homopolymer, but their solubility in THF, chloroform, benzene, ethylene chloride, and acetic acid is still poor. The improvement of solubility should be attributed to the breakage of the regular semi-ladder chain structure containing the DAPh repeat units or cross-linking network with the introduction of comonomer units XY, MA, MT, and AS. Thus, it can be concluded that the solubility is primarily determined by molecular structure. In addition, the intrinsic viscosity of the soluble part of the bipolymers in DMSO is low and their highest intrinsic viscosity (0.26 dL/g) is still lower than that (0.38–1.1 dL/g) of *m*PD/AS/XY terpolymers measured in NMP.<sup>223</sup> Low molecular weight is one of the fateful disadvantages of the aromatic diamine polymers. Apparently both the low solubility and low molecular weight of the aromatic diamine polymers could be an enduring problem, and their enhancement should be our cardinal focus in order for the polymers to go into a practical application field.

## F. Electrical Conductivity

From Tables 6 and 7 it can be seen that the conductivity of three PPDs is much lower than that of PAN (0.01–13 S/cm). Further, the conductivity varies greatly with various polymerization and film-forming conditions. This can also be attributed to the complicated and variable molecular and supramolecular structure of PPDs. The PPD film formed with DMSO as solvent exhibits the highest electrical conductivity and the highest thermostability versus that with *m*-cresol and NMP. Therefore, the technique of modifying the structure to improve conductivity may be a key for practical application of PPDs.

*Po*PD synthesized by oxidative polymerization without catalyst is not a good conductor because its

conductivity is lower than  $10^{-6}$  S/cm at room temperature. The poor conductivity could be due to lack of charge carriers (i.e., protonation at amine sites) on its main structures such as Nos. 28 and 29 in Scheme 4 or due to low mobility of carriers.<sup>70</sup>

*PpPD* is also a semiconductor with high resistivity, because the electronic structure for *PpPD* is similar to pernigraniline.<sup>62</sup> Its specific conductivity is  $6.3 \times 10^{-6}$  S/cm, and its band gap calculated from its electronic spectrum is 2.37 eV. The conductivity of the *PpPD* will decrease from  $6.86 \times 10^{-6}$  to  $1.51 \times 10^{-8}$  S/cm after heating at 150 °C for 2 h and then cooling to room temperature, due to the exclusion of water and dopant.<sup>116</sup> The activation energy of conductance of *PpPD* in the semiconducting region is 0.016 eV.<sup>116</sup>

The electroconductivity of three PD polymers has been easily compared with the HCl concentration in polymerization medium in Table 7. No regular variation of the conductivity of three polymers is found with changing the doping level of HCl. Similarly, no significant variation of the conductivity of the *PpPD* with the dopant is found.<sup>210</sup> It is suggested that *PpPD* prepared with  $(\text{NH}_4)_2\text{S}_2\text{O}_8$  as oxidant at elevated temperature has an electroconductivity of  $8.3 \times 10^{-9}$  (undoped),  $1.3 \times 10^{-8}$  (doped by  $\text{LiClO}_4$ ),  $1.6 \times 10^{-8}$  (doped by  $\text{ICl}_3$ ), and  $2.8 \times 10^{-8}$  (doped by  $\text{Ce}(\text{NO}_3)_3$ ) S/cm.

The electrical conductivity of *PmPD* is 0.064 S/cm, which is 2 orders of magnitude lower than that obtained for PAN but is higher than that of *PoPD* and *PpPD*. This may be caused by the lower amount of dopant incorporated between the proposed more sterically hindered cross-linking structures compared to PAN.<sup>69</sup> The more complicated three-dimensional structure of *PmPD* would also lead to greater structural defects which may interfere with the formation of polarons and bipolarons, which are believed to be responsible for the conduction in organic polymer. As compared with PAN and PPY, the aromatic diamine polymers have the better mechanical property but the conductivity is not as good as that of PAN and PPY, possibly due to more complicated structure and relatively low-level conjugation resulting from the low molecular weight of the polymers.

Prasad et al. revealed a significant influence of acidic aqueous solution on the conductivity and magnetic susceptibility of *PoPD*.<sup>155</sup> It is found that the conductivity increases from  $2.5 \times 10^{-10}$ ,  $3.6 \times 10^{-9}$ ,  $8.9 \times 10^{-8}$ , to  $5.7 \times 10^{-7}$  S/cm with changing acid from  $\text{CH}_3\text{COOH}$ ,  $\text{H}_2\text{C}_2\text{O}_4$ ,  $\text{H}_2\text{SO}_4$ , to  $\text{HClO}_4$ . The magnetic susceptibility increases from  $3 \times 10^{-4}$ ,  $5.4 \times 10^{-4}$ , to  $2.9 \times 10^{-3}$  emu/two-ring unit with changing acid from  $\text{H}_2\text{SO}_4$ ,  $\text{H}_2\text{C}_2\text{O}_4$ , to  $\text{HClO}_4$ . However, the *PoPD* obtained in  $\text{CH}_3\text{COOH}$  does not exhibit magnetic susceptibility.

PBZ and poly(4,4'-diaminodiphenyl ether) are less conducting than *PpPD*. Their conductivity is  $1.71 \times 10^{-7}$  and  $1.38 \times 10^{-9}$  S/cm, respectively.<sup>116</sup> Apparently, an additional phenyl ring and ether linkages cause a decrease in the conductivity. The  $\text{NH}_4\text{OH}$  and thermal treatment at 150 °C for 2 h of the PBZ will significantly decrease conductivity to  $1.4 \times 10^{-10}$  or  $2.95 \times 10^{-9}$  S/cm, respectively, owing to the exclusion

of dopant. However, the conductivity in the PBZ rises by about 2000 and 1000 times upon doping with  $\text{H}_2\text{SO}_4$  and  $\text{HNO}_3$ , respectively.<sup>235</sup>

The electrical conductivity behavior of doped and undoped PBZs has been studied for various concentrations of dopants including nitrate, sulfate, chloride, and acetate ions between room temperature and 200 °C.<sup>116,235</sup> The conductivity of undoped and nitrate- and sulfate-doped PBZs increased slightly with temperature from 31 to ca. 55 °C (a semiconducting behavior), then decreased significantly with a further increase in temperature (a metallic behavior), and later increased dramatically (switching to semiconducting behavior).<sup>235</sup> Different behaviors were found for acetic acid- and HCl-doped and basic PBZs. Acetic acid-doped and basic PBZs exhibit a significantly enhanced conductivity with increasing temperature from 42 to 200 °C except for a narrow temperature range of 125–154 °C.<sup>235</sup> The conductivity of HCl-doped PBZ increases initially from  $1.71 \times 10^{-7}$  to  $1 \times 10^{-6}$  S/cm with elevating temperature from 26 to 41 °C, then decreases until 100 °C, and finally increases again up to 195 °C.<sup>116</sup> Basic PBZ exhibits only one increase stage of conductivity from  $1.4 \times 10^{-10}$  to  $2.8 \times 10^{-6}$  S/cm with a temperature increase from 100 to 290 °C. Moreover, the variation of the conductivity with temperature in a higher temperature range seems somewhat reversible. The metallic behavior in the intermediate range of temperature might be due to elimination of moisture content. Therefore, the water-free doped PBZ prepared by annealing exhibits a steady increase in the conductivity with increasing temperature from 42 to 200 °C. The activation energies of the charge carriers for all the samples in the semiconducting region show dependence on the treatment, dopant, and dopant concentration. Treatment-free PBZ exhibits lower activation energy (0.02–0.13 eV) than heat- and  $\text{NH}_4\text{-OH}$ -treated PBZ (0.08–0.2 eV).<sup>116,235</sup> The PBZs doped by  $\text{H}_2\text{SO}_4$ ,  $\text{HNO}_3$ , and HCl also exhibit lower activation energy (0.02–0.13 eV) than that by acetic acid (0.08–0.2 eV).<sup>116,235</sup> With changing dopant concentration from 0.1 to 1.0 M, all PBZs exhibit the highest activation energy of 0.12 eV ( $\text{H}_2\text{SO}_4$ ), 0.10 ( $\text{HNO}_3$ ), 0.20 (acetic acid) eV at the same dopant concentration of 0.5 due to the effective charge formation from ion pair association.

The binary and ternary copolymers of three PD isomers are also semiconductors. It is found that as-prepared oxidative copolymers from *oPD/mPD*, *oPD/pPD*, *mPD/pPD*, and *oPD/mPD/pPD* with iodine as oxidant at elevated temperature exhibit electroconductivity of  $1.7 \times 10^{-8}$ ,  $1.9 \times 10^{-8}$ ,  $3.4 \times 10^{-8}$ , and  $5.3 \times 10^{-8}$  S/cm, respectively.<sup>210</sup> In conclusion, the electroconductivity of three PPDs obtained by chemically oxidative polymerization is low. Additionally, the electroconductivity of PDANs, P14DAAQ, and P15DAAQ prepared by the chemically oxidative polymerization is unknown because of almost no report on the chemically oxidative polymerization of PDANs, P14DAAQ, and P15DAAQ.

To enhance the conductivity of the PPD polymers, the copolymers of PDs with AN have been synthesized,<sup>194,195</sup> as shown in Table 6. The copolymers of

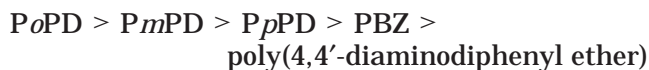
PDs and AN can tune the electrical conductivity of the products by changing the composition of the reaction mixture.<sup>194</sup> The conductivity of the copolymers increases with the increase of AN component in different ways for three copolymers. About 30 mol % of AN can increase the conductivity of *o*PD/AN copolymer by several orders of magnitude. For example, *o*PD/AN copolymer exhibits an abrupt increase in conductivity from  $10^{-11}$  to 1 S/cm with adding AN content from 30 to 50 mol %. At AN content of higher than 50 mol %, the conductivity of *o*PD/AN copolymer is nearly the same as the PAN. However, even 60 mol % of AN does not substantially increase the conductivity of *m*PD/AN copolymer. Only more than 60 mol % AN can dramatically enhance the electrical conductivity of the *m*PD/AN copolymer. With incorporating AN content from 60 to 100 mol %, the conductivity of *m*PD/AN copolymer increases steadily from  $10^{-10}$  to 1 S/cm. For the copolymer of *p*PD and AN, the conductivity changes in the semi-logarithmic scale steadily from  $10^{-9}$  to 14 S/cm over a whole range of composition from 0 to 94 mol %.<sup>194,195,201</sup> In addition, their conductivity changes in a wide interval of reaction mixture composition, which makes poly(*p*PD/AN) more suitable for the control of electrical properties than poly(*m*PD/AN) and poly(*o*PD/AN). In contrast to copolymers, the blends of PPDs and PAN show nearly the same trend in all three blends. There is an abrupt conductivity change from  $10^{-11}$  to 0.1 S/cm in a narrow AN range from 0 to 15 vol %. Therefore, it was induced that the conductivity is not primarily connected with the macroscopic size and structure of a conduction subsystem but rather with the changes in its submicroscopic structure, which is related to a spatial distribution of PD and AN constitutional units. In summary, the conductivity of three PD/AN copolymers depends strongly on the PD structure.

### G. Miscellaneous Properties

Besides electrical conductivity, aromatic diamine polymers also exhibit other interesting properties. Tsuchida et al. suggested that the polymer of *p*PD oxidized by  $\text{Fe}^{3+}$  chelate/oxygen shows reversible redox properties.<sup>211</sup> The polymer in methanol solution can be reduced by an aqueous sodium hydrosulfite ( $\text{Na}_2\text{S}_2\text{O}_4$ ) solution, resulting a light yellow solution, which is reoxidized by air to the original black polymer.

Krivka et al. studied the alternating current properties including complex permittivity and dielectric modulus of *p*PD/AN copolymers.<sup>238</sup> It is found that the real part of the permittivity has a plateau in the low-frequency region, while the peak in the imaginary part is masked by the direct current conductivity. A temperature dependence of loss peak frequency has been found based on the dielectric modulus–frequency curves at 110–190 K. The real part of the alternating current conductivity is almost constant and equal to the direct current conductivity up to the loss peak frequency. With increasing *p*PD content at a constant temperature, the copolymer conductivity seems more dependent on frequency, i.e., the copolymer becomes less metallic.

On the other hand, the complicated structure of cross-linking (or double-stranded ladder) *Pm*PD results in higher thermal stability than that of the normal linear polymer such as PAN,<sup>239–241</sup> as listed in Table 16. Among the five aromatic diamine homopolymers prepared with persulfate as oxidant in acidic aqueous solution, *Po*PD exhibits the highest degradation temperature  $T_d$  and the highest temperature  $T_{dm}$  at the maximum weight-loss rate in nitrogen and air atmospheres while poly(4,4'-diaminodiphenyl ether) exhibits the lowest  $T_d$  and  $T_{dm}$  owing to the presence of ether linkages. The thermal decomposition temperature of the homopolymers decreases in the following order



The *Po*PD also exhibits the highest char yield at 600 °C, but the PBZ exhibits the lowest char yield at 600 °C, although the PBZ prepared by electropolymerization exhibits a higher char yield of 37–50 wt % at 573 °C.<sup>116</sup> Noteworthy is that the PBZ has the highest weight-loss rate  $(da/dt)_m$  and the largest activation energy for decomposition in nitrogen. These results indicate that the *Po*PD has the highest thermostability, possibly due to its higher molecular weight than the other homopolymers. Upon copolymerization, their  $T_d$  value usually decreases. Furthermore, the higher the comonomer content, the more apparent the decrease in the  $T_d$  value is. The thermal decomposition temperature of the PBZ also decreases upon treatment with  $\text{NH}_4\text{OH}$ . It should be noted that *m*PD homopolymer and copolymers, PBZ, and poly(4,4'-diaminodiphenyl ether) exhibit two maximum weight-loss rates, suggesting that they decompose in two steps. In addition, it is seen from Table 16 both *o*PD and *m*PD homopolymers exhibit a higher degradation temperature in nitrogen and air than the PAN emeraldine base synthesized by chemically oxidative polymerization,<sup>220,221,223,224</sup> because the *o*PD and *m*PD homopolymers are highly aromatic ladder and cross-linking polymers, respectively, whereas PAN is linear. Furthermore, the strong interchain van der Waals forces existing between the layers of *o*PD and *m*PD homopolymers would contribute to the overall stability, which is analogous to that found in graphite. Note that the *Pp*PDs prepared with  $\text{Cu}^{2+}$ ,  $(\text{NH}_4)_2\text{S}_2\text{O}_8$ , iodine, and acetic acid as oxidant in aqueous solution showed much lower thermal stability because of so many  $-\text{N}=\text{N}-$  and  $-\text{NH}-\text{NH}-$  bonds plus low molecular weight.<sup>210,214</sup> Similarly, the homopolymers from *o*PD and *m*PD with  $(\text{NH}_4)_2\text{S}_2\text{O}_8$  as oxidant in acid-free solution are also not very thermostable. These polymers showed a weight loss of 2–10% in 150–200 °C and are thermally unstable above 200–300 °C. However, three homopolymers obtained with  $(\text{NH}_4)_2\text{S}_2\text{O}_8$  as oxidant in acid-free solution as well as the *p*PD homopolymers doped by  $\text{LiClO}_4$  and  $\text{Ce}(\text{NO}_3)_3$  exhibit a high char yield of 60–75 wt % at 600 °C.

Le et al. suggested that longitudinal-field spectra of the  $\text{I}_2$ -doped PPD exhibit the typical behavior of a spin-glass with a freezing temperature (100 K) and a spontaneous static local field (500 G) at low tem-

**Table 16. Thermostability of the Homopolymers and Copolymers of Phenylenediamines (PDs) with Aromatic Amines by Chemically Oxidative Polymerization Measured at 10 °C/min**

polymers	$T_d/T_{dm}$ (°C)	$(d\alpha/dt)_m$ (%/min)	char yield at 600 °C wt %	$E$ (kJ/mol)	$n$	$\ln Z$ (min <sup>-1</sup> )	refs
in nitrogen							
PoPD	562/677	2.7	63	43	1.0	2.6	220
<i>o</i> PD/XY (70/30)	499/598	4.9	27	50	0.4	4.5	220
<i>Pm</i> PD	472/384,722	0.9, 1.9	54	11, 18			223
<i>m</i> PD/MT (90/10)	447/377, 697	1.1, 2.1	45	11, 17			215
<i>m</i> PD/MT (70/30)	431/385, 691	1.1, 2.1	48	11, 17			215
<i>m</i> PD/MT (50/50)	419/359, 693	1.0, 2.0	49	13, 16			215
<i>m</i> PD/MA (90/10)	250/377	0.9	56				215
<i>m</i> PD/MA (70/30)	224/308	1.0	63				215
<i>m</i> PD/MA (50/50)	202/294	1.1	59				215
<i>Pp</i> PD	436/603	2.1	47	19	0.7	-0.7	224
<i>p</i> PD/XY (90/10)	452/614	4.0	24	25	0.1	0.4	224
PBZ	347/370,545	16, 4.3	19	136, 82	1.5, 0.8		116
PBZ base	320/344, 560	4.2, 2.9	28	98, 71	1.0, 1.0		116
poly(4,4'-diaminodiphenyl ether)	240/280, 590	1.9, 1.9	55	85, 63	1.0, 1.1		116
PAN	430-500/520-545		57-60				239
in air							
PoPD	554/670	2.8	57	53	1.3	4.3	220
<i>o</i> PD/XY (70/30)	485/575	5.0	15	53	0.6	5.2	220
<i>Pm</i> PD	520/540	6.3	20				69
<i>Pm</i> PD	375/373, 554	2.1, 2.6	14	17			223
<i>m</i> PD/MT (90/10)	353/383, 504	2.0, 2.8	5.1	18			215
<i>m</i> PD/MT (70/30)	338/374, 499	2.2, 2.9	4.4	17			215
<i>m</i> PD/MT (50/50)	364/390, 525	2.0, 2.9	11	19			215
<i>m</i> PD/MA (90/10)	378/529	3.4	13				215
<i>m</i> PD/MA (70/30)	361/533	3.6	12				215
<i>m</i> PD/MA (50/50)	354/529	3.3	11				215
<i>Pp</i> PD	429/601	3.3	27	25	0.4	0.5	224
<i>p</i> PD/XY (90/10)	418/540	4.2	2	29	0.3	1.5	224
PAN	450/473	7.3	0	38	0.5	3.8	240

peratures.<sup>242</sup> Their magnetization measurements hint of antiferromagnetic spin coupling and hysteretic behavior. These features indicate possible spin-glass and/or antiferromagnetic spin freezing with a high transition temperature due to the doped radical spins in PPD.

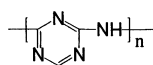
TAB polymer could be the first organic ferromagnet; however, its ferromagnetic behavior is thermally unstable.<sup>219</sup> With increasing temperature, the magnet moment decreases continuously and irreversibly and finally disappears at 420 °C due to thermal degradation in a range of 300–420 °C. Other problems concerning ferromagnetic TAB polymer are very low yield with a maximum of 2% and extreme lack of reproducibility. From the viewpoint of inducing the stronger ferromagnetic interaction by heteroatom substitution, the electronic structures of the dication diradicals of *m*PD and 2,4-diamino-1,3,5-triazine have been calculated for the two possible high-spin polymers, *Pm*PD and poly(imino-1,3,5-triazinediyl) (Scheme 8).<sup>243</sup> It is speculated that *m*-1,3,5-triazinediyl coupler effectively enhances the ferromagnetic interaction between aminium radical centers.

In addition, Trlica et al.<sup>244,245</sup> investigated suspensions of protonated *Pp*PD and poly(*p*PD/AN) and corresponding bases in silicone oil in a DC electric field and found that *Pp*PD displays a fair elec-

trorheological effect, and both the electrorheological efficiency and particle dipole coefficient characterizing particle polarizability decreased with the increase of the *p*PD unit content in the copolymer. Poly(*p*PD/AN) may be an excellent model material both for a study of the relations between the electrorheological properties of suspensions and particle polarizability as well as for the elucidation of particle-chain formation in an electric field. It is seen that the report on these properties is very exiguous, though the properties could be useful for the development of new applications of aromatic diamine polymers.

Chemically oxidative polymerization has been basically successful in preparing oxidative polymers and copolymers from *o*PD, *m*PD, and *p*PD and their derivatives with NH<sub>4</sub><sup>+</sup>, Na<sup>+</sup>, and K<sup>+</sup> persulfates as well as Fe<sup>3+</sup> chelate/EDTA/oxygen as oxidants. However, there are several major classes of aromatic diamine and multiamine monomers, i.e., diaminonaphthalenes, diaminoanthraquinones, diaminopyridines, triaminobenzene, melamine, and tetraaminobenzene, which have not yet been triumphantly polymerized by chemically oxidative polymerization, regardless of two investigations on the polymerization of TAB.<sup>218,219</sup> It could be predicted that TAB, melamine, and *sym*-tetraaminobenzene might be oxidatively polymerized into network polymers. Dendritic polymers could be obtained on the basis of oxidative polymerization of a very small amount of TAB, melamine, or *sym*-tetraaminobenzene with a large amount of aromatic diamines or monoamines.

#### Scheme 8



34: Poly(imino-1,3,5-triazinediyl)

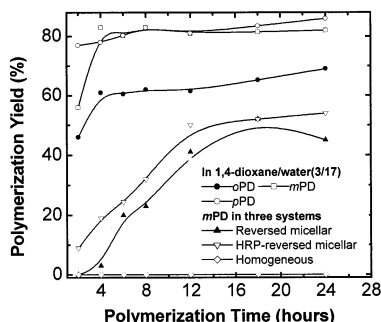


**Figure 11.** Enzyme-catalyzed oxidative polymerization yield of three PPDs as a function of reaction time<sup>72,73</sup>

## V. Enzyme-Catalyzed Oxidative Polymerization and Polymers of Aromatic Diamines

### A. Enzyme-Catalyzed Oxidative Polymerization

Recently the application of enzyme catalysis for oxidative polymerization has attracted some interests. The enzyme-catalyzed oxidative polymerization is chemically mild and environmentally safe.<sup>186</sup> The method is expected to have great potential for providing polymers with new structure and properties of PPD. The enzyme that was often used as a catalyst for oxidative polymerization of aromatic diamines was redox enzyme horseradish peroxidase (HRP). It is reported that HRP can catalyze the oxidative polymerization of aromatic amines, phenol, and their derivatives.<sup>71</sup> Reversed micellar systems were also applicable to HRP-catalyzed polymerization of PD.<sup>73</sup> A typical polymerization procedure in a homogeneous system is as follows: A solution of PD and HRP in a mixture of 1,4-dioxane, phosphate, and 4-(2-hydroxyethyl)-1-piperazineethanesulfonic acid (HEPES) buffer solution was first prepared. The reaction was initiated by adding the same volume of oxidant ( $\text{H}_2\text{O}_2$ ) solution three times at an interval of 30 min. The mixture was magnetically stirred at 30 °C for 24 h. The oxidative polymerization reaction is also carried out in reversed micelles using sodium di(2-ethylhexyl) sulfosuccinate (SESS) as a surfactant and isooctane as solvent; a reversed micellar solution was prepared by dissolving SESS and pure water in isooctane, then PD and HRP in a HEPES buffer solution were added to the micellar solution, and finally the mixture was magnetically stirred at 30 °C overnight. Enzymatic oxidation copolymerization of *o*PD with phenol was performed by using HRP as the catalyst in a mixture of 1,4-dioxane and phosphate buffer to produce polymeric materials.<sup>246</sup>

It is reported that the enzyme-catalyzed oxidative polymerization of aromatic diamines exhibits a significant dependence of reaction time, solvent composition, monomer and its concentration, and oxidant amount. Figure 11 shows the variation of polymerization yields of PPDs with reaction time.<sup>72,73</sup> It can be seen that three isomers appear to exhibit different yield–time relations. The time at which the yield reaches the maximum value and the final yield is different with isomer. *p*mPD has the highest value, while *o*PD has the lowest. This may be due to a difference of the polymerization reactivity caused by the different structure of isomer monomers. The

polymerization yield of three isomeric PDs in a reversed micellar system has been compared.<sup>73</sup> Among them, *m*PD was the most reactive, followed by *p*PD and *o*PD. Apparently the enzyme-catalyzed polymerizing reactivity is different from the activity of chemical oxidative polymerization. However, the increased extent of polymer yield by addition of HRP was larger for *o*PD and *p*PD than for *m*PD. The observed difference of the catalytic activity of HRP for these monomers may be ascribed to the substrate specificity of the enzyme.<sup>73</sup> The reaction of PDs with  $\text{H}_2\text{O}_2$  using HRP as a catalyst in water/1,4-dioxane afforded precipitates as products. No precipitates were obtained without HRP.<sup>71–73</sup> However, for the reaction in reversed micelles without HRP, the yield of the product increased with reaction time and reached 50% in 12 h, as shown in Figure 11.<sup>72,73</sup> Furthermore, only small amounts of precipitates were obtained by a direct reaction of PD with aqueous  $\text{H}_2\text{O}_2$  (30 wt %).<sup>73</sup> These results indicate that HRP and reversed micelles played a catalytic role in the polymerization.

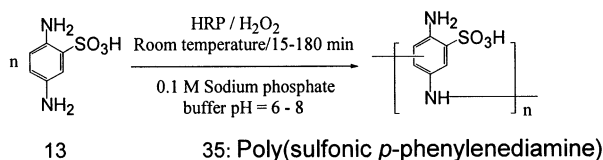
Solvent composition is the most important factor for the yield of enzyme-catalyzed oxidative polymerization of PPD. In mixtures of 1,4-dioxane and phosphate, HEPES, or tris[tris(hydroxymethyl)aminomethane] buffer solutions (0.1 M, pH = 7.1), products were obtained in 80% or higher yields at 15/85 (v/v) 1,4-dioxane/buffer solution. Application of solvents with higher contents of 1,4-dioxane resulted in a sharp decrease in polymerization yield, probably because the buffer components contaminate the products, which was proved by IR,<sup>72</sup> or because the catalytic activity of HRP is decreased due to denaturation by 1,4-dioxane.<sup>71</sup> To avoid contamination, the reactions were carried out in pure water instead of buffer solutions. It is found that the polymerization yield is strongly dependent on the solvent (1,4-dioxane/water) composition.<sup>72</sup> The maximum yield was obtained at 15–30% 1,4-dioxane, and the product yield decreased sharply at higher contents of 1,4-dioxane, which is similar to the reaction in 1,4-dioxane/buffer solutions. Moreover, the initial reaction rate of HRP was the highest at 20% 1,4-dioxane, and it decreased sharply at higher 1,4-dioxane solutions. By means of CD spectra,<sup>72</sup> it was found that the structure of the prosthetic groups of HRP was not significantly altered by a change of solvent composite. HRP retained its natively structure at 20% 1,4-dioxane. However, at higher contents of 1,4-dioxane, HRP structure probably changed because partial unfolding of the proteins enhanced the flexibility of peptide chains around aromatic amino acid residues. Therefore, it was proposed that the decrease of polymer yield at high 1,4-dioxane contents is most likely due to the structural changes of HRP. Ichinohe et al. also investigated the effects of the  $\text{H}_2\text{O}_2$  amount on the polymerization yield of PDs for reactions in reversed micelles.<sup>73</sup> They found the polymer yield increased with an increase in  $\text{H}_2\text{O}_2$ , but it remained almost unchanged above 7.5 mmol of  $\text{H}_2\text{O}_2$ . In addition, they found that the yield of PD polymer in reversed micelles increased by addition of HRP. The results suggest that intermicellar exchange of the

monomers occurred during polymerization. CD spectra indicate that HRP molecules are entrapped in water pools of the reversed micelle and protected from direct contact with organic solvent. Therefore, the nativelike structure and hence catalytic activity of HRP can be retained in the reversed micelles.<sup>73</sup> It can be seen that the enzymatic oxidation in reversed micelles possesses a great potential to create a new conducting polymer.

Shan and Cao also investigated the influence of polymerization conditions on polymerization yield of three PDs via the catalysis of HRP in dioxane at ambient temperature with H<sub>2</sub>O<sub>2</sub> as the oxidant.<sup>247</sup> The black, powdered polymers with a weight-average molecular weight of higher than 10 000 have been obtained in good yields and are soluble in DMF and DMSO. It is found that the variation of pH value from 6 to 7 had nearly no influence on the polymerization yields, while the polymerization yields increase with increasing monomer concentration and oxidant amount. The yield of *o*PD polymerization is achieved up to 77.8% under optimized conditions.

It should be particularly noticed that the enzyme (HRP)-catalyzed oxidative polymerization in the presence of H<sub>2</sub>O<sub>2</sub> has been used to rapidly synthesize a novel water-soluble and dark brown sulfonic *p*PD polymer (Scheme 9) with a polymerization yield of

#### Scheme 9



80% and high weight-average molecular weight of 18 000.<sup>186</sup> The polymerization reaction is as follows. As the polymerization progresses, the <sup>1</sup>H NMR peak pattern at 7.0, 7.15, and 7.5 ppm changes together with the appearance of new peaks at 8.15 ppm. These peaks show multiple splitting patterns and become sharper due to the long-range couplings of the neighboring protons as compared with monomer. The peak intensities of three aromatic protons decrease to 62–72% at 13-min polymerization, implying that all three positions have almost identical probabilities of participating in oxidative coupling. PBZ can be synthesized by the oxidation of H<sub>2</sub>O<sub>2</sub> catalyzed by HRP at room temperature in a monophasic organic solvent with a small amount of water at pH 7.5.<sup>248</sup>

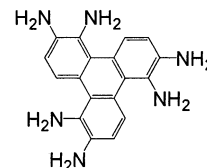
## B. Enzyme-Catalyzed Oxidative Oligomerization

Although the oxidative reaction of *o*PD did not occur effectively by cytochrome *c* in water, the cytochrome *c* solubilized in reversed micelles formulated with di-2-ethylhexyl sulfosuccinate could catalyze the oxidation of *o*PD with H<sub>2</sub>O<sub>2</sub> and finally form an oligomer with the structure shown in Scheme 3 since the nanostructural environment activated cytochrome *c* entrapped in reversed micelles and facilitated the enzymatic oxidation of *o*PD in a nonpolar solvent.<sup>249</sup> In addition, the di-2-ethylhexyl sulfosuccinate molecules play an important role in the

specificity of *o*PD oxidation by electrostatic interaction with di-2-ethylhexyl sulfosuccinate molecules.

When HRP is replaced with cytochrome *c*, the cytochrome *c* catalyzed H<sub>2</sub>O<sub>2</sub>-dependent oxidation reaction of *o*PD in 0.1 M phosphate buffer pH 6.8 facilely gives only a trimer with the structure shown in Scheme 10.<sup>250</sup>

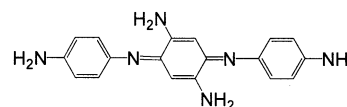
#### Scheme 10



36: *o*-Phenylenediamine trimer

It is interesting that a *p*PD linear trimer, i.e., 2,5-diamino-*N,N*-di-(4-aminophenyl)-2,5-cyclohexadiene-1,4-diimine (Scheme 11), is the end product from the HRP-catalyzed reaction of H<sub>2</sub>O<sub>2</sub> oxidizing *p*PD in the pH 3.0–7.0 B-R buffer solution.<sup>251</sup> The formation of the trimer has been used in voltammetric enzyme immunoassay.

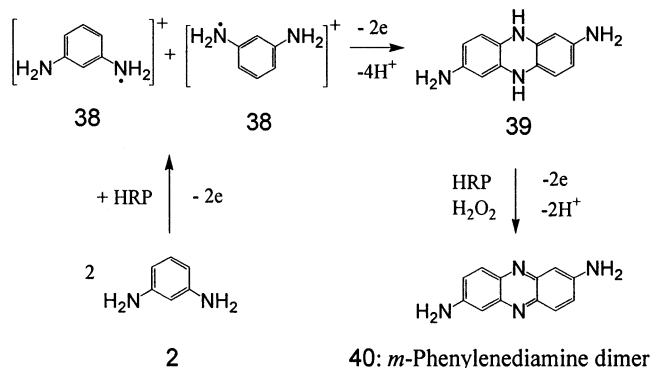
#### Scheme 11



37: *p*-Phenylenediamine trimer

Niu and Jiao indicated that only a dimer (Scheme 12) could be obtained by oxidation of *m*PD (20 mmol) with H<sub>2</sub>O<sub>2</sub> (9 mmol) and HRP (1 mg) as oxidant and catalyst, respectively, in buffer pH 8.5 without dioxane at ambient temperature for 24 h.<sup>252</sup> It can be seen that the organic additive is important for the enzyme-catalyzed oxidative polymerization of *m*PD. The dimerization mechanism is shown in Scheme 12.

#### Scheme 12



In summary, general enzyme-catalyzed oxidative reactions only lead to the formation of the oligomers (dimer and trimer) of aromatic diamines. It appears that aromatic diamine polymers can be formed only under optimal enzyme-catalyzed oxidative conditions.

## C. Structure and Properties of Enzyme-Catalyzed Oxidative Polymers

Ichinohe et al. thought that *p*PD polymerization with H<sub>2</sub>O<sub>2</sub>/HRP as oxidant/catalyst proceeds mainly

via N–N coupling reactions to form linear hydrazine polymer as shown in Scheme 6 according to the results of IR spectra.<sup>72</sup> In this case, excess oxidation would lead to the formation of azo linkages or quinoneimine (quinoid) moieties (Scheme 13). This structure is similar to those obtained with  $\text{Fe}^{3+}$ –chelate complex/oxygen as oxidant.

### Scheme 13



41: Poly(azo/hydrazine phenylene)

42: Quinoid-containing polymer

The  $PpPD$  prepared by oxidative polymerization with  $\text{H}_2\text{O}_2/\text{HRP}$  as the oxidant/catalyst exhibits a very weak  $^1\text{H}$  NMR broad peak at 4–6 ppm due to the NH proton and a very broad peak at 6–8 ppm due to aromatic protons.<sup>72</sup> However, HRP/ $\text{H}_2\text{O}_2$ -catalyzed/oxidized sulfonic  $pPD$  polymer shows three splitting strong peaks at 7.0, 7.15, and 7.5 ppm and a weak doublet peak at 8.15 ppm.<sup>186</sup>

Enzyme-catalyzed oxidative  $PpPD$  exhibits a broad UV–vis absorption at ca. 480 nm.<sup>253</sup> With increasing number-average molecular weight from 912, 1670, to 2040 g/mol, the peak of the broad UV–vis absorption increases from 474, 480, to 482 nm, indicating an enhanced conjugation structure. It is found that a systematic change of the electronic spectra of  $pPD$  polymer in NMP was observed by addition of acetic acid.<sup>72</sup> The intensity of the bands at 337 and 497 nm was reduced, and a new band at ca. 636 nm developed. Four isosbestic points appeared at 308, 360, 405, and 543 nm, indicating a reversible equilibrium between two chromophores,<sup>72</sup> possibly due to changes of  $\pi$ -electron conjugation systems by protonation at nitrogen atoms of azo and quinoneimine groups. However, the UV–vis spectra of  $oPD$  and  $mPD$  polymers slightly changed with adding acetic acid.

HRP-catalyzed  $\text{H}_2\text{O}_2$ -oxidized sulfonic  $pPD$  polymer also exhibits a strong pH dependence of UV–vis absorption and emission characteristics due to rapid doping and undoping processes.<sup>186</sup> The polymer at pH 1.2 has an emission only in the blue region with an emission maximum at 380 nm and an excitation maximum at 320 nm. A new emission band at 530 nm appears at pH 3.0. The excitation spectrum shows multiple bands with peak maxima at 340, 380, and 460 nm unlike that at pH 1.2. With increasing the pH to 6.0, the intensity of the emission at 530 nm increases to about an order of magnitude higher than that in low pH solution. These results show that the polymer exists predominantly in doped form at pH 1.2 but in undoped form at pH 6.0, whereas at pH 3.0 the doped and undoped states coexist. The conversion from the doped to the undoped form is found to be instantaneous due to rapid undoping kinetics.

The enzyme-catalyzed oxidative polymers prepared in solutions of 60% or higher contents of 1,4-dioxane were hardly ever soluble in THF. The polymers prepared in lower 1,4-dioxane contents were partly soluble in THF, depending on the structure of the monomer. With increasing dioxane concentration from 20% to 90% in the polymerization system, the

number-average molecular weight of enzyme-catalyzed oxidative  $PpPD$  increases from 1900 to 3700 g/mol, passing a maximum value of 3800 g/mol at 80%.<sup>253</sup> The HRP-catalyzed  $oPD$ /phenol copolymer was also partly soluble in DMF and DMSO; however, it was insoluble in other common solvents such as acetone, toluene, and water.<sup>246</sup>

It is found from Table 14 that enzyme HRP is very vital for obtaining higher molecular weight ( $M = 20\,000$ )  $PoPD$  because in the absence of HRP the molecular weight of  $PoPD$  formed is much lower ( $M = 800$ ) but with a higher polymerization yield (67%).<sup>117</sup>

The solubility, film-forming ability, electroconductivity, and thermal stability of the HRP/ $\text{H}_2\text{O}_2$ -catalyzed/oxidized sulfonic  $pPD$  polymer were found to be better than those of  $PpPD$ .<sup>186</sup> The sulfonic  $pPD$  polymer is very soluble in water at all pH conditions due to the presence of sulfonic acid and free amino groups. An optically clear and thin polymer film with an absorption maximum of 530 nm was easily made by casting its aqueous solution. Obviously, the presence of the sulfonic substituent on  $PpPD$  is crucial for excellent solubility in water and good solution processibility. The as-prepared polymer shows conductivity of  $10^{-5}$  S/cm at pH 6.0. The first and second significant weight losses of 8% and 19% were observed for the polymer at 201 and 332 °C. Even at 500 °C, less than 25% weight loss was found. It is proposed that the electroactive sulfonic  $pPD$  polymer could be self-assembled into multilayer structure by interweaving with a variety of polyelectrolytes, for the fabrication of thin films of biomaterials through a layer-by-layer deposition technique.

Ichinohe et al. synthesized magnetically active PD polymers by HRP-catalyzed polymerization of three PPDs using  $\text{H}_2\text{O}_2$  as an oxidizing agent in homogeneous or reversed micellar solutions consisting of an anionic surfactant and water in organic solvents, followed by treatment of the polymers with stainless steel sticks.<sup>71,254</sup> These polymers responded to a permanent magnet at room temperature in air. It is considered that the magnetic properties are affected by spin interactions of PPDs and Fe or Ni. The plot of magnetization against applied field at 5 K is almost the same as that at 300 K. The magnetization–magnetic field curves of these polymers showed sigmoid behavior at 300 K but did not show a residual magnetization and a coercive force, resembling those of soft ferromagnets, and the ferromagnetic properties were maintained at 800 K, though the magnetization of the  $PmPD$  gradually decreased with an increase in temperature at the magnetic field of 5000 G. This indicates a Curie temperature of the  $PmPD$  of higher than 800 K. The curves were different for polymers from isomeric PDs. The  $PoPD$  and  $PpPD$  exhibit lower saturation magnetization (0.29 and 0.07 emuG/g at 300 K, respectively) than  $PmPD$  (0.38 emuG/g), indicating a dependence of the inter- and intramolecular spin interactions on the structure of three PPDs.

The ESR spectra of the magnetically active  $PmPD$  were studied in a magnetic field of  $3280 \pm 2500$  G at room temperature.<sup>71,254</sup> Broad ESR bands due to ferromagnetic metals were observed for the magneti-

cally active *PmPD*, but magnetically inactive *PmPD* did not show bands due to transition metals. The  $g$  value and spin concentration of the magnetically active *PmPD* are 2.004 and  $10^{19}$  spins/ $g$ , respectively. Larger  $g$  values and a wider peak indicate that there are stable and lone free electrons in the polymers because the free electrons conjugate with the phenyl rings and nitrogen atoms in the main chain.

Two-photon absorption in HRP/H<sub>2</sub>O<sub>2</sub>-catalyzed/oxidized PBZ in solution in DMSO/methanol with a volume ratio of 4/1 was studied by degenerate four-wave mixing with nanosecond and picosecond pulses.<sup>248</sup> The third-order nonlinear optical susceptibility are on the order of  $10^{-9}$  to  $10^{-8}$  esu. Measurements on a PBZ thin film agree approximately with the extrapolated values from solution measurements. Picosecond time-resolved measurements indicate a pulse-width-limited response followed by a small slow component. Investigation of the total energy transmission as a function of the incident intensity and fluence at 532 nm for pico- and nanosecond pulses indicates reverse saturable absorption. The nanosecond and picosecond curves are superimposed for the intensity plot but not for fluence. Therefore, the nonlinearity is predominantly due to two photon absorption. It is found based on numerical analysis of the data that the two photon absorption coefficient and the imaginary component of the susceptibility are 12.25 cm/GW and  $5 \times 10^{-9}$  esu, respectively. The PBZ material appears to be a good candidate for applications in optical power limiting and switching.

This section has illustrated advances in the enzyme-catalyzed oxidative polymerization and polymers of aromatic diamines in the past 10 years. As compared with chemically oxidative polymerization, the enzyme-catalyzed oxidative polymerization can provide aromatic diamine polymers with different macromolecular structure and further lead to the formation of a soluble *PmPD*. However, investigations on the enzyme-catalyzed oxidative polymerization and polymers from aromatic diamines are very few. In particular, no report on the electroconductivity of the polymers is found. It is hoped that this paper encourages others to discover the more efficient system of enzyme-catalyzed oxidative polymerization and further to expatiate on the important relationship between the polymerization conditions and macromolecular structure/properties/functionality of the polymers.

## VI. Photocatalyzed Oxidative Polymerization of Aromatic Diamines

### A. Photocatalyzed Oxidative Polymerization

Photocatalyzed oxidative polymerization has been used to synthesize some conducting polymers. Conducting PPY prepared by photooxidative polymerization has been reported by using tris(2,2'-bipyridyl)ruthenium complex and n-TiO<sub>2</sub>.<sup>255</sup> Only recently have there been a few publications on the photocatalyzed oxidative polymerization of two *pPD* derivatives including *N*-phenyl-*pPD* and 2,3,5,6-tetramethyl-*pPD*.<sup>87,205,206,256,257</sup> The photocatalyzed oxidative polymerizability of other aromatic diamines has not been reported.

It seems that the photocatalyzed oxidative polymerization from the photoinduced electron transfer from AN does not occur by illumination of the solution containing only AN. However, after a small amount of *N*-phenyl-*pPD* was added, the polymerization occurs easily. Therefore, the *N*-phenyl-*pPD* should be required as an initiator to induce the photooxidative polymerization of AN with photoinduced electron transfer of tris(2,2'-bipyridyl)ruthenium.<sup>258</sup> The photopolymerization of 300 mM AN and 1 mM *N*-phenyl-*pPD* in 2 M HCl aqueous solution has been investigated by illuminating a bilayer electrode composed of tris(2,2'-bipyridyl)ruthenium complex-incorporated Nafion film and methyl viologen pendant polysiloxane film in the visible region ( $\lambda = 420\text{--}600$  nm, 89.5 mW/cm<sup>2</sup>) from the ITO electrode side with a 500 W xenon lamp.<sup>256</sup> The formation of PAN has been confirmed by the absorption spectra, FT-IR spectra, and an increase in the electrode mass, because the absorption peaks at ca. 800 and 400 nm assigned to the conjugated polaron structure and semiquinone cation radical structure of PAN, respectively, appear and are enhanced with illumination time up to 90 min.

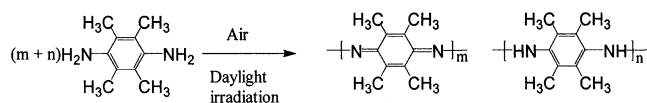
The solution containing only 1 mM *N*-phenyl-*pPD* has been illuminated, and the photopolymerization was brought out despite the very low concentration of *N*-phenyl-*pPD*. The big difference between the photopolymerizations of a AN(300 mM)/*N*-phenyl-*pPD*(1 mM) mixture and *N*-phenyl-*pPD*(1 mM) is a much slower polymerization rate of the latter system due to much lower monomer concentration.

A representative procedure of photopolymerization is as follows. (1) The *N*-phenyl-*pPD* and AN mixture solution for the photopolymerization can be first prepared by a special technique because *N*-phenyl-*pPD* shows poor solubility in HCl aqueous solution. *N*-phenyl-*pPD* (1mM) could not be solubilized in 2 M HCl solution unless 200 W sonication was performed for over 30 min.<sup>258</sup> Teshima et al. proposed a technique for preparing a homogeneous polymerization solution instantly, i.e., *N*-phenyl-*pPD* was first dissolved in AN and then the resulting solution was mixed with HCl aqueous solution.<sup>258</sup> Then tris(2,2'-bipyridyl)ruthenium complex and methyl viologen ion were added. (2) The homogeneous solution containing 1 mM *N*-phenyl-*pPD*, 300 mM AN, 60 mM tris(2,2'-bipyridyl) ruthenium complex, and methyl viologen ion was illuminated under oxygen bubbling with visible light with a wavelength of 420–600 nm and a power of 89.5 mW/cm<sup>2</sup> from the glass substrate side with a 500 W xenon lamp. (3) After illumination, the PAN formed was precipitated by adding NaOH aqueous solution, filtered, and dried under reduced pressure.<sup>87</sup> It is concluded from the similarity in IR and CV spectra of two products that the PAN is almost the same as that obtained by chemically oxidative polymerization except for a small proportion of branched structure in the photopolymerized PAN. However, the PAN obtained by photooxidative polymerization with *N*-phenyl-*pPD* as monomer exhibits a lower molecular weight than that by chemically oxidative polymerization with AN as monomer.



Shao et al. suggested that 2,3,5,6-tetramethyl-*p*PD even at a low concentration of 10 mM can easily polymerize upon sunlight irradiation accompanied with the gradual darkening of the solution color.<sup>205</sup> Original 2,3,5,6-tetramethyl-*p*PD solution is colorless and does not exhibit any absorbency in the visible wavelength range. After irradiation, the solution exhibits three absorbance peaks at 521 (medium), 563 (strong), and 611 (strong) nm in its UV-vis spectrum, implying formation of a highly conjugated structure in a long distance, as shown in Scheme 14. In

Scheme 14



14

43: Poly(2,3,5,6-tetramethyl-*p*-phenylenediamine)

particular, the intensity of the absorbance peak at 563 nm increases linearly from 0 to 0.55 au with prolongating the polymerization time from 0 to 30 min. With further extending the polymerization time from 30 to 45 min, the peak intensity increases from 0.55 to 0.65 au at a relatively slow rate. It can be concluded that the air-oxidative polymerization of 2,3,5,6-tetramethyl-*p*PD could be achieved in 45 min.

It is found that molybdate ammonium [(NH<sub>4</sub>)<sub>6</sub>Mo<sub>2</sub>O<sub>27</sub>·7H<sub>2</sub>O] at acidic aqueous solution (pH = 1) can accelerate the polymerization process of 2,3,5,6-tetramethyl-*p*PD. The mixture solution of molybdate ammonium/2,3,5,6-tetramethyl-*p*PD (1/3 molar ratio) is yellow initially and then turns emerald and immediately precipitates together with the precipitation of MoO<sub>3</sub>. The yellow intermediate might correspond to the intermediate radical, while the emerald precipitate should be 2,3,5,6-tetramethyl-*p*PD polymer. It should be noted that molybdate ammonium does not participate in the air-oxidative polymerization of 2,3,5,6-tetramethyl-*p*PD, since no oxidative polymerization of 2,3,5,6-tetramethyl-*p*PD with molybdate ammonium was found in the nitrogen atmosphere. Therefore, the acceleration of the air-oxidative polymerization of 2,3,5,6-tetramethyl-*p*PD induced by molybdate ammonium might be attributed to its disturbance to the balance between monomer and polymer by entrapping the polymer into MoO<sub>3</sub>.

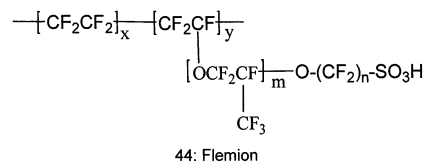
## B. Effect of Reaction Conditions on Photocatalyzed Oxidative Polymerization

There is a significant effect of reaction conditions, such as the organic solvent, pH value, additive, and water content in the polymerization systems, on photocatalyzed oxidative polymerization. The PAN polymerized photocatalyzed oxidatively from *N*-phenyl-*p*PD in AN will have a higher number-average molecular weight (3620 g/mol) and higher polymerization yield (60%) in AN medium than that (1940 g/mol and 40%, respectively) in AN-free acetone because AN not only works as the solvent for *N*-phenyl-*p*PD but also participates in the chain propagation leading to PAN. It is reported that the chemically oxidative polymerization of *N*-phenyl-*p*PD

also gives a linear PAN with a high polymerization yield of 99%.<sup>207</sup> However, the electropolymerization of *N*-phenyl-*p*PD gives a linear AN tetramer which is completely different from the long *para*-substituted polymer chain of the chemically oxidative polymer of AN.<sup>259</sup>

The effect of AN and acetone as photopolymerization solvents was compared for the preparation of PAN image film on an ion-exchange Flemion film (Scheme 15). When the Flemion film containing tris-

Scheme 15



44: Flemion

(2,2'-bipyridyl)ruthenium complex and methyl viologen was illuminated in an acidic aqueous solution of *N*-phenyl-*p*PD, the photopolymerization of *N*-phenyl-*p*PD and AN at higher AN concentration proceeded in the solution rather than on the Flemion film, due to the release of ruthenium tris(2,2'-bipyridyl)<sup>+</sup> from the film by the ion-exchange reaction between ruthenium tris(2,2'-bipyridyl)<sup>+</sup> and protonated AN.<sup>260</sup> This is not good from the viewpoint of PAN image formation on the Flemion film because no PAN image film on the Flemion film can be obtained. Unlike AN, acetone did not take part in the photopolymerization; however, acetone enables *N*-phenyl-*p*PD to be supplied near ruthenium tris(2,2'-bipyridyl)<sup>+</sup> in the film without the release of Ru(bpy)<sub>3</sub><sup>+</sup>. Addition of acetone of even 0.2 vol % is effective for the photopolymerization of *N*-phenyl-*p*PD on the Flemion film, leading to PAN image formation regardless of low effectivity for obtaining high molecular weight PAN in the presence of acetone. It is seen that the photopolymerization sites and product form of *N*-phenyl-*p*PD depend strongly on the solvent used.

The photopolymerization of *N*-phenyl-*p*PD in aerated HCl solution in the presence of an anionic micelle, i.e., sodium dodecyl sulfate, was found to lead to the formation of PAN/micelle complex.<sup>261</sup> It is indicated that in the presence of sodium dodecyl sulfate of more than 1 mM the PAN formed possesses longer conjugation length due to more effective photoinduced electron transfer between Ru(bipyridyl)<sub>3</sub><sup>2+</sup> and *N*-phenyl-*p*PD. The molecular weight of the PAN photopolymerized in the presence of sodium dodecyl sulfate of more than 32 mM is about 5 times higher than that in the absence and presence of sodium dodecyl sulfate of less than 1 mM. It can be concluded that sodium dodecyl sulfate is a good additive of *N*-phenyl-*p*PD and also a good template on the photopolymerization.

The photooxidative polymerization of *N*-phenyl-*p*PD by tris(2,2'-bipyridyl)ruthenium intercalated in a hectorite clay in acidic aqueous solution takes place successfully in the two-dimensional interlayer spaces with anionically charged clay layers acting as templates.<sup>257</sup> The PAN obtained exhibits a longer chain length in the presence of hectorite clay than in the absence of hectorite clay. It should be noted that the

photopolymerization of *N*-phenyl-*p*PD in the interlayer of hectorite clay is less efficient due to slower diffusion of *N*-phenyl-*p*PD in the interlayer than in the solution. It is seen that two-dimensional ordered reaction space will be beneficial to the growth of a long PAN chain in one direction by the photooxidative polymerization of *N*-phenyl-*p*PD.

The effect of solution pH in a range from 0.3 to 5.9 on the photopolymerization of AN and *N*-phenyl-*p*PD has been analyzed by Teshima et al.<sup>258</sup> It is suggested that the photopolymerization leading to the formation of PAN film can be induced effectively by employing the solution at pH -0.3 but not at pH 5.9 or 1.1, although the conductive PAN film can be commonly obtained at the same pH values by electropolymerization. Note that the illumination for the photopolymerization in the solution at pH 5.9 can lead to AN oligomers with lower molecular weight (the degree of polymerization is ca. 4). This result indicates that the photopolymerization leading to PAN film is considerably influenced by the solution pH and the photopolymerization mechanism is different from common electropolymerization. The influence of pH on the initial reaction for the photopolymerization was discussed in detail by quenching reaction of [ruthenium tris(2,2'-bipyridyl)<sup>2+</sup>]<sup>\*</sup> in solution at each pH as a function of *N*-phenyl-*p*PD concentration. It is found that the *N*-phenyl-*p*PD should be fully positively charged at a pH lower than -0.1 due to the protonation to both amino and imino groups but should be neutral at pH 5.9 due to deprotonation. They thought that the pH of the photopolymerization solution plays an important role in the coupling and propagating reactions. At lower pH, the growing intermediate has a protonated form, leading to the formation of PAN with higher molecular weight. At pH 5.9 the growing intermediate has the quinone diimine form that does not show coupling activity because of its stability. Therefore, its coupling and propagating reactions were restricted at the oligomer level.

The electrostatic repulsion between positively charged ruthenium tris(2,2'-bipyridyl)<sup>2+</sup> and *N*-phenyl-*p*PD at the lower pH might influence the electron-transfer process between them.<sup>258</sup> In addition, photoinduced electron transfer may be a key factor as an initial reaction to enhance photopolymerization, but the photopolymerization in solution at lower pH is not effective because of the electrostatic repulsion. It is found that the efficient photopolymerization is induced in the presence of NaCl by continuous illumination for only 3 min because NaCl can increase the ionic strength and then reduce the electrostatic repulsion.

Very recently a deoxyribonucleic acid-PAN complex has been successfully prepared by the photopolymerization of *N*-phenyl-*p*PD via photocatalytic reaction with Ru(bpy)<sub>3</sub><sup>2+</sup> complex in the presence of deoxyribonucleic acid.<sup>262</sup> This polymerization can occur even in solution at pH 3.0–6.5 because of the specific local "lower-pH" environment provided by the phosphate groups of deoxyribonucleic acid. The photopolymerized PAN obtained thus is protonated by deoxyribonucleic acid. *N*-Phenyl-*p*PD in the deoxyribonucleic

acid solution at pH 3.0 can align along the main chain of the deoxyribonucleic acid through intercalation and/or electrostatic interactions, resulting in an expanded-coil PAN structure in the PAN-deoxyribonucleic acid complex. The template effect of structurally ordered deoxyribonucleic acid on the photopolymerization of *N*-phenyl-*p*PD has been observed.

Photooxidative polymerization of *N*-phenyl-*p*PD in the solid state has been studied by Kim in 2001.<sup>206</sup> It is found that the solid-state photopolymerization with Flemion film containing tris(2,2'-bipyridyl) ruthenium and *N*-phenyl-*p*PD is successful,<sup>258</sup> indicating success on the photoinduced electron transfer between tris(2,2'-bipyridyl)ruthenium and *N*-phenyl-*p*PD even in the solid state. Note that a trace amount of water (ca. 1 wt %) in the solid Flemion film is vital for the photopolymerization in the solid state because no photopolymerization was observed for the completely dried film upon illumination. Therefore, it can be concluded that the solid-state photopolymerization of *N*-phenyl-*p*PD in the Flemion film can be induced effectively by a trace amount of water. In addition, since the photopolymerization depends on the intensity of the light source, employment of a laser can cause faster photopolymerization.<sup>258</sup>

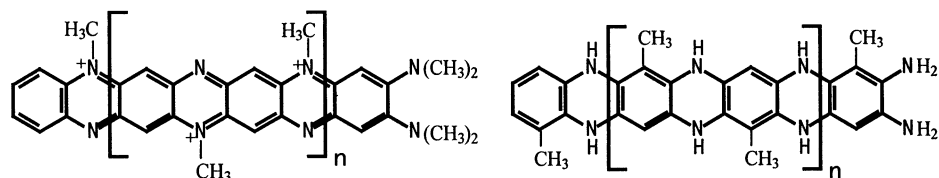
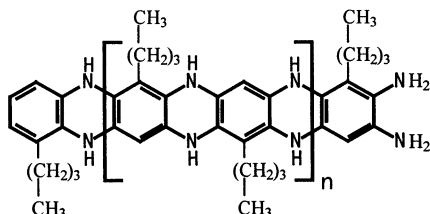
It is clear that some progress in photocatalyzed oxidative polymerization of aromatic diamines has occurred in the last 4 years, since 1998. However, the photocatalyzed oxidative polymerization is still in its early days, particularly in comparison with the wider-researched electrochemically oxidative polymerization. There are many issues, such as the search of new monomers polymerizable photocatalyzed oxidatively, optimization of polymerization condition, characterization of the structure and properties, as well as discovery of functionality of the resulting polymers, which need to be addressed before any industrial development of the photocatalyzed oxidative polymerization can be considered. It is hoped that this section serves as a starting point for further investigation on the photocatalyzed oxidative polymerization and polymers from more aromatic diamines.

## VII. Electrochemically Oxidative Polymerization and Polymers from Aromatic Diamines

In the past, the formation of polymer film initiated electrochemically was avoided whenever possible because the film deposition was considered as electrode "poisoning".<sup>152</sup> Now this type of electrode "poisoning" is being extensively used in preparation of electroconducting polymer, construction of a high-performance sensor, and anticorrosion of metal. Various aromatic polymers, such as PAN, PPY, polypyridylamine, PPD, PDAN, and poly(DAAQ), have been synthesized by the electrochemical method from the corresponding monomers.<sup>4,6–10,18,20–24,31,32,35,36,38,40–42,44–47,139,173–188,227</sup>

Electropolymerization has many advantages compared with other methods as mentioned in section III. It is a process in which polymerization is achieved simply by applying an electrical current through a mix solution of the monomer, solvent, and electrolyte. Preferential solvents for electropolymerization have high specific dielectric constants and dissolve electrolytes, e.g., acetonitrile, propylene carbonate, alco-

## Scheme 16

45: Poly(*N*-methyl-*o*-phenylenediamine)46: Poly(3-methyl-*o*-phenylenediamine)47: Poly(3-*n*-butyl-*o*-phenylenediamine)

hol, and water. Electrolytes mainly include organic solvent-soluble and ion-dissociating organic or inorganic salts and acids, complex salts, e.g.,  $\text{H}_2\text{SO}_4$ ,  $\text{N}(\text{C}_2\text{H}_5)_4\text{BF}_4$ ,  $\text{LiClO}_4$ . The concentrations of the electrolytes and the aromatic diamine monomer are 0.01–1.0 M and 0.001–1.0 M, respectively. The reaction mechanism can be free radical, anionic, cationic, or a combination. The initiation of polymerization may be direct, through oxidation or reduction of an active intermediate from one of the other components in the solution. The polymer formed will either precipitate onto the electrode surface if it is insoluble in the solution or dissolve in the polymerization medium if soluble.<sup>41</sup> Compared to other polymerization methods, electropolymerization is a very convenient method for obtaining a thin coating or film adherent to many metallic substrates. Therefore, the advent of conducting polymers at the end of the 1970s has considerably increased its application fields. Polymer film with controllable thickness and good conducting properties can be now obtained easily. However, it must be emphasized that most of the recent electrochemical work devoted to conducting polymers has been carried out with inert metal or semiconductor electrodes such as Au, Pt, and Ni. A few studies on electropolymerization of conducting polymers on oxidizable metals such as iron, aluminum, and titanium have recently been reported.<sup>38</sup> Moreover, the processibility of many such electroactive polymers is very poor because the films are usually brittle and insoluble, which has prevented them from being put to practical use. Many efforts have been made to resolve this problem, e.g., the development of solubilization of conducting polymers by copolymerizing and blending conducting polymers with nonconducting polymers to form copolymers or composites.

Electrode filming on Pt of *o*PD and *m*PD with a concentration of 1 mM in 100 mM  $\text{N}(\text{C}_2\text{H}_5)_4\text{ClO}_4$ /acetonitrile was reported briefly in 1973.<sup>110</sup> It was found that the filming occurs only in those compounds containing several doubly activated ring positions, leading to the conclusion that films arise

due to multiple ring–ring coupling. Therefore, it was considered that *m*PD filming is possible but *o*PD impossible. However, electrode filming of *o*PD was believed to be absolutely possible later. *Po*PD was first prepared as a stable film onto an electrode by anodic oxidative polymerization of *o*PD in acidic solution.<sup>112,113</sup> It is reported that the *Po*PD film is slightly soluble in common organic solvents,<sup>112</sup> and soluble components are assigned to low molecular weight fractions.<sup>164</sup> Introduction of alkyl side groups to ladder PPD polymers could be one of best methods of improving the solubility. It is reported that 3-methyl-*o*PD and 3-*n*-butyl-*o*PD can electropolymerize by electrooxidation in a potential sweeping between –0.2 and 1.1 V vs SCE at 50 mV/s of 50 mM of corresponding alkyl-substituted *o*PD monomers in  $\text{H}_2\text{SO}_4$  containing  $\text{NaNO}_3$  with Pt (area 2 cm<sup>2</sup>) as working and auxiliary electrodes.<sup>263</sup> Electropolymerization of 4-nitro-*o*PD on Au and GC electrodes and the electrochemical behavior of poly(4-nitro-*o*PD) film formed have been investigated.<sup>264</sup> However, *N*-methyl-*o*PD did not lead to any polymer products under the same polymerization condition. Recently a method of synthesizing poly(*N*-methyl-*o*PD) (Scheme 16) by *N*-methylation of *Po*PD has been reported.<sup>265</sup> The method is that *Po*PD solution in ethanol was mixed with equal molar methyl iodide and refluxed at 60 °C for 24 h. Unfortunately, no systematic investigations on the solubility of poly(*N*-methyl-*o*PD), poly(3-methyl-*o*PD), and poly(3-*n*-butyl-*o*PD) (Scheme 16) have been found.

In addition, the electropolymerization of benzidine and its derivatives including *N,N*-diphenyl benzidine, 3,3',5,5'-tetramethyl benzidine, *N,N,N,N*-tetramethyl benzidine, and *N,N*-diphenyl-*p*PD on ITO has been investigated by cyclic voltammetry.<sup>230</sup> The *N,N,N,N*-tetramethyl benzidine and *N,N*-diphenyl-*p*PD could not electropolymerize successfully, possibly due to the difficulty of deprotonation of the nitrogen atom that is required for the initial electrooxidative step for further polymerization. However, the benzidine, *N,N*-diphenylbenzidine, and 3,3',5,5'-tetramethyl benzidine in  $\text{Et}_4\text{BF}_4/\text{CH}_3\text{CN}$  elec-

**Table 17. Electropolymerization of Aromatic Diamines and the Electroconductivity of the Polymer Films Obtained Directly on Working Electrodes with Pt as Counter Electrode**

polymer	electrical conductivity (S/cm)	electropolymerization solution	working electrode	polymerization parameters	refs
<i>P</i> oPD	0.21 (0.065) <sup>a</sup>	50 mM <i>o</i> PD, 0.1 M H <sub>2</sub> SO <sub>4</sub>	ITO	-0.5 to +0.8 V vs SCE	269
<i>P</i> oPD	1.2 × 10 <sup>-3</sup>	50 mM <i>o</i> PD, 0.1 M H <sub>2</sub> SO <sub>4</sub>	Pt, Au, ITO	-0.4 to +1.2 V vs SCE	164
<i>P</i> oPD	3.1 × 10 <sup>-9</sup>	1 mM <i>o</i> PD, 1.5 M HCl	Pt	0 to +1 V vs SCE	155
<i>P</i> oPD	3.1–4.1 × 10 <sup>-7</sup> (9.2 × 10 <sup>-7</sup> )	100 mM <i>o</i> PD 0.1 M <i>n</i> -Bu <sub>4</sub> NClO <sub>4</sub> / CH <sub>2</sub> ClCH <sub>2</sub> Cl	Pt (Ni)	3.2 mA/cm <sup>2</sup> , 5–20 °C	155
poly(HO- <i>o</i> PD)	5.6 × 10 <sup>-5</sup>	50 mM HO- <i>o</i> PD, 0.1 M N(C <sub>4</sub> H <sub>9</sub> ) <sub>4</sub> BF <sub>4</sub> /CH <sub>3</sub> CN	Pt	2.2 V vs Ag/AgCl	182
poly(3-methyl- <i>o</i> PD)	8 × 10 <sup>-4</sup>	50 mM 3-methyl- <i>o</i> PD 0.1 M H <sub>2</sub> SO <sub>4</sub> , 0.1 M NaNO <sub>3</sub>	Pt	-0.2 to 1.1 V vs SCE	263
poly(3- <i>n</i> -butyl- <i>o</i> PD)	5 × 10 <sup>-4</sup>	50 mM 3- <i>n</i> -butyl- <i>o</i> PD 0.1 M H <sub>2</sub> SO <sub>4</sub> , 0.1 M NaNO <sub>3</sub>	Pt	-0.2 to 1.1 V vs SCE	263
P15DAN	~1 × 10 <sup>-5</sup>	1.1 mM 15DAN, 0.1 M HCl/H <sub>2</sub> O	Pt	-0.1 to 1.0 V vs Ag/AgCl	178
P15DAN	1.5 × 10 <sup>-5</sup>	100 mM 15DAN, 0.1 M LiClO <sub>4</sub> /CH <sub>3</sub> CN	Pt	0.6 V vs SCE	173
P15DAN	10 <sup>-2</sup>	20 mM 15DAN, 0.1 M LiClO <sub>4</sub> /CH <sub>3</sub> CN	Au	-0.3 to +1.0 V vs SSCE	174
P18DAN	0.01(reduced) 2.4 (oxidized)	10 mM 18DAN 0.1 M N(C <sub>2</sub> H <sub>5</sub> ) <sub>4</sub> ClO <sub>4</sub> /CH <sub>3</sub> CN	Pt	-1.0 to +1.2 V vs Ag/AgCl	181
P18DAN	10 <sup>-3</sup> –10 <sup>-2</sup> (oxidized)	20 mM 18DAN, 0.2 M NaClO <sub>4</sub> /CH <sub>3</sub> CN	ITO	-0.8 to +1.2 V vs SSCE	139
P23DAN	2.2 × 10 <sup>-5</sup> (oxidized)	20 mM 18DAN, 0.2 M NaClO <sub>4</sub> /CH <sub>3</sub> CN	ITO	-0.8 to +1.2 V vs SSCE	139
P15DAAQ	0.3–2.0	10 mM 15DAAQ, 0.1 M N(C <sub>2</sub> H <sub>5</sub> ) <sub>4</sub> ClO <sub>4</sub> /0.5 M CF <sub>3</sub> COOH	Pt	-2.0 to +0.8 V vs Ag/AgCl	227
PBZ	3.6 × 10 <sup>-6</sup>	54 mM benzidine, 2 M HCl	Pt	potentiostatic 6 h	116
PDTDA	0.025–0.032	20 mM dithiodianiline, 0.2 M HClO <sub>4</sub> + 0.4 M LiClO <sub>4</sub> /CH <sub>3</sub> CN+H <sub>2</sub> O	Pt	-2.0 to ~+0.8 V vs Ag/AgCl	270
<i>p</i> PD/AN (1/9) copolymer	0.2	19 mM <i>p</i> PD, 163 mM AN, 1 M HCl	IrO <sub>2</sub> /Ti	-0.2 to 0.8 V vs Ag/AgCl	271
sulfonic- <i>p</i> PD/AN (1/9) copolymer	0.023	19 mM sulfonic <i>p</i> PD 163 mM AN, 1 M HCl	IrO <sub>2</sub> /Ti	-0.2 to 0.8 V vs Ag/AgCl	271
<i>P</i> oPD/PVA composite	10 <sup>-4</sup> –10 <sup>-1</sup>	50 mM <i>o</i> PD, 0.1 M H <sub>2</sub> SO <sub>4</sub>	Pt	-0.2 to +0.8 V vs SCE	222, 272

<sup>a</sup> The film was prepared by solution casting method in DMSO.

tropolymerized successfully and yielded electroactive films. The composition of the polymers obtained does not vary with reaction atmosphere, but its doping level will increase with increasing applied potential or electrolyte concentration. As an example of electropolymerization of 0.03 g of *N,N*-diphenylbenzidine in 0.68 g of molybdate-*n*-butylammonium perchlorate, 0.11 g of 2,6-lutidine, and 20 mL of acetonitrile at room temperature on ITO, application of one cycle of triangular wave (from 0 to 2 to 0 V vs SCE) at 50 mV/s can produce a homogeneous yellow film on the surface of the ITO.<sup>266</sup> The film adsorbed strongly to the surface of the electrode. The film was electrochemically active and turned light yellow to green to black, which is used for solar batteries.

A novel 2-dimensional polymer is made by the electropolymerization of *o*PD, with one amine functionality used for an 'in-situ' amide bond with  $\omega$ -mercaptoundecanoic acid forming the self-assembled monolayer on polycrystalline Au electrode.<sup>267</sup> This provides a possibility for fine control of the film thickness to the molecular level. This interesting system could be applicable in such areas as nano-electronics, nonlinear optics, and sensors.

### A. Electrooxidative Polymerization Procedure

Electropolymerization of PDs is carried out in a single- or dual-compartment cell by employing a

three-electrode configuration comprising of working, counter, and reference electrodes in an electrochemical bath consisting of monomer and supporting electrolyte both dissolved in an appropriate solvent. Then a suitable power supply potentiogalvanostatically (cyclic voltammetry), electrical current potentiostatically or galvanostatically, is applied through the solution in the cell. Finally, polymer films are deposited on the working electrode. Generally, potentiogalvanostatic and potentiostatic conditions are recommended to obtain thin films of low conducting aromatic diamine polymers while galvanostatic conditions could give thick films at relatively high current density.<sup>118</sup>

It has been reported that among many isomers of PD, DAN, and diaminopyridine the following isomers including *o*PD, *m*PD, *p*PD, 15DAN, 18DAN, 23DAN, 23DAPy, and 26DAPy<sup>268</sup> can electropolymerize. Each isomer and its polymers have their own individual structure and characteristics. With different electropolymerization conditions, polymer films with various properties are electrodeposited from different solutions onto different electrodes. Table 17 enumerated several kinds of PPD, PDAN, and P15DAAQ films and electropolymerization conditions.

Some kinds of aromatic diamine polymers have been synthesized by electropolymerization, but studies on their properties, especially electrical and

mechanical properties, are very few.<sup>158,273,274</sup> Most studies place attention on blending PD with other components to synthesize copolymer or composite,<sup>142,149,167,169,222,272,275–277</sup> which improves or adds some other properties (showed in Tables 4, 6, and 15–17). The preparation procedure of the copolymer and composite is similar with the procedure mentioned above, except that two or three monomers are added in polymerization solution to polymerize copolymer on another substrate, which must have conducting property. For example, other polymers first deposit on the electrode, and then aromatic diamine polymer film deposits on the substrate to form bilayer or multilayer composite film.

## B. Cyclic Voltammograms of Aromatic Diamines

To date, three electropolymerization techniques including potentiodynamic (potential scanning, i.e., cyclic voltammetry), potentiostatic (constant potential), and galvanostatic (constant current) methods have all been employed for the polymerization of aromatic diamines.<sup>128</sup> These techniques are very often used to quantitatively study the macroscopic growth of polymer films.

### 1. Cyclic Voltammograms of Phenylenediamines

Cyclic voltammetry is a very useful method which qualitatively reveals the reversibility of electron transfer during the electropolymerization and also examines the electroactivity of the polymer film because the oxidation and reduction can be monitored in the form of a current–potential diagram, i.e., CV diagram.<sup>128</sup> The CVs of the film-forming process of aromatic diamine polymers have been extensively studied.<sup>139,164,170,188,227</sup> The CVs recorded continuously during the whole electropolymerization depend on the species and concentration of monomer, electrolyte, and electrode. Generally, there is an anodic irreversible monomer oxidation peak with the largest current on the first scan of the CV during the electropolymerization of almost all aromatic diamines. The first anodic irreversible oxidation peak position is believed to be finger characteristics for each specific monomer. For *o*PD, *p*PD, and *m*PD with Au and Pt as working electrodes in the aqueous solution of KCl, H<sub>2</sub>SO<sub>4</sub>, or buffer at 40–50 mV/s, the anodic irreversible peak current decreased to nearly the background level on the subsequent cycles.<sup>142,149,162–164,167,168,170</sup> Even if the subsequent potential cycling is continued after 1000 cycles, a very low peak current of the anodic oxidation of *o*PD is maintained.<sup>164</sup> Therefore, the thickness of *Po*PD film prepared does not exceed 0.85 nm, because of the blockage arising from the formation of a very compact nonelectroactive polymeric film substantially without holes of the access of monomer to the electrode surface on the following cycles. The polymer films covering the electrode hinder further oxidation of monomer, namely, the polymer film of a certain thickness hinders further growth of the film.<sup>162,164,278</sup> This indicates a low efficiency of *o*PD oxidation on the *Po*PD film as compared to a bare electrode.<sup>162</sup> In addition, the electrooxidative polymerization of the three PD isomers is a self-limiting process since *Po*PD, *Pm*PD, and *Pp*PD are substan-

tially insulating polymers. It is reported that *Po*PD film coated on Au by 20 potential sweeps became totally insulated and therefore could not be coated with any further polymer.<sup>149</sup> This phenomenon is typical for electrochemically grown nonelectroactive polymer films. Malinauskas et al. suggested that the peak current in the CVs depends on *o*PD concentration in electropolymerization solution, showing saturation above 25 mM.<sup>162</sup> Such concentration dependence indicates that at lower *o*PD concentration, a denser *Po*PD film of a diminished redox capacity is obtained, isolating the electrode surface from further polymerization. Substituted *o*PD such as 3-hydroxy-*o*PD exhibits a similar CV feature in aqueous medium.<sup>182</sup>

### 2. Cyclic Voltammograms of Other Aromatic Diamines

The CVs of DANs are different from the CVs of PDs because of the higher electroconductivity of DAN polymers. Meneguzzi et al. reported the CVs taken during the electropolymerization of 15DAN in HClO<sub>4</sub> on a mild steel.<sup>179</sup> The first scan exhibits a broad and irreversible anodic peak due to the monomer oxidation at 0.74 V vs SCE. As cycling continues, this peak shifts to less positive potential, decreases in intensity, and finally disappears. No cathodic peak corresponding to the irreversible anodic peak is observed. In the second scan, one redox system at 0.48 (anodic)/0.44 (cathodic) V vs SCE appears. The currents on the anodic and cathodic waves increase steadily with potential sweep time, reflecting the growth of the conductive P15DAN film. Similar CVs are observed during the electropolymerization of 15DAN in NBu<sub>4</sub>-ClO<sub>4</sub>/HClO<sub>4</sub>/acetonitrile or LiClO<sub>4</sub>/acetonitrile with GC or Pt<sup>173,176</sup> and of 23DAN and 18DAN in NaClO<sub>4</sub> and/or HClO<sub>4</sub> aqueous or acetonitrile solution on GC or BPG electrode.<sup>139,188</sup> The irreversible anodic peak corresponds to the oxidation of the parent amino groups to the corresponding cation radical and of this cation radical to the corresponding dication.<sup>139</sup> No cathodic peak corresponding to the irreversible anodic peaks indicates a fast consumption of the electrogenerated monocation radicals and dications by follow-up chemical reactions to form electroactive PDAN films on the electrode. This is confirmed by the appearance of new redox waves in the second scans in the potential regions more negative (0.1 V anodic/0.05 V vs SCE cathodic for 15DAN,<sup>173</sup> –0.1 V anodic/–0.32 V cathodic for 23DAN and 0.38 V anodic/–0.02 V vs SSCE cathodic for 18DAN<sup>139</sup>) than those at which the irreversible oxidation peak of the monomer appeared and of the formation of the brown films on the electrode.

Skompska, Lee, and colleagues investigated the CVs obtained during the electropolymerization of 18DAN in acetonitrile containing LiClO<sub>4</sub> and N(C<sub>2</sub>H<sub>5</sub>)<sub>4</sub>-ClO<sub>4</sub> on Au and Pt electrodes at 50 and 100 mV/s, respectively.<sup>180,181</sup> Two oxidation peaks appear at 0.62 and 0.98 V in the first potential scan in acetonitrile containing N(C<sub>2</sub>H<sub>5</sub>)<sub>4</sub>ClO<sub>4</sub> along with a reduction peak at –0.51 V corresponding to the 18DAN oligomer formed just during the first scan.<sup>181</sup> However, only one clear oxidation peak appears at 0.44 V in the first potential scan in acetonitrile containing LiClO<sub>4</sub>.<sup>180</sup> As

the scan continues, the oxidation peaks of 18DAN shift in a more positive direction and increase steadily in height until the third scan, but the reduction peak from the oligomer disappears due to the diffusion away from the Pt electrode. Upon further scanning, a slow increase in small oxidation/reduction currents is observed at 0.39/−0.14 V, indicating an accumulation of the electroactive P18DAN film on Pt. These CV characteristics are not in agreement with those reported by Oyama due to the difference of the electrolytes.<sup>139</sup>

Jackowska et al. reported a different CV during the electropolymerization of 15DAN at stationary Au electrode in LiClO<sub>4</sub>/acetonitrile solution.<sup>279</sup> In the successive cycles the CV becomes more complicated. The main anodic peak shifts to more positive potentials; the shoulder and a new anodic peak appear at 0.4 and 0.9 V, respectively, together with a decrease in anodic current. The change of the CV shape is caused by the soluble oxidation products adsorbing and/or reacting on the electrode and confirmed by electropolymerization with a rotating Au disk electrode at 1000 rpm. Only one anodic peak appears at 0.7–0.9 V, characteristic for the oxidation of amino groups when the rotating Au electrode was used. In addition, when stationary Au electrode was used one additional redox couple at 0.06 (anodic)/−0.09 (cathodic) V vs SSCE appears in the subsequent cycles and the corresponding current increases with increasing scan numbers. This couple also corresponds to the redox reaction of the P15DAN film because a yellow-brown film has been formed on the electrode.

Interesting CVs were observed during the electropolymerization of 26DAPy on Pt.<sup>187</sup> The first scan at a scan rate 100 mV/s between 0 and 1.1 V vs Ag/Ag<sup>+</sup> exhibits a broad, irreversible, and strong anodic peak due to the monomer oxidation at 0.4 V followed by a broad shoulder at ca. 0.6 V. With increasing the number of cycles, the two overlapped anodic peaks shift toward more positive potential and their currents decrease gradually. No cathodic peak corresponding to the anodic peaks was observed. A visible golden film formed initially on the electrode and then became light blue and finally purple with increasing deposition charge. If potential cycling at 50 mV/s between 0 and 1.7 V vs Ag/Ag<sup>+</sup>, the CVs are different. The first scan from 0 to 1.7 V exhibits a broad, symmetric, and strong anodic peak at 0.52 V, while the return scan from 1.7 to 0 V exhibits a weak peak centered at 1.2 V. The second scan from 0 to 1.7 V exhibits a weak and broad peak at 0.65 V, but the return scan from 1.7 to 0 V exhibits a medium peak at 1.15 V.

Different CVs were observed for the polymerization of benzidine in NaClO<sub>4</sub>/HClO<sub>4</sub> and naphthidine in NaClO<sub>4</sub>/acetonitrile.<sup>189,190</sup> An anodic peak at 0.58 (or 0.49)V and a cathodic peak at 0.55 (or 0.46) V, which are consistent with two successive charge transfers to form a benzidine (or naphthidine) dication, decrease steadily and fast in intensity on continuous cycling of the potential between 0 and 0.8 (or 1.14) V and disappear at the cycling number of 50. On the contrary, one new reduction/oxidation couple appears at 0.15/0.2 V for benzidine polymerization and 0.95/

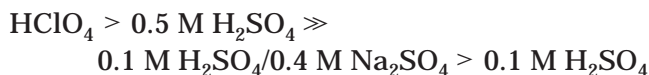
0.92 V for naphthidine polymerization and their peak currents increase steadily with the potential cycling to 50 cycles, showing the characteristic behavior of a deposited electroactive PBZ and polynaphthidine. For the polymerization of the naphthidine, another anodic peak at 0.66 V developed with increasing potential cycles. The CVs do not vary if the solution is stirred during cycling, indicating that the PBZ and polynaphthidine films are electrochemically homogeneous and adhere strongly to the electrode surface.

### 3. Effect of Electrolyte Solutions on the Cyclic Voltammograms

A significant influence of electrolyte solution including solvent, acid concentration, and electrolyte type on the CVs of aromatic diamines has been observed. Del Valle et al. studied the CVs recorded during the electropolymerization of 3-hydroxy-*o*PD in three media.<sup>182</sup> It is found that the CV of 3-hydroxy-*o*PD in 0.1 M Na<sub>2</sub>SO<sub>4</sub> (pH = 1) aqueous solution is analogous to that of *o*PD carried out in aqueous medium,<sup>182</sup> but it is impossible to obtain electrodeposited film on Pt electrode after more than 100 voltammetric cycles with a potential range from −0.7 to 2.0 V even if changing the monomer concentration and the supporting electrolyte because the 3-hydroxy-*o*PD oligomer formed is very soluble in the aqueous medium. There is a much more defined anodic peak of the monomer oxidation with a larger peak current in the CV on the first potential scan if 0.1 M tetrabutylammonium tetrafluoroborate in acetonitrile/water (99/1, vol) is used as the medium for the electropolymerization of 3-hydroxy-*o*PD. A redox couple appears gradually together with an increase in its current and the formation of the poly(3-hydroxy-*o*PD) film on the electrode with increasing number of potential scans. In 0.1 M tetrabutylammonium tetrafluoroborate in anhydrous acetonitrile, a significant current increase in the CVs was observed and a noticeable poly(3-hydroxy-*o*PD) film was obtained on the electrode surface as the number of potentiodynamic cycles increases. It can be concluded that the presence of water in the electrolyte seems to hinder the formation of the 3-hydroxy-*o*PD oligomer films because of the presence of large amount of hydrophilic hydroxyl groups. In addition, the hydroxy groups in the HAN, 3-hydroxy-*o*PD, and ANO generally do not take part in electropolymerization by cyclic voltammetry,<sup>150,182,280</sup> whereas the hydroxy groups in HAN are supposed to do.<sup>228</sup> The existence of free OH groups is very important for the functionalization of the polymers because they can combine with other functional groups. It is reported that poly-(ANO) as a passive layer for corrosion protection presents excellent properties as a 'primer coat' preventing mild steel corrosion.<sup>281</sup>

The effect of electrolyte on the CVs during electropolymerization of 50 mM *o*PD using a gold-plated quartz crystal, ITO, and Pt electrodes has been investigated.<sup>151,159</sup> Although the anodic oxidation peaks during the first positive sweep in 0.1 and 0.5 M H<sub>2</sub>SO<sub>4</sub> are nearly the same, the CVs recorded during the following electropolymerization in 0.5 M H<sub>2</sub>SO<sub>4</sub> are different from those in 0.1 M H<sub>2</sub>SO<sub>4</sub>. The

anodic current of monomer oxidation in the positive sweep from the second cycle in 0.1 M H<sub>2</sub>SO<sub>4</sub> decreased more rapidly than that in 0.5 M H<sub>2</sub>SO<sub>4</sub>. However, the CVs in 0.1 M H<sub>2</sub>SO<sub>4</sub> are very similar to those obtained in 0.1 M H<sub>2</sub>SO<sub>4</sub>/0.4 M Na<sub>2</sub>SO<sub>4</sub>. The number of redox couples containing an additional oxidation peak and an additional reduction peak in 0.1 M H<sub>2</sub>SO<sub>4</sub> and 0.1 M H<sub>2</sub>SO<sub>4</sub>/0.4 M Na<sub>2</sub>SO<sub>4</sub> is more than that in 0.5 M H<sub>2</sub>SO<sub>4</sub>. The appearance of the additional oxidation peak in 0.1 M H<sub>2</sub>SO<sub>4</sub> and 0.1 M H<sub>2</sub>SO<sub>4</sub>/0.4 M Na<sub>2</sub>SO<sub>4</sub> is due to the formation of P*o*PD film, implying that the electropolymerization of *o*PD is much easier in both 0.1 M H<sub>2</sub>SO<sub>4</sub> and 0.1 M H<sub>2</sub>SO<sub>4</sub>/0.4 M Na<sub>2</sub>SO<sub>4</sub> than in 0.5 M H<sub>2</sub>SO<sub>4</sub>. In addition, the formation of P*o*PD proceeded more rapidly in 0.1 M H<sub>2</sub>SO<sub>4</sub> than in 0.1 M H<sub>2</sub>SO<sub>4</sub>/0.4 M Na<sub>2</sub>SO<sub>4</sub>. After 100 cycles in 0.1 M H<sub>2</sub>SO<sub>4</sub> at a scan rate of 100 mV/s, a brown P*o*PD film is clearly seen on the ITO electrode.<sup>164</sup> Note that it is very difficult to deposit P*o*PD film from HClO<sub>4</sub>, and only a P*p*PD with very low molecular weight is formed in HClO<sub>4</sub>,<sup>62</sup> but HClO<sub>4</sub> is indeed a good electrolyte for the electropolymerization of several DAN isomers. The difference of electropolymerization rate of *o*PD in H<sub>2</sub>SO<sub>4</sub> of various concentrations is due to the different solubility of *o*PD oligomer in the electrolytes. The solubility of the *o*PD oligomer formed during the electropolymerization is in the following order



It is found that during the electropolymerization of *o*PD in 0.1, 0.5, and 1.0 M H<sub>2</sub>SO<sub>4</sub>, the electrolyte became red, light brown, and dark red, respectively, due to the formation of more soluble *o*PD oligomers.<sup>161,162,164</sup> The acidity of sulfuric acid electrolyte is more important than the anion concentration in affecting the electropolymerization process of *o*PD due to the difference in solubility of the oligomers.

The CVs during *o*PD (5 mM) polymerization vary significantly with polymerization pH.<sup>154</sup> At pH = 1, only one anodic peak appears, but a second anodic peak also appears during the first cycle at pH = 3, 5, and 7. During successive scans the peak potential shifts toward more positive values at any pH. Note that no reduction peak is found in the reverse scans.

A slightly different dependency of CV curves of *m*PD electropolymerization on the H<sub>2</sub>SO<sub>4</sub> concentration was found.<sup>168</sup> With increasing H<sub>2</sub>SO<sub>4</sub> concentrations from 0.01 to 4 M, similar CV characteristics were observed during the electropolymerization of *m*PD except for a slightly increased peak current of *m*PD monomer oxidation.

Cataldo investigated the CVs on 50 mM *p*PD aqueous solution in 0.1 M HClO<sub>4</sub> on Pt.<sup>62</sup> There is an initial anodic oxidation of *p*PD monomer along with the formation of a bluish cation radical on the electrode, although it has been reported that *p*PD does not electropolymerize in nonaqueous solvents.<sup>230</sup> Upon consecutive cycles, a redox couple appears and its current increases, indicating a continuous oligomerization. Unfortunately, after 10 cycles no further current growth is observed because the low molecular

weight P*p*PD product formed is not able to adhere on Pt electrode and then be dispersed in the solution. It should be appreciated that the electropolymerization of *p*PD is possible at higher monomer concentration.

Pham et al. studied the CVs obtained during the electropolymerization of 15DAN on GC in four different electrolytes.<sup>176,282</sup> The CVs during the film growth of P15DAN in 0.1 M NBU<sub>4</sub>ClO<sub>4</sub>/0.2 M HClO<sub>4</sub>/methanol are different from those recorded in 0.1 M NBU<sub>4</sub>ClO<sub>4</sub>/0.2 M HClO<sub>4</sub>/acetonitrile but similar to those recorded in 0.1 M HCl.<sup>176,178</sup> Note that there is a big difference of CVs recorded from the third potential scan during the electropolymerization of 15DAN on GC and Pt in 0.1 and 2 M HCl solution. Three reduction/oxidation peaks in 0.1 M HCl appear at 0/0.2, 0.4/0.41, 0.45/0.48 V, and their peak current increases with potential cycling to 10 cycles and then decreases. After 40 min of scanning, the peak currents remain steady. In 2 M HCl, only two redox couples at 0/0.2 and 0.45/0.48 V are observed. The oxidation peak at 0.2 V overlaps with the much more intense oxidation peak at 0.48 V. In particular, the peak current still increases even after 40 min of potential scan.

Azzem et al. investigated the variation of CVs during the electropolymerization of 15DAN on Pt with electrolytes.<sup>173,175,177</sup> The CVs recorded in 0.1 M LiClO<sub>4</sub>/acetonitrile<sup>173,175</sup> are different from those in 0.2 M NaClO<sub>4</sub>/0.1 M HClO<sub>4</sub>/water.<sup>175,177</sup> The irreversible oxidation peak of 15DAN monomer during the first scan in LiClO<sub>4</sub>/acetonitrile appears at lower potential and has a larger current than that in NaClO<sub>4</sub>/HClO<sub>4</sub>/water. Upon further scanning, the irreversible oxidation peak of the monomer in LiClO<sub>4</sub>/acetonitrile diminishes gradually with the appearance of a new redox system at 0.1/0.05 V. The irreversible oxidation peak of the monomer in NaClO<sub>4</sub>/0.1 M HClO<sub>4</sub>/water disappears suddenly from the second scan together with the appearance of two new redox systems. After some cyclings, P15DAN appears on the Pt surface as a blue film.<sup>175</sup> In addition, due to the formation of a polymer film on the electrode during electropolymerization, the effect of monomer concentration on the current of the monomer oxidation peak shows no linear proportionality.<sup>173</sup>

Azzem also studied the effect of addition of pyridine on the CVs of 15DAN.<sup>173</sup> An increase in pyridine concentration from 0 to 72 mM produces an increase in the current of the oxidation peak but the cathodic peak at 0.05 V disappears. Only a reduction peak of H<sup>+</sup> appears from -0.08 to -0.15 V due to good nucleophilicity of pyridine that can react with dication dimers and even with [15DAN]<sup>2+</sup>. Note that a different change of CV is found upon addition of HClO<sub>4</sub>. A decrease in the peak current of monomer oxidation with increasing HClO<sub>4</sub> content from 0 to 2.2 and 3.3 mM is observed together with the appearance of a new oxidation peak at 0.52 and 0.63 V, respectively, corresponding to the oxidation of the monoprotonated monomer.

Premkumar et al. reported that in the follow-up cycles during the electropolymerization of 50 mM *o*PD/GC in Na<sub>2</sub>SO<sub>4</sub>/H<sub>2</sub>SO<sub>4</sub> under deaerated condition

the oxidation current decreased rapidly, leaving only a small anodic peak together with a simultaneous appearance of a redox wave from  $-0.1$  to  $-0.08$  V vs SCE.<sup>153,156,158,278</sup> This redox couple is clearly indicative of the formation of P $\sigma$ PD film. The P $\sigma$ PD film formed on GC electrode was always limited to ca. 1 mm in thickness, but the amount of P $\sigma$ PD formed on GC/Nafion electrode was always much larger than that on the plain GC.<sup>153</sup> In addition, the P $\sigma$ PD film coated onto GC does not show any color, whereas the P $\sigma$ PD film prepared on GC/Nafion is a stable light yellow.

Note that the electropolymerization of  $\sigma$ PD in KCl aqueous solution at pH 7 containing a homogeneous nonionic surfactant lyotropic liquid crystalline phase of octaethylene glycol monohexadecyl ether (50 wt %) exhibits a different CV feature as compared with that of  $\sigma$ PD.<sup>283</sup> The peak current corresponding to the oxidation of  $\sigma$ PD is much lower (65 mA) in the liquid crystalline phase than (0.4 mA) in pure aqueous phase. On successive scans, the decrease in current passed is much slower in the liquid crystalline phase than in common aqueous phase.

However, there seems to be no influence of the electroinactive substance on CV. The CV recorded during the electropolymerization of  $\sigma$ PD on a quartz crystal electrode in the presence of glucose has been reported by Malitesta et al.<sup>146</sup> No significant difference is observed in comparison with that obtained under the same conditions (pH and  $\sigma$ PD concentration) but without glucose.

#### 4. Cyclic Voltammograms during the Copolymerization with Aniline

AN strongly affects the CVs of aromatic diamines because it participates in the electrooxidative reaction leading to the formation of aromatic diamine/AN copolymers. The CV of copolymerization of 4 mM  $\sigma$ PD with 160 mM AN in H<sub>2</sub>SO<sub>4</sub> was studied by Peng.<sup>278</sup> It is found that the couples corresponding to the emeraldine/paranigraniline and leucoemeraldine/polaronic emeraldine redox couples in the PAN structure vanish, indicating a decrease in the PAN-like unit content in the copolymer. These suggest a possible growth mechanism of  $\sigma$ PD/AN copolymer, namely,  $\sigma$ PD inserting PAN chain forms a network-like structure. Malinauskas et al. observed a dependence of the CV shape during electrocopolymerization of  $\sigma$ PD and AN on  $\sigma$ PD/AN monomer ratio.<sup>162</sup> At a higher  $\sigma$ PD concentration than AN concentration, the CVs do not differ markedly from those obtained in  $\sigma$ PD solution. Some differences in CVs are observed with  $\sigma$ PD concentrations lower than the AN concentration. At an  $\sigma$ PD/AN ratio of 1/4, two pairs of anodic and cathodic peaks appear in the CVs, the pair at lower potentials corresponding to P $\sigma$ PD and that at higher potentials to PAN. At a lower  $\sigma$ PD/AN ratio of 1/9, the resulting CVs and electropolymerization rate differ from those observed in pure AN solution.  $\sigma$ PD in low concentration can diminish the rate of AN electropolymerization, about 20-fold lower at an  $\sigma$ PD/AN ratio of 1/9 as compared to a pure AN polymerization at nearly the same concentration, because the presence of the P $\sigma$ PD layer with low electroconductivity hinders AN electropolymeriza-

tion. However, it is not clear whether a true  $\sigma$ PD/AN copolymer with repeating different monomer units in the same polymer chain has been obtained. At an  $\sigma$ PD/AN molar ratio of 11/4000, the resulting CVs and electropolymerization rate are identical to those observed in pure AN solution in HCl.<sup>284</sup> The CVs obtained on a PAN-film-coated Pt electrode in 50 mM  $\sigma$ PD in H<sub>2</sub>SO<sub>4</sub> are investigated.<sup>151</sup> The anodic oxidation of  $\sigma$ PD on PAN-film-coated Pt in the first potential sweep proceeds very similarly to that on bare Pt due to the high electroconductivity of PAN film. It is interesting that the anodic peak in the subsequent potential sweeps, corresponding to the leucoemeraldine to emeraldine transition in PAN, grows in height and shifts to positive potentials. The cathodic peak at 0.55 V vs RHE in the subsequent sweeps corresponds to the reduction of P $\sigma$ PD formed during the electropolymerization. This peak shifts to lower positive potential and diminishes in height with repeated potential scans, closely similar to the situation on bare Pt electrode. In addition, a new cathodic peak at 0.2 V vs RHE appears at the fifth potential scan and grows with repeated potential cycling, corresponding to P $\sigma$ PD film. In this way, P $\sigma$ PD/PAN/Pt and PAN/P $\sigma$ PD/Pt bilayer and P $\sigma$ PD/PAN/P $\sigma$ PD/Pt trilayer structures have been prepared and could be very useful for the fabrication of sensor.

Complicated CVs during the electrocopolymerization of  $m$ PD and AN with various  $m$ PD/AN molar ratios have been studied.<sup>168,285</sup> The three redox couples are easily observable at low  $m$ PD concentration on Pt in H<sub>2</sub>SO<sub>4</sub> with the potential cycling from  $-0.1$  to  $+1.0$  V at 100 mV/s.<sup>285</sup> The first and third couples with the respective midpoint potential of 0.33 and 0.70 V obviously correspond to the two well-known redox transitions of PAN. In comparison to the leucoemeraldine-emeraldine transition of PAN, the first redox couple is remarkably shifted toward the positive direction and appears to be more reversible, whereas the potential of the third couple either remains almost unchanged or shifts to lower values, indicating a narrower potential range for the existence of the emeraldine form than PAN. It is unexpected that a high current peak appears in the middle potential region just by mixing a small amount of  $m$ PD to AN solution. A cathodic peak in the middle potential region diminishes in height during the first five scans, whereas its anodic counterpart grows in height by a continuous potential cycling. With increasing  $m$ PD fraction, this middle peak diminishes. At a higher  $m$ PD to AN molar ratio, i.e., equimolar ratio, the first anodic peak overlaps the second one after a few potential scans. When the electrocopolymerization of  $m$ PD with AN was carried out on Au in H<sub>2</sub>SO<sub>4</sub> with the potential cycling from  $-0.1$  to  $+9.2$  V at 40 mV/s, three well-defined redox couples at relatively lower potentials have been observed.<sup>168</sup> With increasing  $m$ PD content from 0 to 4.3 mol %, the intensity of all CV peaks, particularly the peak at the highest potential, decreased. If cycling from  $-0.1$  to 0.8 V, the CV response of the electropolymerization of  $m$ PD with AN was dominated by the polymerization of AN, indicating an unobvious copolymerization between both monomers. Therefore, it



is proposed that the upper switching potential for the electrocopolymerization of *m*PD with AN could be 0.92 V. It can be seen that polymerization conditions strongly influence the CV feature of the electrocopolymerization of *m*PD with AN.

The CVs obtained in various potential scans from  $-0.2$  to  $0.9$  V in *p*PD or sulfonic *p*PD and AN solution in  $\text{H}_2\text{SO}_4$  or HCl on  $\text{IrO}_2$ -coated titanium and Pt electrodes have been studied.<sup>169,271,286</sup> Three anodic peaks at 0.22 (the strongest due to formation of radical cations), 0.5 (the weakest, BQ formation), and 0.81 V (medium, due to formation of diradical dication) corresponding to the three consecutive oxidation steps of AN and anodic peaks at ca. 0.62 and 0.71 V corresponding to respective *p*PD and sulfonic *p*PD are observed. The height and potential values of these peaks depend on the comonomer concentration and the number of potential scans. For example, the *p*PD peak current increases with increasing *p*PD concentration and the number of potential scans. The peak potentials corresponding to AN shift to slightly lower values with increasing *p*PD and sulfonic *p*PD concentrations but to apparently more positive values with increasing the number of potential scans. On the contrary, the peak potential corresponding to *p*PD and sulfonic *p*PD shifts to a more positive value with increasing *p*PD and sulfonic *p*PD concentration but to an apparently lower value with increasing the number of potential scans. These phenomena suggest that the electrocopolymerization between *p*PD or sulfonic *p*PD and AN is easier than the individual electrohomopolymerization of *p*PD, sulfonic *p*PD, and AN. Furthermore, the quinonediimine generated by the *p*PD is more efficient than that by sulfonic *p*PD in the acceleration process of copolymerization, since *p*PD is devoid of an electrostatic interaction between sulfonic group and cation radical nitrogen atom. The mass of polymer deposited on an  $\text{IrO}_2$ -coated titanium electrode is correlated with the anodic peak current, allowing monitoring of the rate of polymer deposition by changing the *p*PD/AN molar ratio. In pure *p*PD solution, only anodic/cathodic peaks at 0.62/0.53 V are observable on prolonged potential cycling. In contrast sharply with *o*PD/AN and *m*PD/AN copolymerization systems, a redox couple due to *p*PD unit appears at ca. 0.45 V and a strong increase of polymer layer growth is observed by mixing a very small amount of *p*PD to AN solution, for example, the *p*PD/AN molar ratio of 11/4000,<sup>284,287</sup> because a presence of *p*PD will facilitate the formation of quinonediimine, resulting in a significant increase in the nucleation rate of polymer deposition.<sup>169</sup> In addition, the CVs during the electrocopolymerization of *p*PD and AN show a dependence on the working electrode. The peak currents of redox couples corresponding to AN are much lower on Pt than those on  $\text{IrO}_2$ -coated titanium electrode.<sup>167,286</sup> The shape of the CVs during the electrocopolymerization of *N*-(3-sulfopropyl) AN and *p*PD also depends on the molar ratio of both monomers. The trend of the variation in CVs with the molar ratio in mixed solutions differs from that for *N*-(3-sulfopropyl) AN and *p*PD used separately. In addition, the CVs of both monomer mixtures are not simply the addition of the individual

CVs of both monomers. This behavior indicates an interaction between both monomers or the corresponding anodic oxidation products.<sup>286</sup> Clearly, a copolymer containing both *N*-(3-sulfopropyl) AN and *p*PD has formed during potential cycling in mixed solutions.

The CV features of two special aromatic diamines, i.e., dithiodianiline (2,2'-diaminodiphenyldithio, No. 24 in Scheme 1) and *N*-phenyl-*o*PD, with AN, respectively, have been studied quite recently. Wen et al. suggested that three distinct oxidation peaks appeared at 0.28 (strong), 0.56 (weak), and 0.64 (weak) V vs Ag/AgCl during the copolymerization of dithiodianiline and AN.<sup>232</sup> The peaks did not show any shift in potentials with increasing cyclic number, indicating that the redox behavior of the growth of dithiodianiline/AN copolymer is totally different from that of PAN under identical conditions. The homopolymerization of dithiodianiline resulted in only limited film growth with two different redox processes at 0.37–0.41 (medium) and 0.50–0.56 (strong) V vs Ag/AgCl. These facts suggest that by cyclic voltammetry the electrocopolymerization of dithiodianiline and AN did occur, which eventually became an adherent and stable copolymer film on the electrode.

Electrochemical copolymerization of *N*-phenyl-*o*PD with AN in aqueous HCl by using cyclic voltammetry also gave a copolymer, based on the differences in CV characteristics of the copolymer in comparison with the corresponding homopolymers, PAN and poly(*N*-phenyl-*o*PD), and the variation of peak currents and potentials between copolymer and PAN films with respect to sweep rates.<sup>288</sup>

As discussed above, the CV characteristics during the electrocopolymerization of PD isomers with AN have been systematically studied. However, it appears that the CV of only one DAN isomer with AN is found. Meneguzzi et al. reported a CV during the electrocopolymerization of 1 mM 15DAN and 100 mM AN in  $\text{HClO}_4$  on a mild steel electrode.<sup>179</sup> In the first scan, two anodic peaks at 0.74 and 1.0 V vs SCE are observed and correspond to the oxidations of 15DAN and AN, respectively. In the second scan, a well-defined redox system was obtained at 0.48 (anodic)/0.44 V(cathodic) (couple I), and after several scans, a second system appears at 0.79 (anodic)/0.75 (cathodic) V vs SCE (couple II). The current on the anodic and cathodic waves increases with scan numbers, reflecting the growth of the copolymer films. Redox couple I is principally due to P15DAN, and redox couple II with a relatively weak current wave is due to PAN. After potential scans for 10 min, the CV exhibits acceleration in the growth of the second redox system due to PAN. In addition, at the beginning the growth of P15DAN is predominant owing to a better adsorption of 15DAN onto mild steel as compared to AN. The growth of PAN is accelerated by 15DAN, just like the acceleration of AN polymerization by *p*PD.<sup>284</sup>

It is obvious that more progress in the cyclic voltammetry of aromatic diamines has occurred in the past 13 years. It can be concluded that CVs provide much important information during the electrocopolymerization and polymer film growth of

aromatic diamines. Furthermore, the electropolymerization of aromatic diamines by cyclic voltammetry through scanning potentials between 0 and +0.8 V at 2–50 mV/s for ca. 12 cycles has been successfully used for the fabrication of sensor,<sup>146,157,278</sup> as discussed in section IX.D.

### C. Constant Potential Electropolymerization

Although the polymer films from aromatic diamines can be prepared by repeated potential cycling, constant potential, and constant current electrolyses, the films prepared by the three techniques show a significant difference in their electroactivity, stability, and yield (or thickness). For example, the repeated potential cycling technique produces P15DAN film with better electroactivity and stability toward repetitive cycling than the constant potential electrolysis.<sup>173,177</sup> However, the polymerization yield is lower with the repetitive potential cycling than with constant potential electrolysis. There are only a few studies of constant potential electropolymerization of PDs and DANs. Malitesta et al. and Murphy studied the current–time profiles obtained during the constant potential electropolymerization of 5 mM three PD isomers in pH 7.4 phosphate buffer and 5 mM four substituted aminonaphthalenes in pH 1.0 NaCl/HCl at 0.65 V vs Ag/AgCl on Pt for 15 min.<sup>142,289</sup> A strongly acidic electrolyte is required for solubilization of the aminonaphthalenes because of their great hydrophobicity. All monomers exhibit a rapid decrease in current in the first 2 min and then a slow decrease in the following 13 min with polymerization time, indicating the formation of insulating films on electrode because the insulating films will block the electrode surface to any further electropolymerization. The current–time plot for P23DAN film formation differed from those for all the other monomers, exhibiting a much slower decrease in current with time, because the most positive oxidation potential of the 23DAN among all the monomers leads to a smaller amount of depositing P23DAN on the electrode than that of other monomer polymers at the same potential and time. It is observed that the constant potential electropolymerization of 23DAN at a higher potential of 0.85 V gave the same current–time profile as that observed for the other monomers at 0.65 V. The potentiostatic transients of 26DAPy at 10 mM in 0.1 M LiClO<sub>4</sub>/CH<sub>3</sub>CN has been studied.<sup>187</sup> For the potential steps from 0 to 0.95 V, the current decreases first very drastically to a very low value in the initial 50 s and then very slowly to a constant value in the following 250 s. At 1.01 V, corresponding to higher overpotential, a slow decrease in current in a period from 30 to 100 s along with a current maximum at 130 s was observed. The current maximum is characteristic of the nucleation and growth process.

It is reported that a thin, stable, and insoluble P*p*PD film can be obtained in 1 h at a constant potential of 0.7 V vs Ag/AgCl in KCl aqueous solution.<sup>170</sup> Similarly, a thin brownish-red P*m*PD film covering homogeneously on an electrode has been obtained also by electropolymerization of *m*PD at a constant potential 0.8 V vs Ag/AgCl in KCl solution

in nitrogen at room temperature.<sup>163</sup> The P*m*PD film is stable in both air and phosphate buffer. It is interesting that at 0.82 V potentiostatically in H<sub>2</sub>-SO<sub>4</sub> the initial electropolymerization rate of *m*PD on the PAN-film-coated Au electrode increased greatly compared with that on bare Au,<sup>168</sup> because the underlying PAN film can promote the *m*PD electropolymerization by providing electrocatalytic sites and nucleation centers. Moreover, the electropolymerization rate of *m*PD increased for at least 16 min with increasing thickness of pre-coated PAN film from 36 to 155 nm. After a certain period the polymerization rate of *m*PD gradually decreased because nonconducting P*m*PD covered the PAN substrate, resulting in the decrease in the electroactive sites.

Additionally, a significant influence of electrolyte composition on the formation of aromatic diamine polymer film by constant potential electrolysis has been revealed. Constant potential electrolysis of 1 mM 15DAN in 0.1 M LiClO<sub>4</sub>/acetonitrile at 0.4 V in the absence and presence of pyridine is studied.<sup>173</sup> The current of the monomer oxidation peak decreases as the quantity of electricity increases in the absence of pyridine. The true current is 0 when electrolysis was stopped, after the passage of a quantity of electricity of 2e<sup>-</sup> per molecule if without pyridine and 4e<sup>-</sup> per molecule in the presence of pyridine because pyridine is a proton acceptor and consequently prevents the protonation of the monomer.

Azzem et al. suggested that a blue thin P15DAN film has been successfully prepared by electrolysis at controlled potentials of 0.6–0.7 V in LiClO<sub>4</sub>/acetonitrile.<sup>175</sup> At higher potentials, the P15DAN film will be destroyed. However, no P15DAN film can be obtained for controlled potentials between 0.4 and 1 V in NaClO<sub>4</sub>/HClO<sub>4</sub>/water. It appears that organic solution is favorable to the constant potential polymerization of 15DAN.

Wei and Wu suggest that the current for the formation of P*o*PD film during the electropolymerization of *o*PD at 0.65 V in 0.1 M deaerated phosphate buffer (pH 7.0) on GC increases significantly upon adding a small amount of HRP and decreases at a lower rate with polymerization time than that without HRP.<sup>290</sup> The increase in electropolymerization rate induced by HRP can be explained by the function of HRP as counteranion into polymer substrate. Consequently, the enzyme plays an important role in constant potential polymerization of aromatic diamines.

Only one aromatic diamine copolymer obtained by constant potential polymerization is mentioned in the literature. Constant potential polymerization of *N*-phenyl-*o*PD with AN on an ITO-coated glass electrode provided a copolymer, which is confirmed by the appearance of an additional band at 520 nm in UV-vis spectra as compared with that of PAN.<sup>288</sup> The result is similar to that by the cyclic voltammetry.

In summary, the constant potential of 0.65–0.85 V could be favorable to the electropolymerization in order to prepare aromatic diamine polymers with electroactivity, redox stability, and environmental stability. Actually, the electropolymerization of aromatic diamines at 0.65 V for 15 min has been

successfully used for the fabrication of a sensor.<sup>289</sup> It should be appreciated that a very high potential varying from 1.8 to 2.2 V seems requisite for the preparation of good amounts of the poly(3-hydroxy-*o*PD) film on Pt by potentiostatic electropolymerization at the optimum time of 3 h.<sup>182</sup> It follows that the presence of a hydroxyl group on the *o*PD ring apparently passivates the electropolymerizing activity of *o*PD.

Sometimes aromatic diamine polymers formed by constant potential polymerization would dissolve in the reaction medium rather than deposit on the electrode. During the controlled potential electrolysis of 23DAPy, 23DAPy polymer is soluble in acidic and alkaline media employed, leading to a series of color variations.<sup>268</sup> For instance, the electrooxidation solution of 23DAPy in acidic medium changed its color from initial straw-yellow into ochre-yellow, orange, red, and finally brown-red. In alkaline medium, the color of the oxidized 23DAPy solutions changed from straw-yellow to ochre-yellow. Unfortunately none of the compounds corresponding to the different colors could be extracted with organic solvents in the whole pH range. By vacuum evaporation of the color solutions, a tar exhibiting brownish-red (in acidic medium) and orange (in alkaline medium) colors has been obtained but could not be purified.

#### D. Constant Current Electropolymerization

The reports of constant current electropolymerization of aromatic diamines are very few,<sup>155,168</sup> but constant current electropolymerization is of practical importance because this technique can produce thick films which are ordinarily difficult to form by constant potential polymerization.<sup>118</sup> Only three investigations on the constant current electropolymerization of three aromatic diamines have been summarized as follows. The constant current electropolymerization of 100 mM *o*PD in 100 mM *n*-Bu<sub>4</sub>NClO<sub>4</sub>/1,2-dichloroethane with an electrolysis time of 4 h on Pt (6.25 cm<sup>2</sup>) has been studied.<sup>155</sup> It is found that blackish-brown polymer forms and covers on the anode together with the precipitation of reddish-brown powder in the solution. The polymerization production of *Po*PD on the anode steadily increases from 135 to 310 mg with increasing current density from 1.6 to 6.4 mA/cm<sup>2</sup> at a constant temperature of 20 °C. The initial conductivity also increases from  $2.35 \times 10^{-7}$  to  $3.80 \times 10^{-7}$  S/cm. If at a fixed current density of 3.2 mA/cm<sup>2</sup>, both the polymerization production and conductivity of *Po*PD significantly increase from 148 to 316 mg and  $6.5 \times 10^{-8}$  to  $4.1 \times 10^{-7}$  S/cm, respectively, with decreasing polymerization temperature from 40 to 5 °C. At a constant optimal current density and temperature, the production, conductivity, and magnetic susceptibility of the *Po*PD obtained depend significantly on polymerization anode, solvent, or electrolyte. It appears that Ni is a better anode than Pt, 1,2-dichloroethane is a better solvent than nitrobenzene, dichloromethane, and acetonitrile, as well as tetra-*n*-butylammonium perchlorate is a better electrolyte than tetraethylammonium bromide and tetramethylammonium chloride. This constant current polymerization also gave

much higher polymerization production and conductivity of *Po*PD than cyclic voltammetric polymerization. These results show that the electropolymerization of *o*PD depends drastically on the reaction conditions.

Si et al. found that the potential for the electrooxidation of *m*PD with AN at a low current density of 26.7 mA/cm<sup>2</sup> increases almost linearly from 0.77 to 1.1 V vs SCE with polymerization time from 0 to 4 min.<sup>168</sup> Furthermore, the rate of the potential enhancement also increases with increasing feed *m*PD content. However, the potential of the AN oxidation decreases slightly because of the electrocatalytic function of PAN formed for the further polymerization of AN. The big difference in the potential variation with polymerization time suggests that the *m*PD attaching to the PAN inhibits the AN electropolymerization, just like the potential cycling copolymerization of *m*PD and AN.

The galvanostatic transient study indicates that a gradual potential rise is evident in the chronopotentiometric curve during the electropolymerization of 10 mM 26DAPy in 0.1 M LiClO<sub>4</sub>/CH<sub>3</sub>CN at a constant current 30 mA/cm<sup>2</sup> on Pt.<sup>187</sup> A sharp potential peak, suggesting the formation of three-dimensional nucleation and growth, appears at a polymerization time of 14 min, and then the potential remains at a medium constant value indicating a steady growth up to at least 37 min. Apparently the constant current for the electropolymerization of aromatic diamines could be a highly variable parameter, which is higher than 6.4 mA/cm<sup>2</sup> for *o*PD or lower than 26.7 mA/cm<sup>2</sup> for *m*PD. The investigation on the constant current electropolymerization of aromatic diamines is very inadequate for the purpose of optimization of reaction conditions in order to prepare novel multifunctional polymers.

#### E. Effect of Reaction Conditions on the Electropolymerization

The preparation conditions, including the type of monomer, polymerization solution, electrode, atmosphere, light, additive, and copolymerization, determine the electropolymerization process and the structure and properties of the resulting polymer film. It is found that *o*PD forms polymer film on electrochemical oxidation at nearly the entire pH range or in most common inorganic acid aqueous solutions listed in Table 2. *m*PD, *p*PD, DAN, and their derivatives all form polymer films on electrochemical oxidation in most common inorganic acid aqueous solutions at a pH value of lower than 7.0 or perchlorate acetonitrile solution listed in Tables 3 and 4. The electropolymerization of *N*-phenyl-*p*PD in aqueous H<sub>2</sub>SO<sub>4</sub> preferably gives an adhesive amorphous polymer film with the molecular structure similar to the AN tetramer,<sup>259</sup> which is quite different from the long and linear *para*-substituted polymer chain of the chemical oxidative polymerization product of AN or a more complicated two-dimensional structure partly containing *ortho*-substitution products obtained by the electropolymerization of AN. Electrode filming also occurs with the electrochemical oxidation of 4-carboxyl-*o*PD, but the film on Pt seems to be

unstable in the entire pH range due to the presence of carboxyl group.<sup>152</sup>

Sabbatini et al. pay attention to the effect of the pH value on polymer.<sup>291</sup> P $\alpha$ PD films were grown by cyclic voltammetry from solutions buffered at pH values of 1, 3, 5, and 7. XPS data show a structure intermediate between polyphenazine and PAN having stronger PAN character with increasing pH value.

The polymer films from the aromatic diamines are generally deposited upon Pt, Au, and graphite substrates. A few oxidizable metal electrodes such as stainless steel, mild steel, and aluminum have been used as substrates. Nevertheless, several metal oxide electrodes have also served as substrates for the formation of electrochemically active thin film. Electrodes of iridium oxide, ITO, OCS, etc., have been reported to be considerably more resistant to degradation in strong acids during the electropolymerization of the aromatic diamines. As shown in Table 17, the polymerization potential is changed with the type of monomers and electrodes. Further, the properties, including conductivity and mechanical properties, are affected. The surface roughness of the electrode (Au) does not affect the formation of the P $\alpha$ PD film; however, the amount of electrochemically active P $\alpha$ PD film is proportional to the real surface area (surface roughness) of the electrode.<sup>156</sup>

Yano et al. reported electronically stabilized P $\alpha$ PD and PHAN films.<sup>150</sup>  $\alpha$ PD and HAN are electrooxidized from H<sub>2</sub>SO<sub>4</sub> aqueous solution on PPTA film-coated ITO electrode. The two monomers can be electropolymerized on the ITO electrode surface because the PPTA film is permeable to the monomers. Furthermore, the PPTA film can serve as the protecting layer. The deposited amount of polymers is increased by the PPTA film because the PPTA film immobilized not only the corresponding polymer but also the oligomer species which are not immobilized by bare ITO electrode. In particular, the immobilized amount of PHAN is greater than that of P $\alpha$ PD. The P $\alpha$ PD and PHAN films are electronically stabilized and durable against oxidative degradation. The electropolymerization efficiency of  $\alpha$ PD at a constant current density of 1 mA/cm<sup>2</sup> for 5 min is also enhanced by the PPTA film. The charge of the P $\alpha$ PD deposited is 1.4 times larger on the PPTA film-coated electrode than on the naked electrode.

Thomas and Euler reported the effect of atmosphere and light on the electropolymerization of DAPh.<sup>292</sup> Both atmospheric oxygen and light catalyze the polymerization of DAPh in 0.2 M Na<sub>2</sub>SO<sub>4</sub>/H<sub>2</sub>SO<sub>4</sub> (pH = 1) at 25 °C by cyclic voltammetry between -0.8 and +1.2 V. They also found that the PDAPh and P $\alpha$ PD films electropolymerized under identical conditions have some similarities but are distinctly different in molecular structure, electrochemical properties, and visible reflectance spectra. The structural differences arise from different coupling positions between monomers during polymerization. Both polymers are primarily PDAPhs, having mostly phenazine repeat units with few extended ladder segments. PDAPh couples repeat units through the 1,3-position and has few quinonediimine segments. In contrast,

P $\alpha$ PD couples the repeat units through the 2,4-positions of the phenazine ring and contains a substantial number of quinonediimine units.

Gao and co-workers found that a laser could induce selective local electropolymerization of  $\alpha$ PD, which is nearly identical to that of the P $\alpha$ PD formed under the normal conditions of electropolymerization.<sup>274</sup> They assumed that the laser-inducing thermal effect is the most likely influence on the electropolymerization kinetics, as the temperature rise at the illuminated surface area results in a considerable shift of the equilibrium potential (from 0.8–0.9 to -0.3–0.5 V).

Yacynych and Mark studied the spectroelectrochemical behaviors on the oxidation of  $\alpha$ PD alone and in the presence of an additive such as Ni(NO<sub>3</sub>)<sub>2</sub> using an optically transparent Pt electrode.<sup>112</sup> It is indicated that almost the same CV characteristics were observed both with and without Ni(NO<sub>3</sub>)<sub>2</sub> in supporting electrolyte of 0.1 M phosphate buffer solution (pH = 7). However, there are significant differences in the rate and nature of the electrode filming on the oxidation of  $\alpha$ PD. The filming nature of  $\alpha$ PD oxidation in Ni(NO<sub>3</sub>)<sub>2</sub>-free solution is independent of time and potential. A conducting film is initially formed, and on top of this, a nonconducting film forms and eventually insulates the electrode. With Ni(NO<sub>3</sub>)<sub>2</sub> present, the oxidation reaction of  $\alpha$ PD is potential dependent but not time dependent. At lower potentials a Ni-containing product is formed which does not coat the electrode, therefore finally forming a precipitate having a relatively high molecular weight. At higher potentials, the polymer is the same insulating film which coated the electrode in the oxidation of  $\alpha$ PD without the presence of Ni<sup>2+</sup>. With adding Ni(NO<sub>3</sub>)<sub>2</sub> at lower potentials, the monocation radical formed by the oxidation of  $\alpha$ PD predominates, but at higher potentials the formation of the dication could predominate. At lower potentials the rate of the monocation polymerization on the electrode is slow compared to the complexation rate with Ni<sup>2+</sup>, which forms a soluble intermediate product. Therefore, the polymer aggregates and precipitates from solution. At high potentials, the dication is preferentially formed, then polymerizing on the electrode surface and forming the insulating film. The polymerization products are pH dependent, with electrode filming occurring at lower and middle pH but not at high pH. In particular, the electrooxidation of  $\alpha$ PD forms a strongly adhering and highly colored film at low pH values. In summary, the electropolymerization conditions should be carefully selected and critically controlled in order to obtain applicable polymer films from aromatic diamines.

Generally, low polymerization yield is a deficiency in the electropolymerization. The relationship between the polymerization conditions and yield is significant to increase the yield. The yield of electropolymerized PBZ has been studied by changing the number of potential cycles, solution pH, temperature, and electrolyte concentration.<sup>116,189</sup> It is found that at a constant pH 2.5 and 35 °C the PBZ yield (i.e., anodic charge) increases linearly with the cycling number from 0 to 50 with a slope of  $3.6 \times 10^{-3} \mu\text{C}$

$\text{cm}^{-2} \text{ cycle}^{-1}$ .<sup>189</sup> A similar linear relation between the anodic charge and cycling number during the electropolymerization of naphthidine was observed but with much larger slope of  $100 \mu\text{C cm}^{-2} \text{ cycle}^{-1}$ .<sup>190</sup> Therefore, the thickness of the PBZ and polynaphthidine films could be controlled by the number of potential cycles. When the pH increases from 1.2 to 3.5 at a fixed potential cycle of 10, the yield of the PBZ reaches a maximum and then decreases in temperature 18–45 °C.<sup>189</sup> The pH corresponding to the maximum increases from 2.2, 2.63, 2.74, to 2.8 with elevating temperature from 18, 26, 35, to 45 °C. However, at 10 °C, the yield seems to increase slightly and monotonically with pH. The polymerization yield increases monotonically with temperature. In particular, the yield in a pH range of 2.4–3.2 increases dramatically with increasing temperature from 10 to 45 °C. A good condition for the formation of the PBZ film is repetitive cycling between 0 and 0.75 V in an aqueous  $\text{HClO}_4$  solution of benzidine at pH 2.5 and 35 °C. It is found that the PBZ yield seems to increase linearly from 2% to 27% with increasing HCl or  $\text{NaClO}_4$  concentration from 0.1 to 2 M.<sup>116</sup>

## F. Electrocopolymerization

A stable conductive polymer is very important for such practical applications as the rechargeable battery and in potential switching application. Electrocopolymerization of AN with a small amount of *p*PD and sulfonic *p*PD will improve the growth rate, stability, molecular weight, and conductivity of PAN film. Addition of a very small amount of *p*PD provides a means of producing large quantities of PAN film rapidly for commercial processes with no undesirable byproducts.<sup>287</sup> However, the function of *m*PD is opposite. Yang and Wen electroprepared the film of *p*PD-AN copolymer.<sup>169</sup> They found that the film-growth rate was strongly dependent on the concentration of *p*PD monomer. At *p*PD concentrations lower than 18.5 mM, the rate of polymer formation on an  $\text{IrO}_2$ -coated titanium electrode increased with increasing *p*PD concentration, while at concentrations larger than 50 mM, the growing rate of the polymer film was depressed. Similarly, a strong increase of polymer layer growth is observed by adding of a small amount of *p*PD to the AN solution.<sup>286</sup> The catalytic effect of *p*PD on the AN electropolymerization included its contributions to both the autocatalysis and the external catalysis. The greatest acceleration of the electropolymerization rate was obtained at the *p*PD/AN molar ratio of ca. 1/5, whereas a further increase in the *p*PD molar fraction leads to a continuous decrease of the electropolymerization rate. Note that even at a *p*PD/AN molar ratio of ca. 1/2 the growth rate of copolymer film exceeds that of pure PAN film. In a solution containing equimolar quantities of both monomers, the growth rate decreases to a small value. In addition, the stability of this film can be promoted about 10% in comparison with that of PAN film if the solution used for polymer growth contained 0.5–18.5 mM *p*PD, but the stability of the film is reduced if higher than 50 mM *p*PD.

It is contrary to the chemical oxidative polymerization that addition of *p*PD with an appropriate

concentration of about 0.5–5 mM resulted in a electropolymerized PAN with higher molecular weight (30 000), narrower molecular weight distribution, and higher conductivity, which were closely related to the contribution of *p*PD to the autocatalysis and external catalysis in the 1.3 M AN polymerization.<sup>203</sup> With increasing *p*PD concentration from 10, 50, to 100 mM, the molecular weight of the polymer obtained decreased from 2200–30000, 1200–6400, to 1200–5000 due to many reactive centers from *p*PD. However, the molecular weight distribution appears to be the widest at a *p*PD concentration at 10 mM. With increasing *p*PD concentration from 0, 0.5, 5, 50, to 100 mM, the conductivity of the polymer obtained is 12.5, 38.7, 43.3, 12.5, to 6.4 S/cm, respectively. *p*PD concentration at 5 mM favored the formation of higher molecular weight and longer  $\pi$ -conjugated PAN, leading to a maximum conductivity. Elemental analysis also indicates an insertion of *p*PD into PAN main chain by a cross-linking function.

During electrocopolymerization of *p*PD and AN, cross-linking reaction and *p*-hydroxyaniline/BQ-imine side reaction occur simultaneously, with the former predominating at *p*PD concentration lower than 18.5 mM, but with the side reaction predominating at *p*PD concentration higher than 50 mM.<sup>169</sup> It is suggested that the resulting *p*PD/AN copolymer has many cross-linking sites between linear PAN chains.<sup>286</sup> Terminal amino groups should be present in the structure of the copolymer, similar to the copolymer of *m*PD and AN.

Similarly, the copolymerization rate of sulfonic *p*PD with AN is also strongly dependent on the amount of sulfonic *p*PD in the comonomer feed.<sup>169</sup> Sulfonic *p*PD acts as an accelerator for AN-sulfonic *p*PD copolymerization and gives rise to more nucleation sites (quinonediimines), thereby increasing the copolymerization rate. More facile quinonediimine formation with adding sulfonic *p*PD s can induce cross-linking sites—phenazinic structure and generate diradical dications in the bipolaronic form of pernigraniline, which establish an equilibrium with their other resonance form, protonated quinonediimine.<sup>173</sup> The four types of resonance structures of *o*PD, *m*PD, and *p*PD dication diradicals with planar conformations have been studied.<sup>293</sup> A special dependence of the benzidine/diphenylamine copolymerization rate on temperature was observed.<sup>189</sup> The rate increases with the temperature from 0 to 37 °C but decreases with a further increase to 50 °C. By increasing the pH of the polymerization solution from 0.8 to 6 or the benzidine content, the yield and rate of the formation of benzidine/diphenylamine copolymer decrease, indicating that the polymerization is accompanied by a proton exchange reaction and the diphenylamine shows much higher electropolymerizing reactivity than benzidine. The optimum conditions for the benzidine/diphenylamine copolymerization were introduced.

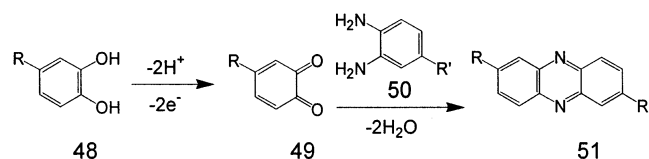
In addition, Park et al. found that resorcinol can also increase the stability of *Po*PD and *Pm*PD films on carbon electrode by the electrocopolymerization of *o*PD and *m*PD with resorcinol for the fabrication of biosensor.<sup>294</sup> Malinauskas et al. prepared copoly-

mer and bilayer structures consisting of PAN and P $\alpha$ PD.<sup>162</sup>

Note that a different electrocopolymerization behavior is observed for *m*PD with AN system. Mazeikiene and Malinauskas prepared *m*PD-AN copolymer in sulfuric acid solution.<sup>285</sup> They found that at a high molar fraction of *m*PD (above 50%), a strong inhibition of electropolymerization appeared, which is contrary to *p*PD and its derivatives. Copolymerization was found to be possible only at low *m*PD/AN molar ratio, but the polymerization rate is low. There may be some side chains in the structure of *m*PD/AN copolymer because of the presence of *m*-amino groups in the *m*PD, leading to low electrical conductivity of the copolymer and, as a result, the low rate of electropolymerization.<sup>295</sup> It appears that the growth of *m*PD/AN copolymer is sustained by the *m*PD attaching to the oxidized AN end group.<sup>168</sup> It is reported that an increase in the electropolymerization rate of *m*PD on an electrode just covered with a layer of PAN was observed. In the opposite case, a significant decrease in AN electropolymerization rate was observed on P*m*PD-film electrode.<sup>285</sup> This rate decreases progressively with thickening of the underlying P*m*PD film. In summary, electrocopolymerization is a really efficient technique of significantly increasing the polymerization rate of AN and enhancing the molecular weight and stability of the polymer films from both AN and aromatic diamines.

It is interesting that the electrocopolymerization of *o*PD and catechol (and two catechol derivatives, 3,4-dihydroxybenzoic acid and 3,4-dihydroxycinnamic acid) in neutral phosphate buffer is used to significantly enhance incorporation of phenazine groups into the polymer backbone, based on the mechanism in Scheme 17.<sup>144</sup>

#### Scheme 17



In Scheme 17 R = H for catechol, COOH for 3,4-dihydroxybenzoic acid, and CH=CHCOOH for 3,4-dihydroxycinnamic acid and R' = H or a polymer chain. As compared with the phenazine unit containing P $\alpha$ PD film grown from HCl solution at pH = 1, the *o*PD/catechol polymer obtained thus exhibits similar redox potentials but enhanced redox activity. The redox peak current of the polymer increases proportionally with increasing catechol concentration from 2 to 10 mM at a constant *o*PD concentration of 10 mM. These results indicate an increase in the content of phenazine redox groups in the polymer chains. Excess catechol results in a further increase but the increasing rate becomes lower.

### G. Spectroscopic Characteristics and Molecular Structure

Several important spectroscopic analyses of aromatic diamine polymers by electropolymerization are reviewed below.

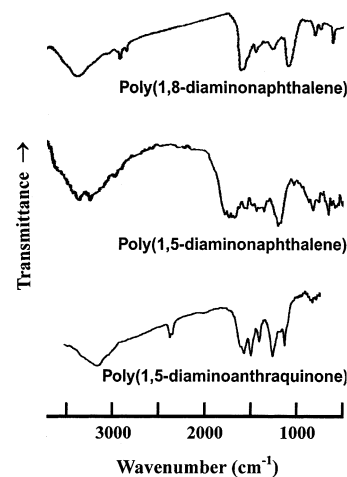


**Figure 12.** FT-IR spectra of poly(1,8-diaminonaphthalene)- (P18DAN),<sup>296</sup> poly(1,5-diaminonaphthalene)(P15DAN),<sup>173</sup> and poly(1,5-diaminoanthraquinone)(P15DAAQ)<sup>227</sup> prepared by electropolymerization.

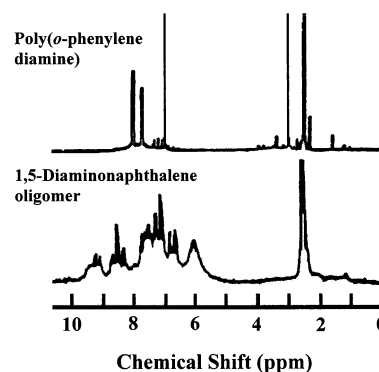


**Figure 13.** <sup>1</sup>H NMR spectra in DMSO-*d*<sub>6</sub> of poly(*o*-phenylenediamine) (P $\alpha$ PD) at 270 MHz<sup>164</sup> and 1,5-diaminonaphthalene oligomer<sup>173</sup> prepared by electropolymerization.

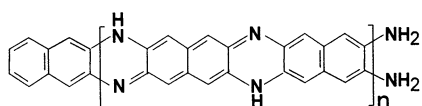
#### 1. IR and <sup>1</sup>H NMR Spectroscopy

The properties and applications of polymers are intrinsically decided by their structure. Each polymer of aromatic diamine has its own structural and spectroscopic character. Until recently, there has been limited research on the spectroscopic characteristics and molecular structure of aromatic diamine polymers prepared by electropolymerization. The molecular chain structure and typical IR and <sup>1</sup>H NMR spectra of the polymers prepared from aromatic diamines by electropolymerization are shown in Figures 12 and 13 and Tables 8 and 10. Apparently the IR and <sup>1</sup>H NMR characteristics of the polymers depend significantly on the aromatic diamine types and polymerization method.<sup>173,164,227,296</sup> The P $\alpha$ PD film prepared by cyclic voltammetry exhibits a different IR spectrum from that by potentiostatic method.<sup>297</sup> The P $\alpha$ PD also exhibits quite different NMR features as compared with that of the P $\alpha$ PD obtained by chemically oxidative polymerization shown in Figures 2–5. It is found from the molecular formula listed in Table 13 that the P $\alpha$ PD shows higher nitrogen content and much higher hydrogen content than the P $\alpha$ PD prepared by chemically oxidative polymerization. All of these indicate that the molecular structure

of the aromatic diamine polymers depends intensively on their polymerization method. Detailed spectroscopic characteristics of the polymers are shown in Tables 8, 10–12, and 18.

Most of aromatic diamines can polymerize and form a ladder structure including the fully reduced form, semi-oxidized form, and fully oxidized form, depending on the electropolymerization conditions. From the result of in-situ electric conductivity, it is proposed that P $\phi$ PD has four kinds of molecular structure and a simple reaction procedure in the redox process. Martinusz et al. studied the accompanying mass change of P $\phi$ PD film electrode in the redox process by using quartz crystal microscale technology and induced the main reaction process in various pH values.<sup>151</sup> There now exist two dominant ideas about the structure of P $\phi$ PD, a ladder-like and linear structure. Chiba et al. considered the P $\phi$ PD structure as a ladder polymer with phenazine rings.<sup>298</sup> Lin et al. also thought of P $\phi$ PD as a semi-ladder polymer with some opening rings.<sup>295</sup> However, Yano speculated P $\phi$ PD as a linear chainlike polymer mainly containing 1,4-substituted benzenoid–quinoid structure,<sup>164</sup> as shown in Table 8. In fact, the diversity of the P $\phi$ PD macromolecular structures resulted from the different polymerization conditions. For example, it is suggested that the structure of P $\phi$ PD is mainly a phenazine unit containing ladder polymer at lower  $\phi$ PD concentration during electropolymerization but a linear polyaminoaniline at higher  $\phi$ PD concentration.<sup>299</sup> Similarly, Oyama et al. proposed nearly the same ladder structure (Scheme 18) for P23DAN.<sup>139,188</sup>

#### Scheme 18



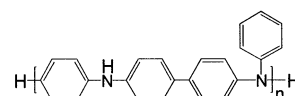
52: Poly(2,3-diaminonaphthalene)

In-situ multiple internal reflection FTIR spectroscopy has been used to investigate the structural development during the formation of P15DAN film in acidic acetonitrile by potential cycling.<sup>282</sup> The P15DAN film formed during the initial 10 potential scans does not seem to exhibit any valuable absorption except for an absorption at 1098  $\text{cm}^{-1}$  due to  $\text{ClO}_4^-$ . The P15DAN film formed after 18–20 potential scans exhibits weak absorptions at ca. 1600 and 800  $\text{cm}^{-1}$ . Only the P15DAN film formed at 30 potential scans exhibits a medium peak at 1602–1576  $\text{cm}^{-1}$  due to a C=C aromatic stretch, a shoulder at 1648  $\text{cm}^{-1}$  due to a C=N stretch, a medium and weak peak at 1300 and 1250/1222  $\text{cm}^{-1}$  due to the C–N stretch in C–NH<sub>2</sub> and C–NH–C, respectively, the bands at 3436/3350 and 3232  $\text{cm}^{-1}$  due to a N–H stretch and bending in –NH<sub>2</sub>, respectively, a band at 3142  $\text{cm}^{-1}$  due to a N–H stretch in the –NH<sub>2</sub> and –NH–, and bands at 752 and 820/797  $\text{cm}^{-1}$  due to C–H out-of-plane vibrations of three and two adjacent aromatic hydrogen atoms, respectively. In-situ IR spectra of the P15DAN films in the oxidized form at +0.7 V and reduced form at 0 V suggest that an alternating sequence of benzenoid and quinoid rings exists in the oxidized form.

The IR spectrum for as-grown PDTDA film by the electropolymerization of 20 mM 2,2'-dithiodianiline in 0.2 M  $\text{HClO}_4$  + 0.4 M  $\text{LiClO}_4/\text{CH}_3\text{CN} + \text{H}_2\text{O}$  was almost the same as that of the quinoid structure of PAN (emeraldine base) itself except for a strong absorption peak at 750  $\text{cm}^{-1}$  due to C–S bond.<sup>270</sup> No absorption peak at 1100  $\text{cm}^{-1}$  due to S=O bond was found, indicating that the disulfide (S–S) bond was not further oxidized but preserved in the polymer during the electropolymerization.

PPBZ electropolymerized at a scan rate of 100 mV/s from –1.0 to +2.2 V vs Ag/AgCl on ITO in 0.15 M  $\text{Et}_4\text{NBF}_4/\text{CH}_3\text{CN}$  exhibits several IR absorption peaks: strong and broad peaks at 690, 745, and 810  $\text{cm}^{-1}$  due to a C–H bend and a weak and broad peak at 3392  $\text{cm}^{-1}$  due to the N–H stretch in secondary amine.<sup>230</sup> The macromolecular structure of PPBZ has been proposed in Scheme 19.

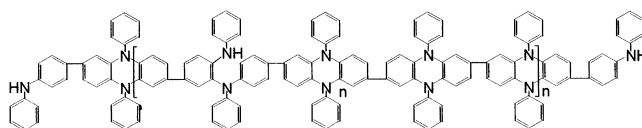
#### Scheme 19



53: The first possible structure of PPBZ

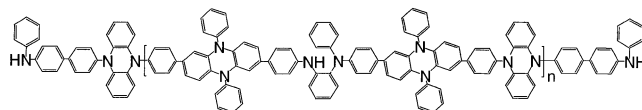
PBZ electropolymerized at the same conditions exhibits a strong absorption at 3380 or 3427  $\text{cm}^{-1}$  due to the N–H stretch in secondary amine,<sup>189,230</sup> several absorptions at 1610  $\text{cm}^{-1}$  due to C=N stretch, 1350 and 1280  $\text{cm}^{-1}$  due to C–N stretch, and 1000  $\text{cm}^{-1}$  due to C–H out-of-plane bending in 1,2,4-trisubstituted benzene rings.<sup>189</sup> Noteworthy is that the IR spectrum of the PBZ prepared by chemically oxidative polymerization with ammonium persulfate in

#### Scheme 20



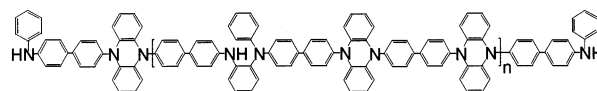
54: The second possible structure of PPBZ

#### Scheme 21



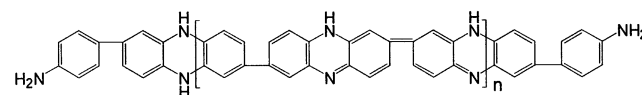
55: The third possible structure of PPBZ

#### Scheme 22



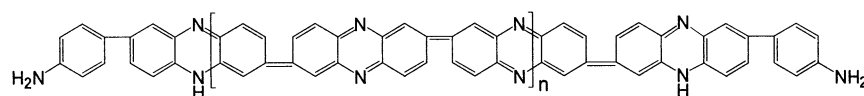
56: The fourth possible structure of PPBZ

#### Scheme 23



57: The possible structure of PBZ formed by electropolymerization

## Scheme 24



58: The possible structure of PBZ by chemically oxidative polymerization

**Table 18. Raman Spectral Characteristics (wavenumber,  $\text{cm}^{-1}$ ) of the Polymers from Aromatic Diamines Prepared by Electropolymerization on Au, Pt, or Ag Electrodes**

polymers	electrode potential (V)	phenazylene					refs
		C=C stretching	C=N stretching	ring stretching	C-N stretching	C-H deformation	
poly( <i>o</i> -phenylenediamine) on Au in 200 mM phosphate buffer (pH = 7)	0.3	1596m	1440m	1396s 1367s	1265br	1032w 711s (C-H stretching)	277
poly( <i>o</i> -phenylenediamine) on Au in 1 M $\text{H}_2\text{SO}_4$	0.5	1606w 1412s	1446w	1375w	1254w	1026 s	99
poly( <i>o</i> -phenylenediamine) on Pt in 1 M $\text{H}_2\text{SO}_4$	0.6	1620w 1580w	1455w 1415s	1365w	1255w	1055w	162
<i>o</i> -phenylenediamine/aniline (1/9) copolymer on Pt in 1 M $\text{H}_2\text{SO}_4$	1.1	1620m (benzenoid) 1585m (quinoid)	1415w	1365w	1175s	1060w	162
poly(1,8-diaminonaphthalene) on Pt in 0.1 M $\text{LiClO}_4/\text{HClO}_4$	-0.6	1590s		1365s 1300s	1130w		296
poly(1,8-diaminonaphthalene) on Au in 0.1 M $\text{LiClO}_4/0.1$ M $\text{HClO}_4$	0.4	1620s		1300b			296
poly(1,8-diaminonaphthalene) on Au in 0.1 M $\text{LiClO}_4/0.1$ M $\text{HClO}_4$	-0.2	1620s 1580b	1470w	1365b 1300m			226
poly(1,8-diaminonaphthalene) on Ag in 0.1 M $\text{LiClO}_4/0.1$ M $\text{HClO}_4$	-0.2	1630s 1580b		1380b 1300m	1280m		226
poly(1,8-diaminonaphthalene) on Pt in 0.1 M $\text{LiClO}_4/0.1$ M $\text{HClO}_4$	0	1620s 1580w		1365w 1300b	1280w		226

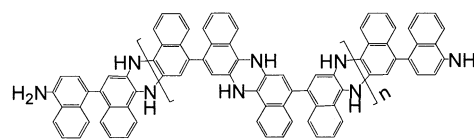
neutral acetonitrile aqueous solution at 5 °C does not exhibit a N-H stretch vibration but exhibits strong absorptions at 1613 (C=N), 1531/1500 (C-C), and 1140, 1090, and 1010  $\text{cm}^{-1}$  (C-H out-of-plane bending in 1,2,4-trisubstituted benzene rings), as well as medium absorptions at 1340/1290  $\text{cm}^{-1}$  (C-N).<sup>235</sup> However, the macromolecular structure of the PBZ has not been mentioned. On the basis of the IR,<sup>189</sup> NMR (Table 10), and UV-vis (Tables 11 and 12) spectra and elemental analysis (Table 13), the authors of this review article speculate the four macromolecular structures of electropolymerized PPBZ and PBZ shown in Schemes 20–23.

The four macromolecular structures of the PPBZ need to be further approved by XPS and solid-state high-resolution NMR spectroscopy. The macromolecular structure of the PBZ polymerized chemically oxidative based on the IR spectrum, high crystallinity, and insolubility<sup>235</sup> is proposed in Scheme 24. This macromolecular structure also needs to be further approved by XPS and solid-state high-resolution NMR, UV-vis spectroscopy, and elemental analysis.

Polynaphthidine electropolymerized at a fixed potential of 1.02 V on Pt of a large area (16  $\text{cm}^2$ ) exhibits several characteristic absorptions at 3420  $\text{cm}^{-1}$  due to the N-H stretch in secondary amine, 1620  $\text{cm}^{-1}$  due to the C=N stretch, 1350 and 1280  $\text{cm}^{-1}$  due to the C-N stretch, and 840/760  $\text{cm}^{-1}$  due to C-H out-of-plane bending in benzene rings with two/four adjacent hydrogens.<sup>190</sup> The IR characteristics of the polynaphthidine are very similar to those of the PBZ due to their similar characteristics of monomer

structure and electropolymerization. Therefore, a possible macromolecular structure of the polynaphthidine is shown in Scheme 25. This structure should

## Scheme 25



59: Polynaphthidine

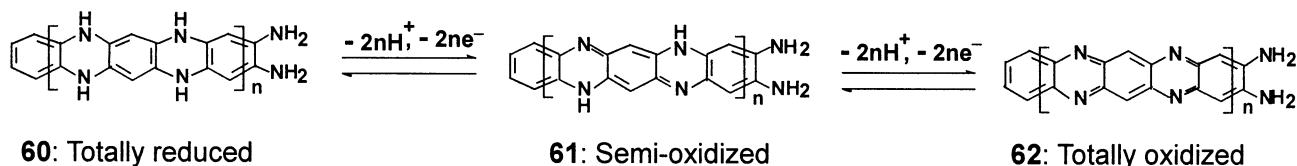
be further confirmed by UV-vis and XPS spectroscopies of the thin film of the polynaphthidine.

## 2. Raman Spectroscopy

Raman spectroscopy is helpful in studying the formation and redox state of macromolecular structure of aromatic diamine polymers during the electropolymerization. Wu et al. studied the redox mechanism of P $\alpha$ PD film in acid solution by electrochemical in-situ resonance Raman and UV-vis substructure reflectance spectroscopy.<sup>99,100</sup> The results of the cyclic voltammetry show that the redox process of P $\alpha$ PD is controlled by the surface process and that there are three steady redox states during the redox process. Qualitatively electrode potential-dependent Raman spectral characteristics of P $\alpha$ PD and PDAN prepared by electropolymerization are summarized in Table 18. It appears that +0.1 V vs SCE is a turnover potential at which the reorientation and electropolymerization of  $\alpha$ PD occurred.<sup>277</sup> The apparent feature is that the



## Scheme 26



intensity of the band at  $1410\text{ cm}^{-1}$  changes significantly with electrode potential and reaches almost the same maximum at 0 and  $+0.2\text{ V}$  vs SCE. This implies that two electrode potentials of 0 and  $+0.2\text{ V}$  vs SCE are correspondent to the same semi-oxidized state of PöPD. When the potential increases to  $0.5\text{ V}$  vs SCE, the intensity at  $1410\text{ cm}^{-1}$  decreases to 65.2% of the maximum, since the transition from a semi-oxidized state of 33.3% to a total-oxidized state occurred. The band at  $1410\text{ cm}^{-1}$  disappears completely at  $-0.2\text{ V}$  vs SCE, which corresponds to the reduced state of PöPD. A recent investigation has also suggested that in Raman spectra of PöPD the band at  $1415\text{ cm}^{-1}$  prevails over others.<sup>162</sup> This band diminishes in intensity after a positive potential shift from 0.1 to 0.6 V vs RHE. The same tendency was also observed with a bilayer PAN–PöPD-modified electrode. In the latter case, the band at  $1415\text{ cm}^{-1}$  is much more intense than in the case of PöPD, indicating the influence of the underlying PAN film which increases the electropolymerization rate of öPD, as compared with bare Pt. Note that both peaks at 1620 and  $1585\text{ cm}^{-1}$  corresponding to benzenoid and quinoid structures, respectively, are present even at low potential values. The relationship between the intensity of the band at  $1415\text{ cm}^{-1}$  and electrode potential shows a clear maximum in a potential range from 0.2 to 0.3 V vs RHE, both in the case PöPD-modified and bilayer PAN–PöPD-modified electrodes. It follows that the band at  $1415\text{ cm}^{-1}$  is the most intense in the partially oxidized form of the PöPD, which bears the maximum concentration of charge carriers. A two-electron redox mechanism, consisting of a few overlapping redox processes, was proposed for PöPD and its derivatives. A fully reduced form of PöPD, consisting of repeat unit of 5,10-dihydrophenazine, is oxidized by one electron to phenazyl or its protonated form depending on the pH value and further by the second electron to the phenazine (fully oxidized form), which may also exist in a protonated state.<sup>162</sup> The strong Raman band at  $1410\text{--}1415\text{ cm}^{-1}$  may correspond to the half-oxidized phenazyl-like structure that has a free radical character and is related to charge carriers. Therefore, it is concluded that there are three structures (Scheme 26) during the redox process of PöPD film in strong acid solution.

Among them, the semi-oxidized structure existing from 0.0 to  $+0.2\text{ V}$  is the most stable state while both the totally reduced structure at  $-0.2\text{ V}$  and the totally oxidized structure at  $+0.5\text{ V}$  are generally unstable.<sup>99</sup> The totally reduced PöPD is almost colorless and unstable in air, for it is oxidized rapidly to semi-oxidized brown PöPD.<sup>100</sup> Therefore, the resonance Raman spectrum of PöPD film in a 1 M  $\text{H}_2\text{SO}_4$  solution is significantly influenced by protonation. Ex situ the resonance Raman spectrum of PöPD

at open circuit potential exhibits a strong and sharp band at  $1410\text{ cm}^{-1}$  and several bands at 1052, 982, and  $898\text{ cm}^{-1}$ , very similar to that at electrode potentials from 0.0 to  $+0.2\text{ V}$ . If the PöPD film is thoroughly rinsed with water to scavenge the residual  $\text{H}_2\text{SO}_4$ , the bands at 1052, 982, and  $898\text{ cm}^{-1}$  due to  $\text{H}_2\text{SO}_4$  vanish and the strongest band at  $1410\text{ cm}^{-1}$  shifts to a lower wavenumber ( $1394\text{ cm}^{-1}$ ) as well as decreases greatly in intensity. When the nonbonding electron pairs of nitrogen atoms are released from bonding with hydrogen ions by deprotonation, the energy level of the highest bonding  $\pi$  orbital in PöPD would shift to that of the lowest antibonding  $\pi^*$  orbitals, resulting in a shift of the electronic absorption bands and a decrease in the Raman intensity. Additionally, the deprotonation would decrease the electronegativity of nitrogen atoms and then weaken the strength of the C–N  $\sigma$  bond in PöPD, leading to a red shift from 1410 to  $1394\text{ cm}^{-1}$  in the Raman spectra. Further, the resonance Raman spectra not only verify the existence of the three redox states of PöPD, but also indicate that the structure of PöPD is dominated by a ladder polymer with phenazine rings.

In-situ surface-enhanced Raman spectroscopy has been employed to confirm the cleavage and recombination of the S–S bond in the electropolymerized film, shown in Figure 14.<sup>231,270</sup> The strong peak at  $540\text{ cm}^{-1}$  due to the stretching vibration of the S–S bond in PDTDA disappeared from  $+0.1$  to  $+0.2\text{ V}$  on reduction or discharging and reversibly appeared at  $+0.4\text{ V}$  on oxidation or charging. In a solution at pH 2.0, the peak at ca.  $440\text{ cm}^{-1}$  assigned as out-of-plane bending C–S–H vibrations appeared again at  $+0.1\text{ V}$  on reduction and disappeared at  $+0.5\text{ V}$  on oxidation, indicating that the electrochemically reduced thiolate is protonated to a thiol. In the case of pH 2.5 and 3.0, unlike that of pH 2.0, the change in peak intensity at ca.  $440\text{ cm}^{-1}$  with the potential was not observed, suggesting that the protonation reaction did not occur, and in these pH values the PDTDA exists as the thiolate form. The PDTDA shows two reduced forms: a thiol form in a more acidic solution with  $\text{pH} < 2.5$  and a thiolate form in a more basic solution with  $\text{pH} > 2.5$ . The thiol and thiolate forms are in equilibrium states at pH 2.5.

In-situ Raman spectroscopy has been used to assess the oxidation state of the metal ion-treated P18DAN films formed at various polarization potentials and compared with the ex-situ Raman spectroscopy.<sup>226,299</sup> It is found from the in-situ resonance Raman spectra that the totally reduced P18DAN at  $-0.6\text{ V}$  on Pt electrode in 0.1 M  $\text{LiClO}_4/0.1\text{ M HClO}_4$  shows a strong band at  $1580\text{ cm}^{-1}$  and two well-separated bands at 1300 (relatively sharp) and  $1365\text{ cm}^{-1}$  (broad) by using the excitation line at 514.5 nm of the  $\text{Ar}^+$  ion laser. The fully oxidized state at  $+0.4$

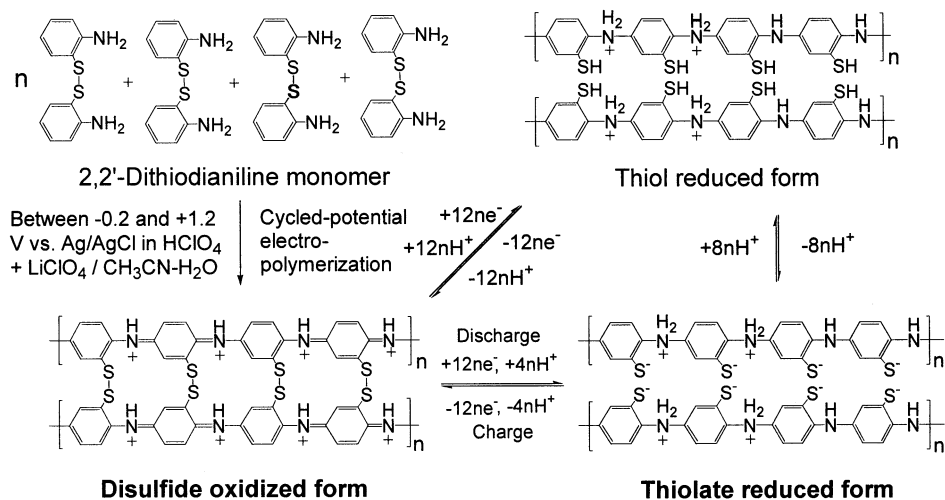


**Figure 14.** Electrochemical cleavage and recombination process of the disulfide (S–S) bond between the conducting polymer chains in poly(2,2'-dithiodianiline) with discharge and charge.<sup>270</sup>

$V$  shows a strong band at  $1620\text{ cm}^{-1}$  and a very broad band at ca.  $1300\text{ cm}^{-1}$ . The Raman spectra of the P18DAN at 0 and  $-0.2\text{ V}$  combine the characteristics at  $-0.6\text{ V}$  with  $+0.4\text{ V}$ . All these bands may involve naphthalene ring motions. In addition, all ex-situ Raman spectra of P18DAN films after keeping for 1 h in four solutions conditioning  $0.1\text{ M HClO}_4/1\text{ mM Hg}^{2+}$ ,  $0.1\text{ M HClO}_4/100\text{ mM Cu}^{2+}$ ,  $0.1\text{ M HClO}_4/100\text{ mM Ag}^+$ , and  $0.1\text{ M HClO}_4/1\text{ mM Ag}^+$  show almost the same strongest band at ca.  $1620\text{ cm}^{-1}$  and slightly different spectral characteristics at  $1580\text{ cm}^{-1}$  as well as between  $1260$  and  $1370\text{ cm}^{-1}$ . These indicate that the majority of all the four films are oxidized, but the films conditioned in acidic  $\text{Cu}^{2+}$  and more dilute  $\text{Ag}^+$  solutions remain partly reduced. Raman spectroscopy has been used to investigate the electrooxidation of 18DAN on gold, silver, and copper electrodes in detail with switching electrode potential from  $-0.2$  to  $+0.2\text{ V}$  and returning to  $-0.2\text{ V}$ .<sup>225</sup>

Raman spectroscopy has also been used to study the redox process of poly(ANO) thin film electropolymerized by cyclic voltammetry between 0 and  $0.7\text{ V}$  vs SCE at  $50\text{ mV/s}$  in four electrolytes including HCl, HClO<sub>4</sub>, *p*-toluenesulfonic acid, and camphorsulfonic acid containing  $1\text{ mM ANO}$  for 15 min.<sup>193,280</sup> The ex-situ Raman spectrum of the film in its oxidized form with  $457.9\text{ nm}$  laser line excitation exhibits a strong band at  $1595\text{ cm}^{-1}$  due to C=C stretch in benzenoid ring, a medium band at  $1372\text{ cm}^{-1}$  due to C–N stretch, and a weak shoulder at  $1635\text{ cm}^{-1}$  due to C=N stretch and a phenazine structure formed by 'ortho coupling' of the aromatic rings during polymerization to some extent. The ex-situ resonance Raman spectrum of the oxidized film with  $350.7\text{ nm}$  excitation exhibits a very strong band at  $1610\text{ cm}^{-1}$  along with a medium broad band at  $1375\text{ cm}^{-1}$  that are not well resolved. In-situ Raman spectra with  $457.9$  (or  $488$ ) nm excitation of the poly(ANO) film formed in HClO<sub>4</sub> or HCl and camphorsulfonic acid vary regularly with potential from  $+0.025$  to  $+0.7\text{ V}$  vs SCE or  $-0.2$  to  $+0.5\text{ V}$  vs Ag/AgCl.<sup>193,280</sup> The spectrum recorded at the lowest potential is similar to the ex-situ Raman spectrum. With increasing potential to the highest potential, the  $1373$  (or  $1367$ )  $\text{cm}^{-1}$  band decreases steadily in intensity,  $1639\text{ cm}^{-1}$

band increases together with the appearance of a shoulder at  $1573\text{ cm}^{-1}$  due to quinoid ring, while  $1596$  (or  $1587$ )  $\text{cm}^{-1}$  band remains constant substantially. If the potential is switched back to  $+0.3\text{ V}$ , the Raman spectrum obtained is the same as that recorded first at this potential. Therefore, some amine units in the films are reversibly transformed into imine groups on oxidation. In-situ resonant Raman spectra obtained at  $632.8\text{ nm}$  change greatly with increasing potential, which is characterized with the appearance of new very well-defined bands at  $1255$ ,  $1280$ – $1330$ , and  $1450$ – $1520\text{ cm}^{-1}$  assigned to the  $\nu\text{C-N}$  mode, semiquinone or polaron ( $-\text{C-N}^+$ ), and oxidized species.

### 3. UV-vis Spectroscopy

UV-vis spectroscopy not only is a rapid and useful technique for tracking the electropolymerization process of the aromatic diamines but also has been used to investigate a significant influence of electropolymerization medium on the structure of aromatic diamine polymers. The UV-vis spectra of the solutions after electropolymerization of *o*PD in three H<sub>2</sub>SO<sub>4</sub> electrolytes for the same period are studied.<sup>161</sup> An absorption maximum of the highest intensity at ca.  $490\text{ nm}$  was observed for the  $0.5\text{ M H}_2\text{SO}_4$  electrolyte. The absorption spectra for  $0.1\text{ M H}_2\text{SO}_4$  and  $0.1\text{ M H}_2\text{SO}_4/0.4\text{ M Na}_2\text{SO}_4$  electrolytes are characterized by two overlapping maxima at ca.  $465$  and  $490\text{ nm}$ , both of the peaks exhibit much lower intensity than that for the  $0.5\text{ M H}_2\text{SO}_4$  electrolyte. This implies that less phenazine content exists in the former case than that in the latter case.

A red shift monotonically occurs in the maximum absorption of *Po*PD from  $416$  to  $480\text{ nm}$  when its electropolymerization medium changes from neutral ( $\text{pH} = 7$ ) to acidic ( $\text{pH} = 1$ ).<sup>154</sup> This indicates that the conjugation of the *Po*PD is extended with lowering the polymerization pH.

Yacynych and Mark reported the difference between the UV-vis spectra of *Po*PD in the reaction solution with and without Ni(NO<sub>3</sub>)<sub>2</sub> and oxygen.<sup>112</sup> The *Po*PD formed in deaerated Ni(NO<sub>3</sub>)<sub>2</sub>-free solution at  $0.25$  and  $0.30\text{ V}$  exhibits a weak absorbance peak

at 460 nm and a strong absorbance peak at 360 nm, respectively. If the potential increases to 0.6 V, the two peaks mentioned above both become stronger. The P $\phi$ PD formed in deaerated Ni(NO<sub>3</sub>)<sub>2</sub>-containing solution at 0.27 and 0.35 V exhibits absorbance peaks at 480 and 360 nm, respectively. The two absorbances resulted from two different species: an intermediate at 460 nm and the final product at 360 nm. In addition, the common air oxidation product of  $\phi$ PD alone and in Ni(NO<sub>3</sub>)<sub>2</sub>-containing solution has an absorbance peak at 415 nm due to 3,5-dihydro-2-amino-3-imino-phenazine, a tautomeric form of DAPh. The peak at 415 nm was not observed in any other spectra obtained in deaerated solution covered by nitrogen atmosphere during the electropolymerization. This shows that the mechanism and product of the electrooxidation of  $\phi$ PD are totally different from those obtained by air oxidation.

It should be noted that the testing solvent influences the UV-vis absorption spectra of electrochemically prepared P $\phi$ PD.<sup>269</sup> A maximum in the visible region shifts from 420 to 440 nm with changing the solvent from acetone, pyridine, DMF, methanol, to DMSO. This bathochromic shift of the absorption spectra in more polar solvents except for methanol suggests the solvatochromism of P $\phi$ PD solution. The maximum absorbance at ca. 460 nm increases apparently and slightly with an increase in the film thickness from 100 to 800 nm for the electropolymerized and cast P $\phi$ PD films, respectively, due to an apparently enhanced doping level of the electropolymerized film. Although the UV-vis spectroscopy of P $\phi$ PD film depends on the testing solvent and film-forming method, the wavelength  $\lambda_{\text{max}}$  (449–452 nm) of the UV-vis maximal absorption of P $\phi$ PD film appears to be independent of the external fields such as magnetic field.<sup>300</sup>

In addition, the changes in UV-vis absorbance were well correlated with the redox wave. The absorption maximum at 468 nm for P $\phi$ PD film gradually decreases as the oxidation level of the film is lowered electrochemically with decreasing polarizing potential from -0.2 to -0.6 V vs SCE.<sup>164</sup> The absorption maximum at ca. 515 nm for P15DAAQ decreases slightly with decreasing potential from 0 to -1.8 V vs Ag/AgCl.<sup>227</sup> The intensity of the absorption maximum at 640–650 nm due to the quinoid structure for PDTDA and PPBZ steadily decreases with decreasing potential from 0.6 to -0.05 and +2.0 to -1.0 V vs Ag/AgCl, respectively, due to the decrease of the quinoid structure content.<sup>230,231</sup> The intensity of a broad absorption maximum at ca. 560 nm decreases steadily with decreasing applied potential from +0.6 to -0.2 V vs SCE, along with a well-defined isobestic point at 415 nm.<sup>189</sup> The wavelength of the absorption maximum also decreases from 580, 570, to 560 nm with a decrease in the potential from +0.6, +0.38, to +0.28 V vs SCE. The variation of the absorbances on the potential indicates a fixed stoichiometric ratio and reversible transform between the oxidized and reduced forms of the PBZ, a Nernstian behavior with interaction between active sites. On the contrary, an increase in UV-vis absorbance at 670 nm for P15DAAQ was observed as the poten-

tial decreased from 0 to -1.4 V vs Ag/AgCl.<sup>227</sup> When the potential is taken further negative than -1.4 V, the peak intensity remains essentially constant. As the potential is taken further positive than 0 V, the absorbance for the peak at 640 nm increases, suggesting an increase in the polaron concentration. A similar increase in the UV-vis absorbance at 570–670 nm with increasing potential from 0 to 0.75 V was observed for 5-aminoquinoline/AN (1/5) copolymer film.<sup>35</sup> The change in UV-vis absorption spectra with time after stepping the potential for 5-aminoquinoline/AN (1/5) copolymer film is studied.<sup>35</sup> The absorption at ca. 500–700 nm increases as the oxidation time increases from 1 to 20 s until the copolymer film is completely oxidized. The reduction showed the opposite trend. Note that the intensity of the absorption maximum at 300–330 nm for PPBZ steadily increases with decreasing potential from +2.0 to -1.0 V vs Ag/AgCl.<sup>230</sup>

In-situ UV-vis subtractive reflectance spectroscopy has been used to study the reaction kinetics of a P $\phi$ PD film in H<sub>2</sub>SO<sub>4</sub>.<sup>301</sup> The semi-oxidized state and totally oxidized state of P $\phi$ PD having electronic absorption bands in the UV spectra at ca. 300, 430, and 500 nm and 300, 450, 530, and 735 nm indicated three redox states of P $\phi$ PD existing in the redox process. New absorption bands in the time-resolved UV-vis spectra with a high time resolution appeared at 465, 550, and 625 nm for the reduction of the totally oxidized state to the semi-oxidized state of P $\phi$ PD and 445, 520, and 685 nm for the reduction of the semi-oxidized state to the reduced state of P $\phi$ PD, suggesting that at least two and one intermediate structures of P $\phi$ PD are produced in the two reduction process, respectively. These intermediate states of P $\phi$ PD, whose exact structures remain unknown, are more unstable than its three redox states. Steady-state potential-resolved UV-vis spectra demonstrate that only one-third of the semi-oxidized state of P $\phi$ PD can be oxidized to the totally oxidized state of P $\phi$ PD.

Wen et al. investigated the in-situ spectroelectrochemical characteristics of the copolymers of sulfonic  $p$ PD with AN, OT, and *N*-methylaniline.<sup>302</sup> It is proposed that the three bands at 310, 375, and 518 nm during polymerization of sulfonic  $p$ PD are assigned to  $\pi$ - $\pi^*$ , polaronic, and excitonic transitions in the polymer. For copolymerization of sulfonic  $p$ PD with AN, OT, and *N*-methylaniline the appearance of a new peak at 672, 633, and 668 nm has been attributed to excitonic transition from benzenoid to quinoid structure of the oxidized state of the AN, OT, and *N*-methylaniline segments, respectively. The decrease in absorbance of the excitonic band arising from the dedoping caused by sulfonic acid groups in the copolymer showed variations in the copolymerization of sulfonic  $p$ PD with AN, OT, and *N*-methylaniline. The following trend was noticed: AN > *N*-methylaniline > OT. The  $\pi$ - $\pi^*$  transition band showed a red shift from 310 to 316, 326, and 392 nm in the sulfonic  $p$ PD/AN, sulfonic  $p$ PD/*N*-methylaniline, and sulfonic  $p$ PD/OT copolymerization, respectively, with the same monomer molar ratio of 95/5 at a constant potential of 0.8 V, indicating that the three copolymers are expected to have longer

**Table 19. Binding Energies and Percentage for the Components of C<sub>1s</sub> and N<sub>1s</sub> XPS Spectra of the P $\alpha$ PD Films Electropolymerized at Four pH Values<sup>154</sup>**

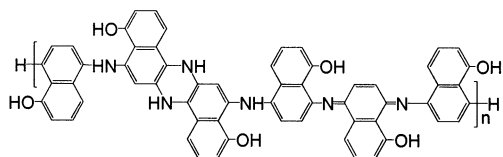
	pH values	binding energy (eV)				percentage (%)			
		1	3	5	7	1	3	5	7
C <sub>1s</sub>	C–C	284.8	284.8	284.8	284.8	59.7	65.6	77.0	64.2
	C–N, C=N	286.2	286.1	286.2	286.2	43.7	29.8	20.7	33.2
	C=O	288.3	288.2	288.4	288.1	5.6	4.6	2.3	2.6
N <sub>1s</sub>	C=N–C	398.7	398.5	398.4	398.3	19.2	14.9	25.4	16.6
	NH <sub>2</sub> , C–NH–C	399.7	399.7	399.5	399.5	55.4	72.3	58.6	66.3
	C=N–OH	401.1	400.8	400.8	400.8	25.4	12.8	16.0	17.1

conjugation length than the sulfonic *p*PD homopolymer. In particular, sulfonic *p*PD/OT copolymer exhibits the longest conjugation length.

As shown in Table 11, almost all aromatic diamine polymers exhibit the maximum absorptions in a shorter wavelength range of 530–735 nm. However, in the case of electroactive PAN, the wavelength of the peaks usually appears at 800 nm. Doped dithio-dianiline/AN copolymer containing 98.9 mol % AN also exhibits the maximum absorption at 780 nm.<sup>232</sup> The appearance of the quinoid structure at a lower wavelength indicates that either the conjugation length or the molecular weight of the polymers is shorter or lower than the PAN. In fact, a shorter conjugation length of the polymers has been confirmed by both the lower conductivity and lower molecular weight than the PAN.

In addition, the in-situ UV–vis spectra of poly(ANO) film in the reduced state from –0.5 to –0.2 V and in the oxidized state at +0.3–+0.7 V show an absorption band at 415–450 and 500 nm, respectively, along with a strong absorption at 313 nm and a broad absorption at 820 nm.<sup>193,280</sup> The band at 415–500 nm might be associated with the  $\pi$ – $\pi^*$  electronic transition in the phenazine rings. A combination of UV–vis and Raman spectra suggests that poly(ANO) should exhibit PAN-like macromolecular structure containing amine (–NH–C), imine (–N=C–), and phenazine ring with hydroxyl side groups, as shown in Scheme 27.

#### Scheme 27



63: Poly(5-amino-1-naphthol)

#### 4. XPS Spectroscopy

XPS spectroscopy has become a powerful characterization technique in the bulk molecular structure investigation on the polymer thin films prepared from aromatic diamines by electropolymerization in recent years. It is successfully employed to differentiate the different carbon and nitrogen environments and calculate the composition, reactivity ratio, and sequence structure. XPS spectroscopy is definitely one of the most powerful characterization methods for insoluble polymers, especially for a small amount of

polymer sample (several milligrams). Some representative investigations are summarized as follows.

An earlier investigation indicates that XPS spectra of electropolymerized P $\alpha$ PD and P*p*PD films are characterized by three peaks,<sup>145</sup> the same binding energy of C<sub>1s</sub> at 285 eV in benzenic form, the same binding energy of N<sub>1s</sub> at 399.4 eV, but a slightly different binding energy of O<sub>1s</sub> at 532.3–532.4 eV.

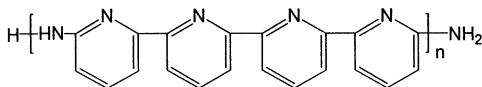
Malitesta et al. suggested that there are three C<sub>1s</sub> signals due to the carbons coupled with carbon, nitrogen, and oxygen atoms, respectively, and also three N<sub>1s</sub> signals ascribed to nitrogen atoms in the C=N, –NH–/–NH<sub>2</sub>, and C=N–OH, respectively, in the XPS spectra of the P $\alpha$ PD prepared by electropolymerization.<sup>146</sup> These XPS spectra have been employed to compare the chemical structure of the P $\alpha$ PD and imprinted P $\alpha$ PD. Only minor differences were observed. The XPS spectrum of the imprinted P $\alpha$ PD treated with 10 mM glucose was further investigated. There is a strong and a weak O<sub>1s</sub> signal due to the oxygen in the C=N–OH/C–OH at 533 eV and C=O at 531.5 eV, respectively. It is found that the O<sub>1s</sub> peak at higher binding energy (ca. 533 eV) was attributed to groups (N–OH) also present in P $\alpha$ PD and to groups (C–OH) belonging to glucose in the sites of imprinted P $\alpha$ PD.

Losito et al. investigated the structure of P $\alpha$ PD films prepared by electropolymerization on Pt at different pH values from 1 to 7 by XPS.<sup>154</sup> They suggested that XPS might be a “bulk” technique for the analysis of P $\alpha$ PD films due to their extremely low thickness, although XPS is usually used as a surface analysis for thick samples. The XPS survey scan for P $\alpha$ PD film electropolymerized at pH 1.0 exhibits three sharp peaks: strongest C<sub>1s</sub> (284.8 eV), weak N<sub>1s</sub> (399.7 eV), and weakest O<sub>1s</sub> (538.3 eV). The presence of primary amino (–NH<sub>2</sub>) and hydroxyl (–OH) groups in the P $\alpha$ PD even at low pH values was confirmed by use of chemical derivatization reaction-XPS. There are three carbons and three nitrogens whose corresponding binding energies and percentage are listed in Table 19.<sup>154</sup> The major component of C<sub>1s</sub> is due both to P $\alpha$ PD benzenic carbons not linked to nitrogen and to contamination carbon. Amino/imino nitrogen (–NH<sub>2</sub>/–NH–) is the predominant type of N<sub>1s</sub>. The amount of carbonyl and oximic (C=N–OH) groups is the smallest. Although the binding energies vary slightly with the pH value, the percentages of every carbon and nitrogen vary significantly. In particular, C–C and NH<sub>2</sub>/C–NH–C percentages appear to be the maximum at pH 5 and 3, respectively. These results plus the UV–vis spectra suggested that a P $\alpha$ PD mainly with a phenazine-like

structure could be electropolymerized at low pH (=1) while a *PoPD* mainly with an amino-1,4-substituted benzenoid–quinoid structure at high pH (=7).

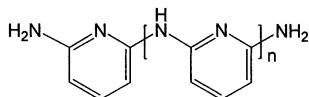
The XPS spectroscopy of 26DAPy polymer films grown at different constant potentials has been investigated.<sup>187</sup> It is found that the XPS spectra of the films formed vary significantly with the potential. Three  $C_{1s}$  peaks at 284.6, 286.3, and 288.2 eV attributed to C–N, N–C=N/N–C–N, and C≡N/C=N<sup>+</sup>, respectively, were observed for the all-26DAPy polymer films. The area ratio of the three peaks was found to be 6/2/1 and 6/4/1 for the films formed at +0.4 and +1.4 V, respectively. Both of the films exhibit two  $N_{1s}$  peaks at 398.8 and 400.0 eV due to C–N=C and N–H, respectively. The area ratio of the two peaks is ca. 1.7/1 and 2.4/1 at +0.4 and +1.4 V, respectively. On the basis of the XPS data, the carbon over nitrogen atomic ratios are 4.1, 4.3, 2.6, and 2.4 for the 26DAPy polymer films formed at 0.4, 0.6, 1.0, and 1.4 V, respectively. A regular and sharp change in the C/N ratio with the potential is noteworthy. A loss of nitrogen with respect to the monomer is evident from the polymer films formed, especially at lower potentials, which is confirmed further by the ammonia production during electrolysis at 0.3 V and the disappearance of the band at 240 nm due to –NH<sub>2</sub> in the UV spectra. These results together with the IR spectrum (strong N–H stretch band at 3351 cm<sup>-1</sup>, strong and sharp C=C and C=N stretch band at 1624 cm<sup>-1</sup>, medium C=C stretch band at 1496 cm<sup>-1</sup>, and weak C–N stretch band at 1283 cm<sup>-1</sup> for the film formed at potential 1.9 V) and UV–vis spectra (a strong and sharp absorbance at 300, 297, 293 nm due to pyridyl ring and a very broad and medium absorption centered at 354, 362, and 382 nm due to the conjugated chain for the film obtained at 1.4, 0.6, and 0.4 V, respectively) suggest the possible macromolecular chain structures in Scheme 28 at 0.4 V and Scheme 29 at 1.4 V.

#### Scheme 28



64: Poly(2,6-diaminopyridyl) prepared at 0.4 V

#### Scheme 29



65: Poly(2,6-diaminopyridyl) prepared at 1.4 V

XPS analysis has been performed *ex situ* on P15DAN film formed by cyclic voltammetry by Pham et al.<sup>176</sup> It is found that the  $C_{1s}$  spectrum displays two peaks: one strong peak at 285 eV due to the carbons coupled to carbon atoms of the same type and another medium peak at 286.3 eV ascribed to carbons coupled singly to oxygen atoms or to N atoms (C–N and C=N). No peak at ca. 288 eV was detected, implying no quinone group present in the polymer chain. The  $N_{1s}$  spectrum displays four peaks. The

strongest peak at the lowest energy and centered 398.8 eV and the second strongest peak at 400 eV can be attributed to the neutral imine (–N=) and amine (–NH–) nitrogen atoms, respectively. Two weak peaks at higher energy centered at 401 and 402.5 eV should be assigned to protonated amine and imine nitrogen atoms. These results suggest that there are two carbon environments and four nitrogen environments in the P15DAN. Their binding energy is very close to that of the *PmPD* prepared by chemically oxidative polymerization discussed in section IV.C. The difference is that there are four carbon environments in the *PmPD*.

Besides the aromatic diamine homopolymers, the XPS spectroscopy of the copolymers of aromatic diamines with AN has been also investigated and successfully and uniquely used to calculate their composition and sequence distribution. The ESCA survey spectrum of *pPD/AN* (1/26) copolymer has been found to exhibit the core level of  $C_{1s}$ ,  $N_{1s}$ , and  $O_{1s}$  at ca. 286, 402, and 534 eV, respectively.<sup>203</sup> Yang and Wen suggested that three XPS  $C_{1s}$  spectra of PAN, *pPD-AN*, and sulfonic *pPD-AN* copolymer films with the thickness of 25 nm are virtually identical regardless of the difference of bonding carbon atom such as C–H, C–N, C–SO<sub>3</sub>H, and C–O.<sup>185,271</sup>  $N_{1s}$  core level spectra of three polymers exhibit three peaks at binding energies of 399.1, 400.4, and 402.2 eV corresponding to –N=, –NH–, and N<sup>+</sup>, respectively. The binding energies for  $O_{1s}$ ,  $N_{1s}$ ,  $C_{1s}$ ,  $Cl_{2p}$ , and  $S_{2p}$  are 531.5–532.4, 399.4–400.0, 285, 197.2–198.0, and 168.0–168.4 eV, respectively, for sulfonic *pPD/AN* copolymer film. With increasing sulfonic *pPD* unit content, the binding energies of  $O_{1s}$  and  $S_{2p}$  decrease slightly, the binding energies of  $N_{1s}$  and  $Cl_{2p}$  increase slightly, but the binding energy of  $C_{1s}$  remains constant. The XPS peak area has been used to calculate the relative content of C, N, S, O, and Cl in the copolymer films. Excess of carbon and oxygen in the sulfonic *pPD/AN* copolymer film was found and attributed to the degradation of the film via hydrolysis to BQ. In *pPD/AN* copolymer film, excess of carbon was also found. Cross-linking/branching structure was revealed in the two copolymers at sulfonic *pPD* and *pPD* molar contents of higher than 20.6% and 10.2%, respectively. Dithiodianiline/AN (2/98) copolymer doped with HCl exhibits the core level of  $C_{1s}$ ,  $N_{1s}$ ,  $O_{1s}$ ,  $S_{2p}$ , and  $Cl_{2p}$  at ca. 284.5 (atomic percentage 76.2%), 400.4 (12.2%), 532(9.2%), 164(0.6%), and 197.5(1.6%) eV, respectively.<sup>232</sup> Three nitrogen forms of =N– (399.1 eV, element percentage 18.6%), –NH– (400.2 eV, 67.9%), and N<sup>+</sup> (400.9 eV, 13.5%) and two carbon forms of C–N (286 eV, 45.2%) and C–C/C–H (284.3 eV, 54.8%) are found.

The actual composition, reactivity ratio, and sequence distribution in the copolymers for sulfonic *pPD/AN* copolymerization calculated based on the XPS spectra are listed in Table 20.<sup>185</sup> It is apparent that different feed content of sulfonic *pPD* leads to different molar content of the sulfonic *pPD* units in the resulting copolymer. At  $f_1 < 0.15$ ,  $F_1 > f_1$ , indicating a faster deposition rate of sulfonic *pPD* than AN, whereas  $F_1 < f_1$  at  $f_1 > 0.15$ , indicating a slower deposition rate of sulfonic *pPD* than AN. A

**Table 20. Composition, Reactivity Ratio, and Sequence Distribution for Electrocopolymerization between Sulfonic *p*PD and AN at the Conversion 0.2% to Polymer<sup>185</sup>**

sulfonic <i>p</i> PD content		reactivity ratio		sequence distribution parameters					
feed( $f_1$ )	resulting( $F_1$ )	$r_1$	$r_2$	$P_{11}$	$P_{12}$	$P_{22}$	$P_{21}$	$\bar{N}_1$	$\bar{N}_2$
0.025	0.051	0	0.369	0	1	0.935	0.065	1	15.35
0.102	0.120	0	0.719	0	1	0.863	0.137	1	7.30
0.206	0.173	0	0.981	0	1	0.791	0.209	1	4.78
0.333	0.235	0	1.126	0	1	0.693	0.307	1	3.26
0.500	0.295	0	1.378	0	1	0.579	0.421	1	2.37

similar relationship between feed content of *p*PD and *p*PD unit content in the resulting copolymer has been observed in the *p*PD/AN copolymer.<sup>271</sup>  $r_1 = 0$  implies that the rate constant of sulfonic *p*PD homopolymerization is 0 due to the polymer chain failing to link further between sulfonic *p*PD monomers despite the variation of the sulfonic *p*PD/AN monomer ratio.<sup>183</sup> The fact that the  $r_2$  value increases with increasing sulfonic *p*PD content might be ascribed to sulfonic *p*PD addition facilitating formation of quinonediimines on the electrode surface, leading to an easier attachment of AN to polymer chain.  $P_{11}$  and  $P_{12}$  keep constant values of 0 and 1, respectively, indicating that polymer chains cannot be propagated between sulfonic *p*PD active end group and sulfonic *p*PD monomer because sulfonic *p*PD active end group prefers to link AN.  $P_{22}$  decreases with increasing sulfonic *p*PD content, while  $P_{21}$  increases because larger sulfonic *p*PD content should increase sulfonic *p*PD attachment for growing polymer chains with AN active end group. Therefore, the sequence length of  $\bar{N}_1$  equals 1 while  $\bar{N}_2$  decreases with increasing sulfonic *p*PD content.

### 5. EPR Spectroscopy

EPR spectroscopy studies on aromatic diamine polymers have recently been carried out in only a few laboratories. Therefore, the EPR spectroscopic characteristics are still not well understood. Only two articles concerning EPR spectroscopy of aromatic diamine polymers have been found and are discussed below. In-situ EPR spectrum of P15DAN electropolymerized on Pt exhibits a wide peak with the peak-to-peak line width of 13 G and a  $g$  value of 2.0009, almost Lorentzian in shape, indicating the presence of a three-dimensional interaction, similar to the EPR of AN oligomers but not the Gaussian line shape in emeraldine base PAN.<sup>303</sup> The  $g$  value and line width were found to be potential independent.<sup>304</sup> A relationship between EPR intensity and the electrode potential for the P15DAN was presented. The maximum of the EPR signal is observed for the reduced form of the P15DAN. A simple model of spin recombination during the oxidation process was used to describe the unusual changes of observed experimental values of EPR intensity. Until now, no investigation on the EPR spectroscopy of other PDANs and PPDs was found. In particular, the EPR spectroscopy of the metal complex of aromatic diamine polymers, such as charge-transfer complexes of DAAQ oxidized by metal ions, should be valuable.

### 6. Electrochemical Impedance and Admittance Spectroscopy

Although the temperature and frequency dependences of the impedance and permittivity of *p*PD/AN

copolymers prepared by chemical oxidation with ammonium persulfate in aqueous medium have been measured,<sup>195</sup> generally electrochemical impedance spectroscopy is considered to be a more advanced and very powerful technique to investigate the electron transfer (electronic resistance) and ionic conductivity as well as examine the film roughness of the conductive polymer film electrode.<sup>127</sup> A wealth of information on the kinetic processes in the electrodes and on ohmic resistance, double layer, and redox capacitances can be obtained.<sup>156,201,305,306</sup> A few investigations on the electrochemical impedance and admittance spectroscopies of aromatic diamine polymers are found. The impedance spectra of *Po*PD-coated electrodes were studied as a function of electrode potential, solution pH, and *Po*PD film thickness.<sup>305</sup> Typical impedance spectra of a *Po*PD-coated GC electrode in 0.4 M HClO<sub>4</sub>/NaClO<sub>4</sub> solution show a linear 45° region corresponding to semi-infinite diffusion in the medium-frequency range and a nearly vertical line due to a finite film thickness in the low-frequency range.

The impedance spectra of Au or Pt/*Po*PD electrodes in 1 M HClO<sub>4</sub> at potentials from -0.14 to +0.16 V vs SCE have been reported.<sup>307</sup> All spectra show a Warburg impedance (a linear 45° region) at higher frequencies, a transition to a capacitive behavior at medium frequencies, and a slightly curved even nearly vertical capacitive line at low frequencies.<sup>308</sup> The Warburg coefficient and the width of the linear 45° region in an impedance diagram showed their minima near the formal potential. The width of the linear 45° region is roughly proportional to the film thickness in a range from 0 to 5 mm. Due to the potential dependence of the Warburg coefficient and low-frequency capacitance, the impedance spectra are potential dependent. The potential dependence of low-frequency capacitance attests to strong interactions within the film that depend on the nature of anions but to a lesser extent on the pH because the charge transport diffusion coefficient strongly decreases with increasing potentials.<sup>307</sup> The impedance results have been explained based on the diffusion-migration transport of both electron and ion within the *Po*PD film because charge transport across *Po*PD film electrode requires the concurrent transport of two charge carriers in order to maintain electroneutrality of the film. Therefore, electron transport should be ensured by interchain electron hopping, accompanied by intermolecular proton exchange, which contributes to the interchain conduction between different conjugated segments on the same chain.

At pH > 4, the impedance spectrum showed a semicircle due to a parallel resistance-capacitance element in the high-frequency range.<sup>305</sup> The diameter

of the semicircle was considered to correspond to interfacial charge-transfer resistance because of its independence of the film thickness in a range from 0 to 2 mm.<sup>309</sup> It is found that charge-transfer resistance changed with the oxidation level of the P $\phi$ PD, which depends on the electrode potential. The relationship between the charge-transfer resistance and the potential at a given pH shows a minimum. This minimum increased with a shift of ca. 230 W/pH as the pH value increased from 4 to 6. The pH dependence of the charge-transfer resistance may be due to a much larger rate constant for the redox reaction of protonated group  $-\text{NH}_2^+$  than nonprotonated group  $-\text{NH}-$ . At a uniform distribution of time-independent proton concentration throughout the film, the heterogeneous rate constant is proportional to the protonation constant of P $\phi$ PD and the proton concentration in solution. Therefore, a decreasing proton concentration leads to an increase in the charge-transfer resistance. The low-frequency capacitance of the P $\phi$ PD film was proportional to the film thickness and showed a maximum at the formal potential of the P $\phi$ PD.<sup>308</sup> In fact, the impedance is purely capacitive in the low-frequency range because charge-carrier concentrations at each instant are almost constant inside the film. In addition, it is interesting that the ohmic resistance obtained from the high-frequency intercept of impedance plots keeps a constant value of 32–34 W and does not vary with both the P $\phi$ PD film thickness from 0 to 5 mm and potential from 0.3 to  $-0.3$  V. This indicates that the film resistance is much lower than the solution resistance.

The effect of surface roughness of electrode on the impedance spectra of gold/P $\phi$ PD electrodes in contact with 1 M HClO<sub>4</sub> has been investigated by systematically changing potentials and P $\phi$ PD film thickness.<sup>156</sup> It is found that the character of the impedance spectra is connected more with P $\phi$ PD film nonuniformity than with the surface roughness of the underlying gold substrate, but the high-frequency capacitance depends on the roughness of the gold substrate and increases significantly due to an increase in real surface area. Recently a model for the impedance of gold/P $\phi$ PD film electrode in 1 M HClO<sub>4</sub> was developed on the basis of three mobile charge carriers, electron diffusion, counterion transport, and hydrogen ion transfer processes, in the course of redox transformation in the P $\phi$ PD film.<sup>306</sup> A general expression for the impedance was discussed, and an analytical solution was obtained for the complex impedance in the case of low-amplitude variation of the electrode polarization of P $\phi$ PD film.

Electrochemical impedance spectroscopy has been used to investigate the dependence of redox-kinetic parameters, the charge-transfer resistance, the redox capacitance, and the diffusion coefficient of charge carriers at GC/P $\phi$ PD electrodes on the oxidation and protonation levels of the P $\phi$ PD.<sup>309</sup> The coupled diffusion coefficient shows a maximum at a medium oxidation level of the polymer near the formal potential of the polymer, indicating that the rate of charge transport within the film may be controlled by interchain electron hopping. The coupled diffusion coefficient decreases exponentially with increasing

solution pH, implying that the electron-hopping process is accompanied by intermolecular proton exchange, due to a decrease in the homogeneous electron-transfer rate constant with deprotonation of the polymer. The charge-transfer resistance and the width of the Warburg region show their minima near the formal potential of the polymer and increase with increasing pH of the solution. In contrast, the low-frequency capacitance shows a maximum at the formal potential and the maximum value is nearly independent of the pH. The capacitance and width of the Warburg region at a given potential are approximately proportional to the P $\phi$ PD film thickness in the range 0–3  $\mu\text{m}$ , with an increase of 10 mF  $\text{cm}^{-2} \mu\text{m}^{-1}$ . These results have been interpreted in terms of the diffusion-migration transport of both electron and proton through the film.

The temperature dependence of impedance of pPD/AN copolymer has been investigated and is found to be different from that of PpPD/PAN blend.<sup>201</sup> The impedance of the copolymer at 100 kHz decreases with increasing the AN unit content. The convex shape of the temperature dependence of the impedance is converted into a concave form at 75 mol % AN unit. Furthermore, the pPD/AN (25/75) copolymer exhibits the largest dependence of impedance which decreases from ca.  $10^6$  to  $10^2$  W cm with elevating temperature from 80 to 300 K. This composition may correspond to the intermolecular analogy of the percolation threshold, at which the chain structure of the copolymer is a critical state from essentially nonconducting (resembling PpPD) to basically conducting (close to PAN). For PpPD/PAN blend, the transition from convex to concave shape occurs between 5 and 10 vol % PAN, at the macroscopic percolation threshold.

Crystal admittance spectra have been used to dynamically monitor the viscoelastic properties of depositing P18DAN films during electropolymerization.<sup>180</sup> It is found that the maxima of successive crystal admittance spectra for the reduced P18DAN film during electropolymerization of 18DAN in acetonitrile increase slightly first and then decrease relatively significantly from 2.61 mS to 2.74 mS then to 2.46 mS and the frequency corresponding to the maxima decreases steadily from 10.0315 to 10.0237 MHz over the course of 12 potentiodynamic deposition cycles at the cathodic end ( $E \leq 0.2$  V), which can be due to the changes in mass of electrode and film. The admittance spectra of the P18DAN film-coated Au electrode are not significantly different from that of the bare Au electrode, indicating that the P18DAN film deposited is rigid.

The admittance spectra during P18DAN film deposition in higher 18DAN concentration 20 mM exhibit an appreciable decrease in peak admittance from 3.31 to 1.86 mS with increasing deposition cycles up to 11. This is because the P18DAN film prepared is nonrigid, in which the decreased rigidity is a consequence of a more open structure at a faster deposition rate at a higher monomer concentration.

The admittance spectrum of the initially rigid P18DAN film in 0.1 M HClO<sub>4</sub> will change remarkably upon the addition of Hg(ClO<sub>4</sub>)<sub>2</sub>. With exposure to 1

mM  $\text{Hg}^{2+}$  ions in solution, both the peak admittance and corresponding frequency decrease because  $\text{Hg}^{2+}$  ions are complexed by free amino groups in the film. However, there is little viscoelastic change occasioned by  $\text{Hg}^{2+}$  uptake into nonrigid P18DAN film. The complex of  $\text{Hg}^{2+}$  ions at a concentration from 1 to 4 mM by nonrigid P18DAN film results primarily in a slight decrease in peak frequency as well as an initial increase and then slight decrease in peak admittance.

Also, a spectroelectrochemical study indicated that the P $\sigma$ PD composited in PAN film could accelerate relaxation process in PAN.<sup>310</sup>

## H. Solubility and Molecular Weight

Generally, the aromatic diamine polymers prepared by electrochemical and chemical oxidative polymerizations exhibit similar solubility in most solvents. The P $\sigma$ PD film prepared by electropolymerization was soluble at 25 °C in DMSO (the solubility 17.0 g/L), DMF (13.0 g/L), methanol (5 g/L), ethanol (4.2 g/L), acetone (0.8 g/L), pyridine (0.5 g/L), and THF (0.3 g/L)<sup>164</sup> but insoluble in acetonitrile, dioxane, chloroform, benzene, and propylene carbonate. Ogura and Yano found a semiquantitative relationship between the solubility of electrosynthesized P $\sigma$ PD and the dielectric constant of the solvents, i.e., its solubility becomes larger with an increase of the dielectric constant of the solvent except for acetonitrile.<sup>164,269</sup>

It is reported that the PBZ and PPBZ films obtained in  $\text{HClO}_4/\text{NaClO}_4$  aqueous solution and  $\text{N}(\text{C}_4\text{H}_9)_4\text{ClO}_4/2,6\text{-lutidine}/\text{CH}_3\text{CN}$ , respectively, and the polynaphthidine obtained in  $\text{NaClO}_4/\text{acetonitrile}$  solution by cyclic voltammetry seem insoluble in most solvents including dichloromethane, chloroform, benzene, toluene, hexane, methanol, ethanol, acetonitrile, DMF, DMSO, acidic aqueous solutions at various pH values, and sulfochromic and sulfonitric solutions.<sup>189,190,266</sup> Fortunately, the insolubility problem of the PBZ and PPBZ has been solved by electropolymerization in different electrolytes like  $\text{Et}_4\text{BF}_4/\text{CH}_3\text{CN}$  by cyclic voltammetry.<sup>230</sup> The PBZ and PPBZ films in doped and undoped forms obtained thus are soluble in several solvents except for  $\text{CH}_2\text{-Cl}_2$  and water.<sup>230</sup> The solubility of PPBZ in acetonitrile, chloroform, and DMF is 0.1 wt % (solution color, brown), 0.3 wt % (purple brown), and 0.7 wt % (purple brown), respectively. The much better solubility of PBZ in acetonitrile, chloroform, NMP, and DMF is found to be 1.9 wt % (light yellow-green), 3.1 wt % (yellow-green), 3.4 wt % (yellow-green), and 3.5 wt % (yellow-green), respectively. In particular, both polymers can be completely dissolved in DMF and NMP without leaving any residue in dissolution, being reprocessable from solution yielding films with the properties substantially identical to virgin films. The different solubility might be due to the change of polymerization medium, resulting in a difference of molecular weight as well as macromolecular structure. Insoluble PBZ generally exhibits higher molecular weight and more rigid chain structure.

The neutral form of dithiodianiline/AN electrocopolymer by treating with  $\text{NH}_4\text{OH}$  exhibits some solubility in NMP and DMF, and even THF, acetone, and ethanol, which should be due to the branched

structure and the presence of  $-\text{S}-\text{S}-$  links.<sup>232</sup> For example, the undoped form of dithiodianiline/AN (2/98) copolymer is more soluble in NMP and DMF as well as partially soluble in THF, acetone, and ethanol. However, the doped form of the dithiodianiline/AN (2/98) copolymer is insoluble in all of the five solvents. Unfortunately, the electrooxidative products (an orange or brownish-red tar) of 23DAPy and 26DAPy appear to be insoluble in organic solvents because the products are amine-linked polymers.<sup>268</sup> It can be seen that the electropolymer of 23DAPy exhibits lower solubility in organic solvents than that of  $\sigma$ PD with similar monomer structure. However, investigation on the solubility of P $m$ PD, P $p$ PD, PDAN, and PDAAQ prepared by electropolymerization has not been reported in detail.

As revealed above, due to the limited solubility of aromatic diamine polymers in most common solvents, the polymers generally exhibit low solution processibility. Unfortunately, the aromatic diamine polymers prepared by four oxidative polymerization techniques also appear to exhibit poor thermal stability and fusibility because a steady weight loss at 230 °C (P $\sigma$ PD),<sup>220</sup> 110 °C (P $m$ PD),<sup>69,223</sup> and 270 °C (P $p$ PD)<sup>224</sup> as well as a broad exothermic peak at ca. 200 °C (P $m$ PD) and 165 °C (P $p$ PD), possibly corresponding to cross-linking reaction,<sup>229</sup> have been found. These lead to undiscovered melt processibility of aromatic diamine polymers. However, it can be predicted that the incorporation of some aliphatic substituents from ethyl to hexyl groups as side chains of the polymers might improve their solubility and fusibility because the aliphatic substituents could serve as internal solubilizer and plasticizer.

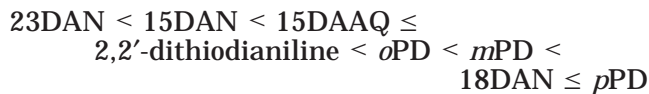
Until now only a few reports concerning the molecular weight of aromatic diamine polymers formed by electropolymerization have been found. The mean molecular weight of P $\sigma$ PD dissolved in DMF was found to be 11000<sup>164</sup> and 20000–30000<sup>311</sup> by means of gel permeation chromatography. The degree of polymerization is not very high, and the polymer is composed of ca. 100–300 units of monomeric  $\sigma$ PD. Compared to the PPD prepared by chemically and enzyme-catalyzed oxidative polymerizations (Table 14), the molecular weight of P $\sigma$ PD by electropolymerization is usually higher. It is difficult to find the reason since the polymerization method and solvent are different. The weight-average molecular weight of electropolymerized PDTDA was ca. 4000 from the gel permeation chromatography analysis.<sup>231</sup> The average molecular weight of electropolymerized P15DAAQ was ca. 3000 from the gel permeation chromatography analysis, composed of ca. 10 monomer units.<sup>312</sup> The molecular weight study on P15DAN suggests that the polymer consists mainly of trimer and pentamer with molecular weights of 452 and 844, respectively.<sup>173</sup> It is clear from Tables 14 and 15 as well as section VI.B that the aromatic diamine polymers and copolymers prepared by the four oxidative polymerizations all exhibit relatively low molecular weight. Actually, the aromatic diamine polymers and copolymers are oligomers.

Perhaps one of the major challenges for the industrial application and commercialization of the oxida-



tive polymers of aromatic diamines is the enhancement of their molecular weight. There are several approaches for effectively enhancing their molecular weight. For *o*PD with a relatively low oxidative polymerizability with  $(\text{NH}_4)_2\text{S}_2\text{O}_8$  as oxidant, elevating the polymerization temperature to 118 °C together with the application of glacial acetic acid of high boiling point rather than HCl aqueous solution is one of the better methods to prepare the polyaminophenazine of relatively high molecular weight.<sup>70</sup> For the polymerization system of *o*PD with  $\text{H}_2\text{O}_2$  in 1,4-dioxane/phosphate buffer pH = 7 at room temperature, addition of HRP dramatically increases the molecular weight of the resulting polyaminoaniline.<sup>117</sup> The electropolymerization of *o*PD in 0.1 M  $\text{H}_2\text{SO}_4$  also gives polyaminoaniline with relatively high molecular weight.<sup>164</sup> In contrast with *o*PD, lowering the reaction temperature to 0 °C for the oxidative polymerization of *p*PD with  $(\text{NH}_4)_2\text{S}_2\text{O}_8$  will produce phenazine ring-containing P*p*PD of relatively high molecular weight.<sup>194</sup> Therefore, it can be reasonably anticipated that the molecular weight of aromatic diamine polymers will become higher at the optimum polymerization conditions including monomer/oxidant ratio, temperature, and reaction medium. Unfortunately, no investigation on the dependence of the molecular weight on the oxidative polymerization conditions is found. Therefore, more efforts should be made in order to prepare really high molecular weight aromatic diamine polymers with high mechanical, stable, reversible redox, and electroconductive properties.

Up to now, the monomer oxidation potential, polymerization yield, and molecular weight of the polymers prepared by the four oxidative polymerizations have been discussed in detail. Generally, the oxidative polymerization activity could be substantially appraised in terms of the above-said three aspects comprehensively. Therefore, a rough order for the oxidative polymerization activity of eight types of aromatic diamines is ranked as follows



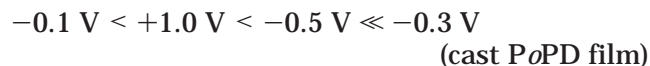
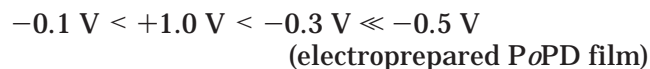
### I. Morphological and Supramolecular Structures

As compared with the other three oxidative polymerizations, one of the greatest predominances of electrooxidative polymerization is that ultrathin, homogeneous, and dense polymer film can be easily prepared from aromatic diamine monomers. Electropolymerization parameters such as monomer type, the number of potential cycles, electrodeposition time, doping level, applied potential, solvent, magnetic field, and copolymerization exhibit a strong influence on the morphology of aromatic diamine polymers, as discussed in the following section. The film thickness can be easily accommodated by altering electropolymerization conditions. The thickness of P*o*PD film prepared by electropolymerization has been controlled by altering the number of potential cycles, but a film thicker than 1 mm was not obtainable.<sup>164</sup> The film thickness electrodeposited increases linearly from 50 to 800 nm with increasing the number of

potential cycles from 60 to 360 and remains at a nearly constant value 800–850 nm when the number of potential cycles is more than 360. With prolonging electrodeposition time from 20 to 120 min, the P*o*PD film thickness increases concavely from 50 to 800 nm,<sup>269</sup> revealing an accelerated deposition of *o*PD with time due to the catalytic formation of reaction sites. ESCA has been used to analyze a Pt sheet covered with P*o*PD film.<sup>142</sup> There is the Pt 4f signal in the ESCA, indicating the presence of a very thin P*o*PD film on the Pt. Angle-dependent ESCA measurements gave a thickness value ranging from 5 to 8 nm. It is found that a brownish P*m*PD film with a thickness of 1 mm was obtained on Pt electrode.<sup>313</sup>

It is seen that there is usually a limitation of the thickness of electrodeposited PPD films due to their nonconductivity. In contrast, no limitation of the cast film thickness is observed because thicker film can be prepared by casting more polymer solution. A linear positive relationship between the thickness and the amount of P*o*PD solution in DMSO was found.<sup>164,269</sup> A solution of 17 g of P*o*PD in 1 L of DMSO corresponded to a cast-film thickness of 175 nm. Furthermore, the thickness of cast P*o*PD film increases linearly from 130 to 760 nm with increasing P*o*PD-saturated casting solution from 130 to 800 mL on the ITO substrate area of 3.28 cm<sup>2</sup>.

The electroprepared P*o*PD film has a rough surface morphology similar to the electroprepared PAN film, except that the nuclei size is slightly smaller than that of the PAN film, whereas cast P*o*PD film shows higher uniformity.<sup>164</sup> Scanning electron microscopy observation revealed that P*o*PD film doped by  $\text{HClO}_4$  shows regular network structure where the dopants are trapped as dispersed phase.<sup>155</sup> Scanning tunneling microscopic observation reveals that the surface morphology of P*o*PD film varies with the potential from -0.5 to +1.0 V.<sup>269</sup> Both electroprepared and cast P*o*PD films show the roughest surface at -0.1 V due to the interaction between positively charged sites in the film and counteranions. The electroprepared P*o*PD film is the smoothest at -0.5 V, whereas the surface of the cast P*o*PD film (-0.5 V) is not as smooth as that of the electroprepared P*o*PD film possibly owing to the involvement of some dopant anions in the cast film. In conclusion, the smoothness of the P*o*PD films increases with the potential in the order



It is speculated that the polymer chains are coarsely stacked in the electroprepared P*o*PD film but connected with each other to a large extent, leading to readily doping and undoping of counteranions during the electrochemical oxidation and reduction of the film. On the contrary, the piled chains in the cast film are crowded, causing restricted doping and undoping of counteranions.

The thickness of the P*o*PD film deposited by cyclic voltammetry could be theoretically predicted. Myler

et al. estimated the number of monomer units deposited and the film thickness based on the  $\alpha$ PD polymerization via a  $2e^-$  process and if the charge under each polymerization curve is integrated.<sup>149</sup> Assuming that the monomer has cross-sectional dimensions of ca.  $0.3 \times 0.5 \text{ nm}^2$  and that each polymer monolayer has a depth of ca. 0.14 nm, the depth of a film coated via 20 potential sweeps is estimated to be 30 nm, which is slightly smaller than the cross-sectional depth of 35 nm observed by scanning electron microscopy.

Although the transmission electron microscopy imaging of the P $\alpha$ PD film seems unsuccessful due to the disintegration of the film under the electron beam, atomic force microscopy has proven especially powerful for the investigation of the P $\alpha$ PD film prepared by electropolymerization. Atomic force microscopy in tapping mode was used for the characterization of the film morphology on highly ordered pyrolytic graphite electrode.<sup>141</sup> The P $\alpha$ PD film obtained in pure aqueous phase shows a smooth and uniform surface consistent with an insulating film. In contrast, the P $\alpha$ PD film obtained in liquid crystalline aqueous phase is rougher but without pores in the film. The surface morphology of the P $\alpha$ PD film electroprepared in a magnetic field was observed by atomic force microscopy.<sup>300,311</sup> The surface of the P $\alpha$ PD film becomes flatter in the order 6 T(+), 0 T, 6 T(-) with the average roughness of 3.23, 3.14, and 2.70 nm and much flatter than PPY film with the corresponding average roughness of 10.7, 13.3, and 8.2 nm. Therefore, the surface morphology and roughness of P $\alpha$ PD film changed with the strength of the magnetic field.<sup>300</sup> The flatness of the P $\alpha$ PD filmed-electrode surfaces was dependent on magnetic field direction.<sup>311</sup> When the directions of magnetic field and electrode face are parallel to each other, a flat surface is observed due to the magnetohydrodynamic flow of the electrolyte solution by electromagnetic force. When the directions of magnetic field and electrode face are perpendicular to each other, the modified surface is very rough owing to the diamagnetic property of P $\alpha$ PD. The image of the electrode surface prepared with no magnetic field is the intermediate one between the two cases above. This structural difference leads to different electroactivity and impedance response: (1) lower electroactivity at 6 T perpendicular than 0 T; (2) lower limit resistance at 6 T perpendicular than 6 T parallel and 0 T; (3) the highest limit resistance at 0 T.

It was recently reported that a nano-organized  $\alpha$ PD oligomer film in two dimensions has been successfully fabricated using electrochemical-assembly technique.<sup>277</sup> The  $\alpha$ PD oligomer film assembled on a bare Au surface shows a nanoscale dot array structure under the action of the potential pulse sequence. At the same time,  $\alpha$ PD oligomer film formed on gold covered by *p*-aminothiophenol self-assembly exhibits a nanoscale line array structure. The growth of  $\alpha$ PD oligomer film in the early stage was observed by electrochemical scanning tunneling microscopy. When the first potential pulse was applied to the electrode, some dots appeared on the gold surface, indicating the formation of P $\alpha$ PD crystal nuclei. With the applica-

tion of the second and third potential pulses to the electrode, not only the number of the dots increased, but also the size of the dots got bigger. After five potential pulses were applied, a slightly disordered sparse ridge structure for P $\alpha$ PD with a dot size distribution from 5 to 15 nm was obtained. After subsection to 30 potential pulses, a two-dimension close-packed dot array structure for P $\alpha$ PD with the dot size mainly ranging from 7 to 10 nm, higher density, and more organization formed. The electropolymerization of  $\alpha$ PD on gold includes three stages: crystal nucleus formation, crystalline grain growth, and orientation at the first five stages of potential pulses. *p*-Aminothiophenol self-assembly on gold can significantly improve the binding force of P $\alpha$ PD film on the substrate since it can take part in electropolymerization of  $\alpha$ PD as a crystal nucleus.

Owing to a rapid deposition of P $\alpha$ PD in 0.1 M  $\text{H}_2\text{SO}_4$  and 0.1 M  $\text{H}_2\text{SO}_4/0.4 \text{ M Na}_2\text{SO}_4$ , the P $\alpha$ PD film formed initially is very porous and fibrous in nature, leading to dramatic changes in the structure and/or morphology of the P $\alpha$ PD.<sup>161</sup> Malinauskas et al. suggested that at lower  $\alpha$ PD concentration more compact P $\alpha$ PD films are obtained by cyclic voltammetry.<sup>162</sup>

The morphology and thickness of P15DAN, P18DAN, and P23DAN films prepared by electropolymerization have been investigated.<sup>139,173</sup> Three films displayed nonspecific amorphous, nonfibrillar, and fairly smooth surface features with almost uniform thickness over the whole film. These three PDAN films showing smooth surface and uniform thickness could be valuable in electronic applications that require extremely smooth surfaces. The film thickness increased with increasing the amount of charge passed during electropolymerization. When the amount of charge is 100 mC, the thickness of the P15DAN film is 300 nm, and when the amount of charge is 600 mC, the thickness of P15DAN film is 1 mm. Typical thickness is 680 nm for P18DAN film and 1.2 mm for P23DAN film. The morphology of P23DAN film is granular and different from that of P18DAN film. The P15DAN film is a thin, rather compact and uniform morphology and very adherent to the mild steel and GC electrodes.<sup>176,179</sup> P15DAN films obtained by scanning the potential from -0.1 to 0.95 V and -0.2 to 1 V vs SCE at 50 mV/s for 45 and 30 min in 0.1 M  $\text{NBu}_4\text{ClO}_4/0.2 \text{ M HClO}_4/\text{acetonitrile}$  and HCl have thicknesses of 65 and 125 nm, respectively.<sup>176</sup> It is also reported that the P15DAN film prepared by cyclic voltammetry between -0.2 and 0.8 V after 10 scans has a thickness of 1 mm.<sup>175</sup>

Besides the aromatic diamine homopolymers, the morphology of electrocopolymer films of aromatic diamine with AN has been also investigated.<sup>169,185,284</sup> At the electrodeposition of the initial 20th cycle for pure AN, the polymer exhibits a rather uniform globular microstructure, whereas at the 80th cycle, a 0.2 mm thick fibrous structure exhibiting some branching develops.<sup>284</sup> In contrast to the initial globular deposit, the later fibrous deposit is not entirely uniform over the  $\text{IrO}_2$ -coated titanium electrode, indicating that the fibers are preferred sites for further polymer growth. Upon addition of 0.5 mM *p*PD to 199 mM AN, the *p*PD/AN copolymer film



lymerization of 15DAAQ does not appear to change the original stacking pattern of the 15DAAQ monomer. Therefore, the P15DAAQ might be a supermolecule with a  $\pi$ - $\pi$  stacking structure observed rarely for traditional conducting polymers. It is the peculiar crystalline structure that leads to a 3-dimensional-extended  $\pi$ -conjugated structure, finally endowing a potential-independent enhanced electroconductivity, better cyclability, and durability.

## J. Properties

There are only a small number of articles concerning the properties of electrochemically oxidative polymers from the aromatic diamines, despite relatively more work already done in electropolymerization of the aromatic diamines. One of the important and useful properties of the aromatic diamine polymers is electroconductivity. Generally, the P $\phi$ PD prepared by electropolymerization exhibits higher electroconductivity than those by chemically oxidative polymerization possibly due to the higher molecular weight and better doping level realized by the former technique, as listed in Tables 6, 7, and 17. The higher electroconducting P $\phi$ PD ( $10^{-6}$  S/cm) prepared in boiling glacial acetic acid by chemically oxidative polymerization in Table 6 is evidence that high molecular weight P $\phi$ PD should have high conductivity because the aromatic diamine polymers obtained by the four oxidative polymerizations present are usually of low molecular weight. It is also seen from Table 17 that the P15DAAQ, P $\phi$ PD, and *p*PD/AN (1/9) copolymers obtained by electropolymerization exhibit higher conductivity than other polymers. On the other hand, the electroconductivity of three typical nitrogen heteroaromatic polymers with similar ladder structure prepared by electropolymerization decreases in the order shown in Scheme 31. Among them, the P $\phi$ PD also exhibits the highest electroconductivity.<sup>227</sup>

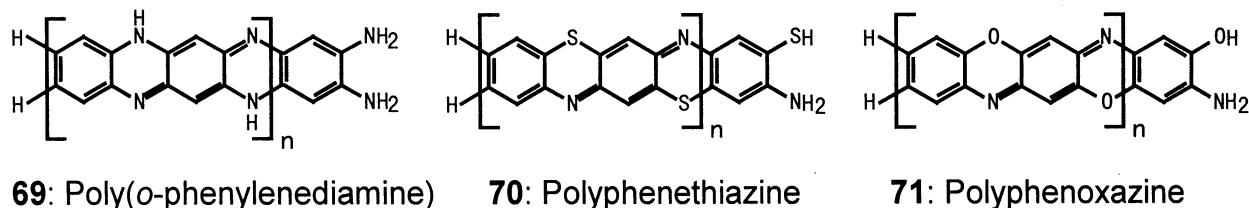
It can be seen from Table 17 that the electroconductivity of aromatic diamine polymers shows an apparent dependence on polymerization conditions (working electrode, electrolyte, solvent, current, temperature), oxidation/reduction state, and film-forming technique. Among the four solvents (1,2-dichloroethane, nitrobenzene, dichloromethane, and 99% aqueous acetonitrile) and three electrolytes (tetra-*n*-butylammonium perchlorate, tetraethylammonium bromide, and tetramethylammonium chloride) it appears that 1,2-dichloroethane and tetra-*n*-butylammonium perchlorate are the best solvent and electrolyte, respectively, for the preparation of P $\phi$ PD film with relatively high conductivity.<sup>155</sup> The increase in current density but decrease in the temperature of

electropolymerization are both beneficial to the enhancement of the electroconductivity of P $\phi$ PD possibly due to the formation of an enhanced conjugation length of polymer chains. It seems that constant current polymerization gives a higher conductivity of P $\phi$ PD than cyclic voltammetry in HCl, while the situation is opposite in H<sub>2</sub>SO<sub>4</sub>.

The electroconductivity of PBZ increases monotonically from  $1.22 \times 10^{-7}$  to  $3.56 \times 10^{-6}$  S/cm with increasing HCl concentration from 0.1 to 2 M or from  $4.1 \times 10^{-9}$  to  $2.12 \times 10^{-8}$  S/cm with increasing NaClO<sub>4</sub> concentration from 0.1 to 1 M, possibly due to an increase in the ratio of anions available for conductivity.<sup>116</sup> The conductivity will decrease by 3–200 times for the PBZ obtained in NaClO<sub>4</sub> and by 150–1000 times for the PBZ in HCl after a cycle of heating to 150 °C for 2 h then cooling to room temperature, because of the conversion from an ionic bond of the anion to a covalent bond or dedoping process. Therefore, the influence of temperature on the conductivity of the PBZ was studied in a wider temperature range. It is observed that the conductivity of the PBZ obtained in 0.1 M HCl increases from  $1.22 \times 10^{-7}$  to  $5.8 \times 10^{-5}$  S/cm with increasing temperature from 26 to 75 °C, then decreases, but with a second increase to  $1.8 \times 10^{-4}$  S/cm at 250 °C. The PBZ obtained in 1 M HCl is similar in the conductivity variation with temperature, i.e., an initial increase from  $3.03 \times 10^{-7}$  to  $1.85 \times 10^{-4}$  S/cm with temperature from 26 to 100 °C, then a decrease, and finally a new increase to  $1.75 \times 10^{-4}$  S/cm at 200 °C. The increase in conductivity with temperature rise suggests that the PBZs are semiconductors, which is similar to the PBZ prepared by chemically oxidative polymerization. A linear relationship between the conductivity logarithm and reciprocal temperature cube root shows a variable range hopping mechanism of conduction. The activation energy of the conductance calculated based on the linear relationship increases from  $1.09 \times 10^{-3}$  to  $1.90 \times 10^{-2}$  eV with decreasing HCl concentration from 2 to 0.1 M or from  $1.33 \times 10^{-2}$  to  $3.83 \times 10^{-2}$  eV with decreasing NaClO<sub>4</sub> concentration from 1 to 0.1 M.

Electropolymerized films of P $\phi$ PD, PBZ, and PPBZ exhibit higher conductivity than the cast film due to a much lower doping level and also partial retention of casting solvent in the cast film.<sup>230,269</sup> Both of the P $\phi$ PD films with the same thickness of 500 nm exhibit a dependence of the conductivity on the exposed time in ambient air. The conductivity of the electropolymerized and solution-cast P $\phi$ PD films is 0.029 and 0.0071 S/cm, respectively, at a dry state but increases to 0.21 and 0.065 S/cm, respectively, after being exposed to air for 24 h since the oxygen molecules absorbed could act as an electron accep-

Scheme 31



tor.<sup>269</sup> The as-electropolymerized PPBZ film with 150 nm thickness with a doping level of 11.1% at +3.6 V in tosylate exhibits an electroconductivity of 2.0 S/cm,<sup>230</sup> whereas solution-cast PPBZ film with the same thickness in the same doping conditions exhibits a low conductivity of 0.1 S/cm. The as-electropolymerized PBZ film with a 150 nm thickness with a doping level of 10.2% at +2.35 V in  $\text{BF}_4^-$  exhibits a conductivity of 0.1 S/cm, whereas solution-cast PBZ film with the same thickness in the same doping conditions exhibits a much lower conductivity of  $2 \times 10^{-5}$  S/cm. There is also a decline of the conductivity after extended electrochemical cycling or prolonged storage for the films. After 1000 electrochemical cycles, the conductivity of the as-electropolymerized and cast PPBZ films decreases from  $2 \times 10^{-5}$  and  $2 \times 10^{-6}$  S/cm to  $9 \times 10^{-6}$  and  $9 \times 10^{-7}$  S/cm, respectively. After storage for 30 days, the conductivity of the as-electropolymerized and cast PBZ films decreases from  $5 \times 10^{-4}$  and  $2 \times 10^{-5}$  S/cm to  $10^{-6}$  and  $2 \times 10^{-8}$  S/cm, respectively. This indicates that the conductivity of both films is not stable.

P18DAN film exhibits a conductivity of 0.01 S/cm when reduced fully at -0.5 V for 5 min and of 2.1–2.7 S/cm when oxidized fully at 0.5 V for 2 min.<sup>181</sup> The electroconductivity of the fully oxidized P18DAN film is 100–1000 times higher than the P18DAN film reported by Oyama<sup>139</sup> because the P18DAN film is prepared in a cleaner solution and thus is somewhat better optimized with the higher molecular weight. When the P18DAN films are silver doped, they become much better conductors. The oxidized form of the Ag-doped film has a high conductivity of 13–35 S/cm, whereas the reduced form of the Ag-doped film appears to have the highest conductivity of 106–309 S/cm. It can be concluded that the conductivity of the Ag-doped polymer is higher than that doped by the redox reaction by at least 2 orders of magnitude. The conductivity of P15DAN is higher ( $10^{-2}$  S/cm)<sup>174</sup> with Au as working electrode than with Pt as working electrode ( $10^{-5}$  S/cm).<sup>173</sup>

The undoped poly(3-hydroxy-*o*PD), behaving practically as an insulator due to the low conductivity of  $(8 \times 10^{-9})$ – $(2.4 \times 10^{-8})$  S/cm does not show conducting properties.<sup>180</sup> The doped poly(3-hydroxy-*o*PD) is a semiconductor, having a relatively high conductivity of  $1.5$ – $5.6 \times 10^{-5}$  S/cm. However, either the geometry or dimensions of the electrode and the electropolymerization conditions have no significant influence on the conductivity of the poly(3-hydroxy-*o*PD). It is seen that the effect of the working electrode on the conductivity of aromatic diamine polymers is complicated.

The conductivity of a composite film of sulfonic *p*PD/AN copolymer with waterborne polyurethane doped by 1 M HCl decreased monotonically from 0.029 to  $10^{-8}$  S/cm with increasing sulfonic *p*PD content from 0 to 50 mol % because the  $\pi$ -conjugation along the polymer backbone is decreased by an increase in the torsional angle between adjacent phenyl rings resulting from the steric effect of the sulfonic groups and the cross-linked/branched structures.<sup>271</sup> It is interesting that *p*PD/AN (1/9 mol)

copolymer doped by 1 M HCl exhibits the maximum conductivity of 0.2 S/cm, which is even higher than that (0.029 S/cm) of AN homopolymers, due to the lower content of HQ/quinone structures in the *p*PD/AN copolymer. It is concluded that there are fundamental differences between *p*PD/AN and sulfonic *p*PD/AN copolymers.

In addition to the electroconductivity, the electroactivity, electrochromism, and permselectivity are also widely studied and will be discussed in section IX.A–C. However, other properties of electrosynthesized polymers from aromatic diamines have been less investigated. It appears that only three reports on their stability and paramagnetism are found and reviewed as follows. The stability of the *p*PD/AN and sulfonic *p*PD/AN copolymer films is also different.<sup>271</sup> It was revealed that the sulfonic *p*PD/AN copolymer film shows higher stability than *p*PD/AN copolymer film and PAN film. Furthermore, the stability of the sulfonic *p*PD/AN copolymer film increases with increasing sulfonic *p*PD unit content due to the existence of the  $-\text{SO}_3\text{H}-\text{NH}$  interaction, leading to difficulty in hydrolyzing the film to degradation. On the other hand, the *p*PD/AN (1/9) copolymer film is more stable than PAN film, also due to the cross-linking structure from *p*PD unit.

Electropolymerized PBZs have much lower thermostability in nitrogen than chemically oxidative PBZs.<sup>116</sup> The decomposition temperature and char yield at elevated temperature of the PBZs are lower at higher electrolyte concentration, but the activation energy of the thermal decomposition appears to be larger. The PBZs generally show an initial weight loss at 50–100 °C due to the elimination of water and acid with an average activation energy 53 kJ/mol and decomposition order of 1.2. Breakage of macromolecular chains occurs at 200 °C with a low average activation energy of 28 kJ/mol and decomposition order of 1.1. The char yield at 573 °C of the PBZ increases from 37 to 46 wt % with decreasing  $\text{NaClO}_4$  concentration from 1.0 to 0.1 M. In particular, the PBZ formed in 1 M HCl shows the largest char yield of 50 wt % at 573 °C. Noteworthy is that the PBZs exhibit high glass transition and melting temperatures. Dithiodianiline/AN (2/175) copolymer shows higher thermal stability than PAN in an inert atmosphere.<sup>116,232</sup> Dithiodianiline/AN (2/175) copolymer at a heating rate of 20 °C/min exhibits the first small weight loss (3%) corresponding to the removal of water and dopant at 100–150 °C, the second weight loss (15%) corresponding to oligomeric products at 300–410 °C, and the third weight loss (25%) due to backbone decomposition from 410 up to 700 °C. At 700 °C, the copolymer shows a higher char yield of 58% than the PAN (42%). The higher thermal stability of the copolymer should be ascribed to the branched structure.

It is interesting that the *po*PD prepared by constant current polymerization exhibits paramagnetism.<sup>155</sup> Its magnetic susceptibility varies significantly with polymerization solvents and increases from  $9 \times 10^{-5}$ ,  $3.8 \times 10^{-4}$ ,  $9.2 \times 10^{-4}$ , to  $1.5 \times 10^{-3}$  emu/two-ring unit with changing solvent from 99% aqueous acetonitrile, dichloromethane, dichloroethane, to

nitrobenzene with Pt as the working electrode. In particular, the highest magnetic susceptibility of  $3.3 \times 10^{-3}$  emu/two-ring unit has been observed in dichloroethane on Ni electrode. The oscillation and chaotic phenomena occurring in electroactive thin *PoPD* films on electrode were studied by W. Kutner (Poland), L. Dunsch (Germany), and G. Inzelt (Hungary). The optical properties of poly(*o*-dianisidine) films on ITO-coated glass electrode are studied by changing the electropolymerization conditions.<sup>316</sup>

### K. Relationship between the Structures of Monomers and Polymers

At this point, four oxidative polymerizations of aromatic diamines have been thoroughly elaborated on in the above sections. The major findings of this review are that several new oxidative polymers with novel and controlled compositions and topologies can be prepared via these oxidative polymerization techniques. Every oxidative polymerization has its own unique characteristics and therefore produces polymers with specific and peculiar macromolecular and morphological structures, form, and properties, as listed in Table 5. However, no systematic comparison of monomer structure and resulting polymer chain structure was found. Apparently, it is necessary to better correlate the structures of the monomers and the polymers formed, although the macromolecular structure of most polymers is still a controversial subject. The controversy lies in the formation of linear or ladder chain structure during the polymerization of aromatic diamines especially for *o*PD. For example, *o*PD, 15DAN, and 18DAN can oxidatively polymerize into linear polymers with one free amino group on each repeated unit under certain conditions. Generally, *o*PD, *m*PD, *p*PD, and 23DAN can oxidatively polymerize into phenazine ring containing ladder polymers sporadically with some free amino groups. 15DAN and 15DAAQ could form special ladder polymers by electrooxidative polymerization. *m*PD, TAB, and tetraaminobenzene would form network polymers. Therefore, oxidative polymerizations are readily suited to synthesize aromatic diamine and multiamine polymers with novel topologies such as linear, semi-ladder, whole ladder, or well-defined network structures. This will be especially important for the macromolecular design of oxidative polymers from aromatic diamines. In fact, the different macromolecular structures of polymers of the same monomers should be attributed to the peculiar mechanisms of the oxidative polymerization at different conditions.

### VIII. Oxidation Polymerization Mechanisms

The mechanisms of four oxidative polymerizations have not, so far, been completely investigated due to their complexity. However, there are few investigations on the mechanism of oxidative polymerizations. The earliest appeared in 1958, when Elving and Krivis proposed that by anodic chronopotentiometry with a graphite electrode three isomeric PDs exhibit a different nature of electrooxidation course.<sup>106,107</sup> At pH values of 2, 5, and 11, *o*PD and *p*PD undergo two-electron oxidation, the latter showing semiquinone

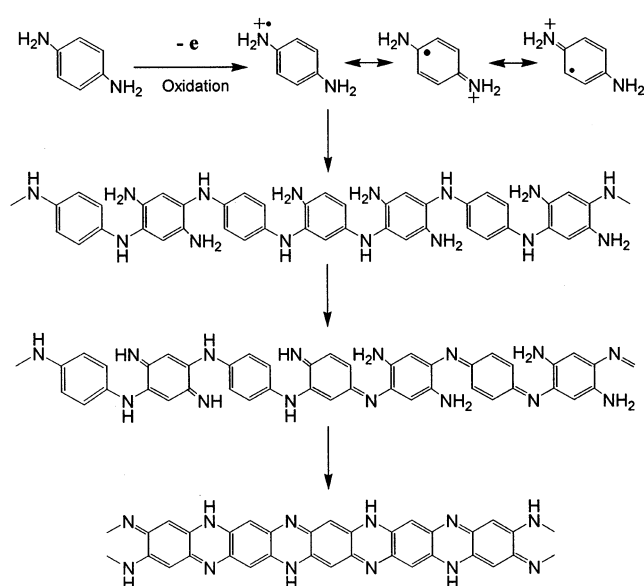


**Figure 15.** Chemically oxidative polymerization mechanism of *p*-phenylenediamine (*p*PD).<sup>62</sup>

diimine formation; at pH = 5.5, *o*PD undergoes a subsequent one-electron process. The latter may be due to reaction of the diimine with *o*PD to produce diaminophenazine, which is further oxidized by a one-electron step to a free radical, which then polymerizes.<sup>107</sup> Although *m*PD shows a one-electron wave due to the formation of a free radical which could polymerize,<sup>106</sup> the *m*PD undergoes at pH = 5.5 a three-electron oxidation to a final polymeric product and at pH = 11.2 a two-electron oxidation which leads to an insoluble polymer.<sup>107</sup> Obviously, only the initiation step of oxidative polymerization was involved in this course.

The mechanism of the oxidative polymerization is believed to be closely related to the position of amino substitution on aromatic diamines. It is reported that the oxidation of *o*PD<sup>297</sup>, *p*PD (Figure 15),<sup>62</sup> and 15DAN<sup>173,174</sup> results in oxidation of both amino groups and sometimes of only one amino group,<sup>164,171,317</sup> while for *m*PD both amino groups are oxidized.<sup>69</sup> The oxidation of 18DAN is reported to result in only one amino group being oxidized,<sup>181</sup> in comparison with 23DAN and 15DAAQ for which both amino groups are oxidized.<sup>139,171,227,289</sup> Also, only the amino group in ANO was oxidized and the hydroxyl group does not take part in the electropolymerization.<sup>317</sup> The different positions of the amino groups on the benzene or naphthalene or anthraquinone ring and the different number of amino groups oxidized per monomer result in polymers of varying macromolecular structure and solubility in organic solvents.<sup>171</sup> Therefore, *Pm*PD, *P23DAN*, and *P15DAAQ* should be ladder polymers, whereas *P18DAN* is a linear polymer containing one free amino group per monomer unit. *Po*PD, *Pp*PD, and *P15DAN* may have ladder or linear chain structures, depending on the oxidative polymerization condition. The prime difference between the ladder and linear structures obtained by oxidation polymerization from aromatic diamines is the absence of free amino groups in the ladder structure but the presence of free amino groups in the linear one.

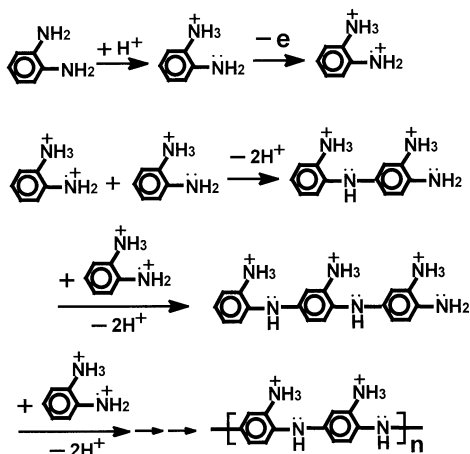


**Figure 16.** Electrochemically oxidative polymerization mechanism of *o*-phenylenediamine(*o*PD).<sup>164</sup>

It has been shown that the oxidative polymerization of aromatic diamines occurs via the combination of a radical cation with a monomeric form of aromatic diamines and its mechanism is very complicated in nature. Some specific mechanisms for the electropolymerization of *o*PD, 15DAN, and 18DAN have been proposed.<sup>62,164,173,181</sup> Yano suggested that one of the amino groups of *o*PD in acidic aqueous solution must be protonated.<sup>164</sup> The positively charged ammonium group without a lone electron pair probably hinders the formation of the phenazine ring during electropolymerization and then has the *meta* orientation effect. Therefore, the head-to-tail coupling is most favorable for the *o*PD polymerization, leading to the formation of poly(aminoaniline). The detailed electropolymerization mechanism of *o*PD is shown in Figure 16.

Dai et al. proposed a slightly different electropolymerization mechanism of *o*PD and HAN.<sup>161</sup> The monomers are initially oxidized anodically to give a monocationic radical, then undergoing chemical coupling to form a dimer, which can be further oxidized to produce a bication. The bication will either undergo polymerization to form a linear chain polymer or become cyclized to yield cyclic ladder polymer. Very similarly, Jang et al. suggested that during electropolymerization of *o*PD at least two different polymeric components which are responsible for electron mediation formed:<sup>318</sup> an active component containing phenazine mainly in the early stage of polymerization

and an inactive component containing noncyclically coupled species. A plausible mechanism for the electropolymerization of *o*PD was proposed. Additionally, an electropolymerization mechanism of sulfonic *p*PD and possible proximity of  $\text{SO}_3\text{H}$  and  $\text{NH}$  groups for self-doping has been mentioned.<sup>302</sup>

The electrooxidative oligomerization of 15DAN is found to consist of a sequence of oxidation, coupling, and deprotonation reactions.<sup>173</sup> As shown in Figure 17, the initial step involves the oxidation of 15DAN on an electrode surface to produce the quite unstable radical cation. This radical cation couples with a 15DAN-monomer molecule to form the neutral radical and protonated monomer species. The neutral radical is oxidized by the transfer of an electron to give the cationic structure. Two cationic molecules suffer a fast and irreversible combination to give rise to the dication of the dihydrodimer, which subsequently deprotonates to produce the dimer. The dimer may be oxidized slightly more easily than the monomer and thus is reoxidized by a reversible transfer of two electrons to the dication. This dication couples with the radical cation and then deprotonates to give the hydrocationic structure of the trimer, which is oxidized and deprotonated to produce the oxidized form of the tetramer to proceed polymerization further.

The electropolymerization mechanism of 18DAN is almost the same as that of 15DAN but the position of combination is different, possibly due to the spatial structural difference between 18DAN and 15DAN. In 18DAN, two amino groups are in the same plane but the both amino groups in 15DAN are in different planes.<sup>177</sup> The first oxidation product of 18DAN is also a radical cation formed on one of two amino groups.<sup>181</sup> The radical cation deprotonates to a nitrene cation, leading to polymerization. The second amino group on each monomer unit may be intact during this sequence of oxidation and protonation reactions because the formation of the second positive charge (dication) on naphthalene requires a very high anodic polarization. It is suggested that the polymerization of 18DAN takes place most likely through the head-to-tail coupling at the *para* position to the oxidized amino group (Figure 18), as in the case of the *o*PD polymerization proposed by Yano.<sup>164</sup> The

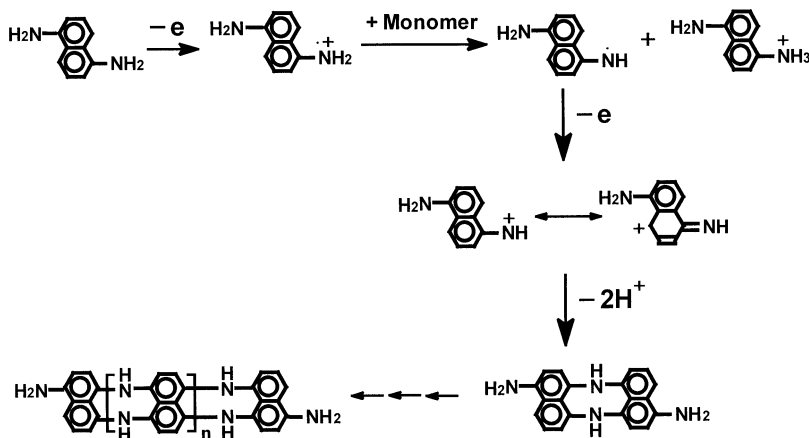


**Figure 17.** Electrochemically oxidative oligomerization mechanism of 1,5-diaminonaphthalene (15DAN).<sup>173</sup>

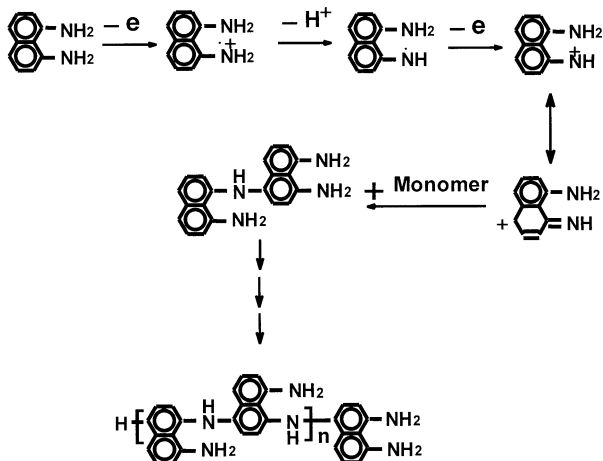


**Figure 18.** Electrochemically oxidative polymerization mechanism of 1,8-diaminonaphthalene (18DAN).<sup>181</sup>

macromolecular structure of resulting P18DAN formed thus is the most favorable for the formation of heavy metal ion–amine complexes. It appears that three mechanisms shown in Figures 16–18 are more probable for the corresponding oxidative polymerizations. Note that there are many factors including electrolyte, solvent, temperature, pH, and electropolymerization method that affect the oxidative reaction mechanism during the electropolymerization of aromatic diamines, thus impacting the characteristics of the polymers coated on the electrode. However, there has been little focus on the influence of the reaction conditions on the electropolymerization mechanism.

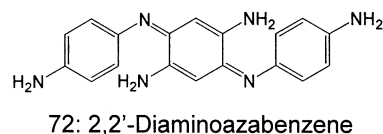
The mechanism of electropolymerization of benzidine has been mentioned.<sup>189</sup> The first step of the polymerization is the formation of the benzidine dication that is stable for several hours in acidic medium (pH < 1). The dication in the medium at 1 < pH < 2.5 may couple with benzidine to give a dimer which initiates the polymerization.

Yacynych and Mark analyzed the effect of the oxidation mechanism on the conductivity of *o*PD film in 1976.<sup>112</sup> They indicated that the conductive film is formed by the polymerization of monocation radicals formed by the oxidation of *o*PD. The insulating film could be formed through the polymerization of the dication of the *o*PD formed on disproportionation or the monocation radical oxidizing at a conducting film surface rather than the electrode surface, yielding a different product, the insulating film.

As compared with the electropolymerization mechanism, the chemical oxidative polymerization mechanism has been studied less frequently to date, though several interesting mechanisms have been presented. Zaki et al. proposed a chemically oxidative condensation mechanism involving six-electron oxidation for *o*PD and *p*PD to get DAPh and 2,2'-diaminoazabenzene (*p*PD trimer) (Scheme 32), respectively, with  $K_3[Mn(C_2O_4)_3]$ ,  $K_3[Co(C_2O_4)_3]$ , and  $K_2[Cu(C_2O_4)_2]$  complexes as oxidants.<sup>319</sup>

The oxidation of *o*PD and *p*PD follows the inner-sphere mechanistic classification. The redox reactions follow first-order kinetics with respect to each of the reactants and first order in amine concentration in

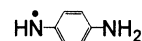
### Scheme 32



homogeneous and heterogeneous phases. However, the specific oxidation rate of *p*PD is larger than that of *o*PD. Additionally, the mechanism of electrocopolymerization between dithiodianiline and AN was proposed.<sup>232</sup>

The chemically oxidative polymerization mechanism for *p*PD has been presented by Cataldo.<sup>62</sup> It is suggested that *p*PD during oxidation is changed directly to a pernigraniline-like structure without passage through intermediate polymeric states involving polymeric radical cations (polarons) or carbocations. The ab initio inter-radical potential for *p*PD radical cation dimer has been studied.<sup>320</sup> In addition to  $K_2S_2O_8$ , other oxidants including ozone, bromine, and chlorine are also able to oxidize *p*PD. The first step during oxidation is the extraction of an electron from the *p*PD molecule with the formation of a radical cation or semiquinone radical. This radical cation is intensely colored and has a tendency to polymerize. The radical cation is stabilized by resonance but may also undergo polymerization or is transformed by further oxidation to unstable *p*-quininediimine. The active sites available in the radical cation are only *ortho* positions to the two-amine groups, as shown in Figure 15.

When the oxidant is changed to  $Fe^{3+}$  chelate, the polymerization mechanism of *p*PD seems different.<sup>212</sup> The first step is the fast formation of the coordination complex between of *p*PD and  $Fe^{3+}$  chelate. The second step is the fast activation of the coordinated *p*PD by electron transfer to the  $Fe^{3+}$  and the formation of *p*PD monoradical



The third step is the coupling of two *p*PD monoradicals to form 4,4'-diaminobenzenehydrazine, which is easily oxidized to a dimer azophenylenediamine by  $Fe^{3+}$  chelate. The dimer is again activated by coordination to  $Fe^{3+}$  chelate and then coupled with an activated monomer *p*PD or dimer until the formation of *p*PD polymer polyazophenylene. The  $Fe^{2+}$  chelate formed can be oxidized at a relatively low rate by oxygen to  $Fe^{3+}$  chelate and again as an oxidant. Therefore, the polymerization rate is mainly controlled by the oxidation of  $Fe^{2+}$  to  $Fe^{3+}$  chelate. There is an equilibrium of  $Fe^{3+}$  and  $Fe^{2+}$  chelates during *p*PD polymerization because the electrochemical potential of reaction system remains a constant value of 100 mV except for a rapid change during the initial stage of the polymerization. It is seen that the chemically oxidative conditions strongly influence the oxidative polymerization mechanism, which renders the investigation of the complete mechanism extremely difficult.

The enzyme-catalyzed oxidative polymerization mechanism of aromatic diamines was briefly mentioned. It is proposed that the initial step of HRP-



catalyzed  $\text{H}_2\text{O}_2$  oxidation of three PD isomers is the formation of the HRP–oxygen complex.<sup>71,72</sup> The complex subsequently reacts with aromatic diamine monomer to form a monomer radical and HRP–OH compound. The monomer radical may be formed also by the reaction between the HRP–OH compound and monomer, accompanying the regeneration of HRP that can serve as an enzyme again. The coupling of the monomer radicals and similar reactions will produce polymers by N–N, N–C, or C–C coupling. The coupling mode seems to be dependent on the monomer structure. It is suggested that the oxidative polymerizations of *o*PD and *p*PD are realized partly through N–N coupling. On the basis of the big difference in the solubility of *Po*PD and *Pp*PD in DMF and NMP listed in Table 14, it can be deduced that the coupling mode of *o*PD and *p*PD for the polymerization is not the same. The oxidative polymerization of *m*PD proceeds irregularly through C–N, N–N, and C–C couplings, leading to the formation of branched or even cross-linked polymers that are hardly ever soluble in THF.

The photocatalyzed oxidative polymerization mechanism was scarcely studied. Teshima et al. thought that the first step of photooxidative polymerization is the formation of active *N*-phenyl-*p*PD cation radicals by photo-oxidation in the *N*-phenyl-*p*PD and AN mixture system, because the oxidation potential of *N*-phenyl-*p*PD is comparatively lower than the redox potential of the ruthenium complex.<sup>256</sup> The electron was transferred from *N*-phenyl-*p*PD to the ruthenium complex and to methyl viologen ion and then consequently to oxygen by photoinduced electron transfer. This continuous and unidirectional photoinduced electron transfer produced *N*-phenyl-*p*PD cation radicals. These electrophilically attacked the AN monomer to yield AN trimer. Because the oxidation potential of the trimer should be even lower than that of *N*-phenyl-*p*PD, the trimer may be easily photooxidized by the photoactivated ruthenium complex. This reaction proceeds successively to form PAN.

For the pure *N*-phenyl-*p*PD system, the *N*-phenyl-*p*PD protonated at the primary amino group at pH = 0 is photooxidized by excited ruthenium tris(2,2'-bipyridyl)<sup>2+</sup> and cation radicals should be generated.<sup>257,258</sup> The ruthenium tris(2,2'-bipyridyl)<sup>+</sup> formed is oxidized back to ruthenium tris(2,2'-bipyridyl)<sup>2+</sup> by oxygen in aerated solution. The polymerization proceeds with the protonated doubly oxidized quinoid form of *N*-phenyl-*p*PD reacting with unoxidized *N*-phenyl-*p*PD, followed by further oxidation at the macromolecular chain end via photoinduced electron transfer. Because of the complexity of the enzyme- and photocatalyzed oxidative systems and conditions, the enzyme- and photocatalyzed oxidative polymerization mechanisms have attracted much less attention than the electrochemically and chemically oxidative mechanisms.

In summary, the oxidative polymerization mechanism of aromatic diamines is a very complicated and diverse process depending on the monomer type, oxidant feature, and polymerization method and conditions. There is no one complete mechanism of

oxidative polymerization that is universally accepted for the whole family of aromatic diamines so far. Perhaps each monomer may be suited to a specific mechanism at a given polymerization condition. More studies on the complete mechanism of oxidative polymerizations are needed because it is especially important for a correlation of oxidative conditions with performance and multifunctionality of the aromatic diamine polymers. It is the diverse polymerization mechanisms that lead to novel colorful polymers with various macromolecular structures, multifunctionalities, and extensive application potentials.

### IX. Multifunctionality and Potential Applications of the Aromatic Diamine Polymers

Since the pioneering studies demonstrate that the oxidative polymers of aromatic diamines have a lot of novel functions such as the variable electrical conductivity with polymer structure,<sup>194</sup> multiple conductivity (polaron, bipolaron, proton, and radical conductivity),<sup>178,214</sup> changeable electroactivity,<sup>177</sup> unique electrochromism,<sup>247,321</sup> high permselectivity to various electroactive species,<sup>289,322</sup> linear sensitivity of the electroconductivity to moisture,<sup>222,275</sup> regular variation in the electroconductivity with temperature<sup>214</sup> and external electric field,<sup>323</sup> high sensibilities of the polymer-modified electrode to the biosubstances at an extremely low concentration,<sup>182,286,306</sup> novel electrode behavior,<sup>149,156,272,276,286</sup> good detecting ability of electroinactive anions,<sup>157</sup> efficient electrocatalysis for the redox reaction,<sup>324,325</sup> effective absorptivity to heavy metal ions,<sup>180,181</sup> active electronic barrier ability and strong adhesion ability to metal,<sup>179,326,327</sup> and high capacitance,<sup>227</sup> there has been an explosion in potential applications in numerous intercrossing fields. These multifunctionalities are being investigated further, and some new significant progress and higher value applications will be achieved again.<sup>328</sup>

#### A. Electroactivity

Cyclic voltammetry is particularly useful in investigating and differentiating the electroactivity from electroinactivity of conducting polymers. The reversible electroactivity is one of the most promising functionalities of conductive polymers for applications in rechargeable batteries because the polymers could serve as light and flexible electrodes exhibiting a large capacity to reversibly accept and donate electrical charge at a relatively low potential. Table 21 summarizes the electroactivity of many polymer films from various aromatic diamines determined by cyclic voltammetry. Almost all polymers prepared from aromatic diamines are electroactive in acidic aqueous solution and sometimes in buffer solution. It is seen that *p*PD/AN copolymer exhibits the narrowest range from 0.42 to 0.66 V vs SCE, whereas P15DAAQ exhibits the widest electroactivity range from –1.8 to +1.0 V vs Ag/AgCl. In fact, it is reported that 14DAAQ, 15DAAQ, and 26DAAQ monomers also exhibit a wider electroactivity range from –2.4 to –0.6 V vs ferrocene/ferrocenium, among which 15DAAQ exhibits the highest electroactivity but 26DAAQ exhibits the lowest electroactivity.<sup>334</sup> All

**Table 21. Electroactivity of Polymer Films Prepared from Aromatic Diamines by an Oxidative Polymerization**

polymer	electrode	electrolyte	electroactivity range	anodic peak oxidation potential, $E_{pa}$	cathodic peak reduction potential, $E_{pc}$	formal potential, $E^{\circ}$	refs
PoPD	GC	0.2 M Na <sub>2</sub> SO <sub>4</sub> 0.1 M H <sub>2</sub> SO <sub>4</sub>	-1.0 to 0.5 V vs SCE	-0.15	-0.13	-0.14	153
PoPD	GC	0.2 M Na <sub>2</sub> SO <sub>4</sub> H <sub>2</sub> SO <sub>4</sub> , N <sub>2</sub> (O <sub>2</sub> )	-0.8 to 0.3 V vs SCE	-0.15 (-0.13)	-0.16 (-0.29)	-0.15 (-0.21)	276
PoPD	GC	0.2 M Na <sub>2</sub> SO <sub>4</sub> H <sub>2</sub> SO <sub>4</sub> , pH = 1, O <sub>2</sub>	-0.8 to 0.4 V vs Ag/AgCl	0	-0.09		292
PoPD	ITO	0.1 M H <sub>2</sub> SO <sub>4</sub>	-0.5 to 0.5 V vs SCE	0.025	-0.25		164
PoPD	Pt	Walpole buffer pH 1.1	-0.2 to 0.15 V vs SCE	-0.06	-0.12	-0.09	272
PoPD	Pt	10 mM KI (KBr) Walpole buffer pH 1.1	-0.2 to 0.65 (-0.2 to 1.3) V vs SCE	-0.06, 0.47 (-0.06, 1.12)	-0.12, 0.35 (-0.12, 0.87)	-	272
PoPD	Pt	1 M H <sub>2</sub> SO <sub>4</sub>	0.05 to 0.75 V vs SCE	0.25 V vs RHE	0.22 V vs RHE	0.23	162
PoPD	Au	0.1 M borate buffer, pH 8.5, N <sub>2</sub>	-0.9 to ~-0.2 V vs SCE	-0.53	-0.8	-0.67	265
PoPD film thin (thick)	Au	1 M HClO <sub>4</sub>	-0.15 to 0.45 V vs SSCE	-0.01 (-0.03)	-0.04 (-0.02)	-0.02 (-0.02)	156
PDAPh	GC	0.2 M Na <sub>2</sub> SO <sub>4</sub> H <sub>2</sub> SO <sub>4</sub> , pH = 1, O <sub>2</sub>	-0.8 to 0.1 V vs Ag/AgCl	no	-0.34		292
poly( <i>N</i> -methyl- <i>o</i> PD)	Au	0.1 M borate buffer, pH 8.5, N <sub>2</sub>	-0.8 to -0.5 V vs SCE	-0.1	-0.46	-0.27	265
poly(3-methyl- <i>o</i> PD)	Pt	1 M HCl	-0.3 to +0.1 V vs SCE	-0.07	-0.23	-0.15	263
Poly(3- <i>n</i> -butyl- <i>o</i> PD)	Pt	1 M HCl	-0.3 to +0.1 V vs SCE	-0.08	-0.15	-0.11	263
P15DAN	mild steel	1 M HClO <sub>4</sub>	0.3 to 1.0 V vs SCE	0.48	0.44	0.46	179
P15DAN	Au	0.1 M KNO <sub>3</sub>	-1 to 1 V vs Ag/AgCl	-0.5	-0.25	-0.37	225
P15DAN	Au	0.1 M LiClO <sub>4</sub> / CH <sub>3</sub> CN	-0.4 to 0.4 V vs SCE	0.18 V vs SSCE	-0.01 V vs SSCE	0.095	174
P15DAN	GC	0.1 M N(C <sub>4</sub> H <sub>9</sub> ) <sub>4</sub> ClO <sub>4</sub> / 0.2 M HClO <sub>4</sub>	0.3 to 1.2 V vs SCE	0.85	0.78	0.81	176
P15DAN	Pt	2 M HClO <sub>4</sub>	-0.05 to 0.75 V vs SCE	0.42	0.39	0.4	176
P15DAN	Pt	0.1 M LiClO <sub>4</sub> /HClO <sub>4</sub> , pH = 2.1	-0.4 to 0.4 V vs SCE	0.23	-0.03		304
P15DAN	GC	0.1 M HCl	-0.2 to 0.7 V vs Ag/AgCl	0.29, 0.47	0.02, 0.44		178
P15DAN	Pt	0.1 M HCl	0 to 0.5 V vs SCE	0.39	0.21	0.3	173
P15DAN	Pt	1 M HCl	0.1 to 0.5 V vs SCE	0.34	0.3	0.32	175
P15DAN	carbon graphite	HCl solution, pH = 0	-0.2 to 0.5 V vs SCE	0.32	0.31	0.31	173
P15DAN	Pt	HCl solution, pH = 0	0 to 0.8 V vs SCE	0.33	0.24	0.28	177
P18DAN	Pt	0.1 M KNO <sub>3</sub>	-0.6 to 0.6 V vs Ag/AgCl	-0.16	0.23		181
P18DAN	Au	0.1 M HClO <sub>4</sub>	-0.3 to 0.7 V vs SCE	0.3	0.02	0.16	296
P18DAN	Au	0.1 M HClO <sub>4</sub>	-0.4 to 0.5 V vs SCE	0.4	0.1	0.25	180
P18DAN	BPG	0.2 M NaClO <sub>4</sub> pH = 1	-1.2 to 0.5 V vs SSCE	0.26	0.07	0.16	139
P23DAN	GC	0.2 M Na <sub>2</sub> SO <sub>4</sub> pH = 1	-0.7 to 0.5 V vs SCE	-0.12	-0.21	-0.16	188
P23DAN	GC	0.2 M Na <sub>2</sub> SO <sub>4</sub> pH = 1, O <sub>2</sub>	-0.7 to 0.5 V vs SCE	-0.12	-0.24	-0.18	188
P23DAN	BPG	0.2 M NaClO <sub>4</sub> pH = 1	-1.2 to 0.2 V vs SSCE	-0.1	-0.3	-0.2	139
P15DAAQ	Pt	0.1 M N(C <sub>2</sub> H <sub>5</sub> ) <sub>4</sub> ClO <sub>4</sub> / propylene carbonate	-1.8 to 1.0 V vs Ag/AgCl	-0.93, 0.72, 0.93	-1.42, -1.1, 0.6, 0.8		227
PBZ	Pt	0.1 M HClO <sub>4</sub> / 0.3 M NaClO <sub>4</sub>	0 to +0.5 V vs SCE	0.25	0.22	0.24	189
PBZ	Au	0.2 M HClO <sub>4</sub> / 0.3 M NaClO <sub>4</sub>	-0.3 to 0.45 V vs SCE	0.19	0.16	0.22	329
PBZ	Pt	0.3 M HClO <sub>4</sub> / 0.3 M NaClO <sub>4</sub>	-0.1 to 0.5 V vs SCE	0.26	0.25	0.25	330

**Table 21 (Continued)**

polymer	electrode	electrolyte	electroactivity range	anodic peak oxidation potential, $E_{pa}$	cathodic peak reduction potential, $E_{pc}$	formal potential, $E^{\circ}$	refs
polynaphthidine	Pt	0.4 M NaClO <sub>4</sub> /CH <sub>3</sub> CN	0.1 to 1.14 V vs SCE	0.99	0.96	0.975	190
<i>m</i> PD-AN copolymer	Au	1.2 M H <sub>2</sub> SO <sub>4</sub>	0 to 0.6 V vs SCE	0.26	0.19	0.23	168
PAN- <i>Pm</i> PD bilayer	Au	1.2 M H <sub>2</sub> SO <sub>4</sub>	-0.1 to ~0.9 V vs SCE	0.2, 0.76	0.05, 0.65		168
PAN- <i>Pm</i> PD bilayer	Pt	0.5 M H <sub>2</sub> SO <sub>4</sub>	0 to 0.6 V vs Ag/AgCl	0.2	0.09	0.14	285
<i>p</i> PD-AN copolymer	IrO <sub>2</sub>	H <sub>2</sub> SO <sub>4</sub> /H <sub>2</sub> O pH = 0	-0.2 to 1.0 V vs Ag/AgCl	0.34, 0.61, 0.79	0.12, 0.52, 0.67		169
<i>p</i> PD-AN copolymer	carbon micro-band gap	1 M H <sub>2</sub> SO <sub>4</sub>	0.42 to 0.66 V vs SCE	0.59	0.55	0.57	331
15DAN-AN copolymer	mild steel	1 M HClO <sub>4</sub>	0.3 to 1.0 V vs SCE	0.48, 0.79	0.44, 0.75		179
poly(phenosafranin)	BPG	0.1 M NaH <sub>2</sub> PO <sub>4</sub>	-1.0 to 0.4 V vs SCE	-0.45	-0.23	-0.34	332
poly( $\beta$ -amino-anthraquinone)	carbon fiber	deaerated pH 5.5 acetate buffer	-1.0 to -0.2 V vs SCE	-0.594	-0.485	-0.53	333

three voltammograms are characterized by two quasi-reversible waves reflecting the sequential uptake of one electron by each anthraquinone monomer.

It is reported that the electroactivity of the oxidative polymers of aromatic diamines depends significantly on the composition and pH value of electrolyte, polymer film thickness, and voltammetric cycles. The electroactivity exhibits a different dependence of gas soluble in the medium for different polymers. In both oxygen-saturated and nitrogen-degassed electrolytes, *Po*PD containing phenazine rings as electroactive sites shows electroactivity.<sup>291</sup> Although PDAPh shows a strong irreversible peak growth at -0.35 V in oxygen-saturated electrolyte, it is nearly electroinactive under nitrogen, showing only a small quasi-reversible couple centered at -0.21 V, possibly due to the distinctly different molecular structure of *Po*PD from PDAPh.

The electroactivity of *Po*PD and PDTDA films in acidic aqueous media depends strongly on the pH value and the nature of counterions.<sup>231,307</sup> The peak potentials of *Po*PD/Au and PDTDA/ITO electrodes steadily shift to more negative potentials with increasing pH of the HClO<sub>4</sub> solution, indicating that the oxidation and reduction processes are accompanied by deprotonation and protonation, respectively. The CV character of the *Po*PD/Au electrode does not change with pH. The peak potentials of the reversible oxidation-reduction wave of *Po*PD film are independent of scan rates in a range from 2 to 200 mV/s, indicating fast charge-transfer kinetics at the film interfaces.<sup>308</sup> The relationship between  $E^{\circ}$  of the PDTDA film and the pH value exhibits two slopes above and below pH 2.5.<sup>230</sup> The slope (0.055 V per pH) in solutions with pH < 2.5 is larger than that (0.018 V per pH) in solutions with pH > 2.5, indicating that the PDTDA may show three distinctly different structures. All CVs of the PDTDA film have one single redox wave in the potential range from -0.2 to +0.6 V.<sup>231</sup> The value of the peak current density decreases as the pH value increases. Therefore, the redox response was not observed in the basic

solutions at pH > 3.5, which is similar to the behavior of electroactive PAN.

P15DAN film is electroactive only in acidic aqueous solutions at pH up to 5.<sup>175,282</sup> However, an electroinactive P15DAN film in a basic aqueous medium can recover its activity when dipped again in an acidic solution. The potential sweep cycling shows a well-defined redox response at 0.37 V due to a proton-electron addition-elimination at NH sites. The peak currents of the redox system of the thin films prepared by 3 and 5 scans vary linearly with the sweep rate up to 200 mV/s. In the case of the films prepared by a higher number of polymerization scans of 10-35, the linearity disappears.<sup>177</sup> Repetitive voltammetric cyclings induce a loss of the electroactivity. The electroactivity decreases 11% and 15%, depending on the film thickness, during the first 3 and 5 cycles, respectively. For the thick P15DAN film prepared by a larger number of scans of 10-35, the electroactivity decreases greatly with increasing sweep rate from 5 to 200 mV/s and its drop percent reaches a maximum for the film prepared by 35 scans (50%).<sup>177</sup>

A linear relationship between the charge  $Q_t$  consumed for the formation of the P15DAN films in two different media and their electroactivity  $Q_f$  in acidic water measured on the first cycle is found<sup>177</sup>

$$Q_t = (454 \pm 3) Q_f$$

(3 mM 15DAN concentration  
in acetonitrile solution) (1)

$$Q_t = (11 \pm 2) Q_f$$

(3 mM 15DAN concentration  
in aqueous acidic solution) (2)

A big difference between the coefficients of the two relationships in acetonitrile and water is explained by the following: (1) the low solubility of the 15DAN monomer in aqueous medium induces a lower charging current; (2) some soluble polymers having lower molecular weight in acetonitrile do not deposit firmly on the electrode in this medium.

There is also a linear relationship between  $Q_t$  and  $Q_f$  at low cycling number following the empirical equation.<sup>156</sup>

$$Q_t = 588 Q_f \quad (100 \text{ mM } 15\text{DAN concentration in acetonitrile}) \quad (3)$$

At larger numbers of cycles, the linearity of the relation disappears, possibly due to no further increase of electroactive thickness of the coating with increasing amount of charge used during the film formation. In acetonitrile, P15DAN films with an optimum of electroactivity are successfully prepared by electrolysis at potentials of 0.6–0.7 V.

The P15DAN film prepared by controlled potential electrolysis at two concentrations of monomer in acetonitrile at 0.5 V exhibits a different linear relation between  $Q_t$  and  $Q_f$ .<sup>173</sup>

$$Q_t = 50 Q_f \quad (100 \text{ mM } 15\text{DAN concentration in acetonitrile}) \quad (4)$$

$$Q_t = 225 Q_f \quad (5 \text{ mM } 15\text{DAN concentration in acetonitrile}) \quad (5)$$

The percentage drop (26% and 16%) in the electroactivity of the P15DAN films in acetonitrile solution during the first 3 and 25 cycles, respectively, in acidic water (pH = 0) is much lower than that observed (83 and 49%), respectively, for those prepared in aqueous acidic solution.

The CV for P18DAN film in acetonitrile displays a chemically reversible but electrochemically irreversible behavior,<sup>188</sup> whereas the CV in  $\text{KNO}_3$  aqueous solution shows a more electrochemically reversible behavior than in acetonitrile. This indicates that electron transfer is more efficient in water than in nonaqueous solution because of different redox mechanisms, depending on the availability of protons in the solutions. The CV peak current for the oxidation of P15DAN and P18DAN films in acetonitrile is a linear function of the square root of the scan rate,<sup>176,188</sup> indicating that the redox reaction is controlled by the diffusion of counterions due to a slow electron transfer through thick films.

Bagheri and Nateghi investigated the electrochemical behavior and charge transport processes of P18DAN by cyclic potential sweep method in aqueous acid solutions.<sup>306</sup> The P18DAN film shows semi-infinite diffusion behavior. The effects of pH and temperature on the peak currents and peak potentials of CVs of P18DAN film are studied. A redox mechanism of P18DAN film is proposed.

A linear pH dependence of the CV peak potential for the oxidation of P $\alpha$ PD, poly(*N*-methyl- $\alpha$ PD), P18DAN, and P23DAN films with respective slopes of  $-70$ ,  $-70$ ,<sup>245</sup>  $-66$ ,<sup>139</sup> and  $-56$ <sup>188</sup> mV/pH in a pH range from 2.2 to 6.2 has been described. With increasing pH, the voltammograms shifted to the negative direction of potential and the anodic and cathodic peak currents decreased. This indicates the following. (1) Electron-transfer reaction in the films accompanies the proton exchange in a 1/1 ratio



where  $n = m$  for each monomer unit. The protonation and deprotonation reactions occur at the methyl group-free nitrogen atom in the redox reaction of the polymers.<sup>264</sup> (2) Electrode kinetics become poorer at higher pH values due to the lower electroactivity of the film.

In summary, three parameters affecting CV peak currents include diffusion coefficients of counterions, concentrations of electroactive species in the film, and the inherent electron-transfer characteristics-exchange current.

Typical steady-state current and mass responses to cyclic voltammetric potential sweeps at different scan rates for P18DAN film exposed to  $\text{HClO}_4$  accompany the redox switching of the polymer.<sup>180</sup> This redox switching of films is characterized by nonmonotonic mass change: proton, counterion, and solvent transfers occur to extents dependent upon the experimental time scale, typically 0.2–2 s. The oxidation of P18DAN is accompanied by an initial increase in film mass, followed by a substantial mass loss for potentials higher than 0.1 V. This changeover potential is roughly centrally located within the region of switching the film between reduced and oxidized forms. The heterogeneous nature of electroactive polymer films generally leads to a distribution of standard potentials. Note that the mass decrease in the anodic region of film oxidation is markedly scan-rate dependent: the largest mass loss at the lowest scan rates. This contrasts with the initial mass increase, which is independent of the scan rate. Therefore, it is concluded that the electroactive behavior for P18DAN is quite different from that of PAN.

It should be noticed that the electroactivity of PBZ and polynaphthidine films is stable and after a few cycles their voltammetric responses are maintained for at least 1 day, indicating neither desorption nor degradation of the films.<sup>189,190</sup> The CVs of the two films, highly asymmetric due to a complex redox, exhibit a dependence on potential scan rate, the film thickness, and the solution pH.<sup>189</sup> The anodic and cathodic peak currents vary linearly with scan rate below 100 mV/s for PBZ and 150 mV/s for polynaphthidine and the anodic peak current shows a higher slope, although the anodic and cathodic peak potentials are independent of the scan rate. The electroactivity of the PBZ film is reproducible at pH from 1 to 3.5 but lost at pH above 4. The electroactivity of PBZ and PPBZ films exhibits a dependence on the film-forming method.<sup>230</sup> Two weak oxidation peaks at +0.45 and +0.95 V vs Ag/AgCl and the corresponding reduction peaks at +0.15 and  $-1.55$  V vs Ag/AgCl were observed for as-electropolymerized PBZ film, while the PBZ film reprocessed by solution casting exhibits strong and different electroactivity. As-electropolymerized PPBZ is a brownish-green electroactive film exhibiting oxidation and reduction peaks at +2.0 and 0 V vs Ag/AgCl, respectively. Reprocessed PPBZ film exhibits slightly different oxidation and reduction peak potentials at +1.5 and +0.1 V vs Ag/AgCl, respectively. It appears that the

reprocessed film exhibits slightly stronger electroactivity than as-formed film. The CV of the polynaphthidine film exhibits a strong dependence on potential scan range.<sup>190</sup> The film can repeatedly and quasi-reversibly be cycled from  $-0.8$  to  $1.14$  V in  $\text{NaClO}_4/\text{acetonitrile}$  without decomposition. If the anodic potential exceeds  $1.14$  V up to  $1.7$  V, the film irreversibly loses its characteristic response but remains adhered on electrode. If the some Lewis bases such as DMSO are added into the electrolytes, the film reversibly and quickly loses its voltammetric response due to the elimination of proton after ca. 13 cycles, though it remains adhered on the electrode. If the film is treated in  $\text{NaClO}_4/\text{acetonitrile}$ , its original redox properties can be recovered in about 1 day due to the addition of proton. However, the film shows great stability by weeks in the reduced state even in contact with air without losing its electrochemical response.

As can be seen from the data in Table 21, some polymers such as *Po*PD, poly(alkyl-*o*PD), and P23-DAN, which are ladder polymers with phenazine rings, exhibit negative  $E^{\circ}$  values which are similar to those of poly(phenosafranin) and poly( $\beta$ -aminoanthraquinone). On the contrary, P15DAN and P18DAN homopolymers, *m*PD/AN, *p*PD/AN, and 15DAN/AN copolymers, as well as *Pm*PD/PAN bilayer exhibit positive  $E^{\circ}$  values which are similar to those of PAN, poly(*N*-alkyl AN), poly(1-naphthylamine), and poly(1-pyrenamine), which are not double-stranded ladder polymers. These results imply that the electroactive sites of both groups of polymers are different. For the *m*PD/AN copolymer,<sup>168</sup> its electroactivity monotonically diminishes with increasing feed *m*PD content, due to the decrease of high electroactive AN unit content in the copolymer. Finally, *m*PD homopolymer does not exhibit a significant redox peak owing to its electroinactivity.

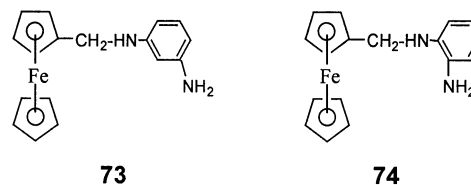
Apparent formal redox potential distribution has been determined and used to analyze the current/potential response of PHAN, *Po*PD, and PBZ in different electrolytic media.<sup>329</sup> The distribution function for the formal redox potential is sigmoidal in shape and interpreted on the basis of a simple statistical thermodynamic model that considers the possibility of expansions and contractions during the oxidation–reduction cycles applied to the polymer. The analysis of the experimental formal redox potential distribution has been used to obtain the number of redox centers per polymer unit, the ratio of the internal partition function of the units, and the formal redox potential of the centers. These units change in size during the oxidation–reduction cycles. The number of centers involved in one unit of PHAN and *Po*PD is twice as much as those of the conducting polymers such as poly(OT) at one-half oxidation. PBZ consisting of a relatively larger repeat unit has almost twice the number of redox center per unit as PHAN and *Po*PD. These results are in agreement with the previous studies on the electrochemical behavior of these polymers.

The electroactivity of electrocopolymer films of *o*PD and 2,5-dimethoxyaniline has been studied, and their CV curves are characterized by two broad redox

couples centered at ca.  $0.1$  and  $0.3$  V vs  $\text{Ag}/\text{AgCl}$ .<sup>335</sup> Both *Po*PD and 2,5-dimethoxyaniline homopolymer contribute possibly to the first redox couple. The second redox couple might originate exclusively from 2,5-dimethoxyaniline units. The exact positions and relative magnitudes of the two redox couples depend on the composition of the electropolymerization bath due to the different electrodeposition mechanism for the equimolar mixture of monomers. Surprisingly, the *o*PD/2,5-dimethoxyaniline films with ratios of  $1/4$  and  $3/4$  exhibit similar cyclic voltammograms, which are however different from that of *o*PD/2,5-dimethoxyaniline (1/1) copolymer film. The *o*PD/2,5-dimethoxyaniline (1/1) copolymer film is characterized by higher capacitive currents and bigger distances between the anodic and cathodic counterparts of the redox pairs. A sensitive IR spectral region to the substitution of the phenyl ring suggested that *o*PD and 2,5-dimethoxyaniline form real copolymer structure rather than a mixture, which is consistent with the cyclic voltammetry and in-situ UV–vis data.

Note that the ferrocene polymer films with *Pm*PD backbones prepared by electropolymerization from *m*PD to one of the cyclopentadienyl rings of ferrocene (Scheme 33) in acetonitrile solution only display well-

Scheme 33



defined responses for the ferrocene portion of the polymer without being complicated by voltammetric responses of the supposed *Pm*PD backbone in supporting electrolyte.<sup>336</sup> The polymerization may occur by coupling of the primary amine nitrogen to the 4 and/or 6 position, both of which are resonance-stabilized radical cations on the adjacent benzene ring. The films are stable to continuous potential cycling, showing less than a 5% decrease in the redox currents over 50 repetitive scans. However, another monomer following Scheme 33 does not electropolymerize regardless of the same oxidation potential of  $0.41$  V.

Yousef and Abdel-Azzem investigated the electroactivity of P15DAN prepared by an electrooxidative polymerization of nickel complex of 15DAN in  $\text{LiClO}_4/\text{acetonitrile}$  using cyclic voltammetry and controlled potential electrolysis.<sup>337</sup> The P15DAN filmed electrode showed an electroactive redox response in acidic aqueous solution only. The stability of the redox response toward repetitive cyclic voltammetry and the factors affecting the electroactivity are studied. The formal redox potential of the P15DAN filmed electrode is  $0.28$  V vs  $\text{Ag}/\text{Ag}^+$  in  $1$  M acidic chloride aqueous solution ( $\text{pH} = 0$ ). The electroconductivity of the P15DAN film in  $10$  mM KCl aqueous solution is  $2.2 \times 10^{-4}$  S/cm.

However, the *Po*PD– $\text{Ni}^{2+}$  complex exhibits electroactivity even in  $0.1$  M NaOH aqueous solution.<sup>338</sup> A couple of redox peaks with the  $E_{\text{pa}}$   $0.43$  V vs SCE

and  $E_{pc}$  0.37 V vs SCE were observed during potential scanning between +0.6 and +0.2 V. The peak current increases with scanning rate, but the peak potential keeps substantially constant. The redox peak currents increase initially with increasing cyclic number and then reach constant values after a certain cyclic number, due to improvement of the position complexing  $Ni^{2+}$ . The redox peak potentials shift positively from 0.32 to 0.50 V ( $E_{pa}$ ) and 0.26 to 0.41 V ( $E_{pc}$ ) with decreasing NaOH concentration from 2 to 0.01 M.

PoPD (polyaminoaniline) solution in DMSO in an anion-doped state was first studied and obviously showed two reversible redox peaks (anodic peaks at -1.1 and -0.5 V vs SCE and cathodic peaks at -1.5 and -0.6 V vs SCE) which are different from that of PoPD film (only one reversible redox peak).<sup>339</sup> With the addition of the halogenide ions, the corresponding redox potential shifted. The relationship between the potential shift and the concentration of the halogenide ion has been used to determine the relative association constant of PoPD for four halogenide ions. It is found that the association constant of PoPD decreases significantly with increasing atomic weight of halogenide ion from  $F^-$  ( $104 \text{ mol}^{-1} \text{ L}^{-1}$ ),  $Cl^-$  ( $32 \text{ mol}^{-1} \text{ L}^{-1}$ ),  $Br^-$  ( $29 \text{ mol}^{-1} \text{ L}^{-1}$ ), to  $I^-$  ( $9 \text{ mol}^{-1} \text{ L}^{-1}$ ).

Two extremities of electroactivity are revealed for P15DAAQ and poly(3-hydroxy-*o*PD). It is interesting that P15DAAQ exhibits two sets of reproducible redox responses for repeated cycles:<sup>227</sup> one appearing in a very negative potential range from -0.7 to -1.8 V vs Ag/AgCl and the other in a more positive range from +0.1 to +1.0 V. These two kinds of redox responses correspond to the quinone group because P15DAAQ has a two-electron process involving a quinone/quinone radical anion process at a reduced peak, which is followed by a radical anion/dianion conversion at another reduction peak.

It should be noticed that the poly(3-hydroxy-*o*PD) prepared by electropolymerization exhibits no significant redox processes in the -0.2 and +1.0 V vs SCE potential range,<sup>182</sup> indicating a scarce electroactivity for aromatic diamine polymers. This feature allows a possible application of the polymers in a very wide electroinactive window.

In conclusion, the aromatic diamine polymers usually exhibit typical and stable electroactivity at a given condition. The electroactivity depends strongly on polymer type, comonomer ratio, electrolyte (composition, pH, additives), and potential scanning rate. There are a number of studies on the electroactivity of aromatic diamine polymers, but systematic results have not been elaborated yet. Thus, a careful polymer structure-electroactivity evaluation is requisite to thoroughly explore the electroactivity and find more suitable applications.

## B. Permselectivity

There are a few investigations on the permselectivity through electropolymerized films of various aromatic diamine polymers because the permselectivity is a vital factor for high performance sensors.<sup>163,166,272,289,322</sup> Yano and co-workers studied the permselective response of a 2.6 mm thick PoPD film electrode to several kinds of inorganic ions.<sup>272</sup> The

PoPD film-coated electrode has electrochemical responses to only two halogenide ions,  $I^-$  and  $Br^-$ , whereas it had no response to other ions such as  $Fe^{2+}$ ,  $Mn^{2+}$ , and  $Tl^+$ . In this case, the film is permeable to the  $I^-$  and  $Br^-$ . The permeability of the ions through the film is controllable by incorporating quinones into the film. Furthermore, the incorporation can enhance the permselectivity of the film to the two halogenide ions.

Ekinici et al. investigated the characteristics of PoPD and PmPD films prepared by electropolymerization as dopamine-selective membranes while preventing electroactive AA permeation through the films.<sup>163,166</sup> It is found that the film thickness is one of the most important factors affecting their permselectivity characteristics. The PoPD and PmPD films having an optimal thickness of 12 and 1.2  $\mu\text{m}$ , respectively, exhibit the largest separation factor of dopamine over AA. The optimum polymerization potentials are found to be 0.7 and 0.8 V vs Ag/AgCl for PoPD and PmPD films, respectively, to ensure a controllable film growth at a slow electrolysis rate at a fixed optimal thickness. It is depicted that the optimal concentrations for monomer *o*PD and electrolyte KCl corresponding to maximum dopamine currents are 50 and 100 mM, respectively, for PoPD film as well as monomer *m*PD and electrolyte KCl of 100 and 150 mM, respectively, for PmPD film. It is claimed that both PoPD and PmPD films can serve as high-performance dopamine-selective permeation membranes while rejecting AA.

To reject the major interferences, in particular acetaminophen, Murphy<sup>289</sup> and Madaras et al.<sup>322</sup> investigated the permselectivity and stability of various electroactive species through insulating aromatic diamine polymer films prepared by electropolymerization on Pt electrode. By using a thin electropolymerized PmPD film, the electrochemical interferences from ascorbate, acetaminophen, urate, and other oxidizable species are greatly diminished but the film is almost completely permeable to  $H_2O_2$ . It is seen from Table 22 that, compared with PoPD film, six films exhibited reduced permeability to  $H_2O_2$  and interferences. The lowest permeability to  $H_2O_2$ , ascorbate, and acetaminophen as well as the highest permselectivity to  $H_2O_2$  against ascorbate and acetaminophen, respectively, were observed for both P23DAN and poly(ANO). All films experienced some deterioration over a period of 21 days, and the poly-(substituted naphthalene) films maintained lower permeability to all species than the three PD polymer films. It is suggested that the extra benzene ring on each substituted naphthalene unit compared with PD unit would confer greater hydrophobicity on the films formed, leading to a lower degree of solvation, closer packing of the macromolecular chains, reduced diffusion of the solvated interference species through the films, and finally lower permeability. The difference in the permeability of four poly(substituted naphthalene) films might result from the different degrees of order of the macromolecular chains. P23DAN and poly(ANO) films exhibit lower permeability because of their higher degree of close chain packing resulting from the ladder structure. In

**Table 22. Permselectivity of Electroactive Species through Electropolymerized Films Grown from Various Aromatic Diamines on a Pt Electrode in Situ within a Microdialysis Electrode from a 5 mM Solution of the Monomer for 10–15 min at 0.65 V vs Ag/AgCl<sup>289,340,341</sup>**

monomer	oxidation potential (V vs SCE)	film thickness (nm)	permeability (%)				selectivity		
			H <sub>2</sub> O <sub>2</sub>	ascorbate	acetaminophen	urate	H <sub>2</sub> O <sub>2</sub> /ascorbate	H <sub>2</sub> O <sub>2</sub> /acetaminophen	H <sub>2</sub> O <sub>2</sub> /urate
<i>o</i> PD		150	97	2.8	44	1.7	35	2.2	57
<i>m</i> PD	1.0	28	78	2.7	1.7	0.1	29	46	780
<i>p</i> PD		650	81	6.4	8.3	0.59	13	9.8	137
15DAN	1.05	27	85	3.7	2.0	0.09	23	43	944
18DAN	0.85	1200	75	2.7	3.4	0.06	28	22	1250
23DAN	1.10	160	39	0.5	0.2	0.14	78	195	279
ANO	0.90	66	20	0.2	0.2	0.07	100	100	286
<i>o</i> PD-GOx		10	100	1.8(AA)		2.9(uric acid)	56 <sup>a</sup>		34 <sup>b</sup>
PPY-GOx/ <i>o</i> PD		-10	86	4(AA)		0(uric acid)	21.5 <sup>a</sup>		very big
PPY-COx/ <i>o</i> PD		-10	100	4(AA)		0(uric acid)	25 <sup>a</sup>		very big

<sup>a</sup> The permselectivity of H<sub>2</sub>O<sub>2</sub> over ascorbic acid. <sup>b</sup> The permselectivity of H<sub>2</sub>O<sub>2</sub> over uric acid.

addition, all the films have low permeability to urate, suggesting no gross defects in the films and therefore good coverage of the films on the electrode. A long response time to H<sub>2</sub>O<sub>2</sub> (60 and 120 s, respectively) at P23DAN and poly(ANO) films does suggest membrane-type diffusion for these films.

As compared with the monolayer modified electrodes discussed above, bilayer modified electrodes exhibit better permselectivity. The first article concerning the permselectivity of *Po*PD film containing bilayer was reported by Centonze et al.<sup>342</sup> The permeability of some organic probes through the bilayer grown onto Pt and GC electrodes has been investigated by cyclic and rotating disk working electrode voltammetry. Vidal et al. investigated the effect of the outer *Po*PD layer on the permselectivity through bilayered Pt/PPY-GOx/*Po*PD, Pt/PPY-COx/*Po*PD, and Pt/PPY-COx/P15DAN electrodes.<sup>340</sup> It is found that the addition of *Po*PD layer results in a slight increase of H<sub>2</sub>O<sub>2</sub> permeation but a considerable suppression of the responses produced by two interfering species, AA and uric acid, compared with monolayer Pt/PPY-GOx and Pt/PPY-COx electrodes, especially where the response of uric acid with two bilayer electrodes is negligible.

Myler et al. investigated the permselectivity of glucose over oxygen across an ultrathin *Po*PD film-containing GOx/Au/polycarbonate composite membrane by electropolymerization of *o*PD on a gold sputter-coated porous polycarbonate membrane.<sup>149</sup> As the pores of the underlying porous polycarbonate were blocked, the glucose/oxygen permselectivity was found to increase and reach a maximum value of 0.95 at the three potential sweeps. Once a homogeneous *Po*PD film formed, the permselectivity fell. The glucose/oxygen permeability ratio is ca. 0.39 when the thickness of *Po*PD film is 30 nm at 20 potential sweeps.

The permselectivity of *Po*PD films obtained at pH = 5 is very high and is attributed to hydrophobic interaction and effective hydrogen bonding. It is suggested that *o*PD can form polymeric film on electrochemical oxidation in phosphate buffer at nearly all pH values and on a variety of electrode materials.<sup>142</sup>

Very recently a controllable permselectivity through templated *Po*PD-modified electrodes was studied by

changing the order of electropolymerization medium.<sup>141</sup> The *Po*PD film deposited in the ordered phase containing 50 wt % liquid crystalline exhibits ion selectivity, allowing a positively charged ion such as the [Ru(NH<sub>3</sub>)<sub>6</sub>]<sup>3+</sup> redox couple through to electrode while excluding a negatively charged ion including the [Ir(Cl)<sub>6</sub>]<sup>3-</sup> or [Fe(CN)<sub>6</sub>]<sup>4-</sup> redox couple, because the film contains a dense array of nanometer-diameter pores representing a direct cast of the structure of the order liquid crystalline phase as a templating agent. Furthermore, this selectivity should arise from a difference in charge rather than the size of the ions since the ions have very similar sizes of 0.5–0.8 nm. Therefore, the *Po*PD film exhibits negative charge or is neutral. In contrast, both types of ions are completely blocked by the films deposited in the nonordered system of traditional aqueous or 20 wt % liquid crystalline phase.

The permselectivity of some ions and H<sub>2</sub>O<sub>2</sub> through aromatic diamine polymer films is primarily controlled by the assembling structure of the films. Closer and more orderly packing of the macromolecular chains in the films leads to larger permselectivity along with lower permeability. Note that the stability of the permselectivity is not good enough. To enhance the stability and maintain the high permselectivity, it is necessary to better understand the relationship between the supramolecular structure and permselectivity through the films. Thus, more systematic studies on the permselectivity and stability are needed to prepare high-performance films of aromatic diamine polymers, which can find many crucial applications as permselective coatings in biosensors and other selective electrodes,<sup>341</sup> as elaborated in section IX.D. The fabrication of a controllable permselective electrode is of great significance in conjunction with amperometric microelectrode sensors with less susceptibility to surface fouling or molecular sieving process.

### C. Electrochromic Film

Electrochromism is a unique property of conductive polymers that change color reversibly in response to an applied external potential.<sup>234</sup> Several novel electrochromic devices such as electrochromic windows (smart windows), antiglare car rear-view mirrors,

and high-performance display panels have been fabricated with electrically conducting polymers. In particular, smart windows are very interesting because of the energy savings and glare attenuation by controlling the amount of sunlight and heat passing through the windows. Smart windows fabricated of conductive polymers can be switched between opaque blue/purple and transparent sky blue. Photoelectrochromism of PAN prepared from *N*-phenyl-*p*PD as monomer in a Ru complex methyl viologen system has been reported.<sup>343</sup> Additionally, nonradiation displays such as electrochromic displays and liquid crystal displays exhibit great application potential because of their softness to human eyes. In particular, the electrochromic displays have advantages over liquid crystal displays because they have memory functions and no limited visual angle, which is inherent to liquid crystal displays. The electrochromic displays are based on an electrochemical reaction of the conducting polymers that expresses a color change upon changing redox state.

Yano and Kitani and co-workers systematically investigated the electrochromism of *Po*PD film and found that the response time of *Po*PD film to the color change is much shorter (4–5 ms) than that of PAN and polyaniline acid films.<sup>113,164,321</sup> The absorption maximum at 468 nm in the dependence curves of the UV–vis spectra of the *Po*PD film on the polarizing potential is independent of the decoloration process, implying that the change in color can be electrochemically controlled without accompanying any color mixture. Therefore, the solution cast *Po*PD film exhibits good electrochromic properties and high redox activity. The CV of electropolymerized and cast *Po*PD films with a thickness of 800 nm showed a reversible redox property accompanied with excellent electrochromism between transparent yellow and brown.<sup>164,269</sup> An anodic peak at –0.05 V is responsible for the color change of the film from transparent yellow to reddish-brown, whereas the color change back to transparent yellow occurs on passing the cathodic peak at –0.22 V. The electropolymerized *Po*PD film exhibits an increased separation between anodic and cathodic peaks from 60 to 190 mV with increasing film thickness from 100 to 800 nm. Thin *Po*PD film on Pt prepared by cyclic voltammetry also changes its color from pale yellow when reduced to brownish-red (the maximum absorption wavelength 512 nm) when oxidized with potential cycling.<sup>113,162</sup> A different electrochromism was found for the *Po*PD film on ITO electrode which exhibits a color change from light green at –0.2 V (the maximum absorption wavelength 680 nm) to brownish-red at 0.2 V (the maximum absorption wavelength 495 nm) with the color transition point at ca. 0 V.<sup>344</sup> The characteristic change of film color during its oxidation and reduction processes is repeated without remarkable changes. The *Po*PD film appears to be slightly darker after 10<sup>6</sup> cycles, indicating that *Po*PD film is undoubtedly durable for more than 10<sup>6</sup> repetitions of the writing–erasing process. The red color, which has never been reported before for PAN and its derivatives, is observed with *Po*PD. A piece of OTE was coated with *Po*PD, and then PAN was deposited on

it in order to prepare a composite film. It is found that the composite film retains the optical characteristics of each component film but without undesirable interference. Yano et al. also reported that the *Po*PD film with a thickness of 800 nm prepared by electropolymerization shows a reversible redox reaction which is accompanied by a readily observable color change between nearly red (vermillion) and colorless.<sup>160</sup> The switching time of the color change is <10 ms.

Similarly, the color of the P18DAN film on Pt and Au prepared by electropolymerization has been observed and depends on the film thickness or the numbers of successive voltage scan.<sup>181,226</sup> Palys et al. found that the electropolymerized P18DAN film on Au electrode is brownish-violet.<sup>226</sup> Lee et al. found that the P18DAN film is light brown for 10 potential cycles, yellow for 20 cycles, orange for 30 cycles, purple for 40 cycles, and green for 50 cycles.<sup>181</sup> The color of P15DAN film changes from yellow to blue, also depending on the number of scans.<sup>179</sup> The sequence of the color change suggests qualitatively that the polymer chains become longer as the number of potential cycles is increased. The P18DAN film thus prepared has excellent quality with a homogeneous texture and good adhesion to the electrode. Note that the film became flaky and peeled off from the electrode when the potential was cycled repeatedly for 12 h, due to a degradation reaction resulting from the overoxidation of the film and inefficient mass transport of counterions through thick P18DAN film. Apparently *Po*PD film exhibits much more stable electrochromism than the two PDAN films.

An as-electrosynthesized PPBZ film of 100 nm thickness exhibits a reversible electrochromic change from transparent at –1.0 V vs Ag/AgCl to dark blue at +2.0 V vs Ag/AgCl.<sup>230</sup> With electrochemical cycling between –0.5 and +2.0 V vs Ag/AgCl, about 2.5% degradation in peak height and no change in peak position over 10 000 cycles under air were observed. The PBZ film is colorless in the reduced state at 0 V and blue in the oxidized state at 0.6 V vs SCE.<sup>189</sup> An as-electrosynthesized PBZ film of 75 nm thickness exhibits a different electrochromic change from light yellow at –0.25 V vs Ag/AgCl to deep purple at +0.65 V vs Ag/AgCl.<sup>230</sup> Note that the PBZ shows marked instability to electrochemical cycling under air. Although under nitrogen the PBZ exhibits reversible electrochromism from +0.5 to +0.65 V vs Ag/AgCl and less degradation, the polymer degradation is observable after ca. 100 cycles. A reprocessed PBZ film of 40 nm thickness by solution cast from a saturated solution in DMF also exhibits a similar reversible electrochromism between –0.5 and +0.675 V vs Ag/AgCl under nitrogen<sup>230</sup> but subsequently degraded over ca. 50 cycles. It is seen that the process of film formation influences the stability of the electrochromism. The polynaphthidine film shows electrochromic properties being yellow in the reduced state and blue in the oxidized state.<sup>190</sup>

In addition to the aromatic diamine homopolymer films discussed above, the electrochromism of the films of their copolymer with AN and composite is



also investigated in order to prepare electrochromic film with better comprehensive performance. Dithio-dianiline/AN (2/175) copolymer film exhibits a pale yellow color at 0 V due to a reduced and nonconducting state and a green color at 0.8 V due to a conducting state.<sup>232</sup> The P $\phi$ PD composite film exhibits a continuous variety of colors by changing the anodizing potential: colorless (−0.4 V), red (0 V), and yellow (0.4 V).<sup>321</sup> Another composite film fabricated by PAN, P $\phi$ PD, and PPTA exhibits three-color electrochromism: vermilion or orange (−0.4 V), green (+0.4 V), and violet (+1.2 V).<sup>324,345</sup> A slightly different color change was also observed with PAN and PPTA composite film: pale yellow (−0.4 V), green (+0.4 V), and violet (+1.2 V). The P $\phi$ PD and PAN were electronically stabilized by the matrix PPTA film, and the color change was clearly observed at least for 1000 repetitions.

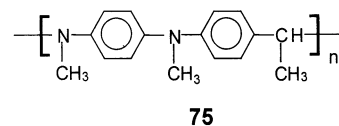
Yano et al. fabricated an especially attractive composite film of PB and P $\phi$ PD because its redox potentials causing the color change are sufficiently separate from each other (larger than 0.2 V) as well as PB and oxidized P $\phi$ PD exhibit blue and nearly red (vermilion), respectively, in the colored state, two of the three primary colors.<sup>159,160</sup> The PB film was electrodeposited on an ITO electrode surface, and then the P $\phi$ PD film was easily electrodeposited to obtain the stable PB/P $\phi$ PD composite film electrode by potential cycling up to 60 cycles. The composite film thickness in the dry state is 2.2 mm. The reduced form of both PB and P $\phi$ PD is colorless. By changing the anodic potential, the composite film exhibits a continuous variety of colors: colorless (−0.2 V), nearly red or vermilion (0.1 V), and violet or emerald green (0.6 V). It is also found that the color of the PB/P $\phi$ PD/ITO composite film is changed by the environmental solution pH. The maximum absorption wavelength in the colored state linearly decreased with the solution pH. The switching time of the color change is <600 ms. The stability in color change of the composite film electrode is good. After 2000 repetitions, the composite film shows bright color change. The composite film remains 60% of the coloration after 100 000 repetitions of a square-wave potential pulse since the P $\phi$ PD worked as a binder, which enhanced the adhesion of PB to the electrode surface. The binder effect of P $\phi$ PD prevents the formation of cracks for the composite film. The composite film retains the electrochromic properties of each component but no undesirable interference. The PB/P $\phi$ PD film electrode has functioned as a three-color-expressible electrochromic display. The preparation of such an electrode would be a new promising method for the fabrication of multicolor-expressible displays. It follows that the investigation on electrochromic film of aromatic diamine polymers has been focused on mainly P $\phi$ PD, P18DAN, and P15DAN. Among them, P $\phi$ PD appears to exhibit the best electrochromism, the highest electrochromic stability, and much faster response to the color change than PAN. Unfortunately, no reports on the electrochromism of P $m$ PD and P $p$ PD films have been made to our knowledge. Obviously investigations on the electrochromism of polymer films from aromatic

diamines are not abundant or available at the present time. Consequently a detailed relationship between the electrochromism and macromolecular structure of the polymer films from aromatic diamines is needed to optimize the electrochromism and even establish a perfect theory of the electrochromism for a practical application in display panels.

In addition, electrodeposited PHAN and poly(ANO) films on ITO electrode displayed the reversible electrochromic response.<sup>228,280</sup> A reversible color change of the PHAN film between brown and colorless was observed when the electrode potential was cycled between 0.7 and −0.7 V vs SSCE.<sup>228</sup> The color of the oxidized form of the PHAN film is brown (the maximum absorption wavelength 440 nm) and the reduced form is almost colorless. The poly(ANO) film is light yellow at −0.5 V and turns dark green at +0.5 V.<sup>280</sup> If the upper switch potential is maintained until 0.5 V, these color changes are reversible and reproducible.<sup>280,191</sup>

Nishikitani et al. synthesized a nonconjugated electrochromic polymer (DDPA) from *N,N*-dimethyl-*N,N*-diphenyl-*p*PD and acetaldehyde having the following structure (Scheme 34).<sup>234</sup>

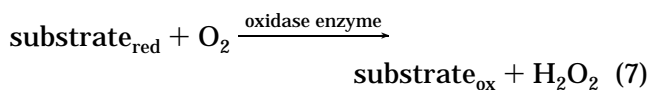
**Scheme 34**



It is found that the color of the monooxidized state of the polymer is blue and that of dioxidized state is purple. A solid-state electrochromatic cell comprising a 0.5 mm thick DDPA layer and a cathodically coloring electrochromic material has been fabricated.<sup>234</sup> This cell can be colored blue by applying a potential of 1.0 V and bleached at 0 V. This applied potential for coloration is low enough to avoid a side reaction.

#### D. Amperometric Biosensors

An important aspect of the extensive applications for the aromatic diamine polymers is the development of amperometric biosensors. The biosensors are based on the amperometric detection of H<sub>2</sub>O<sub>2</sub> after conversion of the analyte of interest by an immobilized oxidoreductase enzyme through electropolymerization of the aromatic diamines. The principle for the sensor to detect most of biosubstances is that the biosubstance oxidase selectively and sensitively catalyzes the oxidation reaction of corresponding biosubstances and the reduction of oxygen, then quantitatively consumes the oxygen in the solution as follows



The biosensors involving the use of electrochemically synthesized PD polymers for enzyme immobilization are widely investigated and of prime importance in bioanalysis owing to the following advantages: (1) The amount of polymers deposited is

readily controlled; (2) Depositions only occur at the electroactive surface; (3) The construction is relatively easy; (4) No components such as mediator could leach from the electrode; (5) A serious problem in the use of enzyme-modified electrodes in biological media, i.e., interference by endogenous electroactive reducing agents, could be prevented or even resolved to a great extent by covering electrosynthesized PD polymers, which block access to the electrode surface of even relatively small organic molecules without affecting sensitivity to  $\text{H}_2\text{O}_2$ ; (6) Conducting PD polymers are ideally suited for sensor applications because they not only exhibit high conductivity and electroactivity but also could be used as general matrix and further modified with other compounds in order to change selectivity.

These advantages that biosensors afford can only be achieved if the sensors meet the required specificity, sensitivity, robustness, and reliability for a particular application.<sup>135</sup> To date, only a relatively small number of biosensors enjoy commercial success, possibly due to a number of common problems that still need to be addressed, particularly those relating to robustness, reliability, and stability.

### 1. Technique of Enzyme Immobilization Involving Aromatic Diamine Polymers

Two seminal articles demonstrated the electrochemical immobilization of enzyme in electrosynthesized P $\alpha$ PD for the first time.<sup>142,346</sup> The possibility of an "in situ" preparation of a GOx/P $\alpha$ PD biosensor has been shown for the first time.<sup>347</sup> Before enzyme immobilization for the fabrication of biosensors, pretreatment or preparation of working electrodes should be done. There are many articles concerning the procedure of enzyme immobilization into aromatic diamine polymers.<sup>340,348–361</sup> However, the pretreatment or fabrication of working electrodes for biosensors is similar. Typically, the Pt or Au disk used as electrode substrate should be cleaned according to standard procedure and polished successively with finer grades of diamond polishing compounds and an aqueous alumina slurry of 0.3–1.5  $\mu\text{m}$ , sometimes subjected to ultrasonication in deionized water for 30 min, soaked overnight in an oxidant solution, and mounted in a Teflon electrode holder which restricted a certain exposed area.<sup>170,264</sup> Besides the Pt and Au electrodes, organic conducting salt (OCS) and carbon including graphite powder, graphite rod, carbon fiber, and carbon microband are often selected as electrode substrate for biosensors. The OCS could be either *N*-methylphenazinium tetracyanoquinodimethanide prepared by metathesis of phenazine methosulfate and 7,7,8,8-tetracyanoquinodimethane<sup>362,363</sup> or tetrathiafulvalene-*p*-tetracyanoquinodimethane.<sup>351</sup> The OCS was tightly pressed onto the paste electrode or used to fill the hole in the working electrode block. When graphite powder was used, the enzyme can be mixed into the graphite powder and the mixture was packed into the well of the working electrode.<sup>355,361</sup>

The one-step immobilization procedure was widely used by a direct electrochemical co-deposition of the enzyme and polymer. The enzyme immobilization into aromatic diamine polymer matrix onto the

electrode substrate is easily, quickly, and successfully performed in one step by electropolymerization from unstirred and deaerated aqueous solution containing enzyme and aromatic diamine monomer in electrolyte.<sup>142,167,170</sup> The enzyme-immobilized polymer film is deposited at a constant potential of 0.4–1.0 V for 2–50 min under nitrogen at room temperature<sup>142,167,170,289,357,364</sup> or by cyclic voltammetry in a range from –0.5 to 1.0 V at a scan rate of 2–50 mV/s for 3–12 scans.<sup>146,157,278</sup> The monomer and enzyme concentrations are 5–100 mM and 100 units/L (or 20 mM), respectively. The thickness of the polymer film can be accurately controlled by the amount of charge passed or scan cycle numbers during the electropolymerization and exhibits good reproducibility.<sup>278</sup> Visual examination reveals the formation of a thin and brownish or purple polymeric film for P $\alpha$ PD and P $\rho$ PD or yellowish film for P $m$ PD on the electrode surface.<sup>157,163,167,170</sup> The resulting enzyme electrode was thoroughly rinsed with doubly distilled water or phosphate-buffered salt solution to remove the weakly bound enzyme to the polymer from the electrode surface. The kinetics and behavior of GOx immobilized in various electropolymerized thin films of P $\alpha$ PD and PAN cross-linked with  $\rho$ PD toward elevated temperature, organic solvent denaturation, and pH were investigated.<sup>365</sup> The amount of entrapped enzyme in the P $\alpha$ PD film can be determined by XPS spectroscopy.<sup>366</sup> It is suggested that an increase in the length of adsorption times prior to electrodeposition of the P $\alpha$ PD leads to greater amounts of entrapped enzyme (GOx) in the film. This one-step immobilization approach can provide the sensors with relatively good sensitivity but need large amounts of expensive enzyme, typically 5 mg/mL.<sup>348</sup>

The one-step immobilization procedure is very efficient for most enzymes. However, this method cannot immobilize some enzymes successfully. Liu et al. indicated that the electropolymerization of  $\alpha$ PD on Pt at or scanned to +0.6 V will make nitrilase lose its activity after the immobilization, while the potential at +0.6 V is required for the  $\alpha$ PD polymerization.<sup>367</sup> Therefore, a two-step immobilization procedure by the first electropolymerization and the second cross-linking is also developed at the same time.

In the two-step immobilization, the enzyme is immobilized on the electrode by cross-linking with a bifunctional reagent, glutaraldehyde. A 10 mL amount of buffer solution containing 410–5000 units/mL enzyme is rapidly mixed with 10 mL of a 0.25–25% solution of glutaraldehyde in the presence of bovine serum albumin.<sup>149,358,368</sup> This mixture is quickly placed directly on the electrosynthesized PD polymer films on the electrode in 5 mL injections, each being left to dry before the subsequent addition. The cross-linking reaction is allowed to proceed in a moist air environment at 4 °C for 0.5–6 h.<sup>322,369–371</sup> The enzyme solution can be also first dispersed on the polymer-coated electrode surface and dried.<sup>359</sup> Then glutaraldehyde solution is added and allowed to dry for 30 min<sup>351</sup> or the enzyme-containing electrode is exposed to glutaraldehyde vapor for 2 h in a desiccator followed by drying for 48 h in ambient conditions.<sup>356</sup>

The electrode surface is then rinsed with cold buffer to eliminate any loose enzyme and unreacted glutaraldehyde. It is indicated that a slower electropolymerization could be better to improve the sensor performance due to better coverage of polymer film over the electrode.<sup>358</sup> Sometimes the mixture solution of enzyme with cross-linking agent glutaraldehyde is directly applied to the surface of each metallized electrode.<sup>360</sup> The exposed metal of the electrode is also dipped into enzyme solution for several minutes to deposit enzyme and then dry.<sup>348</sup> This enzyme-coated electrode is covered with an electroprepared thin P $\alpha$ PD film as an effective diffusional barrier.<sup>149,355,360</sup>

A detailed example of an immobilization method of enzyme is given as follows:<sup>264</sup> (1) Au electrode was immersed in cystamine aqueous solution for 8 h to deposit a self-assembled monolayer of 2-amineethanethiolate; (2) a mixture solution of phosphate buffer containing 8.3 mM enzyme, 1.8 g/L PM $\alpha$ PD, and 80 mM glutaraldehyde was cast on the electrode; (3) the electrode was kept under dry nitrogen at 35 °C for 6 h to allow the binding of amino residues of enzyme molecules with the amino groups of 2-aminoethanethiolate on the Au substrate via glutaraldehyde. In addition, it is indicated that the  $-\text{NH}_2$  groups on the functionalized copolymer produced by electrocopolymerization of *m*PD and AN can be applied for the covalent immobilization of biological materials.<sup>322</sup>

Ryan et al. suggested that the response and reproducibility of the sensors produced by the dip-coating method to deposit enzyme on the electrode prior to the electropolymerization in solution of  $\alpha$ PD are at least as good as the one-step co-deposition procedure.<sup>348</sup> The effect of the number of dip coatings in a 200 units/mL GOx solution followed by polymerization in 300 mM  $\alpha$ PD on the currents for 500 mM glucose recorded with Pt/GOx/P $\alpha$ PD sensor obtained has been studied. It is found that the current at 0.7 V vs SCE is  $0.7 \pm 0.1$  nA for 1 dip,  $3.8 \pm 2.3$  nA for 2 dips,  $5.1 \pm 2.0$  nA for 5 dips,  $10.9 \pm 4.8$  nA for 10 dips, and  $3.1 \pm 1.6$  nA for 20 dips. The maximum response was observed for 10 dips. A different relationship between the response and dipping number was found for Pt/GIOx/P $\alpha$ PD sensor. The amperometric responses at 0.7 V vs SCE for 10 mM glutamic acid, recorded with sensors fabricated by dipping in a 200 units/mL GIOx solution followed by polymerization in 300 mM  $\alpha$ PD, are  $0.62 \pm 0.02$  nA at 1 dip,  $0.59 \pm 0.14$  nA at 2 dips,  $0.78 \pm 0.24$  nA at 5 dips, and  $0.66 \pm 0.35$  nA at 10 dips. No distinct peak in the current vs number of dips was observed, although five dips gave the largest response.

Also, if the electrode is precoated by conducting PAN layer, the amount of the enzyme immobilized on the electrode will increase significantly. It is suggested that the amount of protein (antibody paratyphi A) cross-linked on P*m*PD deposited on PAN-filmed Au is much larger than that on the P*m*PD deposited directly on Au because the underlying fibril PAN film with larger specific area provides richer active sites for immobilizing protein.<sup>168</sup>

Apparently, as compared with one-step immobilization procedure, the biggest characteristics of the

two-step immobilization procedure are the application of cross-linking reagent. Therefore, the two-step immobilization procedure is more complicated but will give biosensors with more stable performance than the one-step immobilization procedure because the enzyme is immobilized by chemical cross-linking during the two-step immobilization procedure.

## 2. Biosensor Applications

Aromatic diamine polymer films are extensively used on amperometric electrodes for the elimination of electrochemical interference from electroactive compounds and fouling from other compounds (e.g., proteins). Thus, many enzymes have successfully been electrochemically deposited into PD polymer films on several electrodes listed in Table 23. Most of the investigations focused on the P $\alpha$ PD film containing biosensors, whereas very few focused on the P*p*PD film containing biosensors. Much attention has been paid in recent years to avoid the effects of electrochemically active interferents, such as AA and acetaminophen, usually present in biological fluids. One approach to avoid interferences is related to the use of selective membranes, which are highly permeable for H<sub>2</sub>O<sub>2</sub> but nonpermeable for interference species. However, many of the known selective membranes do not ensure a full avoidance of interference. Therefore, serious research activities have been taken in creating improved selective membranes useful in interference-free biosensors. The biosensors containing aromatic diamine polymers are very hopeful to serve for a reliable, sensitive, and fast detection and analysis of biological substance species in assayed samples of human blood serum, food, etc. Since the earliest publications of the amperometric biosensors containing aromatic diamine polymers emerged in 1990,<sup>142,372</sup> there have been abundant published articles in this area. Many important studies are listed below.

**a. Detection of Glucose and Cholesterol.** The biosensors containing aromatic diamine polymers have been found to be the most extensively used for the detection of glucose in assayed samples of human blood serum. They can be simply classified into monolayer and multilayer biosensors in terms of the layer number of polymer films. A monolayer P $\alpha$ PD film biosensor on Pt, capable of immobilizing GOx during one-step electropolymerization and at the same time of rejecting ascorbate, was reported by Malitesta et al.<sup>142</sup> They immobilized GOx into a very thin 10 nm thick P $\alpha$ PD film directly during electropolymerization performed by anodic oxidation at an appropriate electrode potential. A resulting sensor was shown to drastically reject ascorbate.<sup>142</sup> In particular, the sensor exhibits a very short response time of less than 1 s, which was never observed before with any enzyme electrode. This characteristic is especially promising for application of enzyme-modified electrodes in flowing systems such as flow injection analysis or high-performance liquid chromatography.

Xu and Chen developed miniaturized Pt/P*p*PD-GOx and Pt/P $\alpha$ PD-GOx sensors for amperometric determination of glucose.<sup>373</sup> It is found that both Pt/P*p*PD-GOx and Pt/P $\alpha$ PD-GOx sensors noticeably

**Table 23. Characteristics of Amperometric Biosensors Containing Phenylenediamine Polymer Films Fabricated by Electropolymerization**

electrode	enzyme immobilized	detection substance	linear range ( $\mu\text{M}$ )	detection limit ( $\mu\text{M}$ )	sensitivity (nA/mM)	response time (s)	lifetime (days)	refs
PoPD/carbon	glutamate dehydrogenase	glutamate	5–78	3.8	460	120	3(O) <sup>a</sup>	355
tetramethoxysilane/PoPD/Pt	glucose oxidase	glucose	2–2000		825	15	15(S) <sup>b</sup>	356
PoPD/Pt	glucose oxidase	glucose	0–10000		550	<1	10(S)	142
PoPD/Pt	lactate oxidase	lactate	0–1500	0.25	36	short	5(S)	357
tetramethoxysilane/PoPD/Pt	galactose oxidase	galactose	20–4000		71	27	6(S)	356
tetramethoxysilane/PoPD/Pt	cholesterol oxidase	cholesterol	60–3000		41	51	32(S)	356
PoPD/Pt	lysine oxidase	lysine	2–2000	0.1		13		358
PmPD/Pt	lysine oxidase	lysine	14–500	10		15		358
PpPD/Pt	lysine oxidase	lysine	20–400	10		15		358
PoPD/Au	lysine oxidase	lysine	100–10000				40(S)	359
PoPD/Ru–Rh/carbon	lysine oxidase	lysine	2–125	2	192	short		360
PoPD/Pt	glucose oxidase	glucose	0–10000		7.15	4–8		349
PoPD/PoPD/Pt	glucose oxidase	glucose	0–8000		6.8			349
PoPD/PoPD/PoPD/Pt	glucose oxidase	glucose	0–14000		2.2			349
PPY derivative/PoPD/Pt	glucose oxidase	glucose	0–5000		340		290(S)	354
PoPD/OCS	glucose oxidase	glucose	1000–11000		24.5		12(O)	351
PoPD/PPY/OCS	glucose oxidase	glucose	1000–12000		18.4		8(O)	351
PoPD/PPY/Pt	glucose oxidase	glucose	0–6000	5.14	18.7	5.1	15(S)	340
PoPD/PPY/Pt	cholesterol oxidase	glucose	0–300	0.68	35.8	7	15(S)	340
PoPD/PPY/PB/Pt	glucose oxidase	glucose	0–7000		19	30		352
PoPD/graphite- <i>n</i> -eicosane/PVC	oxalacetate decarboxylase	oxalacetate	50–1200	10	53	180		361
PVC/PmPD/Pt	glucose oxidase	glucose	0–37700		1.8	35	56(S)/5(O)	361
PmPD/Pt	glucose oxidase	glucose	0–6000		8.3	4	90(S)	167
PpPD/Pt	glucose oxidase	glucose	0–6000		3.8	<4	>30(S)	170
PmPD/Pt	glutamate oxidase	glutamate	100–2000		800		180(S)/21(O)	369
Nafion-PHMA/PmPD/Pt–Au	creatininase	creatinine	0–1200	10		60	30(S)	322
PmPD/dimethylferrocene/carbon	glucose oxidase	glucose	2000–76000		220	20	72(S)	368
PVC/PmPD/Pt	lactate oxidase	lactate	1000–15000		10–15	60	280(S)/9(O)	370

<sup>a</sup> O means continuously operational lifetime. <sup>b</sup> S means shelf lifetime or storage lifetime.

eliminated the interferences of AA, uric acid, and cysteine. The Pt/PpPD-GOx sensor under optimal conditions exhibited a linear response to glucose in a concentration range of 10–3000 mM, high stability over 2 months, and far greater current density of responding to glucose than the Pt/PoPD-GOx sensor. Ju et al. prepared an amperometric Au/PoPD-GOx sensor based on a nanometer-sized (88 nm) microband Au electrode.<sup>374</sup> The sensor also eliminates the interference of AA and shows a linear response to glucose in a range from 0.5 to 10 mM.

Furthermore, Pt/resorcinol-*m*PD copolymer-GOx microsensor was found to show good reversibility of the electrode process, short response time of 1–10 s, low detection limit of 25  $\mu\text{M}$ , and linear range from 25  $\mu\text{M}$  to 2 mM glucose. Therefore, the microsensor could serve for interference-free and antifouling measurement in blood and plasma,<sup>375</sup> because the resorcinol-*m*PD copolymer film blocks acetaminophen completely in concentrations higher than physiological values.

Myler et al. prepared an amperometric polycarbonate/Au/GOx-bovine serum albumin/PoPD electrode by electropolymerization of PoPD on a gold sputter-coated porous polycarbonate membrane for the determination of glucose concentration in whole blood.<sup>149</sup> The electrode can facilitate the screening of biological anionic interferents such as ascorbate and urate due to charge repulsion by the GOx and protein immobilized. The PoPD film offers an enhanced biocompatibility as compared with polycarbonate.

Wang et al. reported a one-step electropolymeric co-immobilization of GOx and heparin within a PoPD film on Pt electrode for amperometric biosensing of glucose.<sup>376</sup> It is found that the co-deposition of GOx and heparin imparts both biocatalytic and anticoagulation activities onto the PoPD film-modified electrode and greatly improves the sensor performance after exposure to whole blood. Although the PoPD film alone does provide the necessary biocompatibility, exposure to the blood sample resulted in a substantial (>50%) suppression of the response of the Pt/PoPD-GOx electrode and the formation of a fibrin "clot", whereas only a negligible change of the response and electrode surface is observed for Pt/PoPD-GOx-heparin electrode before and after blood exposure. This indicates that the bioactivity of heparin is retained on its entrapment within the PoPD film and the surface-confined heparin prevents coagulation during exposure to whole blood. The Pt/PoPD-GOx-heparin sensor exhibits a fast response, good reproducibility, extended linear range, and the absence of carryover/memory effects but decreased sensitivity. In addition, the negatively charged heparin may facilitate the rejection of common anionic interferences and hence impart enhanced permselectivity. The simultaneous localization of the enzyme and heparin offers great promise for simplifying the preparation of enzyme electrodes and fabricating a miniaturized, implantable, biocompatible glucose needle-type biosensor.

Reynolds and Yacynych constructed Pt/PoPD-GOx ultramicrobiosensors for direct measurement of glucose in complex samples.<sup>377,378</sup> The sensors are very effective on preventing interferences, together with a response time (100%) of 15–45 s, linear response over the human clinical range for glucose (3–7 mM).

Ji, Sasso, and co-workers immobilized GOx in electropolymerized PoPD film onto a platinized, reticulated vitreous carbon or GC electrode and used the resulting sensor for determination of glucose in human serum by flow injection analysis.<sup>341,372</sup> The PoPD film thickness and GOx molecular diameter in the sensor were <10 and 8.6 nm, respectively. They reported a drastic reduction of interferences caused by AA, uric acid, and cysteine as well as a virtual elimination of electrode fouling by proteins in blood serum, whereas high H<sub>2</sub>O<sub>2</sub> permeability was maintained through the PoPD film. The sensor has the following advantages: (1) longer working lifetime of 1.5–2 months (600 runs of repetitive detections) and shelf lifetime of at least 3 months, (2) higher sample throughput of 130 samples per hour, (3) larger reproducibility with an error in precision of  $\pm 1\%$ ,

(4) practical recovery of 100.6%, (5) easier miniaturization. Notably, the linear detection range of the sensor exhibits a dependence on oxygen. At ambient conditions, the linear detection range is to 10 mM and usable to 30 mM. If the carrier stream and samples are saturated with oxygen, the sensor is linear to 30 mM and useful to 100 mM.

Centonze et al. studied the influence of AA on the response of a Pt/PoPD-GOx glucose biosensor and found that the homogeneous reaction between AA and H<sub>2</sub>O<sub>2</sub> is too slow to influence the response of typical glucose biosensors and similar H<sub>2</sub>O<sub>2</sub> detecting biosensors.<sup>379</sup> Therefore, the decrease in the sensor response, observable when working in batch under typical experimental conditions, can in no way be ascribed to depletion of H<sub>2</sub>O<sub>2</sub>, which is produced in the biocatalytic cycle via the homogeneous reaction with AA. While the purely additive Faradic interference can practically be nullified by the entrapping membranes, electrode fouling by electrooxidation products of AA (responsible for the observed decrease in glucose sensitivity) has no effect in flow injection analysis but might still represent a problem when working in continuous flow or batch systems at high ascorbate concentration. In summary, Pt/PoPD-GOx sensor can be employed in flow injection analysis to accurately monitor glucose in the presence of AA.

Dumont and Fortier compared the performance of PoPD/GOx, PAN/GOx, PPY/GOx, and PoPD-cross-linking PAN/GOx sensors.<sup>365</sup> It is found that the PoPD/GOx sensor gave the best signal/noise ratio though the linearity to glucose for the most of the sensors is 7–10 mM and all the sensors exhibited permselectivity toward electroactive species.

Multilayer biosensors based on the aromatic diamine polymer films are also widely studied. Garmjonyte and Malinauskas reported the effect of multilayer structure on the performance of biosensor.<sup>349,352</sup> It is found that the greatest response to glucose and ascorbate is observed at a single-layered Pt/PoPD-GOx electrode, whereas introduction of an intermediate PoPD layer, i.e., Pt/PoPD/PoPD-GOx electrode, diminishes the response to some extent, especially at higher glucose concentration. Placing the third PoPD layer as the top layer over Pt/PoPD/PoPD-GOx, as for Pt/PoPD/PoPD-GOx/PoPD multilayered electrode, diminishes the response by a factor of 3 or 4 as compared with Pt/PoPD/PoPD-GOx or Pt/PoPD-GOx electrodes. It is shown that the sensitivity to both glucose and ascorbate decreases but the linear range of response to glucose increases by placing one or two additional PoPD layers onto Pt/PoPD-GOx electrodes. However, the sensitivity to ascorbate decreases to the greatest extent with the greatest retention of ascorbate of ca. 95% at multilayered Pt/PoPD/PoPD-GOx/PoPD electrode. On the other hand, a multilayered composite Pt/PB/PoPD/PoPD-GOx- and Pt/PB/PPY/PoPD-GOx-based biosensors can be operated at much lower potential together with a very useful combination of higher sensitivity to glucose and weaker interference response to ascorbate than Pt/PoPD/PoPD-GOx- and Pt/PB/PPY-GOx-based biosensors, respectively.<sup>349,352</sup>

Nguyen and Luong suggested that a carbon/polyvinylferrocene-GOx/resorcinol-PD copolymer sensor could determine glucose up to 25 mM with a response time of 1 min for at least 50 repeated analyses with good reproducibility.<sup>380</sup> The presence of ambient oxygen, AA (0.1 mM), and uric acid (0.5 mM) did not affect its performance. When applied for the determination of the glucose level in reconstituted human serum, the results agreed well with those of the reference hexokinase assay. Mulchandani and Pan revealed that HRP/poly(*m*-aminoanilinomethylferrocene)-modified GC electrode biosensor can measure H<sub>2</sub>O<sub>2</sub> and other organic peroxides in both aqueous and organic media by reduction at a low applied potential of -50 mV vs Ag/AgCl without interference from molecular oxygen.<sup>381</sup> When modified with GOx, the new bienzyme electrode can detect glucose sensitively and selectively, demonstrating the suitability of the above peroxide biosensor for other oxidoreductase enzyme-based biosensors.

Vidal et al. also fabricated multilayered carbon/OCS-GOx/PPY/PoPD, Pt/PPY-GOx/PoPD, and Pt/PPY-COx/PoPD composite biosensors by an in-situ flow injection methodology with continuous circulation of a solution containing the monomer.<sup>340,351</sup> The linear range and lifetime of the carbon/OCS-GOx/PPY/PoPD and carbon/OCS-GOx/PoPD electrodes are substantially improved relative to carbon/OCS-GOx/PPY and carbon/OCS-GOx electrodes, respectively.<sup>351</sup> Similarly, the limit of detection, reproducibility, and selectivity of H<sub>2</sub>O<sub>2</sub> over AA and uric acid of the Pt/PPY-GOx/PoPD and Pt/PPY-COx/PoPD electrodes are substantially improved compared with Pt/PPY-GOx and Pt/PPY-COx electrodes, respectively.<sup>340</sup> These results suggested a great importance of the PoPD outer layer. The Pt/PPY-GOx/PoPD- and Pt/PPY-COx/PoPD-based biosensor can be satisfactorily applied to the determination of their respective substrates in assayed samples of human blood serum.

Bartlett et al. fabricated microelectrochemical enzyme transistors by connecting two carbon band electrodes with an anodically grown PAN film and immobilizing GOx or HRP onto the PAN/insulating PoPD bilayer film.<sup>331,364,382</sup> The amperometric response to H<sub>2</sub>O<sub>2</sub> of the bilayer film electrode could be improved if HRP was adsorbed onto the PAN film rather than immobilized in the PoPD film due to the insulating PoPD film interfering with the direct electrochemical interaction between the enzyme and the PAN film.<sup>167</sup> The effect of varying the PAN growth charge on the switching rate of carbon/PAN/PoPD/GOx switch was investigated along with the conditions for immobilization of the GOx. By optimization of the thickness of the polymer film and the deposition condition, the switching time can be reduced to 10 s to switch from fully insulating to fully conducting for moderate glucose concentrations. The further reduction of the switching time should be possible if thinner films are employed. In addition, the transistors can resist the interferences from acetaminophen and L-urate but not L-ascorbate because acetaminophen and L-urate produced no switching response over the ~7 min period studied. As the carbon/PAN/PoPD/HRP device is reused over 15

repeat experiments, the switching rate will fall due to inactivation of the enzyme. The full switching time is ~100 s at saturating H<sub>2</sub>O<sub>2</sub> concentrations, which is much longer than that of the GOx system. The device can be applied to determine H<sub>2</sub>O<sub>2</sub> or HRP content in solution having H<sub>2</sub>O<sub>2</sub> or HRP concentration below 0.5 M. This type of device could form the basis of a simple, disposable device for electrochemical immunoassay or DNA probe using HRP as the label. However, several limitations, such as inhibition by high H<sub>2</sub>O<sub>2</sub> concentrations, need to be overcome in order to achieve fast reproducible switching transients in real analyte solutions.

Yasuzawa et al. prepared Pt/PoPD/poly(5-(1-pyrrolyl)pentyl-2-(trimethylammonium)ethyl phosphate-, poly(3-(1-pyrrolyl) propionic acid)-, and poly(1-(3-D-gluconamidopropyl)pyrrole)-GOx-based sensors.<sup>353,354,383</sup> The insertion of an inner PoPD film not only reduces the influence of uric acid and acetaminophen on the first sensor response, but also increases the lifetime significantly of the first two sensors.<sup>353,354</sup> Note that an interference of AA and acetaminophen to the glucose response was largely lowered by using PoPD film as the inner film of the third sensor but the influence of uric acid still remained.<sup>383</sup> The use of both Nafion and PoPD films as the inner film produced the best results in preventing the interference. A covalent bonding treatment between GOx and PPY derivative with 1-ethyl-3-(3-dimethylaminopropyl)carbodiimide is effective to improve the stability and linear range of the glucose response for the second sensor.<sup>353</sup>

Similarly, an inner PoPD film in Pt/PoPD/GOx/Nafion sensor is also very efficient for the enhancement of the performance of implanted needle-type glucose sensors in a biological matrix.<sup>384</sup> A flow rate independent signal has been led by a careful design of the various PoPD film thicknesses. In this design, both GOx and PoPD can reduce cracking of the outer Nafion layer by enhancing adhesion. Electrodeposition of PoPD for 15 min prior with GOx and Nafion gave complete protection against uric and ascorbic acids and urea. If the electrodeposition time of PoPD was reduced to 5 min, the influence of uric acid becomes a little bit more apparent. The interference of acetaminophen to the glucose response was apparent for the electrodeposition time of PoPD from 5 to 15 min. Notably, however, L-cysteine poisoned the sensors. Blood could also decrease the electrode sensitivity due to the adsorption of blood proteins on the Nafion. Fortunately, the sensors deteriorated by L-cysteine or blood can be refreshed by rinsing the sensor in fresh buffer. It is found that a 5-min PoPD film gives an excellent compromise between protection from interferences and stir rate independence. In in vitro testing a needle-type sensor, configured with a 5-min PoPD/GOx/Nafion trilayer, exhibits a nearly linear response up to 20 mM glucose, a detection limit below 0.1 mM, a response time of 33 s, a stabilization time of 10–30 min, sensitivity of 25 nA/mM, and precision of 2–5%. In in vivo tests, the same multilayer sensor was implanted subcutaneously in a conscious dog. Although a longer stabilization time of 30–40 min was required, the sensor signal matched the glycemia of the dog very well,

with a delay of 3 min, corresponding to the known lag time for subcutaneous glucose levels. The sensor remained functional after 1 week of implantation but failed after 2 weeks due to degradation of the reference electrode. Noteworthy is that a heat-curing procedure of the entire needle-type sensor of P $\phi$ PD/GOx/Nafion trilayer at 120 °C can significantly improve sensor stability in vivo and selectivity for glucose against uric acid and acetaminophen of the sensor, because the heat-curing procedure could seal pinholes or cracks in the Nafion and increase the crystallinity of the Nafion but hardly ever affect the GOx activity.<sup>385</sup> Several heat-cured needle-type sensors of P $\phi$ PD/GOx/Nafion trilayer remained functional for at least 10 days after subcutaneous implantation in dogs, without degradation of their sensitivity of 3 nA/mM in vivo and 6 nA/mM in vitro in pH 7.4 buffer at 37 °C.

Yegnaraman and Yacynych fabricated a Pt/GOx ultramicroelectrode immobilized by electropolymerized films of PPY and P $m$ PD.<sup>386</sup> The polymer film thickness was varied from 10 to 466 nm by controlling the charge during electropolymerization. The influences of the film thickness and the oxygenation/deoxygenation of the solutions on the amperometric response are studied.

Zamboni and Losito reported a H<sub>2</sub>O<sub>2</sub> sensor completely free from ascorbate interference based on a bilayer polymeric membrane of overoxidized PPY/P $\phi$ PD.<sup>387</sup> The sensor was used to study the kinetics of ascorbate oxidation by oxygen. Centonze et al. fabricated an oxygen-independent and interference-free OCS/P $\phi$ PD-GOx sensor for detection of glucose.<sup>382</sup> It is found that the sensor exhibits a response time to glucose of 10–16 s, a linear range up to 20 mM, an operational lifetime of 4 days, and a shelf lifetime of longer than 30 days. In the glucose determination, the sensor can reject the interferents such as uric acid, ascorbate, and cysteine with the rejection of higher than 95%.

Two bilayered electrodes, poly(OT)/P $m$ PD and poly(OT)/P $\phi$ PD, were prepared by electropolymerization on Pt at constant potential.<sup>388</sup> The factors affecting permselectivity characteristics to electroactive species such as AA, oxalic acid, and H<sub>2</sub>O<sub>2</sub> of the prepared double-layered polymeric electrodes were optimized systematically. It was found that AA and oxalic acid could not pass through polymeric films but a regular response for H<sub>2</sub>O<sub>2</sub> injections was seen. As a result, poly(OT)/P $\phi$ PD-GOx enzyme electrode prepared by enzyme immobilization using OT homopolymer working electrode gave regular responses for the glucose injections.

Additionally, Malitesta et al. prepared an electro-synthesized P $\phi$ PD molecularly imprinted by glucose with molecular recognition properties to be applied in biomimetic sensors.<sup>146</sup> The assembled sensor showed a shelf life of at least 1 month and a linear range up to 20 mM glucose.

Note that the homogeneous interference at Pt/P $\phi$ PD-GOx electrode in vitro between AA and H<sub>2</sub>O<sub>2</sub> could be catalyzed by trace metal impurities in the buffer.<sup>389</sup> The presence of the metal chelator EDTA in solution might eliminate the negative interference.

However, the homogeneous redox reaction in the mammalian brain is absent presumably due to a deficiency of suitable catalysts. Therefore, the good performance of Pt/P $\phi$ PD-GOx sensor is not compromised by lipids in vitro and can remain for several days following implantation in brain tissue.

Pt/P $\phi$ PD-GOx biosensors implanted in the right striatum of freely moving rats have been used for real-time measurements of the effects of anesthesia on extracellular brain glucose concentrations in order to real-time monitor brain energy metabolism in freely moving animals in vivo.<sup>390,391</sup> The biosensor responded to changing glucose levels in brain extracellular fluid by intraperitoneal injection of insulin that caused a decrease in the Pt/PPD-GOx current and by local administration of glucose (1 mM) via an adjacent microdialysis probe that resulted in an increase in the biosensor current. The change in temperature from in vitro to in vivo conditions has a minimal effect on the response of the biosensor, due to highly insulating thin PPD film (ca. 10 nm) immobilizing the GOx (diameter 8.6 nm) close to the electrode surface and acting as an efficient diffusion barrier preventing glucose from penetrating the film but not preventing it from reaching the active site and producing H<sub>2</sub>O<sub>2</sub>. Interferents involving administering AA and subanaesthetic doses of ketamine intraperitoneal have a minimal effect on the response of the biosensors. The sensor exhibits a detection limit of 3.53 mM and operational stability of longer than a 5-day period after implantation. Therefore, the sensor is reliable for glucose monitoring in brain extracellular fluid in vivo.

Carbon fiber/P $m$ PD-GOx sensor has also been investigated for in vivo brain glucose measurements by differential normal pulse voltammetry.<sup>392</sup> The calibration curves obtained based on the peak height and glucose concentration were linear from 0.5 to 5 mM and showed a sensitivity of 2.2 mA M<sup>-1</sup> cm<sup>-2</sup>, selectivity of 0.71 of H<sub>2</sub>O<sub>2</sub> over peptides. However, the sensor lost its selectivity and/or sensitivity properties after the differential normal pulse voltammetry measurements of 16 h, possibly due to a gradual alteration of the P $m$ PD film. Because of the poor stability, the sensor could not be used for glucose monitoring in the living brain.

On the other hand, Trojanowicz et al. compared the performance of amperometric glucose biosensors fabricated by the immobilization of GOx during the electropolymerization of P $\phi$ PD with PPY, PMPY, and PAN on Pt or Au electrodes.<sup>393</sup> It was found that Pt/P $\phi$ PD-GOx sensor exhibits the highest sensitivity of response to glucose together with a wide linear range and better durability. It is also found that P $\phi$ PD/poly(phenol red)-coated electrode exhibits the more favorable electrochemical behavior (lower overpotential required and higher selectivity against interferents) of the NAD<sup>+</sup>/NADH redox couple than poly(3-methylthiophene)/poly(phenol red) coated electrode.<sup>394</sup> An amperometric biosensor for glucose based on polystyrene-immobilized enzyme over an electro-synthesized P $\phi$ PD layer has been fabricated.<sup>395</sup>

By electropolymerization of  $m$ PD,  $p$ PD in the presence of pyrroloquinolinequinone, a new sensor

based on glucose dehydrogenase enzyme has been assembled.<sup>165</sup> The Au/*Pm*PD/pyrroloquinolinequinone-glucose dehydrogenase sensor exhibits a short response time (5–10 s) and detection limit (50 mM) in a linear glucose concentration range of 0.1–3 mM. The Au/*Pp*PD/pyrroloquinolinequinone-glucose dehydrogenase sensor exhibits substantially the same response time (8–10 s) but a lower detection limit (10 mM). The sensors under nondynamic conditions showed a decrease of 10% over 1 month and a residual activity of 50% over 2 months. A biosensor with the light-harvesting protein (phycoerythrin) has been fabricated by electropolymerization of *o*-dianisidine with GOx and HRP on ITO-coated glass electrode for bioanalytical application.<sup>319</sup>

**b. Detection of Lysine.** The rapid detection of L-lysine in food is very important for food production and quality control. For the rapid and specific determination of L-lysine in food with good reproducibility (4–6%), Kelly et al. fabricated an interferent-free and fast response amperometric biosensor by electropolymerization of *o*PD, *m*PD, and *p*PD directly on Pt or electropolymerization of *o*PD over a Ru/Rh-coated GC electrode.<sup>358,360</sup> The selectivity of the enzyme was optimized by choosing enzyme source, controlling the pH, electropolymerization time, temperature, and flow rate of the system. The optimum flow rate and pH were 0.5 mL/min and 7.5, respectively. It is found that all three PPDs can cover the Pt electrode surface to some extent and that the best polymer is *Po*PD. *Po*PD film reduced the interferent response as follows: AA by 100%, citric acid by 99.9%, phenylalanine by 99.8%, uric acid by 99.6%, acetaminophen by 98.8%, cysteine by 96%, compared with the bare Pt.<sup>358</sup> Carbon/Ru/Rh/*Po*PD-LOx biosensor generated the lowest relative response to AA and the second lowest response to L-cysteine.<sup>377</sup>

Karalemas et al. constructed an amperometric lysine biosensor by electropolymerization of *o*PD on Si–Au strip electrode, followed by LOx immobilization with glutaraldehyde.<sup>359</sup> The unique feature of a smooth and uniform surface of the electrode allows a highly controllable electropolymerization procedure, such as enzyme amount, pH, immobilization time, which is low cost, simple, and repeatable. It is proved that *Po*PD film exhibits high selectivity of lysine against ornithine, phenylalanine, arginine, and histidine. The selectivity can be further controlled and even improved by optimizing the polymerization conditions. However, the biosensor does not exhibit high selectivity of lysine against tyrosine and cysteine.

**c. Detection for Lactate and Lactic Acid.** *Po*PD-LAOx-based biosensor has been successfully employed for a reliable, sensitive, and fast quantification of lactate and lactic acid in clinical processes, food processes, and bioprocesses. Dempsey et al. constructed a Pt/*Po*PD-LAOx biosensor by a one-step electropolymerization procedure of *o*PD and LAOx in deaerated unstirred phosphate buffer solutions by applying a constant potential of 0.65 V vs Ag/AgCl for 20 min.<sup>357</sup> It is suggested that a thinner *Po*PD film appears to incorporate more enzyme resulting in faster response. A thicker film implies a slower

response and lower sensitivity but results in a wider linear range, because the diffusion of the product H<sub>2</sub>O<sub>2</sub> through the *Po*PD film may be a limiting factor as the thickness is increased and the enzymatic reaction occurs more readily in the outer portion of the film near the solution side than in the interior of the film. The Pt/*Po*PD-LAOx electrode exhibits 0%, 19%, 94%, and 90% responses of glucose, ascorbate, uric acid, and L-lactate, respectively, while these responses significantly decreased to 0%, 11%, 50%, and 64% by covering an additional cellulose membrane with a 12000–14000 molecular weight cutoff over the electrode. Distinctive features of the sensor are a high sample throughput of 180/h and precision of 3.53% for 25 injections when the sensor is used in flow injection analysis.

Krawczyk et al. suggested that Pt/*Po*PD-LAOx monolayer biosensor does not provide sufficient discrimination from several interfering species in physiological fluids.<sup>396</sup> However, Pt/polyphenol/PPY/*Po*PD-LAOx trilayer sensor exhibits high selectivity of response to lactate over interfering species. Despite a continued decrease in biosensor sensitivity, this trilayer biosensor has been successfully applied in flow injection determination of lactate in both undiluted and diluted human blood serum samples over a 10-day period. Excellent reproducibility and low detection limit were found to be 0.6% during the measurement for 1:10 diluted serum and 2 μM, respectively.

Palmisano et al. constructed an in-situ electrosynthesized *Po*PD/LAOx biosensor for determination of lactate in serum by flow injection analysis.<sup>346</sup> At a flow rate of 50 mL/min, linearity is up to 0.2 mM lactate and detection limits of about 2 mM could be easily achieved. Faradic interferences caused by ascorbate, urate, cysteine, and acetaminophen were sufficiently minimized to permit lactate determination in diluted serum by flow injection analysis. At a flow rate of 1 mL/min, a sample throughput higher than 70 sample/hour was achieved. After 1 week of continuous use in the flow injection analysis, a 75% decrease in biosensor sensitivity was observed. Palmisano et al. also reported an efficient rejection of ascorbate in H<sub>2</sub>O<sub>2</sub> detecting *Po*PD-based biosensors modified by placing an additional electroactive layer between the substrate electrode and *Po*PD film<sup>397–399</sup> and systematically described the lactate sensitivity of the Pt/PPY/*Po*PD-LAOx biosensor fabricated. The sensor displays a very short response time of 4 s, linear range of response up to 10 mM lactate, high efficiency of rejecting interferent, high sample throughput, and no sample pretreatment with an operational lifetime of at least 6 days. Ascorbate, urate, cysteine, and paracetamol produce a nondetectable bias even at their maximum physiological concentration in blood. The sensor can successfully determine lactate in complex media such as serum, milk, and yogurt.

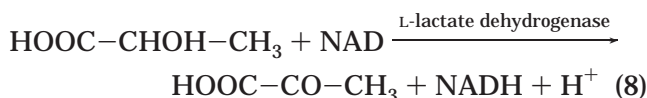
Shu et al. suggested that the production of D-lactic acid during fermentation could be monitored on-line with a reagentless carbon paste electrode modified by D-lactate dehydrogenase, NAD<sup>+</sup>, and mediator containing an electropolymerized *Po*PD membrane in a flow injection system integrated with a filtration



sampling device.<sup>400</sup> The time delay between sampling and detection was approximately 6 min, which is much shorter than traditional spectrophotometry. In particular, the use of the *PoPD* membrane on the electrode resulted in a very selective sensor response with acceptable stability and sensitivity. The response for D-lactic acid is linear to 10 mM together with the detection limit of 0.7 mM, the operational stability of 20 h, and a throughput of 20/h. The D-lactate concentrations determined on-line also agreed well with those determined by a standard method, implying that this sensor system is suitable for on-line monitoring of D-lactate production in batch fermentation.

The electropolymerization of *mPD*, *pPD* in the presence of pyrroloquinolinequinone using cyclic voltammetry on Au electrode has been also used to fabricate a sensor based on L-lactate dehydrogenase enzyme.<sup>165</sup> The Au/*PmPD*/pyrroloquinolinequinone electrode exhibits high selectivity of the electrooxidation of  $\beta$ -NAD<sup>+</sup> over the oxidation of paracetamol, ascorbic, and uric acid with a detection limit of  $5 \times 10^{-5}$  M ( $\beta$ -NAD<sup>+</sup>, reduced form) and response time of 10 s. The Au/*PmPD*/pyrroloquinolinequinone-lactate dehydrogenase sensor exhibits a response time (7–10 s) and detection limit (50  $\mu$ M) to lactate in a linear lactate range 0–7 mM. The Au/*PpPD*/pyrroloquinoline-quinone-lactate dehydrogenase sensor exhibits substantially the same response time (8–10 s) but lower detection limit (10  $\mu$ M). The stability of the both sensors under nondynamic conditions is good.

A bienzyme-*PoPD*-modified carbon paste electrode has been constructed for the amperometric detection of L-lactate.<sup>401</sup> The bienzyme is glutamic pyruvic transaminase and L-lactate dehydrogenase together with its cofactor NAD<sup>+</sup>. The response of the electrode is based on the electrocatalytic oxidation of the enzymatically produced NADH as follows



The oxidation of the liberated NADH allows the measurement of lactate because the electrocatalytic oxidation of NADH yields an analytical signal to the lactate concentration. Due to the fact that oxygen is not involved, this measurement of lactate shows more promise than that of the lactate oxidase enzymatically produced H<sub>2</sub>O<sub>2</sub>. The interference of uric acid, AA, cysteine, glutathione, and paracetamol will be practically reduced by covering the bienzyme-*PoPD* electrode with a second electrosynthesized PHAN nonconducting film. The bienzyme-*PoPD*/PHAN double-filmed electrode obtained thus gives a linear response for lactate of 0.6–85 mM, a response time of 80 s, high selectivity of lactate over other hydroxyacids including malonic, glycolic, quinic, isocitric, and malic acids even at higher concentration of 1mM, and stability for at least 1 month at room temperature. The sensor could be used for the quantification of lactic acid in cider and also for a reliable, sensitive, and fast determination and analysis of lactate in clinical processes, food processes, and bioprocesses.

**d. Detection for Glutamate, Glutamic Acid, and Inosine.** Zilkha et al. described a *PoPD*-GLOx/Pt amperometric detector for flow analysis of glutamate in dialysate emerging from an implanted microdialysis probe.<sup>402</sup> The *PoPD* film eliminates interferences from AA and other endogenous electroactive compounds. The high sensitivity (<0.5  $\mu$ M) and short response time of the detector (90% of the maximum response in 30 s) make it particularly suitable for investigating conditions that produce rapid changes in brain extracellular glutamate. In particular, its small size allows it to be placed within a few centimeters of the animal preparation, reducing the delay for data acquisition to ca. 2 min.

Cooper et al. invented biomolecular sensors for neurotransmitter determination by adsorption of GLOx onto 10 and 25 mm (inside diameter) Pt microelectrodes followed by immobilization in an electrochemically polymerized nonconducting *PoPD* film.<sup>403,404</sup> The sensors exhibit a detection limit of 100  $\mu$ M and sensitivities of 13 and 120 pA/mM for 10 and 25 mm (inside diameter) Pt microelectrodes, respectively. The response of the enzyme electrodes for the amperometric determination of glutamate was proportional to the size or area of the electrode and highly reproducible from day to day with a linear dynamic range from 100  $\mu$ M to 15 mM. The sensor was stable over a period of 30 days, and the *PoPD* film can reduce interference from the electroactive compounds, uric acid (wholly excluded) and AA (partially excluded) but not dopamine. The response time of the sensors is shorter than 15 s.

Similarly, Ryan et al. constructed an amperometric biosensor for neurotransmitter L-glutamic acid by dip coating of L-glutamate oxidase (GLOx, 200 units/mL phosphate buffer, pH 7.4) onto 60  $\mu$ m radius Teflon-coated Pt wire with an exposed length of 1 mm, followed by electropolymerization of *oPD*.<sup>348</sup> The sensor has a fast response time of 10 s, a high sensitivity to L-glutamic acid of  $3.8 \pm 1.3$  nA/(cm<sup>2</sup> mM) in the linear range of 0–100  $\mu$ M, a low detection limit of 300 nM, and the selectivity for L-glutamic acid over AA of  $92 \pm 3\%$ , indicating suitability for neurochemical applications in vivo.

Curulli et al. suggested that the Au/*PmPD*/pyrroloquinolinequinone-glutamate dehydrogenase sensor exhibits a response time (8–10 s) and detection limit (10  $\mu$ M) to glutamate in a linear range 0–5.5 mM.<sup>165</sup> The Au/*PpPD*/pyrroloquinolinequinone-lactate dehydrogenase sensor exhibits substantially the same response time (9–15 s) but lower detection limit (5  $\mu$ M).

Matsumoto et al. investigated a simultaneous biosensing of glutamate and inosine monophosphate by using immobilized enzyme reactors.<sup>405</sup> The ghost response caused by the interference in real sample and electrode fouling was reduced through covering the Pt electrode with *PoPD* film. The system may be applicable to the quality evaluation of food seasoning.

**e. Detection for Hypoxanthine, Galactose, Choline, Sorbitol, and Ethanol.** The published articles concerning the detection for hypoxanthine, galactose, choline, sorbitol, and ethanol through aromatic diamine polymer film-based sensors are

very deficient. Nguyen et al. constructed an amperometric biosensor by forming a layer of cross-linked xanthine oxidase on Pt, followed by electropolymerization of a submonolayer PpPD-resorcinol copolymer film.<sup>406</sup> It is interesting that optimal performance was obtained with enzyme-based electrodes sparsely covered with PpPD-resorcinol copolymer film formed by electropolymerization in shorter than 6 min. The resulting electrodes exhibited a linear response to hypoxanthine in a range 5–300  $\mu\text{M}$  with a response time of 2 min. The biosensor has been successfully and continuously applied in monitoring hypoxanthine content of fish extracts for 6 h with over 50 assays together with a storage lifetime of 60 days when stored at 4 °C in phosphate buffer.

Manowitz et al. fabricated a carbon/Pt/*m*PD-resorcinol copolymer-Nafion composite-galactose oxidase biosensor to prevent interferences for a flow injection analysis system for the detection of galactose in human plasma.<sup>407,408</sup> The sensor showed high selectivity of  $\text{H}_2\text{O}_2$  over urate, ascorbate and acetaminophen, a detection limit of 50 nM, a linear range from 0.05 to 6 mM, a storage stability of longer than 30 days, a recovery of 105%, and a high sample throughput of 120 samples/h. Note that a composite of *m*PD-resorcinol copolymer and Nafion can realize high selectivity (4.17) to  $\text{H}_2\text{O}_2$ , because the carbon/Pt/*m*PD-resorcinol copolymer-galactose oxidase biosensor without Nafion exhibits a low selectivity (1.77) to  $\text{H}_2\text{O}_2$ . It is seen that inclusion of the composite polymers facilitated the development of a sensitive galactose biosensor.

PoPD has been used for satisfactory fabrication of a Pt/PoPD/PoPD-choline oxidase sensor for the detection of choline.<sup>393</sup> A significant influence of enzyme concentration and the electropolymerization time on the sensitivity of the biosensors was found. Among all the conditions examined, the biosensor with the largest sensitivity of response to choline but also with a relatively high background current (30–50 nA) and short lifetime (5 days) was obtained using a 5 min electropolymerization from a solution containing 100 units/mL choline oxidase. An increase of the electropolymerization time up to 30 min significantly improves the long-term stability of detection (10 days), although after 1 day of use its sensitivity dropped by about 50% due to the decrease of the enzyme activity in solution used for the polymerization. In addition, Pt/PoPD/PoPD-choline oxidase sensor can also be used for the detection of butyrylcholine in solution with dissolved esterase.

Saidman et al. systematically describe a carbon-NAD<sup>+</sup>-D-sorbitol dehydrogenase/PoPD biosensor for the amperometric detection of D-sorbitol.<sup>409</sup> The electrocatalytic system for NAD<sup>+</sup> oxidation coupled to the sorbitol oxidation allows developing a biosensor for sorbitol. Electroinactive PoPD films formed at electropolymerization pH higher than 7 can prevent electrode fouling and interference from ascorbate and several polyols. No response was observed for some polyols such as mannitol and dulcitol. However, the biosensor exhibits the same signal of xylitol as sorbitol at 0.5 mM and 1.5 times the signal of sorbitol to iditol. Therefore, xylitol and iditol could be two

major interferences. The resulting biosensor responded to sorbitol up to 800  $\mu\text{M}$  with a detection limit of 40 nM, good reproducibility with a relative standard deviation of 6.1%, a response time of 40 s, and an operational lifetime of longer than 48 h. Unfortunately, the response time was raised to 120 s on the second day after biosensor fabrication. Good agreement is observed between the practical analytical results of the sorbitol content in foods like dietetic ice cream and candy by the biosensor and the spectrophotometric methods. Therefore, the biosensor can be applied for a reliable and rapid determination of sorbitol in a number of different fields, such as food, pharmaceutical, and cosmetic industries.

An electrochemical biosensor for ethanol has been constructed by electropolymerizing PoPD on the surface of an alcohol dehydrogenase–NAD<sup>+</sup>-modified carbon paste electrode.<sup>410</sup> Efficient electrocatalytic oxidation, at low applied potentials, of the enzymatically produced NADH by the conducting film provided a current that was dependent on ethanol concentration. The biosensor exhibits a linear response to ethanol in the range 0.03–3  $\mu\text{M}$  and a response time of 20 s. The trend in sensitivity toward different alcohols is in agreement with the known biospecificity of yeast ADH. Ethanol sensor was applied to the analysis of different alcoholic beverages, resulting in excellent accuracy and precision.

**f. Detection of Dopamine, Ascorbate, and Ascorbic Acid.** Dopamine, ascorbate, and ascorbic acid are generally deemed to be interferences during the amperometric detection of most biosubstances. Therefore, their responses and sensitivities are expected to be as low as possible. However, sometimes in order to detect the concentration of dopamine, ascorbate, and ascorbic acid in extracellular and cerebrospinal fluids quickly and precisely, the responses and sensitivities of the three substances are desired to be high enough. Mo and Dgorevc constructed a carbon/overoxidized PoPD microelectrode containing sodium dodecyl sulfate as the dopant but without any enzyme for a measurement of dopamine and ascorbate,<sup>411</sup> where the PoPD film should be electrosynthesized at the optimum polymerization potential +0.8 V and time 20 min. To effectively turn the PoPD film into an overoxidized PoPD film for the optimum simultaneous detection of dopamine and ascorbate, a high anodic vertex potential of 2.2 V together with a short overoxidation time of 7 s (50 CV runs) at a cycling frequency of 2.3 Hz at pH 7.0 is required. As-prepared overoxidized PoPD electrode, without any pretreatment or conditioning, immediately exhibits the attractive ability to simultaneously measure nanomolar-order dopamine and millimolar-order ascorbate in a pH 7.4 medium because of a high current response to cationic dopamine and a favorably slow response to anionic ascorbate. A linear range for dopamine in the presence of 0.3 mM ascorbate is from 50 nM to 10  $\mu\text{M}$  with an extremely low detection limit of 10 nM. The detection limit for dopamine will lower further to 2 nM (signal/noise = 3) if in the absence of ascorbate. The linear range for ascorbate in the presence of 100 nM dopamine is 0.2–2 mM with a detection limit of 80  $\mu\text{M}$ . The

reproducibility of the measurements of the electrode is 1.6% and 2.5% for 100 nM dopamine and 0.3 mM ascorbate, respectively. Obviously the detection of dopamine exhibits a wider linear range, a lower detection limit, and better reproducibility than the detection of ascorbate. Potential interfering agents including 3,4-dihydroxyphenylacetic acid, uric acid, oxalate, human serum proteins, and glucose at their physiologically relevant or higher concentrations did not have any effect. In particular, the overoxidized *Po*PD-filmed microelectrode exhibits only a minor change in dopamine response even after being stored in air for 1 month and is very easy to refresh by running 20 voltammetric cycles between  $-0.2$  and  $+0.8$  V in phosphate buffer pH 7.4 after the detection of  $1 \mu\text{M}$  dopamine. These imply long storage lifetime and good maintenance of the microelectrode because of the absence of the enzyme with low stability especially at relatively high temperature in air. Therefore, the overoxidized *Po*PD-filmed microelectrode is promising for in vivo and in vitro applications, including measure of dopamine and ascorbate in extracellular and cerebrospinal fluids.

A *Po*PD biosensor for the detection of AA in human serum has been fabricated by electropolymerization of *o*PD and AA oxidase in buffer pH 5.6 at 0.6 V vs Ag/AgCl for 20 min onto GC electrode.<sup>412</sup> Solution pH and temperature significantly influence enzyme activity and the rate of reaction catalyzed by enzyme. It is found that there is a maximum enzyme activity and response current at 5 mM AA, pH 5.6, and 25 °C. The GC/*Po*PD-AA oxidase sensor exhibits a linear detection range of 0.25–10 mM, an extremely low detection limit of 10 nM, a response time of 7s, and repetition (relatively standard deviation 0.7%) for the detection of AA. There is hardly ever interference of the sensor by  $\text{K}^+$ ,  $\text{Na}^+$ ,  $\text{Ca}^{2+}$ ,  $\text{CH}_3\text{COO}^-$ , glucose, sucrose, uric acid, inosine, urea, proline, lysine, glycine, starch, and fructose. However, its response decreases with increasing number of measurements and remains 98% after 100 repetitive measurement or being stored at low temperature for 1 month. In particular, it exhibits a recovery of 98–110% in the practical measurement of human serum.

**g. Detection of Nitric Oxide.** Park, Friedmann, Pontie, and colleagues constructed enzyme-free microsensors for the detection of nitric oxide based on carbon/*Po*PD, carbon/*Po*PD/Nafion, carbon/Nafion/*Po*PD, carbon/Nafion/*Po*PD-resorcinol, and carbon/Nafion/*Pm*PD-resorcinol.<sup>294,413–415</sup> As shown in Table 24, every sensor exhibits different characteristics. For instance, the *Pm*PD film containing microsensor exhibits the best selectivity ratio (>1300) of nitric

**Table 24. Effect of Coatings on the Electrode Selectivity Ratio of Response to Nitric Oxide against Each of the Following Three Interferents**

coating	interferents			refs
	ascorbate	dopamine	nitrite	
carbon/ <i>Po</i> PD	679	390	221	413
carbon/ <i>Po</i> PD/Nafion	662	3	495	413
carbon/Nafion/ <i>Po</i> PD	756	175	935	413
carbon/ <i>Pm</i> PD	1300	130	144	294
carbon/ <i>Pm</i> PD-resorcinol	2050	184	417	294
carbon/ <i>Pm</i> PD- <i>Po</i> PD	2200	25	90	294

**Table 25. Permselectivity of Nitrites over Ascorbic Acid through Electropolymerized Films Grown from Various Aromatic Diamines on Pt from a 5 mM Solution of the Monomer in 0.1 M Phosphate Buffer Solution at pH 6.5 in the Potential Cycle from 0 to +0.8 V for PPD and in 0.2 M NaCl and Balanced to pH 1.0 with Concentrated HCl in the Potential Cycle from  $-0.15$  to  $+1.3$  V for PDAN at the Same Scan Rate  $2 \text{ mV/s}$ <sup>417</sup>**

film	permeability (%)		permselectivity nitrites/ascorbic acid
	nitrites	ascorbic acid	
<i>Po</i> PD	3.8	0.15	25
<i>Pm</i> PD	6.3	0.18	35
Poly(ANO)	44	0.6	73
P15DAN	24	0.8	30
P18DAN	35	0.3	117

oxide against ascorbate, carbon/*Po*PD sensor exhibits the highest selectivity ratio (390) of nitric oxide against dopamine, and carbon/Nafion/*Po*PD sensor exhibits the highest selectivity ratio (935) of nitric oxide against nitrite. Carbon/Nafion/*Po*PD and carbon/Nafion/*Pm*PD-resorcinol sensors are capable of detecting nitric oxide very selectively against L-arginine, serotonin, and xanthine besides ascorbate and nitrite. Carbon/Nafion/*Pm*PD-resorcinol sensor exhibits high sensitivity of 560 nA/mM to nitric oxide, a low detection limit, defined as a signal-to-noise ratio of 3, from 60 to 80 nM nitric oxide concentrations along with a linear range of 0.2–10  $\mu\text{M}$  and lifetime of 7 days.<sup>294</sup> In particular, carbon/Nafion/*Po*PD and carbon/nickel porphyrin/Nafion/*Po*PD sensors show very low detection limits of 35 and 40 nM nitric oxide concentrations, respectively. In addition, these sensors exhibit a very rapid response with one-half response time of 284 ms and excellent linearity in a range of 0–6  $\mu\text{M}$ . It appears that the sensitivity of the carbon electrode to nitric oxide increases when the electrode is coated with Nafion/*Po*PD, and the sensitivity of the carbon/Nafion/*Po*PD microsensor fabricated thus is much higher to nitric oxide (9.6 nA/ $\mu\text{M}$ ) than those to the interfering analytes such as ascorbate, L-arginine, nitrite, serotonin, dopamine, 5-acetamidophenol, epinephrine, 4-metcatechol, 5-hydroxyindol, norepi-nephrine, and dopac. Therefore, the carbon/Nafion/*Po*PD microsensor can discriminate between nanomolar changes of nitric oxide and micromolar changes of the other analytes, due to a better size exclusion from *Po*PD film having a compact stacked structure. Note that the carbon/Nafion/*Po*PD sensor also displays recording characteristics that were necessary for the reliable detection of nitric oxide in biological systems. These sensors are useful for direct monitoring of nitric oxide in the rat brain following an ischemic injury, for the measurement of nitric oxide diffusion in the extracellular space of the rat brain, and for the detection of nitric oxide release from isolated rat renal arterioles. A carbon fiber/*Po*PD/porphyrine/Nafion sensor has been used to measure the extracellular nitric oxide level in anesthetized cats by in vivo voltammetry.<sup>416</sup>

**h. Detection of Nitrites and Nitrates.** Very recently a new Pt/P18DAN sensor was assembled and used for rapid amperometric detection of nitrites and nitrates in water by batch and flow injection analysis for the first time.<sup>417</sup> As seen in Table 25, among

several electropolymerized films from aromatic diamines, P18DAN film exhibits the highest permselectivity of nitrite over AA, possibly due to its highest hydrophobicity and lowest solvation. After 48 h the permselectivity remained constant only for the P18DAN film, whereas poly(ANO) showed a permselectivity decrease of 30%. It is found from batch analysis that the Pt/P18DAN sensor for the detection of nitrites exhibits a good linearity from 0.5 to 100  $\mu\text{M}$ , sensitivity of 0.7 nA/ $\mu\text{M}$ , low detection limit of 0.1  $\mu\text{M}$ , short response time of 10 s, and a stable response for at least 4 months. Note that the Pt/P18DAN sensor needed about one night of stabilization in pH 4 acetate buffer at +0.9 V before the first use. The influence of the nitrate/nitrite ratio on Pt/P18DAN sensor response depends on the column used for flow injection analysis. For all the nitrite/nitrate ratios from 9/1 to 1/9 in a solution of 100  $\mu\text{M}$ , the response current decreased slightly from 35.4 to 34.6 nA if through a Cu/Cd column but decreased significantly from 33.3 to 3.8 nA if bypassing a Cu/Cd column. The detection limit in flow injection analysis was 0.25  $\mu\text{M}$ , which is slightly higher than that in batch analysis. Furthermore, the presence of  $\text{Cl}^-$ ,  $\text{SO}_4^{2-}$ ,  $\text{Ca}^{2+}$ ,  $\text{Mg}^{2+}$ ,  $\text{Na}^+$ ,  $\text{K}^+$ ,  $\text{Al}^{3+}$ ,  $\text{CO}_3^{2-}$ ,  $\text{Mn}^{2+}$ ,  $\text{Cu}^{2+}$ ,  $\text{Zn}^{2+}$ , and  $\text{PO}_4^{3-}$  in water, the most common coexisting species at their maximum admissible concentrations, did not affect the nitrite determination. By adding standard solutions of nitrates to mineral water samples, the Pt/P18DAN nitrite sensor exhibits a recovery 96–98% and a relative standard deviation lower than 0.8%. Almost all performances of the Pt/P18DAN nitrite sensor are better than those of Pt/cellulose acetate sensor. Comparison between a standard colorimetric method and the flow injection analysis by the Pt/P18DAN sensor for nitrate determinations in tap water and mineral water suggests a difference of less than  $\pm 4\%$ . Contrary to the standard colorimetric method based on carcinogenic reagents, the amperometric detection of nitrites and nitrates in water is very simple and rapid and does not require any reagent. Also, this method could be extended easily to the analysis of nitrites and nitrates in various types of samples such as food, soils, vegetables, and fertilizers.

These performances are slightly better than those of nitrate biosensor based on ultrathin poly(1-methyl-3-(pyrrol-1-ylmethyl)pyridinium tetrafluoroborate) film.<sup>418</sup> The biosensor exhibits a detection limit 5.4 mM, a linear range up to 100 mM, a response time of 10 s, an operational lifetime of >3 weeks, a high sensitivity to nitrate of 5.5 nA/ $\mu\text{M}$ , and no interference from nitrite (2 times the nitrate concentration).

**i. Detection of Immune Antigens.** Aromatic diamine polymer film-based immunoelectrodes for the detection of hepatitis B surface antigen (HBsAg) and mouse immunoglobulin G (MIgG) are prepared through the following three steps.<sup>419,420</sup> (1) A dense PmPD film is formed by an electropolymerization of mPD at 2.5 V onto graphite electrode. (2) The PmPD on the electrode is activated by 3% glutaraldehyde at 15 °C, and hepatitis B surface antibody (HBsAb) or MIgG antibody is immobilized to the free amino groups on the activated PmPD at 4 °C. (3) The

electrode is blocked out with a 10 g/L bovine serum albumin solution in pH 7.2 phosphate buffer at 4 °C.

The immunoelectrodes exhibit good selectivity and repetition (relatively standard deviation 5.6%) with linear ranges of 0.1–3.2  $\mu\text{g/mL}$  HBsAg and 0.1–20  $\mu\text{g/mL}$  MIgG at the optimal pH 8.0, the sensitivity and specificity to HBsAg of 86.1% and 100%, respectively. The immunosensor can be satisfactorily used for over 15 times and stored stably for over one-half a year at 4 °C. Notably, however, the response times to HBsAg and MIgG are longer (8 and 6 min, respectively) than those of other biosensors.

### 3. Factors Affecting the Characteristics of the Biosensors

**a. Electropolymerization Conditions.** The electropolymerization conditions including monomer concentration, solution pH, electropolymerization method, polymerization temperature, and time for the fabrication of the biosensors exhibit a significant effect on the characteristics of the sensors. The effect of monomer concentration on the selectivity coefficient of Pt/GlOx/PoPD biosensors has been investigated by Ryan et al.<sup>348</sup> At oPD concentrations from 20, 100, 200, 300, to 400 mM, a concentration close to saturation, the selectivity coefficient for glutamic acid over AA rose steadily from  $-360 \pm 250\%$ ,  $-50 \pm 50\%$ ,  $15 \pm 30\%$ , to a peak value of  $83 \pm 9\%$  and declined again to  $66 \pm 27\%$ , respectively. It appears that an oPD concentration of 300 mM is best to maximize the selectivity. Ryan et al. also found that the selectivity varies with polymerization time in a fixed oPD monomer concentration of 300 mM mainly due to a decrease in AA response for a certain period of time. The selectivity coefficient for glutamic acid over AA is  $12 \pm 16\%$  at a polymerization time of 1 min,  $-10 \pm 100\%$  at 5 min,  $86 \pm 9\%$  at 15 min, and  $83 \pm 9\%$  at 30 min. Therefore, a polymerization time of 15 min is necessary in order to minimize any small pores in the PoPD film.

The effect of pH value on the enzyme-catalyzed reaction rate and enzyme activity of the biosensors is very strong. The pH value at which the biosensors exhibit the best performance depends on the sensor composition. The effect of the solution pH on the sensitivity of the Pt/PmPD electrode to L-glutamate was studied by varying the pH of the phosphate buffer (0.1 M) between 5.5 and 7.5.<sup>369</sup> It is found that the response of the electrode is the highest and most stable at pH between 6.0 and 6.5 and does not interfere with electroactive species and oxygen. The Pt/L-GlOx-PmPD sensor has been used to determine the L-glutamate concentration in broth samples<sup>369</sup> and exhibits a good accuracy as compared with the results obtained by using glutamate dehydrogenase. Pt/PoPD/silicate-GOx and Au/PoPD-GOx sensors show the greatest electrochemical response at pH 6.0–7.0<sup>356</sup> and 7.0–7.5,<sup>421</sup> respectively. A bienzyme-PoPD-carbon electrode exhibited a maximum response of 10  $\mu\text{M}$  lactate in a range of pH 9–10 at the optimum detection potential of 150 mV.<sup>401</sup> It is seen that every biosensor exhibits the optimal performance in its own suitable pH value range.

A pH-sensing biosensor for amperometric detection of oxalacetate has been prepared from graphite

composite electrode modified with *PoPD* based on the use of pH-sensitive redox probe molecules, where  $H^+$  ions are liberated from the oxalacetate decarboxylation catalyzed by the enzyme



The *PoPD* is used as a redox mediator in the biosensors, and its electrochemical properties are pH-dependent in the buffer pH from 3.9 to 9.8. This biosensor exhibits a series of advantages including low detection limit, insensitivity to a small variation in the ion concentrations, and good accuracy and storage stability together with the ease of preparation and application,<sup>361</sup> which extend the range of analytes detectable using the amperometric transduction technology, such as substrates of decarboxylases, amidohydrolases, esterases, and other hydrolases. It is suggested that the oxalacetate-*PoPD* biosensor is comparable to the classical amperometric one utilizing co-immobilized oxalacetate decarboxylase and pyruvate oxidase with a relatively narrow linear range and lower stability that was caused by the fragility of pyruvate oxidase.<sup>361</sup>

The performance of *Au/PoPD-GOx* sensor has been investigated by changing the enzyme immobilizing method from potentiostatic to cyclic voltammetric electropolymerizations.<sup>421</sup> It is revealed that the potentiostatic technique may provide better repetition.

Ekinici et al. studied the optimum conditions of *Pt/PmPD-GOx* and *Pt/PpPD-GOx* electrodes fabricated by one-step anodic electropolymerization of *mPD*, *pPD* and concomitant incorporation of *GOx* with *KCl* aqueous electrolyte at 0.8 and 0.7 V vs *Ag/AgCl*, respectively.<sup>167,170</sup> It is found that the optimal temperature and buffer concentration corresponding to the maximum steady-state amperometric response of *Pt/PmPD-GOx* electrode are 323 K and 5 mM, respectively.<sup>167</sup> The optimal temperature and pH corresponding to the maximum response of *Pt/PpPD-GOx* electrode are 308 K and 6.2, respectively.<sup>170</sup> The response of both electrode-based sensors was unaffected by the interfering substances, such as lactose, sucrose, urea, uric acid, paracetamol, and *AA*, showing that the sensors would be used in biomedical analysis for diabetic patients.

**b. Mediator.** Geise et al. reported a 1,1'-dimethylferrocene-mediated biosensor which was easily and quickly constructed by cross-linking *GOx* with glutaraldehyde on nonconducting electropolymerized *PmPD* film-modified graphite electrode<sup>368</sup> or *Pt* disk electrode.<sup>422</sup> The electron mediator could be in contact with the active site of the enzyme and the electrode surface through a network of ferrocene as well as the electron mediation occurs by charge transfer from one ferrocene to another ferrocene. *PmPD* film can prevent fouling and signals from interfering species. Therefore, the graphite/*PmPD-GOx* biosensor exhibits little or no interference from ambient oxygen together with a long lifetime of up to 72–129 days. Note that the *PmPD* film is a very important protecting layer to performance stability because mediator/

*GOx* biosensor with *PmPD* film loses 25–50% of their absolute current response and 30–55% of their sensitivity within 3 days of construction due to leaching of the mediator from the electrode.<sup>368</sup> *Pt/PmPD-GOx* biosensor has small background currents and a short response time of 15–30 s (100% response). 1,1'-Dimethylferrocene electron-mediated *Pt/PmPD-GOx* biosensor has a linear response up to 76 mM glucose and little interference from oxygen together with a lifetime of 3 months.<sup>422</sup> Curulli et al. investigated enzyme electrode probes obtained by electropolymerization of *oPD*, *mPD*, and *pPD* with  $NAD^+$  (phosphate) and a mediator 5-methylphenazonium methylsulfate using cyclic voltammetry.<sup>423</sup> Dong described a *GC/Nafion/PoPD* biosensor and found that cobalt porphyrins modifying *GC* and carbon fiber electrodes can greatly decrease the overpotential and increase the sensitivity of detection.<sup>424</sup> *PoPD* and *Nafion* layers can avoid the interference from *AA* and uric acid. He fabricated an amino acid enzyme electrode with double enzymes by using ferrocene derivatives as the mediator. He also prepared dehydrogenase (lactic acid, alcohol, and malic acid dehydrogenases) enzyme electrodes with double mediators. It is found that this kind of biosensor can overcome the disadvantage of poor selectivity and reproducibility by using the mediators for direct determination of  $\beta-NAD^+$ , reduced form.

Nakaminami et al. found that *PMoPD* possesses the electron mediation ability for *UOx* and fabricated an *Au/PMoPD-UOx* electrode-based sensor, which does not require the use of special reagents in test solutions.<sup>265</sup> In particular, the sensor exhibited fast amperometric responses ( $\sim 30$  s) to uric acid and can be applied as a reagentless amperometric determination in a uric acid concentration range covering that in the blood of a healthy human being of 150–400  $\mu M$ .

Nakabayashi et al. fabricated amperometric carbon/poly(3-hydroxyaniline)-*HRP*-ferrocene (as a mediator) biosensor for sensing  $H_2O_2$ .<sup>425</sup> The  $H_2O_2$  sensor shows a linear response to  $H_2O_2$  in 0.6–20  $\mu M$  and sensitivity of 10.1 nA/mM and especially is not influenced by easily oxidizable species, *AA*, and uric acid due to the presence of mediator ferrocene. In conclusion, the mediator plays an important role in the performance enhancement of the biosensors based on the aromatic diamine polymer.

**c. Temperature.** The characteristics of the biosensors exhibit a significant dependence on testing temperature since the enzyme activity and molecular diffusion rate in the sensors vary with temperature. Wilkins et al. fabricated needle-type glucose and lactate biosensor for continuous intravascular glucose and lactate monitoring by employing *GOx* and *LAOx*-entrapping *PmPD* as the inner layer on the *Pt* and *PVC*, polyurethane, or cellulose as the external diffusion control and protective layer.<sup>370,371</sup> The effect of temperature on the sensor performance was studied, and the sensitivity of *Pt/PmPD-LAOx/PVC* to lactate is increased with increasing temperature from 25 to 37 °C, but the linear range and time of the sensor response decrease from over 15 to 10 mM and from 60 to 45 s, respectively,<sup>369</sup> because the enzyme

activity and molecular diffusion rate increase. Similar decreasing trends of the sensitivity of Pt/*Pm*PD-GOx/(PVC or polyurethane, or cellulose acetate) sensors to glucose with increasing temperature were observed.<sup>371</sup>

It is found that Pt/GOx/*Po*PD sensor, where the GOx was immobilized by using covalent attachment (carbodiimide), exhibits a complex relationship between the peak current and temperature.<sup>371</sup> With increasing temperature from 25 to 50 °C, the current minimum and maximum occur at approximately 29 and 43 °C, respectively. If the GOx was immobilized by cross-linking with glutaraldehyde, the minimum seems to disappear but the maximum is observed at a higher temperature of 47 °C. Also, the Pt/GOx sensor without *Po*PD protective film exhibits a current maximum at 33 and 43 °C if the GOx was immobilized by carbodiimide and cross-linking, respectively. Apparently cross-linking, especially *Po*PD protective film, significantly increases the thermal stability of the enzyme immobilized in the sensor.

Thermodeactivation studies at 55, 60, and 65 °C have shown *Po*PD/GOx films to be the most resistant enzymatic films and offered the best protection against GOx deactivation in hexane, chloroform, ether, THF, and acetonitrile when compared with the other electropolymerized films such as PAN, PPY, polyindole, and *p*PD-cross-linking PAN films.<sup>365</sup> However, enzymatic activity decreased rapidly when pH was raised above 7.5.

**d. Protective Layer.** As discussed above, the biosensors based on aromatic diamine polymers exhibit good performance. Moreover, the biosensors will show better performance if they are covered by a thin protective layer made of traditional polymers. Among the three biosensors with different protective layers, it is found that the Pt/*Pm*PD-LAOx/PVC sensor exhibits excellent reproducibility of response within an acceptable 2% error limit, continuously operational lifetime of 9 days, and very long inactive storage lifetime of 280 days. A slightly lower reproducibility of 5%, shorter operational lifetime of 7 days, and much shorter storage lifetime of 14 days are observed for the Pt/*Pm*PD-GOx/PVC, Pt/*Pm*PD-GOx/polyurethane, or Pt/*Pm*PD-GOx/cellulose acetate sensors.<sup>371</sup> The interference caused by urea, glycine, and AA is very minimal. However, the response of all of these needle sensors to acetaminophen and uric acid cannot be neglected.<sup>370,371</sup> Nevertheless, a satisfactory result was obtained when testing the sensor in blood and bovine plasmas. For Pt/*Pm*PD-GOx/PVC, Pt/*Pm*PD-GOx/polyurethane, or Pt/*Pm*PD-GOx/cellulose acetate sensors,<sup>371</sup> increasing the coating solution concentrations from 0.2 to 15 mg % of three protective polymers extends the linear response range from 2.2 to 37.7 mM but is accompanied by a decrease in the sensitivity from 34.7 to 1.4 nA/mM as well as an increase in the response time from 19 to 183 s, because thicker or less porous coatings were obtained at higher concentrations. At a fixed coating concentration of 10 mg %, Pt/*Pm*PD-GOx/PVC sensor shows the widest linearity of up to 37.7 mM, Pt/*Pm*PD-GOx/polyurethane sensor shows the largest sensitivity of 2.2 nA/mM and the shortest

response time of 24 s, while Pt/*Pm*PD-GOx/cellulose acetate sensor shows the smallest sensitivity of 1.6 nA/mM and the longest response time of 183 s. Therefore, PVC coating has an advantage in increasing the linear range while preserving the medium sensitivity and response time.<sup>371</sup>

**e. Enzyme.** Enzyme should be one of the most important components in the biosensor. Therefore, the enzyme feature controls the major behavior of the biosensor to some extent. The biosensors consisting of the same aromatic diamine polymer and electrode but different enzymes exhibit different characteristics for different detection substances. Yao constructed Pt/*Po*PD-GOx, Pt/*Po*PD-COx, Pt/*Po*PD-uricase, and Pt/*Po*PD-lactate dehydrogenase-GAOx electrodes for the amperometric flow injection determination of glucose, urate, cholesterol, and lactate-pyruvate, respectively, in blood serum by detecting selectively H<sub>2</sub>O<sub>2</sub> generated enzymatically into the enzyme reactors, without any interference from oxidizable species and protein such as L-AA and uric acid present in serum.<sup>426–428</sup> The first three electrodes exhibit a linear range of 5–500 mg/dL for glucose, 5–200 mg/dL for cholesterol, and 1–50 mg/dL for urate and detection limits of 1.7 mg/dL for glucose, 0.88 mg/dL for cholesterol, and 0.19 mg/dL for urate. The electrodes are stable enough to be used repeatedly for 3 weeks with the assay precision of better than 2% for the simultaneous assay of the three species in human control serum at an assay speed of up to 38 samples per hour.<sup>426</sup> When the lactate dehydrogenase-GAOx was used in the flow injection analysis system for highly sensitive detection of lactate and pyruvate, both lactate and pyruvate can be determined with a 400-fold increase in sensitivity compared with the unamplified responses with an extremely low detection limit of 2 nM for a 10 mL sample injection.<sup>427</sup>

Yao et al. compared the performance of Pt/*Po*PD/silicate-GOx and Pt/*Po*PD/silicate-galactose oxidase with Pt/*Po*PD/silicate-COx biosensors containing different enzymes.<sup>356</sup> It is found that these three sensors responded to glucose, galactose, and cholesterol, respectively, with a response time of 15, 27, and 51 s, respectively, without any interference from electroactive species such as L-ascorbate and urate below 0.2 mM,<sup>356</sup> because *Po*PD film had a size-exclusion function and blocked the access of the electroactive interferents to the electrode surface. In particular, the three sensors in turn exhibit a different linear range from 2 μM to 2 mM for glucose detection, 20 μM to 4 mM for galactose detection, and 60 μM to 3 mM for cholesterol detection, different sensitivities of 825, 71, and 41 nA/mM, as well as different storage stabilities of 15, 6, and 32 days, respectively. It can be concluded that a series of detection parameters of the biosensors are strongly relative to the enzymes immobilized.

**f. Lipid and Protein.** Ryan et al. investigated the effect of addition of lipid and protein on the performance of the Pt/GIOx/*Po*PD sensors operating at 0.7 V vs SCE.<sup>348</sup> It is found that precoating Pt disks with the lipid phosphatidyl ethanol amine by drop coating in chloroform before enzyme immobilization and electropolymerization exhibit enhanced interference

blocking properties of biosensors because the presence of the lipid can decrease the response of AA but has no significant effect on the response of glutamic acid and on the sensitivity to the  $H_2O_2$ .

Upon incorporation of protein (enzyme and non-enzyme) into the P $\phi$ PD layer, the Pt/GlOx/P $\phi$ PD sensor obtained exhibits better selectivity because the P $\phi$ PD layer is more compact when formed by electropolymerization in  $\phi$ PD solution containing protein. Ryan et al. observed a significant enhancement in the selectivity for glutamic acid over AA when bovine serum albumin was incorporated into the sensor.<sup>348</sup> It is believed that the enhancement is due to both an increase in the response of glutamic acid and a decrease in the response of AA. Therefore, the co-deposition of protein with the P $\phi$ PD might protect some GlOx molecules from inactivation during electropolymerization, which is similar to cross-linking with glutaraldehyde. Furthermore, modification of the Pt with lipid(phosphatidylethanolamine)/GlOx/P $\phi$ PD-protein(bovine serum albumin) reduced its sensitivity to dopamine, 3,4-dihydroxyphenylacetic acid, and uric acid about 100 fold.<sup>348</sup> A more complicated modification of Nafion, ascorbate oxidase, cellulose acetate, glutaraldehyde, bovine serum albumin, and GlOx on Pt might produce a sensor with a high selectivity of glutamic acid over AA of about 99%. It is certain that the introduction of lipid and protein onto the electrode would be beneficial to improvement of the performance of final biosensors.

#### 4. Bifunctional Biosensor

The carbon/overoxidized P $\phi$ PD microelectrode without immobilization of any enzyme is typical of a bifunctional biosensor for a measurement of dopamine and ascorbate, as discussed in section IX.D.2.f.<sup>407</sup> Other biosensors discussed above are monofunctional generally, i.e., they can detect a single biosubstance at the same time. Marzouk et al. described a simple flow injection system for simultaneous amperometric determination of glucose and lactate by using two parallel Pt/P $m$ PD-GOx and Pt/P $m$ PD-LAOx electrodes.<sup>429</sup> The reliability of the system assessed by measuring glucose and lactate simultaneously in several samples of blood plasma, urine, and dairy products was in good agreement with those obtained by standard spectrophotometric methods. The flow system proved to offer advantages of (1) simplicity, (2) operational stability, up to 3 months, (3) simultaneous determination of glucose and lactate using a single 20 mL sample injection, (4) stability of the signal of a detective component by wide variations in the concentration of a nondetective component, (5) high sample throughput, more than 50 samples/h, (6) high accuracy and precision, and (7) a reasonable dynamic range of about two orders of magnitude.

Very recently, Rhemrev-Boom et al. reported an on-line continuous monitoring of glucose or lactate by ultraslow microdialysis combined with a miniaturized flow-through nanoliter biosensor based on P $m$ PD ultrathin membrane.<sup>313</sup> The effect of  $m$ PD electropolymerization time at +0.8 V on the performance of Pt/P $m$ PD-GOx biosensor was analyzed in a standard solution containing 5 mM glucose in Dulbecco's

buffer. It is found that the CV peak height was 0.23, 0.48, 1.83, 0.82, and 0.58 nA when the polymerization time was 15, 30, 60, 90, and 120 min, respectively. It is seen that a polymerization time of 60 min is suitable to obtain the biosensor with high sensitivity. The linearity and stability can be extended by increasing the electropolymerization time of  $m$ PD. It is also found that the stability toward denaturation and immobilization within the P $m$ PD film is significantly better for GOx than LAOx. Therefore, the linear range ( $\sim$ 30 mM), response time (several seconds), and operational lifetime (70 h) of Pt/P $m$ PD-GOx biosensor are much better than those ( $\sim$ 5mM, in the order of seconds, and 5 h, respectively) of Pt/P $m$ PD-LAOx biosensor. Additionally, Pt/P $m$ PD-GOx biosensor also exhibits a very low detection limit of 50 nM glucose.

#### 5. Summary

As indicated above, the enzyme-immobilized electrodes prepared by the electropolymerization of PDs can serve as high-performance amperometric biosensors due to their good sensitivity and reproducibility, excellent repeatability, high (perm)selectivity, high enzyme activity, excellent biocompatibility, wide detection range, low detection limit, short response time, high sample throughput, long lifetime, relative ease of construction, and absence of any components such as mediator leaching from the electrode. These favorable features offer great promise for in vitro and in vivo application of the aromatic diamine polymer film-modified biosensors in detecting a number of biological substances directly and diagnosing disease clinically. All of these characteristics should mainly result from the ultrathin, dense, and semiconducting film of three PPDs. Note that there are also many other aromatic diamine polymers such as PDAAQ and polydiaminopyridine which have not yet been studied as a key component for the fabrication of biosensors. A simple overview of the important factors evidently influencing the performance of the biosensors, including electropolymerization condition, mediator, detecting temperature, protective layer, enzyme, and protein, has been found. However, none of the factors are fully investigated, but they do establish the basis for further disquisition. Perhaps a closer investigation on the relationship between the macromolecular/supramolecular/morphological structures of aromatic diamine polymers and the comprehensive performance of the biosensors obtained may inspire development of more powerful and more efficient biosensors.

#### E. Miscellaneous Sensors and Detectors

In addition to amperometric biosensors, there are several important applications of aromatic diamine polymers in other sensors and detectors, although the fabricated approaches appear similar.

##### 1. Acoustic Wave Sensor

Very exciting applications of aromatic diamine polymers are continually emerging for the detection of atropine sulfate. A bulk acoustic wave sensor based

on P $\phi$ PD and copoly( $\phi$ PD-AN) was fabricated as the first case of imprinting atropine sulfate by using electrochemical methods.<sup>148,278</sup> A compact and rigid P $\phi$ PD film was believed to be a molecular imprinting material based on an in-situ quartz crystal impedance study. The thickness shear mode acoustic sensor modified with the P $\phi$ PD film exhibits molecular recognition ability to the template molecule of D,L-phenylalanine with a linear concentration range of 2–20 mM.<sup>148</sup> The effect of  $\phi$ PD/AN ratio on the sensor response to atropine sulfate was studied. The copoly-( $\phi$ PD-AN) film-modified sensor exhibited (1) high sensitivity to atropine mainly due to weak nonspecific adsorption of imprinting copolymer coating, (2) good selectivity of atropine against inorganic compounds and some common organic compounds, (3) wide linear range from 8  $\mu$ M to 4 mM, (4) a detection limit of lower than 2  $\mu$ M, (5) a recovery of higher than 98%; (6) higher stability and a longer shelf life than biosensor due to no biological components in the sensor, and (7) very simple and reproducible preparation of the sensor as well as the possibility for sensor miniaturization. The sensor was successfully applied for the determination of atropine sulfate in media of serum and urine.

## 2. Capacitive Sensor

A novel glucose biosensor has been developed using molecularly imprinted polymers containing a non-conducting P $\phi$ PD-sensitive layer for the capacitive detection of glucose.<sup>147</sup> The whole procedure for sensor preparation includes three steps: (1) the preparation of P $\phi$ PD layer by electropolymerization of  $\phi$ PD on a gold electrode in the presence of the template (glucose), (2) surface plugging of uncovered areas with 1-dodecanethiol to make the layer dense and insulating, and (3) removal of template molecules and nonbound thiol from the modified electrode surface by washing with distilled water. The sites of the removed template molecule, 'imprint sites', can recognize the template molecule or close structural molecules because its size, shape, and chemical functions have been recorded in the polymer. The capacitance decreased as the P $\phi$ PD layer became thicker, and the P $\phi$ PD film thickness of ca. 95 nm is suitable for capacitive detection. The binding between glucose and imprint sites can be detected directly because an additional layer decreasing the capacitance will form further when glucose binds to the imprint sites. The capacitive sensor fabricated thus exhibits a linear detection range of the glucose concentration from 0.1 to 20 mM, a detection limit of 50  $\mu$ M, and a relative standard deviation less than 14%. It is found that AA did not cause any observable interference and fructose, similar to glucose structure, caused a very small capacitance change (less than 7%) under the same conditions. However, the stability of the sensor is not good enough because the capacitance response to 20 mM glucose is constant at room temperature only during the initial 10 h. Apparently this capacitive sensor is not as powerful as an amperometric sensor but it does not need expensive and instable enzyme. In conclusion, the bioassay ability for the acoustic wave and capacitive sensors fabricated by molecularly imprinting, without

immobilization of bienzyme, along with the good anti-interference suggests that these sensors will continue to gain popularity as important detection tools in the biosciences.

## 3. Piezoelectric Immunosensor

A piezoelectric immunosensor for the detection of salmonella paratyphi A was prepared by immobilization of an antibody (anti-salmonella paratyphi A) on electropolymerized P $\phi$ PD, P $m$ PD, or PHAN films onto a gold-plated crystal.<sup>430</sup> The amino groups containing P $m$ PD film gave the best results for immobilizing the antibody because the amino groups are vital for chemical immobilization of active protein with glutaraldehyde. The PHAN and P $\phi$ PD films gave relatively inferior results for immobilizing antibody due to the absence of amino groups in the ladder structures of the HAN and  $\phi$ PD polymers. With antibody cross-linked on the P $m$ PD film, a piezoelectric immunoassay was proposed for the detection of salmonella paratyphi A and a shorter assay time was achieved. The salmonella paratyphi A concentration in the range of  $10^5$ – $10^9$  cells/mL can be measured by this method. A loss of 8% of the original activity occurred after the modified crystals were stored in a brown desiccator over silica gel blue for 4 weeks. The response of the sensor is greater at higher incubation temperatures, but its reusability decreased quickly at temperatures higher than 35 °C, which is one major obstacle to widespread application of the piezoelectric immunosensor. In any case, this sensor could be applied to clinical diagnosis and the determination of food contamination.

## 4. Amperometric Ion Detector

Another important application of aromatic diamine polymers that has only begun to emerge since 2000 is the amperometric detection of electroinactive anions in the solution. As discussed above, amperometric detection is a useful and important testing method with advantages of rapid response, low detection limit, low cost, and ease of fabrication and miniaturization. Conducting polymer-modified electrodes have been applied in the amperometric detection of many electroinactive ions, based on the fact that oxidation of the polymer involves the incorporation of an anionic species to counterbalance the positive sites generated in the oxidation process. Although Martinusz et al. stated that the protonation of P $\phi$ PD film is not an indispensable step during the redox processes,<sup>431</sup> the redox transformation of Au/P $\phi$ PD films is indeed accompanied by the sorption–desorption of anions by the protonation and deprotonation of the  $-\text{NH}-$ ,  $-\text{NH}_2$ , and  $=\text{N}-$  groups in the phenazine rings and free amine groups in the P $\phi$ PD chains.<sup>432</sup> Therefore, a complicated equilibrium between protons and anions should be established in order to compensate for the charge on the protonated groups by the charge of coadsorbed anions. P $\phi$ PD film, especially reduced film, exhibits more pronounced selectivity of sulfate ions over perchlorate, phosphate, and chloride ions owing to a strong interaction between  $\text{SO}_4^{2-}/\text{HSO}_4^-$  ions and the protonated sites of the P $\phi$ PD.<sup>431</sup> Xu et al. prepared an amperometric



Au/PoPD detector and found that the detector can be successfully, conveniently, and reproducibly used for the determination of electroinactive anions such as  $\text{SO}_4^{2-}$ ,  $\text{Cl}^-$ ,  $\text{NO}_3^-$ ,  $\text{F}^-$ ,  $\text{CH}_3\text{COO}^-$ , and  $\text{PO}_4^{3-}$  by single-column ion-exclusion chromatography at the optimum concentration of D,L-malic acid in the mobile phase of 5 mM and the optimum flow rate of 1.0 mL/min.<sup>157</sup> The main advantages of the detector are lower redox potential, better stability, lower detection limit, and higher precision. It is reported that the detector exhibits (1) a linear concentration range of 0.01–5 mM for all of the anions, (2) detection limits of 2.1  $\mu\text{M}$  for  $\text{SO}_4^{2-}$ , 2.47  $\mu\text{M}$  for  $\text{Cl}^-$ , 3.53  $\mu\text{M}$  for  $\text{NO}_3^-$ , 3.41  $\mu\text{M}$  for  $\text{F}^-$ , 5.82  $\mu\text{M}$  for  $\text{CH}_3\text{COO}^-$ , and 3.86  $\mu\text{M}$  for  $\text{PO}_4^{3-}$  at a signal-to-noise ratio of 3, (3) big electrochemical responses to all the anions in the order of  $\text{SO}_4^{2-} > \text{F}^- > \text{Cl}^- > \text{NO}_3^- > \text{PO}_4^{3-} > \text{CH}_3\text{COO}^-$ , (4) excellent reproducibility of 3.6%, and (5) operational stability of 14 days. The detector has been applied to the detection of common anions in real water samples with high precision.

### 5. pH Sensor

The first report on PoPD-filmed electrode as sensor is a potentiometric pH sensor in 1980.<sup>152</sup> A PoPD-filmed electrode was fabricated by galvanostatically electrochemical polymerization of oPD on wire electrode with perchlorate or bovine serum albumin dopants in a propylene carbonate or universal buffer electrolytes including phosphate buffer pH 7.0, respectively.<sup>152,433</sup> The potentiometric characteristics of the resulting films show sub-Nernstian to nearly Nernstian responses possibly due to the protonation of amine linkages in the PoPD. The electrode sensitivity at 25 °C is from -50.7 to 53.0 mV/pH. The electrode has a linear working range of pH 3–10 and an average response time of 3–5 min together with response reproducibility of 5%. An ITO/PoPD electrode prepared by cyclic voltammetry of 100 min from -0.2 to 1.2 V vs SCE at 50 mV/s in 1 M HCl exhibits good pH-sensitive function including good repetition, high stability, large electrode sensitivity of -55.3 mV/pH, and short response time in a pH range of 4–10.<sup>344</sup> The response time decreases from 4 to 2 min with increasing pH value from 4 to 10. In particular, the electrode stability was maintained without the need of pretreatment prior to use or immersion in solution when not in use.<sup>152,433</sup> One problem is that the PoPD film is unstable at pH 1 and 13. Therefore, the PoPD can offer potential for a pH sensor device in a range of pH values from 3 to 10 and could find wide applications.

### 6. Humidity Sensor

An important aspect of the aromatic diamine polymers taking into account their possible applications is the development of a humidity sensor composited with hydrophilic polymers. Ogura et al. first used electropolymerization to prepare PoPD/PVA composite film for application as a humidity sensor as follows.<sup>222,275</sup> Two solutions saturated with PoPD and PVA in DMSO are first made, respectively, and the PoPD solution was then added to the PVA solution. After this was stirred thoroughly, the mixed

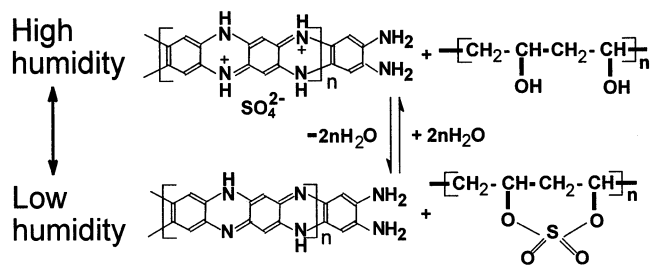


**Figure 19.** Equilibrium involved in the moistening and desiccating processes of the humidity sensor fabricated with poly(*o*-phenylenediamine) (PoPD) and poly(vinyl alcohol).<sup>222</sup>

solution was cast on a microelectrode and the solution evaporated to form the composite film of PoPD/PVA. Shim and Park reported the fabrication of a humidity sensor using chemically synthesized P15DAN.<sup>225</sup> The sensor is a solid-state microelectrochemical device consisting of two split Au electrodes and a sensing compartment. A 50  $\mu\text{m}$  wide gap between the split Au electrodes was bridged with the composite polymer slurry by a spin-coating method at 150 rpm. The polymer slurry was prepared by mixing the P15DAN powder with acetylene carbon black with polyvinylidene fluoride in NMP. The composite film-coated split electrodes were dried under vacuum at 100 °C.

It is found that the conductivity of the PoPD/PVA composite film rose sharply at about 0.1 vol % of the PoPD and reached a value of  $\sim 10^{-2}$  S/cm, due to percolation behavior in which the percolation threshold appeared at a very low volume of conducting polymer. The conductivity of the film was linearly related to the humidity, extending from  $2.5 \times 10^{-5}$  to  $1.5 \times 10^{-1}$  S/cm between the wet and dry states with the relative humidity covering more than 5 orders of magnitude.<sup>434</sup> For example, the PoPD/PVA composite exhibits electrical resistances of  $3 \times 10^5$  and  $1.2 \times 10^{11}$   $\Omega$  at 68% and 20% RH, respectively. There was no hysteresis in the measurement of conductivity when the humidity varied. The change in conductivity was caused by a shift of the equilibrium between the conducting and insulating PoPD depending on the atmospheric humidity. For example, in the drying process reaction of the protonated and conjugated PoPD with the OH group of PVA occurred to form the insulating PoPD and a water molecule resulting in a decrease of the conductivity of the composite film. The equilibrium is considered to be involved in the moistening and desiccating processes, as shown in Figure 19.<sup>222</sup> The role of different types of water for the linear dependence of the conductivity of PmPD/PVA and PHAN/PVA composites on the atmospheric humidity was studied using thermogravimetry, mass, and FT-IR spectroscopies.<sup>435</sup> The weakly bound water molecules equilibrate with the atmospheric moisture, but the strongly bound water stays at PVA unit even in a dry state (<130 °C). With the decrease in the amount of weakly bound water, the protonic acid is dedoped from the conducting polymer and is sheltered in the strongly bound water. Thus, their conductivity decreases with decreasing the humidity. In the moistening stage, water is again bound to the whole surface of the composites and the protonic acid

diffuses toward the conducting polymers, resulting in the recovery of the conductivity. Ogura et al. studied AC impedance spectroscopy of humidity sensor using P $\phi$ PD/PVA composite film.<sup>434</sup> They proposed two different equivalent circuits for the humidity-sensing process in the humidity region lower and higher than 70% RH. The logarithmic value of the film impedance changes linearly over larger than eight orders upon variation of relative humidity from 20% to 95% RH, and the capacitive contribution (interfacial impedance) at the film/electrode interface becomes appreciable for the composite films with larger thickness (>50 nm) and/or larger weight ratio of P $\phi$ PD to PVA (>0.25). AC impedance measurements have been used to investigate the effect of the protonation level of P $\phi$ PD on the response of the P $\phi$ PD/PVA composite film to humidity.<sup>436</sup> It is found that the film resistance increased with decreasing protonation level of the P $\phi$ PD in relative humidity regions higher than 40% but hardly ever depended on the protonation level in humidity of lower than 40%. Additionally, the film possesses satisfactory mechanical strength. In contrast with the P $\phi$ PD/PVA composite, there is no such linear relationship for P $m$ PD/PVA and poly(OT)/PVA composites.

All the things mentioned above show that the conductivity of the P $\phi$ PD/PVA composite film is very sensitive to atmospheric humidity and therefore the film is very suitable for humidity sensor, which can be used in air conditioning systems and automatic cooking systems.<sup>222</sup> In addition, the composite P15DAN sensor has been applied to the amperometric and the resistance-type humidity sensor employing chronoamperometry and impedance spectroscopy.<sup>225</sup> The current drift was less than  $\pm 1\%$  for lower humidity. The advantages of using the composite sensor are reversible and linear response to the changes in relative humidity and the composite film for resistive-type humidity sensors is insoluble in high humidity without chemical modification.<sup>225</sup> Recently, the effect of hygroscopicity of the insulating unit of the composite of PHAN with five normal polymers including PVP, poly(acrylic acid), poly(ethylene oxide), and polymethyl methacrylate on their response to relative humidity was investigated in detail.<sup>437</sup> The hygroscopicity of these insulating polymers decreases in the sequence

poly(acrylic acid) >  
 poly(vinylpyrrolidone) (PVP) >  
 poly(ethylene oxide) > polymethyl methacrylate

The electroconductivity of the PHAN/PVP composite was linearly proportional to the relative humidity, covering more than 4 orders of magnitude, due to acid–base transition of conducting polymer in the composite, which depends on the presence of weakly and strongly bound water. PHAN/hydrophilic poly(acrylic acid) composite has a large amount of water molecules, and consequently PHAN is completely transformed to the salt form at humidity higher than 70%, resulting in the approach to a constant conductivity independent of humidity. On the other hand,

the nonlinear dependence of the conductivity on the humidity was observed for PHAN/poly(ethylene oxide) or polymethyl methacrylate composite due to a smaller amount of strongly bound water in the composite. After all, an insulating polymer like PVP or PVA with moderate hygroscopic characteristics is most suitable for developing an aromatic diamine polymer composite sensitive to humidity.

### 7. Chemiluminescence Biodetector

Electropolymerized P $\phi$ PD has been used to construct an enzyme-modified chemiluminescence detector for H<sub>2</sub>O<sub>2</sub>, GOx, and LAOx substrates with a combination of high sensitivity with a good signal stability.<sup>438</sup> GOx and LAOx are immobilized in a poly(carbamoylsulfonate) hydrogel, which is adsorbed on the fungal peroxidase-modified graphite paste. The bienzyme optrodes obtained thus show rapid response to H<sub>2</sub>O<sub>2</sub>, glucose, and L-lactate in the linear range of 1–200, 80–8000, and 50–2000  $\mu$ M, respectively, together with respective sensitivity of 1.53, 1.23, and 1.38 mV/M. The detection limit and throughput are ca. 10  $\mu$ M and 60 injections per hour at a flow rate of 0.4 mL/min for a residence time of shorter than 0.5 s.

In addition, the  $\phi$ PD/catechol electropolymer can reduce cytochrome *c* in solution, indicating that the polymer has potential for the construction of reagent-less biosensors for the detection of cytochrome *c*.<sup>144</sup>

### 8. Summary

It is seen from only a few investigations elucidated above that aromatic diamine polymers can serve as a versatile sensor and detector for precise and inexpensive detection of the biosubstances, electroinactive anions, pH value, and humidity, as well as clinical diagnosis and determination of food contamination. However, these new applications are obviously imperfect since only a few studies have been found. Before these applications come into practical fields, the sensor and detector first require very precise control of the multifunctionalities. The fabrication technique of the polymer-containing sensor and detector with stable multifunctionalities should be optimized. A reliable relationship between the macromolecular structure/property of the polymers and sensing mechanism deserves further investigations in order to optimize the performance of the sensor and detector. Note that no investigation on the sensors and detectors fabricated by PBZ and PDAAQ is found.

### F. Electrocatalyst of Redox Reactions

The electrodes coated by aromatic diamine polymer films can potentially serve as a new type of powerful electrocatalyst for many important redox reactions on electrodes. Ohsaka et al. reported the excellent electrocatalysis of GC/P $\phi$ PD and GC/P23DAN electrodes for irreversible O<sub>2</sub> reduction to H<sub>2</sub>O<sub>2</sub> in acidic aqueous media (pH = 1), with an activation potential of ca. 300 mV lower than that of the bare electrode.<sup>188,276</sup> The electrodes were prepared in situ by electropolymerization of the corresponding monomers

in acidic aqueous solution. On the basis of the results of CVs, it is found that the P $\phi$ PD and P23DAN films catalyze considerably the reduction of oxygen via the mediating phenazine redox couple in 1,4-diazine ring-containing polymer films, during which mainly H<sub>2</sub>O<sub>2</sub> is formed, but four-electron reduction of O<sub>2</sub> and/or decomposition of the H<sub>2</sub>O<sub>2</sub> formed may occur.<sup>439</sup> It is found that Ni-doping P $\phi$ PD-filmed electrode has good electrocatalytic activity for the electroreduction of oxygen by reducing the overpotential and enhancing peak current of the oxygen reduction.<sup>440</sup> However, the situation is slightly different for P23DAN-filmed Pt electrode.<sup>188</sup> A direct two-electron reduction of O<sub>2</sub> to H<sub>2</sub>O<sub>2</sub> at the Pt-film interface and the two-electron reduction mediated by the film occur concurrently.

Note that the PHAN film exhibits very little catalyzing activity, although PHAN has a structure similar to that of P $\phi$ PD. A different reactivity of the 1,4-diazine ring in P $\phi$ PD and 1,4-oxazine ring in PHAN with O<sub>2</sub> may result from the different electrocatalysis of P $\phi$ PD and PHAN films for O<sub>2</sub> reduction. Apparently this function is related to the molecular structure of the P $\phi$ PD film. A reaction mechanism of P $\phi$ PD (or PDAPh) with O<sub>2</sub> is proposed on a molecular basis. Thus, using some suitable methods such as copolymerizing and composing could improve the electrocatalytic function of the PHAN film.

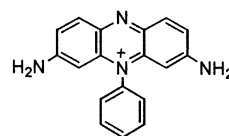
It is suggested that the composite electrodes fabricated by electrodeposited aromatic diamine polymer onto the electrodes precoated by another component such as Nafion and zeolite-L films exhibit greatly enhanced electrocatalysis. Permkumar et al. prepared 1  $\mu$ m-thick PPD thin film/Nafion composite film.<sup>153</sup> The formation of PPD within the Nafion film showed a greatly enhanced electrocatalytic reduction of oxygen coupled with the permeation of oxygen through the Nafion film. When GC/Nafion/P $\phi$ PD electrode was used, the rate of oxygen reduction was enhanced, and this clearly indicates that the protonated form of reduced P $\phi$ PD mediates catalytic reduction of O<sub>2</sub> to H<sub>2</sub>O<sub>2</sub>. The migration of proton and supporting electrolyte ion is enhanced in the Nafion/P $\phi$ PD film when compared with P $\phi$ PD film. Additionally, an irreversible reduction of O<sub>2</sub> was also observed as follows



This can be explained based on the oxygen permeation through the Nafion film. When compared to the GC electrode, a 10% increase in the yield of the reduction product, H<sub>2</sub>O<sub>2</sub>, was found at the GC/P $\phi$ PD electrode. Furthermore, the amount of H<sub>2</sub>O<sub>2</sub> observed at GC/Nafion/P $\phi$ PD is 35–40% higher than that observed at GC/P $\phi$ PD.

It is reported that the insertion of zeolite-L into the composite film can significantly increase the efficiency of catalytic reduction of O<sub>2</sub> to H<sub>2</sub>O<sub>2</sub>. A poly(phenosafranine)-modified electrode was fabricated by electropolymerization of 0.5 mM phenosafranine, a phenazine dye having the structure shown in Scheme 35 in H<sub>2</sub>SO<sub>4</sub> by cycling the potential between –0.5 and +1.3 V on respective basal plane graphite (BPG) and zeolite-L-coated BPG electrodes for the

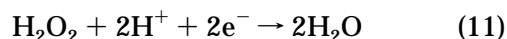
Scheme 35



## 76: Phenosafranine

mediated reduction of oxygen.<sup>332</sup> The poly(phenosafranine) is believed to be an insoluble, oligomeric, probably cross-linked film with electroactivity. It is found that the oxygen reduction potentials due to the catalytic reduction of oxygen by the reduced polymer to H<sub>2</sub>O<sub>2</sub> are –0.48 and –0.45 V at the BPG/poly(phenosafranine) and BPG/zeolite-L/poly(phenosafranine) electrodes, respectively. BPG/zeolite-L/poly(phenosafranine) electrode exhibited larger amount of H<sub>2</sub>O<sub>2</sub> and turnover numbers than the BPG/poly(phenosafranine) electrode. At an applied potential of –0.5 V vs SCE for 30 min in the presence of oxygen, BPG/zeolite-L/poly(phenosafranine) electrode produced 0.24 mmol of H<sub>2</sub>O<sub>2</sub> (turnover number 348 and percentage of formation of H<sub>2</sub>O<sub>2</sub> 71%), whereas BPG/poly(phenosafranine) electrode produced 0.19 mmol of H<sub>2</sub>O<sub>2</sub> (turnover number 189 and percentage of formation of H<sub>2</sub>O<sub>2</sub> 62%). Thus, the presence of zeolite-L increases the turnover numbers and the percentage formation of H<sub>2</sub>O<sub>2</sub> because zeolite can concentrate oxygen inside their cages and channels in the composite film. Therefore, the BPG/zeolite-L/poly(phenosafranine) electrode is more stable and efficient for the catalytic reduction of oxygen than the BPG/poly(phenosafranine) electrode.

Additionally, it is illustrated that electrosynthesized-P $\phi$ PD film (0.1 mm thickness) modified with highly dispersed Pt microparticles exhibits a great increase in the electroactivity and the electrocatalytic reduction for H<sub>2</sub>O<sub>2</sub> to H<sub>2</sub>O.<sup>325</sup> The CVs of catalytic reduction are irreversible



It is believed that the dispersed Pt particles may act as the catalytically active centers with a highly electrocatalytic activity and sensitivity of electrochemical response to H<sub>2</sub>O<sub>2</sub> and P $\phi$ PD acts as an electron-transfer matrix and a protective layer with a long time stability of the electrode. It is interesting that the inner Pt layer at the electrode can also improve the catalytic activity because small H<sub>2</sub>O<sub>2</sub> molecules can permeate through the P $\phi$ PD film and then be catalyzed by Pt microparticles. The electrocatalysis of the H<sub>2</sub>O<sub>2</sub>/H<sub>2</sub>O couple proceeds under diffusion control and depends on the potential scan rate, the pH value, and the H<sub>2</sub>O<sub>2</sub> content.

If incorporating some enzyme into the electrodes filmed by aromatic diamine polymers, the electrodes possessing bioelectrocatalysis will be constructed. Bartlett, Chen, and their coworkers studied the bioelectrocatalysis to H<sub>2</sub>O<sub>2</sub> reduction of PAN/P $\phi$ PD-HRP enzyme electrode,<sup>273,440</sup> suggesting that a direct electron transfer between the enzyme and the P $\phi$ PD takes place in the biocatalytic process. Catalysis of the reduction of H<sub>2</sub>O<sub>2</sub> by HRP adsorbed on PAN and

then immobilized with *PoPD* is very efficient. At low  $\text{H}_2\text{O}_2$  concentration, the reaction is under a large measure of measure-transport control, especially at slightly elevated temperature.<sup>440</sup> In particular, the phenazine rings in *PoPD* can increase markedly the concentration of  $\text{H}_2\text{O}_2$  that may be rapidly reduced. However, the lifetime of the *PoPD*-HRP enzyme electrode could not meet the requirements of a commercial process of at least several months. Some *oPD* oligomers incorporated in the enzyme film can play a role in electron-transfer mediators to accelerate the regeneration of the oxidized enzyme.

Wei et al. investigated the reduction of BQ at the *PoPD* electrode in the electroactive potential range of the *PoPD*,<sup>441</sup> indicating that the BQ can penetrate into the *PoPD* matrix and exchange an electron with *PoPD*. The kinetics of the bioelectrocatalytic oxidation of HQ at *PoPD*/HRP membrane electrode has been studied at different potentials. The optimum operational potential was found for the detection of HQ to be  $-0.15\text{ V}$ .<sup>442</sup>

Besides the redox reactions of  $\text{O}_2/\text{H}_2\text{O}_2$ ,  $\text{H}_2\text{O}_2/\text{H}_2\text{O}$ , and BQ/HQ, the redox reactions of KI,  $\text{K}_3\text{Fe}(\text{CN})_6$ ,  $\text{FeSO}_4$ , and AA have been studied by using electrocatalysis of *PoPD*-filmed electrode.<sup>443</sup> It is demonstrated that *PoPD*-filmed electrode can catalyze reversible redox processes of KI and AA but not  $\text{K}_3\text{-Fe}(\text{CN})_6$  and  $\text{FeSO}_4$  due to the barrier of *PoPD* film with positive charges to  $\text{Fe}^{2+}$  permeation. Ni-doping *PoPD*-filmed electrode also presents a good electrocatalytic activity for the electrooxidation of AA by reducing the overpotential and enhancing peak current of the AA oxidation, followed by a parallel catalysis mechanism.<sup>444</sup> It is revealed that the peak current of the AA oxidation is linearly proportional to AA concentration in a certain range.

In addition to single-polymer-modified electrodes, copolymer- and bilayer-filmed electrodes are also interesting in electrocatalytic processes. Mazeikiene and Malinauskas observed an electrocatalytic effect for the HQ/BQ redox couple on a *pPD*/AN copolymer-filmed electrode.<sup>286</sup> They showed that electrocatalysis of the HQ/BQ couple depends on the film thickness and *pPD*/AN molar ratio. With increasing the thickness, the electrocatalytic effect becomes more evident. There is a definite optimum molar ratio of both monomers. The electrode modified by the *pPD*/AN copolymer with the optimum molar ratio exhibits the greatest electrocatalytic efficiency, but the *pPD*/AN copolymer film cannot catalyze the electrode reduction of  $\text{Fe}(\text{CN})_6^{-4}/\text{Fe}(\text{CN})_6^{-3}$ .<sup>271</sup> Note that all compositions of sulfonic *pPD*/AN copolymer film will retard the electrode reductions of both  $\text{Fe}(\text{CN})_6^{-4}$  and HQ. The electrode covered by a film of *pPD*/*N*-(3-sulfo-propyl)AN copolymer exhibits a weak electrocatalytic efficiency for the HQ/BQ redox couple. The big difference between these two copolymer-filmed electrodes has been explained by the different potential regions for their redox transformations. On the other hand, electropolymerized Pt/PAN/*PpPD* bilayer-filmed electrode leads to suppression of the electrocatalytic properties compared to a PAN monolayer-filmed electrode. Conversely, electropolymerized Pt/*PpPD*/PAN bilayer-filmed electrode exhibits almost

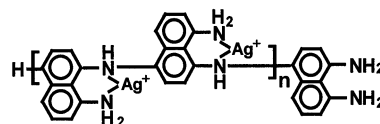
the same electrocatalytic efficiency as a PAN monolayer-filmed electrode.

This shows that the electrodes coated by the polymer films from several aromatic diamines are really good electrocatalysts for several important redox reactions. However, there are only a few correlative studies to our knowledge. None of the film-coated electrodes are ideally designed, but existing reports discussed above do offer foundations for further investigation including obtainment of the aromatic diamine polymers exhibiting optimal electrocatalysis and the establishment of their electrocatalytic theory.

## G. Heavy Metal Ion Complex and Detection

Purification treatment of heavy metal polluting water is a very pressing and tough task to modern industry and has become one of the hottest research subjects in environmental chemistry. Lee et al. described a doping technique for P18DAN with free-amine groups complexing metal ions and an application of this technique to sensing heavy ions such as  $\text{Ag}^+$ ,  $\text{Hg}^{2+}$ ,  $\text{Pb}^{2+}$ ,  $\text{Tl}^{2+}$ ,  $\text{Cd}^{2+}$ , and  $\text{Cu}^{2+}$ .<sup>181</sup> The free amines in the P18DAN form stable complexes with the heavy metal ions, as shown in Scheme 36.

Scheme 36



77: A complex of poly(1,8-diaminonaphthalene) with  $\text{Ag}^+$

The film can concentrate the ions in dilute solutions. Unless amine group and imine group are located adjacent to each other in the polymer chain, an efficient formation of stable complexes is not expected because amine and imine groups are required for  $\text{Ag}(\text{NH}_2)^+$ . A formation constant of  $2.8 \times 10^6\text{ L/mol}$  is estimated for the  $\text{Ag}^+$ -amine complex. It is found from the scan-rate dependence of the CV current for the oxidative stripping of metallic Ag in the polymer film that the stripping current of the surface-bound species is directly proportional to the square root of the scan rate and also controlled by the diffusion of counterions as well as ligand (water molecules) inside the polymer matrix, where the  $\text{Ag}^+$  produced upon oxidation is held as a complex. This indicates that the major fraction of  $\text{Ag}^+$  is inside the polymer matrix rather than on the surface. The diffusion coefficient of  $\text{Ag}^+$  through P18DAN solid film is  $2.1 \times 10^{-13}\text{ cm}^2/\text{s}$ . Therefore, it is proposed that each monomeric unit of P18DAN complexes one  $\text{Ag}^+$ . The rather small diffusion coefficient suggests that the P18DAN film is very dense and the majority of complexation sites with  $\text{Ag}^+$  are inside rather than on the surface of the P18DAN. The dynamic linearity for  $\text{Ag}^+$  collection efficiency indicates that the complexation of  $\text{Ag}^+$  is saturated at high  $\text{Ag}^+$  concentration. The linear detection range and lower detection limit for  $\text{Ag}^+$  are  $0.1\text{--}1.0\text{ }\mu\text{M}$  and  $10\text{ nM}$ , respectively.

Apparently the detection limit is stupendously low and allows the determination of trace amounts of  $\text{Ag}^+$ .

Skompska and Hillman investigated the complexing properties of P18DAN film with  $\text{Hg}^{2+}$  ions in order to explore the ability of the film to extract the  $\text{Hg}^{2+}$  ions from solution.<sup>180</sup> It was found that the nonrigid P18DAN chains have been cross-linked by coordination of  $\text{Hg}^{2+}$  ions to amine groups on neighboring chains by the formation of  $-\text{NH}_2 \cdots \text{Hg}^{2+} \cdots \text{H}_2\text{N}-$  interchain linkages with a 1:1 Hg:amine complexation stoichiometry, thereby rigidifying the film. The amine groups are not in excess of one per Hg. Saturation of these amine sites occurs at Hg solution concentration of 4 mM.

Palys et al. gave direct evidence for P18DAN to bind the heavy metal ions.<sup>296</sup> They investigated the sensitivity of P18DAN to the ions by electrochemical and spectroscopic methods. It is found that  $\text{Ag}^+$  and  $\text{Hg}^{2+}$  ions from the solution are able to oxidize P18DAN in both acidic and neutral media while  $\text{Cu}^{2+}$  ions do not since the  $\text{Cu}^{2+}/\text{Cu}$  couple has a lower redox potential than that of the polymer. At the same time,  $\text{Ag}^+$  ions are reduced at the polymer surface whereas  $\text{Cu}^{2+}$  and  $\text{Hg}^{2+}$  or  $\text{Hg}_2^{2+}$  ions are complexed by the amino groups of the polymer. In summary, through free amine groups, P18DAN films are able to rapidly and efficiently extract heavy metal ions from aqueous solution without having to apply any potential.

Jackowska et al. fabricated a P18DAN-modified electrode-based sensor for heavy metal ions by the electropolymerization of 18DAN.<sup>445</sup> In-situ EPR spectra were applied to detect and follow the changes in concentration of  $\text{Cu}^{2+}$  ion in the polymer matrix.

Similarly, P15DAN film with free  $-\text{NH}_2$  groups can chelate  $\text{Cu}^{2+}$  ions and is transformed into a very stable complexed film, which was confirmed by XPS spectra.<sup>176</sup> It is found that the XPS spectrum of  $\text{Cu}_{2\text{P}}$  in the complexed film displays the  $\text{Cu}_{2\text{P}_{3/2}}$  peak centered at 934.3 eV with full width at half-maximum larger than that of the same peak in the  $\text{CuCl}_2$  spectrum. The signal intensity ratio  $S_{1/S2}$  of the satellite peak is lower for the P15DAN- $\text{Cu}^{2+}$  complex than that for  $\text{CuCl}_2$ , due to a multiplet splitting from the 2P<sub>3/2</sub> core shells in paramagnetic species. These two subtle changes in the  $\text{Cu}_{2\text{P}}$  peak indicate an effective change in the ligands of  $\text{Cu}^{2+}$  species. The electroactivity of the  $\text{Cu}^{2+}$ -complexed P15DAN film also changed. The CV redox peaks of the complex in 2 M  $\text{HClO}_4$  were observed at more negative potentials ( $E_{\text{pa}} \sim 0.2\text{V}$ ,  $E_{\text{pc}} \sim 0.04\text{V}$ ) than those of the same film before complexation with  $\text{Cu}^{2+}$  ions ( $E_{\text{pa}} \sim 0.42\text{V}$ ,  $E_{\text{pc}} \sim 0.394\text{V}$ ).

It must be stressed that not all aromatic amine polymers can complex metal ions. For example, the CV response of the PAN film treated with  $\text{CuCl}_2$  is the same as untreated PAN. No  $\text{Cu}^{2+}$  was detected in the XPS spectra of the treated film. This result clearly shows that  $\text{Cu}^{2+}$  ions cannot be complexed by the secondary amino groups in the PAN chain. However, it can be speculated that one of the two P $\phi$ PDs with different macromolecular structures, i.e., poly(aminoaniline), prepared by electropolymeriza-

tion, could complex the heavy metal ions in the solution because there is one free  $-\text{NH}_2$  group in every repeated unit.<sup>164</sup> Theoretically, the  $-\text{NH}_2$  group content in the aromatic diamine polymers can be determined by the amount of heavy metal ions complexed, but a corresponding report is not found. Fortunately, another method is proposed by which the relative content of the  $-\text{NH}_2$  group in the polymers could be estimated by the amount of immobilized protein (or the amount of cross-linked glutaraldehyde) because the  $-\text{NH}_2$  group can be quantitatively bonded with glutaraldehyde, of which the terminal aldehyde couples the protein.<sup>168</sup>

PBZ film electrode was successfully used for electrochemical detection of  $\text{Ag}^+$  ions.<sup>330</sup> The PBZ film was obtained on Pt by cyclic voltammetry between 0 and 0.8 V at 100 mV/s from 0.5 mM benzidine in  $\text{NaClO}_4 + \text{HClO}_4$  aqueous solutions at pH 2.5 at 35 °C and exhibited good adherence on Pt, mechanical stability, and very reproducible electrochemical response.  $\text{Ag}^+$  ions were preconcentrated efficiently at open circuit from aqueous silver nitrate solution into PBZ film electrodes because of a strong specific interaction between  $\text{Ag}^+$  ions and the film mainly due to differences between the chemical potentials of  $\text{Ag}^+$  ions in solution and the film. A diffusion model is triumphantly proposed as a mechanism for the incorporation of the  $\text{Ag}^+$  ion into the film. It was found that preconcentration of  $\text{Ag}^+$  ions into the film is highly dependent on the pH, being more favored at neutral pH, that is, when the nitrogen in imine-amine groups in the polymer chain is not protonated. In acidic media the  $\text{Ag}^+$  ions do not compete with the  $\text{H}^+$  ions for the same site in the film. However, the poor interaction of the nitrogen species of the PBZ film with  $\text{Ag}^+$  in acidic media provided a simple and convenient method for the removal of preconcentrated  $\text{Ag}^+$  ions from the modified electrode and then renovate the film. The ability for PBZ film to capture  $\text{Ag}^+$  in solution was analyzed based on the stripping response due to silver oxidation obtained after reduction of the preconcentrated  $\text{Ag}^+$  ions. The analytical method of detection is promising. However, at concentrations of  $\text{AgNO}_3$  lower than 1 mM,  $\text{Ag}^+$  ion concentration could not be correctly detected, which is a serious complication for electroanalytical purposes. Three parameters influence the preconcentration of  $\text{Ag}^+$  ion at pH 7 at a given temperature: (1) the thickness of polymer film, (2) the preconcentration time, and (3) the concentration of  $\text{AgNO}_3$  solution. The optimization of these variables permitted control of the incorporation of  $\text{Ag}^+$  ions in the polymer matrix. The amount of  $\text{Ag}^+$  ions incorporated into the film decreased when the thickness of the film increased. The PBZ electrodes with an anodic charge of 30–80  $\mu\text{C cm}^{-2}$  and preconcentration time of 55–80 min could be optimal. This method for the analytical determination of  $\text{Ag}^+$  shows a linear detection range between 0 and 0.15 mM  $\text{AgNO}_3$ . Theoretically, all electroactive imine ( $=\text{N}-$ ) nitrogen-containing polymers such as PAN that can be doped with silver ions in a neutral medium could be used for the electrochemical detection of silver ions.

## H. Electric and Electronic Materials

### 1. Switch

The regular change in resistance of PD polymers with temperature suggests a possibility of the polymers to be served as a thermoelectric switch. It is reported that the variation in resistance with temperature of PpPD film synthesized by the reaction catalyzed with  $\text{Co}^{2+}$  and  $\text{Cu}^{2+}$  follows a normal Gaussian shape in the region 100–200 °C.<sup>214</sup> The resistance reaches a maximum value at 150 °C for  $\text{Co}^{2+}$  and 160 °C for  $\text{Cu}^{2+}$ . This behavior may arise from the combined effect of proton conductivity (due to hydrogen bonding network) and radical conductivity present in the polymer. The resistance of the polymer will increase with the disruption of the hydrogen-bonding network due to an increase in temperature, whereas the radical conductivity in the polymer takes over above a particular temperature. There is a transformation between two thermally interconvertible states by binding a water molecule in order to obtain the thermoelectric switch property.

Popok et al. demonstrated a sandwich structure insulator/conductor/insulator combining the ion implantation with the electrochemical deposition of dielectric P $\phi$ PD in order to fabricate a transistor-like electronic switch.<sup>323</sup> The deposition of dielectric P $\phi$ PD in the pores of the implanted layer by electrochemical oxidation of  $\phi$ PD yields a more perfect sandwich structure insulator/conductor/insulator, and the transistor devices fabricated exhibit lower switching voltages and controllable conductivity of the buried layer by applying external electric field.

### 2. Electrochemical Capacitor

More recently conjugated conductive polymers including PAN and PPY and several aromatic diamine polymers have been studied for application as electrochemical capacitors. P15DAAQ could be used as a proton battery or an aqueous electrochemical supercapacitor material.<sup>227,312</sup> The electrochemical window of P15DAAQ is ca. 2.3 V, and it has a high conductivity of 0.4–2 S/cm even at a reduced states due to the presence of charge carriers in a wide potential range and to the two- or three-dimensional expansion of the  $\pi$ -conjugated system. By using the P15DAAQ film as both anode and cathode, a novel type of electrochemical capacitor device has been constructed. The P15DAAQ/P15DAAQ capacitor exhibited high specific energy and power from 25 to 46 Wh/kg and from 10.2 to 30.5 kW/kg, respectively, which are more or less than the specific energy and power from 20 to 50 Wh/kg and from 2 to 20 kW/kg, respectively, for the electrochemical capacitors based on polythiophene derivatives. The P15DAAQ film can also serve as a polymer cathode in a rechargeable polymer battery system.<sup>227</sup> The P15DAAQ has the following advantages over traditional conductive polymers: (1) high specific capacity of 238 Ah/kg (theoretical specific capacity 338 Ah/kg),<sup>312</sup> because the redox reaction of its quinone and 3-electron  $\pi$ -conjugated system occurs separately and/or cross over with exchanging three protons per monomer unit; the specific capacity of P15DAAQ is much

higher than those for PAN (25 Ah/kg) and PPY (2 Ah/kg) on the same substrate; (2) wide potential window (ca. 2.3 V); (3) fast redox reaction; (4) high electric conductivity; (5) high electrocatalytic activity; and (6) electrochemical durability.<sup>312</sup>

Conducting PDTDA film containing disulfide bonds is a proton-exchange type of high-energy storage material.<sup>270</sup> Due to an intramolecular electrocatalytic effect of aniline/anilinium and thiol/thiolate redox couples at almost the same potential, the PDTDA exhibits four advantages, such as high energy density 675 Wh/kg-cathode, high charge capacity 270 Ah/kg-cathode, good redox cyclicability ( $10^3$ – $10^4$  cycles), and faster kinetics as a cathode in secondary lithium batteries.<sup>270,446</sup> The charge capacity of the PDTDA exceeds the theoretical capacity of PAN/ $\text{ClO}_4^-$  (150 Ah/kg-cathode) and that of a composite cathode containing 2,5-dimercapto-1,3,4-thiadiazole, PAN, and gel electrolyte (303 Wh/kg)<sup>447</sup> but is much lower than that (1500–3500 Wh/kg) of polysulfide containing multiple sulfur atoms in its molecule ( $-\text{[S]}_n-$ ). Therefore, the PDTDA could be an advanced material in energy storage devices such as electrochemical ultracapacitors or proton-exchange batteries.<sup>231,446</sup>

The chronoamperometry, chronocoulometry, and chronovoltabsorptometry studies suggest reversible behavior for PPBZ film over several thousand cycles for pulses from 0.1 to 100 s but considerable degradation for PBZ.<sup>230</sup> It is found that the film thickness exhibits an important influence on the charging characteristics of PPBZ by a coulometry.<sup>230</sup> With increasing the thickness from 5 to 210 nm at a fixed film area of 4 cm<sup>2</sup>, the charging capacity increased from  $4.3 \times 10^{-4}$  C to a maximum  $13 \times 10^{-4}$  C at a thickness of 60 nm and then decreased to  $8.6 \times 10^{-4}$  C, whereas the switching time, for achievement of 90% of the total coulometric change, increased almost linearly from 1.45 to 16.2 s, which is much longer than switching time of other conducting polymers (0.08 s). These data indicate that neither PPBZ nor PBZ would be promising as a rapid optical switch by purely electrochemical means.

### 3. Modifying Film of Cell Electrodes

Electrosynthesized P $\phi$ PD film is a film of effectively improving power efficiency of photoelectrochemical and fuel cells. The dark electropolymerization of  $\phi$ PD on electrodes occurs only at surface imperfections (edges and steps).<sup>448</sup> The P $\phi$ PD film formed thus can effectively prevent electron exchange with solution species and then significantly decrease energy losses via recombination processes at electrode imperfections in the photoactive surface. Indeed, after coating P $\phi$ PD film on n-WSe<sub>2</sub> and n-MoSe<sub>2</sub> single crystal electrodes, increases in their solar-to-electrical power efficiency generally range from 30% to 100% and reach the highest value of 317% for n-WSe<sub>2</sub>/Fe(CN)<sub>6</sub><sup>4-/3-</sup> cell.

The effect of P $\phi$ PD on the performance of polymer electrolyte fuel cells based on the proton exchange Nafion membrane was described.<sup>449</sup> The ion conductivity of the Nafion membrane is strongly influenced by the water content. The effect of a P $\phi$ PD layer

electropolymerized onto the cathode electrode on the fuel cell performance measured with dry gases  $H_2/O_2$  at atmospheric pressure has been investigated. The measured voltage vs current density relationship for Nafion plus P $\phi$ PD showed a remarkable improvement over the case with Nafion only. It is seen that P $\phi$ PD film plays an important role in improving the power efficiency of photoelectrochemical and fuel cells.

The PPD films prepared from chemically oxidative PPD powders by solution casting technique also served as a high-density positive electrode for polymer film battery.<sup>450</sup> Composite cathodes for polymer film battery have been prepared from solutions of 2,5-dimercapto-1,3,4-thiadiazole and PPD. The electrochemical characteristics of the composite cathodes were investigated using cyclic voltammetry.<sup>451</sup>

It is obvious that the polymers from aromatic diamines are very promising as key electric and electronic materials. It should be noted that investigation on these electric and electronic materials is very sporadic and not thorough. Therefore, more systematic work needs to be done in order to optimize the corresponding performance and finally develop these new applications.

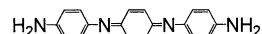
### I. Anticorrosion Coating for Metals

There is huge commercial potential for the application of conducting polymers as anticorrosion coatings for metals. It was estimated that corrosion costs U.S. industries tens of billions of dollars per year.<sup>132</sup> It is shown that the conducting polymer coatings on iron, nickel, aluminum, and steel can either act as an active electronic barrier to corrosion or as inhibitor by shifting the corrosion potential of the substrate to higher values or both and therefore enormously reduce the corrosion rate.<sup>327,452,453</sup> However, less work on corrosion protection has focused on aromatic diamine polymers until now. The anticorrosion mechanism of aromatic diamine polymers for metals has not been found yet. Recent investigations on the protection of metal surface against corrosion by aromatic diamine polymers were reported in the 1998 and 2001. The corrosion protection properties of aromatic diamine polymers have been studied on iron,<sup>327</sup> mild steel,<sup>179</sup> and stainless steel.<sup>326</sup> It is reported that P15DAN and P15DAN/AN composite films can be successfully deposited on iron and mild steel from acidic solutions by cyclic voltammetry.<sup>179,327</sup> The films have a uniform and compact structure together with controlled thickness and exhibit excellent adhesion properties on iron and mild steel and similar electroactivity to those of the corresponding films generated on Pt. The P15DAN film formed on iron after 30 min of polarization is ca. 75 nm thick and adherence is 100%. In particular, the composite film imparts a form of anodic protection for at least 9 days in pH = 4 sulfate medium and protects iron better than PAN film alone. By electropolymerization of  $\phi$ PD in  $H_3PO_4$  on 304 stainless steel under potentiostatic conditions, adherent electroactive P $\phi$ PD films have been obtained.<sup>326</sup> It is suggested that the P $\phi$ PD-coated steel electrodes in chloride aqueous solution show a positive shift of the corrosion poten-

tial. Therefore, the aromatic diamine polymer coatings can provide significant corrosion protection to iron and steel exposed to severe corrosion environments. It is reported that an adherent coating containing an air-oxidizable  $p$ PD moiety or a mixture of the  $p$ PD and its air oxidation product can protect metal articles from corrosion under prolonged exposure to normal ambient atmospheric conditions.<sup>454</sup>

In addition, electrochemical studies suggest that a  $p$ PD derivative exhibits excellent anticorrosion properties.<sup>455</sup> In particular, both an epoxy cured by  $N,N$ -bis(4'-aminophenyl)-1,4-quinonenediimine (Scheme 37) and cross-linked  $p$ PD films demonstrated better corrosion protection property at relatively low thickness without a topcoat than conventional PAN and two-pack epoxy reference systems.

#### Scheme 37



78:  $N,N'$ -Bis(4'-aminophenyl)-1,4-quinonenediimine

### J. Micropatterning Films

Another promising application of the photooxidative PAN prepared from aromatic diamine derivative in lithographic fields has emerged since 1999.<sup>87,456</sup> It is found that photoillumination through a photomask to Flemion film containing ruthenium trisbipyridyl and methyl viologen in the  $N$ -phenyl- $p$ PD polymerization solution can give a micropattern of PAN on an electrode surface, because photopolymerized PAN was only obtained on the illuminated part of the Flemion film. A clearly defined micropattern with less than 2 mm has been easily induced by visible light illumination with a xenon lamp.

Upon illumination in the visible region of 420–600 nm with a 500 W xenon lamp through UV and IR cutoff filters, a well-defined photoimage or micropattern with less than 1 mm has been successfully obtained by a solid-state photooxidative polymerization with Flemion film that was prepared by casting the Flemion solution containing ruthenium trisbipyridyl and methyl viologen ions as well as  $N$ -phenyl- $p$ PD on glass under dark.<sup>206</sup> The PAN photopolymerized thus exhibits a conducting state because the micropattern is green in color. It is believed that using a laser rather than a xenon lamp will form a much finer micropattern.

Kim et al. suggested that the photoredox reactions of PAN photopolymerized with  $N$ -phenyl- $p$ PD as monomer in 5 M HCl aqueous acetone solution have been carried out successfully by UV-vis illuminations.<sup>456</sup> In particular, the photoredox proceeds more effectively when the reaction solutions are deaerated with nitrogen. Good reversibility for the photoredox of PAN is observed. However, the PAN may hydrolyze during excessive photooxidation in the acidic aqueous solution.<sup>457</sup> The PAN hydrolysis has been prevented by using nonaqueous dichloroethane solution containing  $CF_3COOH$  and methanol. Furthermore, improvement of photoreduction efficiency of the PAN polyelectrolyte composite film was observed because the rate of photoreduction in the organic solution was very fast as compared with that in acidic

aqueous solution. Further analysis must be done to prepare a more effective photorewritable system and to realize this reversible photoelectrochromic in a dry state.

Therefore, the fact that the conducting PAN can form at any place and any geometry as well as change its state with UV–vis illumination reversibly might endow it with various potential applications as optoelectronic devices including optical rewriting system, photofunctional wire, memory device, and image formation. For example, a photorewritable conducting PAN image obtained by the polymerization of *N*-phenyl-*p*PD for Flemion composite film containing ruthenium trisbipyridyl and TiO<sub>2</sub> can be erased and regenerated by consecutive photoreduction and photooxidation via photoinduced electron transfer with ruthenium trisbipyridyl and TiO<sub>2</sub> in 1 M HCl aqueous solution containing 10 vol % methanol.<sup>456</sup> The green PAN image was obtained by the photopolymerization of *N*-phenyl-*p*PD induced by visible illumination passing through a suitable mask. Therefore, the illuminated part was colored, i.e., the photopolymerized PAN provided a negative type image. Since the PAN was formed on only photopolymerized parts, the unpolymerized parts of the film do not have the photorewritable properties. The photoreduced image is yellow, corresponding to the color of both reduced PAN and Ru(bpy)<sub>3</sub>. The repeatable process between the photoreduction and photooxidation gave a constant cycle for more than 10 times. Further, the photogenerated PAN image in ambient conditions was stable for about 0.5 years. Without doubt, this application will attract increasing attention because it inaugurates a new area of high-value applications for the aromatic diamine polymers.

### K. Additives in Lubricating Oil

The *P**o*PD fine particles could serve as additives in lubricating oil in order to decrease friction and abrasion.<sup>458</sup> The tribological properties of *P**o*PD fine particles with a diameter on the order of 1 μm prepared by emulsion oxidative polymerization were studied as lubricating additives. It was found that the fine *P**o*PD particles, formed at the optimum polymerization conditions of 0.6 M HCl and *o*PD/K<sub>2</sub>S<sub>2</sub>O<sub>8</sub> molar ratio of 2/1 in the presence of sodium dodecylbenzene sulfonate and PVA, exhibit some antiwear and antifricition performance and then improve the loading capacity of basic oil, since the particles could fill and level up the friction surface and elastically roll on the surface. Detailed research mainly concerning the relationship between the diameters/shapes and preparation conditions of the fine particles of *o*PD and other aromatic diamine polymers should be performed in the future in order to develop this new application field.

### L. Applications of the Oxidation of Aromatic Diamines

In addition to the many important applications of the aromatic diamine polymers elaborated above, there are a number of interesting applications of aromatic diamines that do not fit well into the

disciplinary categories described above. It is found that the oxidation reactions of aromatic diamines are also very valuable in several application fields including the immunosorbent assay, detection of hemoglobin and H<sub>2</sub>O<sub>2</sub>, determination of traces of metal ions, and the surface area of the particles of noble metal catalysts, despite there not being more or full correlative investigations. Therefore, this work establishes the foundation for further studies. More similar applications of the polymers and redox reactions from the aromatic diamines may be expected in coming years.

#### 1. Immunosorbent Assay

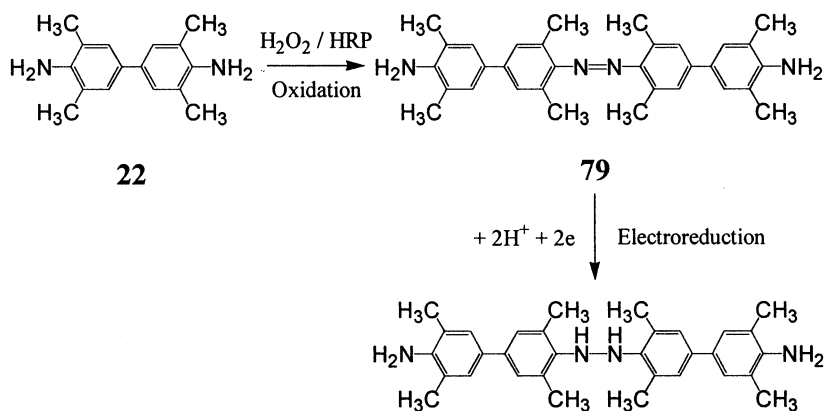
The electroactive trimer of *p*PD oxidized/catalyzed by H<sub>2</sub>O<sub>2</sub>/HRP, respectively, exhibits a sensitive voltammetric peak current at a potential of -0.97 V vs Ag/AgCl in pH 10 B–R buffer solution,<sup>251</sup> which can be used to measure HRP with a detection limit of 0.95 m units/L and a linear range of 1.75–750 m units/L. On the basis of the combination of a *p*PD–H<sub>2</sub>O<sub>2</sub>–HRP voltammetric enzyme-linked immunoassay system with direct antigen coating enzyme-linked immunosorbent assay, cucumber mosaic virus can be easily detected as low as 0.5 ng/mL even in the presence of 10–100 ng/mL tobacco mosaic virus, southern bean mosaic virus, and tobacco ringspot virus, respectively, which is 10 times lower than that of the conventional spectrophotometric *o*PD enzyme-linked immunosorbent assay method. This method can be applied for the serological detection of plant viruses.

A sensitive technique of HRP detection using high-purity *o*PD as a substrate was proposed.<sup>459</sup> A colorimetric enzyme-linked immunosorbent assay amplified photochemically consists of two successive steps. The first step is a conventional HRP-mediated enzyme-linked immunosorbent assay at which DAPh was formed in the dark. At the second step, the sample is illuminated at 400–500 nm for several minutes, which results in a large increase of DAPh concentration. The final DAPh concentration is proportional to the concentration of DAPh formed by HRP. The low limit of HRP detection by these techniques was about 0.6 units/mL. Detection of HRP was restricted by the rate of background formation of DAPh (*K*<sub>b</sub>) in the *o*PD substrate solution. An *o*PD substrate solution exhibiting a minimal ratio of *K*<sub>b</sub>/*K*<sub>HRP</sub> was composed of 2 mM *o*PD and 5mM H<sub>2</sub>O<sub>2</sub> in 0.01 M citric acid buffer at pH 5. The much lower limits of HRP and carcinoembryonic antigen detection of 0.56 m units/mL and 0.04 ng/mL, respectively, were obtained by spectrofluorimetric method if the DAPh was embedded in the micelles of a detergent in the aqueous buffer solution.<sup>460</sup> The detection of carcinoembryonic antigen also exhibits a wide linear range of 0.04–5 ng/mL and a relatively standard derivative of 7% at a carcinoembryonic antigen concentration of 0.5 ng/mL. The spectrofluorimetric method can be conveniently combined with standard chromogenic enzyme-linked immunosorbent assay.

The coupling reaction of 3,3',5,5'-tetramethylbenzidine oxidized and catalyzed by H<sub>2</sub>O<sub>2</sub> and HRP, respectively, has been used to determine the helicobacter pylori specific IgG antibody in human serum



## Scheme 38



80: 4,4'-Di(3,5-dimethyl-4-amino)-2,2',6,6'-tetramethylazobenzene

by differential pulse voltammetric enzyme-linked immunoassay, because the electroreduction of the enzyme product 4,4'-di(3,5-dimethyl-4-amino)-2,2',6,6'-tetramethylazobenzene (Scheme 38) exhibits a sensitive differential pulse voltammetric response at 0.1 V vs Ag/AgCl in pH 4.0 acetate buffer solution.<sup>461</sup> The helicobacter pylori specific IgG antibody could be detected with a detection limit of 1 unit/mL in a linear range of 0–100 units/mL and relatively standard derivative of 7.6%. The immunoassay with electrochemical detection shows high sensitivity, high accuracy, and short detecting time of 0.5 min, as well as two inherent advantages including a much lower detection limit and wider detection range than the more widely used spectrophotometric techniques.

### 2. Detection of Hemoglobin, H<sub>2</sub>O<sub>2</sub>, and Laccase

The enzymatic activity for the oxidation of *o*PD with H<sub>2</sub>O<sub>2</sub> to form DAPH that is determined spectrophotometrically has been used for the detection of hemoglobin, HRP, carcinoembryonic antigen, and laccase, where hemoglobin, HRP, and laccase, could be excellent enzymes for catalyzing the oxidation reaction.<sup>459,460,462,463</sup> This detection method exhibits a wide linear range of hemoglobin concentration from 0.065 nM to 85 μM, a highly low detection limit of 3.2 × 10<sup>-3</sup> nM, a small relative standard deviation of within 5% for the determination of different concentrations of hemoglobin, and recovery of 105% for the detection of hemoglobin in urine sample.<sup>462</sup> Excess of bovine serum albumin, Ca<sup>2+</sup>, Mg<sup>2+</sup>, Cu<sup>2+</sup>, and glucose did not interfere. Caffeine and theophylline interfere slightly. Fe<sup>2+</sup> is the active metal ion of the heme and hence interferes with the determination.

An automatic flow-injection stopped-flow kinetic spectrophotometric method for laccase activity by measuring variation of absorbance at 420 nm with time at 55 °C can give a linear range over 0–2 U and a detection limitation of 0.012 U.<sup>463</sup> The proposed method has been applied to the analysis of laccase activity of real samples at 30 samples per hour. Note that a spectrofluorometric method in organic solvents will provide a wider linear range for determination of laccase activity.<sup>464</sup> The optimal conditions for laccase in organic media are 55 °C, pH = 6.5, and 10

mM *o*PD in 1.25 mL of ethanol, 4-dioxane, or acetone. The linear range of the method proposed in ethanol, 1,4-dioxane, and acetone media was 0.44–19.33, 0.11–20.85, and 0.38–21.05 U with the relatively high detection limit of 0.088, 0.022, and 0.076 U, respectively. It is believed that the method is simple, sensitive, and reliable for the determination of hemoglobin and laccase in real samples.

Also, Ju et al. constructed an amperometric hemoglobin biosensor using a poly(2-aminoanthraquinone)-modified carbon fiber electrode.<sup>333</sup> It is found that the electrode showed excellent electrocatalytic activity for the reduction of hemoglobin in a weakly acidic solution with a linear increase in the catalytic current in cyclic voltammetry with a wide hemoglobin linear concentration range of 0.5–340 μM, high sensitivity of 5 μA/mM, response time of 20 s, and long storage lifetime of 30 days. The hemoglobin concentration in the whole blood determined by the sensor agreed well with the one obtained with the reference instrument.

The oxidation of *o*PD by H<sub>2</sub>O<sub>2</sub> catalyzed by hemoglobin has been used as a rapid and sensitive method for stopped-flow spectrophotometric determination of H<sub>2</sub>O<sub>2</sub>.<sup>465</sup> The initial rate of the formation of the oxidation product DAPH at the wavelength of 425 nm was monitored, permitting an intertemporally low detection limit of 9.2 nM H<sub>2</sub>O<sub>2</sub>, a wide linear H<sub>2</sub>O<sub>2</sub> concentration range from 50 nM to 3.5 μM, and a small relative standard deviation of 2.1%. Satisfied results with recoveries from 94% to 110% were found in the determination of H<sub>2</sub>O<sub>2</sub> in real samples (rain-water) by this method. Note that some inorganic ions (SO<sub>4</sub><sup>2-</sup>, NO<sub>3</sub><sup>-</sup>, Ca<sup>2+</sup>, Mg<sup>2+</sup>, Al<sup>3+</sup>, Cu<sup>2+</sup> except for SO<sub>3</sub><sup>2-</sup>, NO<sub>2</sub><sup>-</sup>) and several organic compounds (glucose, caffeine, theophylline, uric acid) have interference.

### 3. Detection of Traces of Metal Ions

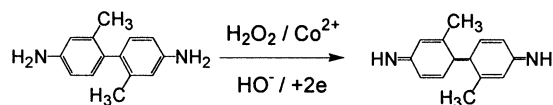
The detection of traces of metal ions is rapidly becoming more important in environmental and medicinal analyses that require high sensitivity. Some of the metal ions such as the most toxic organomercury(II) are harmful to animal and human health. On the basis of the inhibitory effect of Hg<sup>2+</sup> on the catalytic activity of HRP immobilized, several aromatic diamines including *o*-dianisidine, *o*PD, and 3,3',5,5'-tetramethylbenzidine have been used as

indicators for the determination of organomercury compounds at concentrations from 20 nM to 1 mM because the oxidation of the aromatic diamines by  $\text{H}_2\text{O}_2$  by using immobilized peroxidase as catalysts accompanies an obvious color change.<sup>466</sup> For example, during the oxidation of *o*-dianisidine catalyzed by immobilized peroxidase in the presence of phenylthiourea, the solution changes color from green to yellow to red in wells on a polystyrene plate or from green to violet to red on chromatography paper. *o*PD is oxidized by  $\text{H}_2\text{O}_2$  accompanied by a color change from pale blue to pale brown on a polystyrene plate or from pale red to pale blue on chromatography paper. A color change from pale blue to gray to colorless on a polystyrene plate and on chromatography paper follows the oxidation of 3,3',5,5'-tetramethylbenzidine by  $\text{H}_2\text{O}_2$ . The most contrasting change of colors was observed in the case of *o*-dianisidine oxidation. Better color contrast from blue to brown also occurred in 3,3',5,5'-tetramethylbenzidine oxidation only in the presence of diethyldithiocarbamate. This method has been recommended for a rapid and easy determination of organomercury compounds in natural water.

*o*-Dianisidine has been used for determination of their inorganic and organic effectors because the effectors are the inhibitors of the peroxidase activity toward *o*-dianisidine for all the enzymes.<sup>467</sup> The detection limits are 50 ng/mL for  $\text{Bi}^{3+}$  and  $\text{Cd}^{2+}$ , 0.2–50 mM for phenols and their derivatives, and 5  $\mu\text{M}$ , 0.5  $\mu\text{M}$ , 0.6 nM, 0.009 nM, 0.1  $\mu\text{M}$ , and 0.5 nM for tartaric, oxalic, salicylic, salicylic–sulfonic acids, fluoride, and cyanide, respectively. The indicator reactions of the oxidation of *o*-dianisidine, *o*PD, and 3,3',5,5'-tetramethylbenzidine have been used for determination of  $\text{Hg}^{2+}$  with extremely low detection limits of 10, 0.8, and 0.3 ng/L, respectively.

The colorizing oxidation reaction of *o*-tolidine with  $\text{H}_2\text{O}_2$  has been used to determine trace  $\text{Co}^{2+}$  based on a strong catalysis of  $\text{Co}^{2+}$  to the oxidation in basic solution (Scheme 39).<sup>468</sup> The detection limit and

Scheme 39



25: Achromatism

81: Jasmine

linear range for the determination of  $\text{Co}^{2+}$  are 1.78 and 0.8–3.6  $\mu\text{g/L}$ , respectively. Although  $\text{Ni}^{2+}$  of 2 ng interferes with the examination of  $\text{Co}^{2+}$  of 3.2  $\mu\text{g/L}$ , only  $\pm 5\%$  relative error was found in the presence of  $\text{Zn}^{2+}$  (50  $\mu\text{g}$ ),  $\text{Fe}^{3+}$  (8  $\mu\text{g}$ ),  $\text{Ca}^{2+}$  (5  $\mu\text{g}$ ),  $\text{Mg}^{2+}$  (1  $\mu\text{g}$ ),  $\text{Cu}^{2+}$  (1  $\mu\text{g}$ ),  $\text{Pb}^{2+}$  (0.5  $\mu\text{g}$ ), and  $\text{Mn}^{2+}$  (0.2  $\mu\text{g}$ ). In addition, determination of  $\text{Co}^{2+}$  does not appear to be influenced by a large amount of  $\text{SO}_4^{2-}$ ,  $\text{NO}_3^-$ ,  $\text{Cl}^-$ ,  $\text{K}^+$ , and  $\text{Na}^+$ . This method has been recommended for a satisfactory determination of trace  $\text{Co}^{2+}$  in vitamin  $\text{B}_{12}$  with a relative standard error of 1.3% and recovery of 98.7–99.1%. It can be anticipated that the oxidation reaction of *o*-tolidine with  $\text{H}_2\text{O}_2$  could be similarly used for determination of trace  $\text{Ni}^{2+}$  without interference from the other ions men-

tioned above except for  $\text{Co}^{2+}$ . The oxidation of aromatic diamines could play an important role in the inspection of  $\text{Hg}^{2+}$  and  $\text{Co}^{2+}$  in food, medicine, and wastewater.

The organomercury compounds (methyl-, ethyl-, phenylmercury) can be enzymatically determined based on their effect on the induction period caused by the introduction of sodium diethyldithiocarbamate to the oxidation of *o*-dianisidine, *o*PD, and 3,3',5,5'-tetramethylbenzidine by  $\text{H}_2\text{O}_2$  catalyzed by native HRP.<sup>469</sup> The enzymatic determination of the induction period is inversely proportional to organomercury compound concentration over a range of 0.05–10  $\mu\text{M}$  for methylmercury and 0.6–5  $\mu\text{M}$  for ethylmercury as well as phenylmercury. The lowest detection limit is 30 nM for methylmercury, 400 nM for ethylmercury, and 900 nM for phenylmercury. The standard relative deviation is lower than 3%. The interfering effect was observed for such metal ions as  $\text{Bi}^{3+}$ ,  $\text{Cu}^{2+}$ ,  $\text{Pb}^{2+}$ , and  $\text{Fe}^{3+}$ . However, the interference could be masked or even eliminated by adding potassium ethylenediaminetetraacetate. The proposed method is simple, inexpensive, and rapid and does not require the preliminary conversion of organomercury compounds to elemental or ionic mercury. The most sensitive procedure using 3,3',5,5'-tetramethylbenzidine oxidation is applied successfully to determination of the most toxic methylmercury in Kara Seawater.

#### 4. Determination of the Surface Area of Noble Metal Catalysts

The electrocatalytic oxidation of *N,N*-dimethyl-*p*PD with chloropentaamine– $\text{Co}^{3+}$  chloride has been used for determination of the blank surface area of silver and other noble metal sols acting as catalyst, where the sols can be either large (4.6 mm diameter) or small particles (22.6 nm),<sup>470</sup> because the first oxidation product of *N,N*-dimethyl-*p*PD is a stable radical cation *p*-semiquinonediimine, which absorbs strongly in the visible region of the spectrum followed photometrically. The determining principle is that the rate of the electrocatalytic reaction between *N,N*-dimethyl-*p*-phenylenediamine and the chloropentaamine– $\text{Co}^{3+}$  chloride is proportional to the surface area of noble metals.

#### 5. Determination of Phenol, Catechol, and Ascorbic Acid

The oxidation of *o*PD with dehydroascorbic acid, forming a highly fluorescent quinoxaline derivative (3-(1,2-dihydroxyethyl)furo[3,4-*b*]chinoxaline-1-one) that is excited at the 345 nm and detected at 410 nm, has been developed to determine phenol and catechol fluorimetrically by a highly sensitive, enzymatic flow injection analysis.<sup>471</sup> Upon contact with tyrosinase immobilized in a packed bed flow reactor, phenol is oxidized to *o*-benzoquinone, which oxidizes ascorbic acid to dehydroascorbic acid producing catechol, which is enzymatically reoxidized to *o*-benzoquinone. The chemoenzymatic substrate recycling enhances the sensitivity of the detection of phenol, catechol, and dehydroascorbic acid with a detection limit of 20, 20, and 100 nM, respectively. Phenol, catechol, and dehydroascorbic acid can be determined in the linear

ranges between 0.1 and 2  $\mu\text{M}$ , between 0.02 and 2  $\mu\text{M}$ , and between 0.5 and 100  $\mu\text{M}$ , respectively, with the throughput of 20 phenol detections per hour with relative standard deviations from 0.8% to 3.5% by automatic flow injection analysis with high operational stability of 96 h. Chloride,  $\text{Cd}^{2+}$ ,  $\text{Pb}^{2+}$ , and  $\text{Ni}^{2+}$  showed no significant influence.  $\text{Zn}^{2+}$  seems to slightly activate the tyrosinase.  $\text{Cu}^{2+}$ ,  $\text{Hg}^{2+}$ , and NO oxidize the AA and therefore cause a more or less positive bias. The high sensitivity and precision recommend the proposed method for the precise determination of phenol traces in water samples. In addition, a reproducible method is described for determination of AA and dehydroascorbic acid by ion-pairing reversed-phase HPLC with fluorometric detection based on the oxidation of AA, *o*PD $\cdot$ 2HCl, and 3,4-dimethyl-*o*PD $\cdot$ 2HCl by copper sulfate or acetate.<sup>472</sup> The method applied to human plasma exhibits a detection limit of 16 ng for AA and 3 ng for dehydroascorbic acid with a recovery of 98%.

### X. Conclusions and Prospects

This review has comprehensively summarized research in the rapidly developing and very active field of oxidative polymerizations and polymers from aromatic diamines since the first report in 1943 to the beginning of 2002. The number of chemists who are interested in the oxidative polymerizations and polymers is steadily increasing. Tremendous new advances in the syntheses, structures, fabrication, properties, multifunctionalities, and applications of the polymers have been achieved over the past 15 years, especially in the last 5 years. The oxidative polymerizations and polymers of aromatic diamines are growing into a mature field with widespread and fast growing potential applications. The oxidative polymerization of aromatic diamines has not only opened new and promising areas of fundamental research in the field of electroconducting polymers, but also boosted the high value applications for the polymers.

Although a complete theory of oxidative polymerizations and polymers from aromatic diamines has not been established until now, some important conclusions can be made based on the existing research achievements. A careful comparison of chemically, enzyme-catalyzed, photocatalyzed, and electrochemically oxidative polymerizations of the aromatic diamines with regard to polymerization conditions and characteristics of the resulting polymers clearly demonstrates that each oxidative polymerization has its own unique feature for the synthesis of the polymers and copolymers of three PD isomers, three DAN isomers, two DAAQ isomers, benzidine, dithiodianiline, naphthidine, and their derivatives. The electrochemically oxidative polymerization for the preparation of fine products is generally preferred over other three oxidative polymerizations, while the chemically oxidative polymerization is desirable from the viewpoint of mass production. Enzyme-catalytic and photocatalytic activities for the oxidative polymerization of the aromatic diamines, however, are not high enough to obtain high molecular weight polymers at the present

time. It is therefore necessary to devise new highly efficient systems of catalytically oxidative polymerization. The oxidation potential of aromatic diamines, a basic and important parameter for the oxidative polymerization, varies significantly with the monomer type and oxidation conditions. The oxidative polymerization conditions strongly influence the polymerization yield, molecular structure, morphological structure, molecular weight and its distribution, and solubility of the resulted polymers. A rough activity order for the oxidative polymerization of aromatic diamine monomers based on a comprehensive consideration of their oxidation potential, polymerization yield, and molecular weight is found to be 23DAN < 15DAN < 15DAAQ  $\leq$  2,2'-dithiodianiline < *o*PD < *m*PD < 18DAN  $\leq$  *p*PD. An apparent dependence of the solubility of the polymers on the molecular structure rather than on the molecular weight is revealed. The solubility of aromatic diamine polymers can be significantly improved by copolymerization with aromatic monoamines and their derivatives. There is a close relationship between the molecular chain structures of the polymers and the monomers as well as conditions of polymerization. The relative substituted position of two amino groups on the naphthalene ring and the types of oxidants used for the phenylenediamine polymerization are two key factors for the final molecular structure of the resulting polymers. A combination of Fourier transform IR,  $^1\text{H}/^{13}\text{C}$  NMR, UV-vis, laser Raman, X-ray photoelectron, circular dichroic, ESR, EPR, and electrochemical impedance spectroscopies with elemental analysis could basically reveal features of the complicated macromolecular and electronic structures of aromatic diamine polymers on the basis of the comparison of the precise assignments of the characteristic absorbance and resonance peaks in the spectra for the various polymers from different monomers. A series of reasonable macromolecular chain structures for the polymers has been proposed. The linear PAN-like *Po*PD, linear azophenylene-like *Pp*PD, linear polyaminonaphthylamine-like P15DAN and P18DAN, ladder phenazine-like structure (*Po*PD, *Pm*PD, *Pp*PD, P23DAN, P15DAAQ), and network poly(*sym*-triaminobenzene) are the common conclusion although the definite structures have not been determined.

Oxidative polymerization is believed to be a powerful technique for the design, synthesis, and architecture of novel multifunctional polymers from several types of aromatic diamines under facile reaction conditions. However, due to the complexity of the multicomponent oxidative polymerization and the variability of oxidation potentials of aromatic diamines with reaction conditions, it is vital to better understand and consider all of its components and monomer oxidation potential to make full use of this methodology and find the optimum polymerization conditions for the preparation of specific materials in particular application field to provide a commercially practical technique for the oxidative polymerization. Fundamental theories of the oxidative polymerization mechanism for four oxidative polymerization procedures have been roughly established,

but the final theory needs to be searched for further in order to explore the most probable mechanism.

Aromatic diamine polymers are now available as materials with a unique combination of many novel properties and functionalities including variable electrical conductivity, unique electrochromism, high permselectivity to electroactive species, high sensitivities of the electrode modified by the polymers to the biosubstances at a low concentration, good detecting ability of electroinactive anions, efficient electrocatalysis for redox reaction, effective absorptivity to heavy metal ions, anticorrosion ability for metal, and high capacitivity. These properties and functionalities clearly establish the fact that the initial expectation of potentially wide applications for the polymers from aromatic diamines in numerous areas has become a reality. Among the three isomeric PPD films prepared by electropolymerization, P $\alpha$ PD film-modified electrode exhibits the highest built-in permselectivity of H<sub>2</sub>O<sub>2</sub> over ascorbate and the most excellent electrochromism and will serve as a very promising material for designing fast-response, interference-free, and long-term stable amperometric biosensors and high-performance display panels. PDAN and PDAAQ and PDTDA can be used as a heavy metal ion complex and electrochemical capacitor material, respectively. In addition, the oxidative polymers and redox reaction from the aromatic diamines can also be applied in an amperometric anion detector, a chemiluminescence biodetector, a capacitive biosensor, a pH sensor, a piezoelectric immunosensor, immunoassay, modifying film of battery electrode, and other fields such as micropatterning, additives in lubricating oil, detection of hemoglobin and H<sub>2</sub>O<sub>2</sub>, determination of metal ions, and determination of the surface area of the noble metal particles as catalysts. Apparently the development of oxidative polymers from the aromatic diamines must have a significant impact on chemical and biochemical research as well as electric and electronic material industries. However, despite the amount of research in this area, the study on these multifunctionalities is not final and these potential applications are on the horizon. Therefore, there are several issues that need to be addressed before any commercial development of aromatic diamine polymers can be considered. In summary, the art and science of the oxidative polymerization and polymers of aromatic diamines have not reached a sophisticated level yet.

A possible way to solve the several key problems existing, including low solution processibility, low molecular weight, poor fusibility that leads to undiscovered melt processibility, and poor mechanical properties of the polymers, which are very important factors for the fabrication and application of self-supporting polymer materials, is systematically recommended for the first time, involving the incorporation of aliphatic substituents and the optimization of oxidative polymerization conditions. Some further challenges remain for the future: polymerization mechanism, macromolecular chain structure, multifunctionalization, and practical applications. Perhaps the efficient preparation of aromatic diamine polymers exhibiting both high molecular weight and good

processibility will be the first challenge explored. A variety of oxidative polymers from aromatic diamines need to be thoroughly evaluated to comprehend the correlation between synthetic condition–macromolecular structure–macroscopic properties. Therefore, it is anticipated that future research in the oxidative polymerization and polymers of aromatic diamines will be focused on the following areas: (1) quantitative influence of monomer structure and polymerization conditions on the macromolecular chain structure of final oxidative polymers; (2) acquiring polymers with both high molecular weight and mechanical properties; (3) final characterization technique of the macromolecular structure of insoluble polymers of aromatic diamines; (4) remarkable improvement of the solubility and fusibility of the polymers and their solution and melt processibilities as well as exploration of the direct formation of insoluble polymer products (fiber, film, sheet, blend, composite, etc.) from oxidative polymerization; (5) fabrication of the articles of aromatic diamine polymers and the precise measurement of multifunctionalities; (6) the development of industrially practical applications. Obviously the aromatic diamine polymers will attract increasing attention and lead to more applications in numerous areas if the thorny problems mentioned above are solved thoroughly. It is expected that this review will encourage even more exciting future endeavors.

## XI. Nomenclature

AA	ascorbic acid
AN	aniline
ANO	5-amino-1-naphthol
AS	<i>o</i> -anisidine
BPG	basal-plane pyrolytic graphite
BQ	benzoquinone
CD	circular dichroic
CHCl <sub>3</sub>	chloroform
CO <sub>x</sub>	cholesterol oxidase
CV	cyclic voltammogram
DAAQ	diaminoanthraquinone
14DAAQ	1,4-diaminoanthraquinone
15DAAQ	1,5-diaminoanthraquinone
26DAAQ	2,6-diaminoanthraquinone
DAN	diaminonaphthalene
12DAN	1,2-diaminonaphthalene
15DAN	1,5-diaminonaphthalene
18DAN	1,8-diaminonaphthalene
23DAN	2,3-diaminonaphthalene
DAPh	2,3-diaminophenazine
23DAPy	2,3-Diaminopyridine
26DAPy	2,6-Diaminopyridine
DMF	<i>N,N</i> -dimethylformamide
DMSO	dimethyl sulfoxide
EPR	electron paramagnetic resonance
ESCA	electron spectroscopy for chemical analysis
ESR	electron spin resonance
FT-IR	Fourier transform-infrared
GC	glassy carbon
GLOx	glutamate oxidase
GOx	glucose oxidase
HAN	<i>o</i> -hydroxyaniline
HEPE	4-(2-hydroxyethyl)-1-piperazineethanesulfonic acid
HPC	hydroxypropylcellulose
HQ	hydroquinone
HR P	horseradish peroxidase
ITO	indium tin oxide

LAOx	lactate oxidase
LOx	lysine oxidase
MA	2-pyrimidylamine
MT	<i>m</i> -toluidine
NAD <sup>+</sup>	nicotinamide adenine dinucleotide
NMP	<i>N</i> -methylpyrrolidone
NMR	nuclear magnetic resonance
OCS	organic conducting salt
OT	<i>o</i> -toluidine
PAN	polyaniline
PB	prussian blue
PBZ	polybenzidine
PD	phenylenediamine
<i>m</i> PD	<i>m</i> -phenylenediamine
<i>o</i> PD	<i>o</i> -phenylenediamine
<i>p</i> PD	<i>p</i> -phenylenediamine
P14DAAQ	poly(1,4-diaminoanthraquinone)
P15DAAQ	poly(1,5-diaminoanthraquinone)
PDAN	polydiaminonaphthalene
P15DAN	poly(1,5-diaminonaphthalene)
P18DAN	poly(1,8-diaminonaphthalene)
P23DAN	poly(2,3-diaminonaphthalene)
PDAPh	poly(2,3-diaminophenazine)
PDTDA	poly(2,2'-dithiodianiline)
PHAN	poly( <i>o</i> -hydroxyaniline)
PHMA	poly(2-hydroxyethyl methacrylate)
PHT	<i>o</i> -phenetidine
PMoPD	poly( <i>N</i> -methyl- <i>o</i> -phenylenediamine)
PPD	polyphenylenediamine
<i>Pm</i> PD	poly( <i>m</i> -phenylenediamine)
<i>Po</i> PD	poly( <i>o</i> -phenylenediamine)
<i>Pp</i> PD	poly( <i>p</i> -phenylenediamine)
PPBZ	poly( <i>N,N</i> -diphenylbenzidine)
PPTA	poly( <i>p</i> -phenylene terephthalamide)
PPY	polypyrrole
PVA	poly(vinyl alcohol)
PVP	poly( <i>N</i> -vinylpyrrolidone)
SESS	sodium di(2-ethylhexyl) sulfosuccinate
TAB	<i>sym</i> -triaminobenzene
TFA	trifluoroacetic acid
THF	tetrahydrofuran
UOx	uric acid oxidase
UV-vis	ultraviolet-visible
WAXD	wide-angle X-ray diffraction
XPS	X-ray photoelectron spectroscopy
XY	2,3-xylydine

## XII. Acknowledgments

The project was supported by (1) the two National Natural Science Foundations of China (20174028 and 29804008), (2) the Foundation of the University Key Teacher of Chinese Ministry of Education (GG-430-10247-1186), (3) the State Key Laboratory for the Modifications of Fiber and Polymer Materials, Donghua University, China, and (4) the Key Laboratory of Optics and Magnetic Resonance Spectroscopy of Education Ministry, East China Normal University.

## XIII. References

- Letheby, H. *J. Chem. Soc.* **1862**, 15, 161.
- Green, A. G.; Woodhead, A. E. *J. Chem. Soc.* **1910**, 97, 2338.
- Wei, Y.; Tang, X.; Sun, Y. *J. Polym. Sci., Part A: Polym. Chem.* **1989**, 27, 2385.
- Wei, Y.; Focke, W. W.; Wnek, G. E.; Ray, A.; MacDiarmid, A. G. *J. Phys. Chem.* **1989**, 93, 495.
- Cao, Y.; Andreatta, A.; Heeger, A. J.; Smith, P. *Polymer* **1989**, 30, 2305.
- Wu, T. S.; Yang, C. H. *J. Electrochem. Soc.* **1996**, 143, 4019.
- Sherman, B. C.; Euler, W. B.; Ren, F. R. *J. Chem. Educ.* **1994**, 71 (4), A94.
- Johnson, B. J.; Park, S. M. *J. Electrochem. Soc.* **1996**, 143, 1269.
- Johnson, B. J.; Park, S. M. *J. Electrochem. Soc.* **1996**, 143, 1277.
- Mattoso, L. H. C.; Faria, R. M.; Buhoess, L. O. S.; MacDiarmid, A. G. *Polymer* **1994**, 35, 5104.
- Joo, J.; Prigodin, V. N.; Min, Y. G.; MacDiarmid, A. G.; Epstein, A. J. *Phys. Rev. B* **1994**—II, 50, 12226.
- Anand, I.; Palaniappan, S.; Sathyanarayana, D. N. *J. Polym. Sci., Part A: Polym. Chem.* **1998**, 36, 2291.
- Anand, J.; Palaniappan, S.; Sathyanarayana, D. N. *Polymer* **1998**, 39, 6819.
- Wu, S. Z.; Zeng, F.; Li, F. X.; Zhu, Y. L. *Eur. Polym. J.* **2000**, 36, 679.
- Mazeikiene, R.; Malinauskas, A. *Eur. Polym. J.* **2000**, 36, 1347.
- Wang, H. L.; Romero, R. J.; Mattes, B. R.; Zhu, Y. T.; Winokur, M. J. *J. Polym. Sci., Part B: Polym. Phys.* **2000**, 38, 194.
- Chen, S. A.; Hwang, G. W. *J. Am. Chem. Soc.* **1995**, 117, 10055.
- Karakisla, M.; Sacak, M.; Erdem, E.; Akbulut, U. *J. Appl. Electrochem.* **1997**, 27, 309.
- Li, X.-G.; Kresse, I.; Springer, J.; Nissen, J.; Yang, Y. L. *Polymer* **2001**, 42, 6859.
- Biaggio, S. R.; Oliveira, C. L. F.; Aguirre, M. J.; Zagal, J. H. *J. Appl. Electrochem.* **1994**, 24, 1059.
- Brett, C. M. A.; Oliverira Brett, A. M. C. F.; Pereira, J. L. C.; Rebelo, C. J. *J. Appl. Electrochem.* **1993**, 23, 332.
- Tang, H.; Kitani, A.; Shiotani, M. *J. Electrochem. Soc.* **1996**, 143, 3079.
- Yonezawa, S.; Kanamura, K.; Takehara, Z. I. *J. Electrochem. Soc.* **1995**, 142, 3309.
- Dhawan, S. K.; Trivedi, D. C. *J. Appl. Electrochem.* **1992**, 22, 563.
- Duran, R. S.; Zhou, H. C. *Polymer* **1992**, 33, 4019.
- Li, X.-G.; Huang, M.-R.; Jin, Y.; Yang, Y. L. *Polymer* **2001**, 42, 3427.
- Li, X.-G.; Huang, M.-R.; Zhu, L.-H.; Yang, Y. L. *J. Appl. Polym. Sci.* **2001**, 82, 790.
- Huang, M.-R.; Li, X.-G.; Yang, Y. L.; Wang, X.-S.; Yan, D. *J. Appl. Polym. Sci.* **2001**, 81, 1838.
- Li, X.-G.; Huang, M.-R.; Gu, G.-F.; Qiu, W.; Lu, J.-Y. *J. Appl. Polym. Sci.* **2000**, 75, 458.
- Li, X.-G.; Huang, M.-R.; Yang, Y. L. *Polym. J. (Tokyo)* **2000**, 32, 348.
- Koketsu, J.; Kato, K.; Ando, F.; Fujimura, Y. *Synth. Met.* **1993**, 60, 45.
- Hayat, U.; Bartlett, P. N.; Dodd, G. H. *Polym. Commun.* **1986**, 27, 362.
- Li, X.-G.; Huang, M.-R.; Li, F.; Cai, W. J.; Jin, Z.; Yang, Y. L. *J. Polym. Sci., Part A: Polym. Chem.* **2000**, 38, 4407.
- Li, X.-G.; Huang, M.-R.; Pan, P.; Zhu, Z.-L.; Yang, Y. L. *Polym. Degrad. Stab.* **2001**, 71, 333.
- El-Rahman, H. A. A. *J. Appl. Electrochem.* **1997**, 27, 1061.
- An, H.; Seki, M.; Sato, K.; Kadoi, K.; Yosomiya, R. *Polymer* **1989**, 30, 1076.
- Karakisla, M.; Sacak, M. *J. Polym. Sci., Part A: Polym. Chem.* **2000**, 38, 51.
- Petitjean, J.; Aeiyaeh, S.; Ferreira, C. A.; Lacaze, P. C.; Tak-enouti, H. *J. Electrochem. Soc.* **1995**, 142, 136.
- Sutton, S. J.; Vaughan, A. S. *Polymer* **1995**, 36, 1849.
- Sun, H.; Sun, B. *J. Appl. Electrochem.* **1993**, 23, 212.
- Sun, H.; Sun, B. *J. Appl. Electrochem.* **1993**, 23, 741.
- Naoi, K.; Oura, Y.; Maeda, M.; Nakamura, S. *J. Electrochem. Soc.* **1995**, 142, 417.
- Moon, D. K.; Padias, A. B.; Hall, H. K.; Huntoon, J. T.; Calvert, P. D. *Macromolecules* **1995**, 28, 6205.
- Nishio, K.; Fujimoto, M.; Ando, O. *J. Appl. Electrochem.* **1996**, 26, 425.
- Lee, J. Y.; Ong, L. G.; Chuah, G. K. *J. Appl. Electrochem.* **1992**, 22, 738.
- Kim, H.; Pyo, M. *J. Appl. Electrochem.* **2000**, 30, 49.
- Chiu, H. T.; Lin, J. S.; Huang, C. M. *J. Appl. Electrochem.* **1992**, 22, 358.
- Nakata, M.; Shiraiishi, Y.; Taga, M. *Makromol. Chem.* **1992**, 193, 765.
- Ouyang, J. Y.; Li, Y. F. *Polymer* **1997**, 38, 3997.
- Wainright, J. S.; Zorman, C. A. *J. Electrochem. Soc.* **1995**, 142, 379.
- Reynolds, J. R.; Katritzky, A. R.; Soloducho, J. *Macromolecules* **1994**, 27, 7225.
- Kim, J. B.; Lim, S. T. *Polym. Bull.* **1996**, 37, 321.
- Kathirgamanathan, P.; Souter, A. M.; Baluch, D. *J. Appl. Electrochem.* **1994**, 24, 283.
- Dahlhaus, M.; Beck, F. *J. Appl. Electrochem.* **1993**, 23, 957.
- Beck, F.; Dahlhaus, M. *J. Appl. Electrochem.* **1993**, 23, 781.
- Li, X.-G.; Wang, L.-X.; Jin, Y.; Zhu, Z.-L.; Yang, Y.-L. *J. Appl. Polym. Sci.* **2001**, 82, 510.
- Li, X.-G.; Wang, L.-X.; Huang, M.-R.; Lu, Y.-Q.; Zhu, M.-F.; Menner, A.; Springer, J. *Polymer* **2001**, 42, 6095.
- Li, X.-G.; Huang, M.-R.; Wang, L.-X.; Zhu, M.-F.; Menner, A.; Springer, J. *Synth. Met.* **2001**, 123, 435.

- (59) Yamamoto, T.; Sanechika, K.; Yamamoto, A. *J. Polym. Sci., Polym. Lett. Ed.* **1980**, *18*, 19.
- (60) Torillon, G.; Garnier, F. *J. Electroanal. Chem.*, **1982**, *135*, 173.
- (61) Englebienne, P.; Weiland, M. *Chem. Commun.* **1996**, 1651.
- (62) Cataldo, F. *Eur. Polym. J.* **1996**, *32*, 43.
- (63) Anderson, M. A.; Mattes, B. R.; Reiss, H.; Kaner, R. B. *Science* **1991**, *252*, 1412.
- (64) Martin, C. R.; Liang, W.; Menon, V.; Parthasarathy, R.; Parthasarathy, A. *Synth. Met.* **1993**, *55–57*, 3766.
- (65) Rebattet, L.; Escoubes, M.; Genies, E.; Pineri, M. *J. Appl. Polym. Sci.* **1995**, *57*, 1595.
- (66) Chang, M. J.; Liao, Y. H.; Myerson, A. S.; Kwei, T. K. *J. Appl. Polym. Sci.* **1996**, *62*, 1427.
- (67) Huang, S. C.; Conklin, J. A.; Su, T. M.; Ball, I. J.; Nguyen, S. L.; Kaner, R. B. *Polym. Mater. Sci. Eng.* **1995**, *72*, 323.
- (68) Kuwabata, S.; Martin, C. R. *J. Membr. Sci.* **1994**, *91*, 1.
- (69) Chan, H. S. O.; Ng, S. C.; Hor, T. S. A.; Sun, J.; Tan, K. L.; Tan, B. T. G. *Eur. Polym. J.* **1991**, *27*, 1303.
- (70) Premasiri, A. H.; Euler, W. B. *Macromol. Chem. Phys.* **1995**, *196*, 3655.
- (71) Ichinohe, D.; Muranaka, T.; Kise, H. *J. Appl. Polym. Sci.* **1998**, *70*, 717.
- (72) Ichinohe, D.; Muranaka, T.; Sasaki, T.; Kobayashi, M.; Kise, H. *J. Polym. Sci., Part A: Polym. Chem.* **1998**, *36*, 2593.
- (73) Ichinohe, D.; Saitoh, N.; Kise, H. *Macromol. Chem. Phys.* **1998**, *199*, 1241.
- (74) Lu, Y. Q.; Shi, G. Q.; Li, C. J. *J. Appl. Polym. Sci.* **1998**, *70*, 2169.
- (75) Yang, J.; Zhao, C.; Cui, D.; Hou, J.; Wan, M.; Xu, M. *J. Appl. Polym. Sci.* **1995**, *56*, 831.
- (76) Sari, B.; Talu, M. *Synth. Met.* **1998**, *94*, 221.
- (77) Huang, Y.; Xiao, S.; Tian, H. *J. Funct. Polym.* (in Chinese) **1998**, *11* (3), 44.
- (78) Cruz, G. J.; Morales, J.; Castillo-Ortega, M. M.; Olayo, R. *Synth. Met.* **1997**, *88*, 213.
- (79) Olayo, M. G.; Morales, J.; Cruz, G. J.; Olayo, R.; Ordóñez, E.; Barocio, S. R. *J. Polym. Sci., Part B: Polym. Phys.* **2001**, *39*, 175.
- (80) Nakata, M.; Shiraiishi, Y.; Taga, M.; Kise, H. *Makromol. Chem.* **1992**, *193*, 765.
- (81) Kurachi, K.; Kise, H. *Polym. J.* **1994**, *26*, 1325.
- (82) Zhao, H.; Price, W. E.; Wallace, G. G. *Synth. Met.* **1998**, *148*, 161.
- (83) Xiao, S.; Xu, J.; Huang, Y.; Li, L. *J. South China Univ. Technol.* (in Chinese) **1998**, *26* (1), 95.
- (84) Morales, J.; Olayo, M. G.; Cruz, G. J.; Castillo Ortega, M. M.; Olayo, R. *J. Polym. Sci. B: Polym. Phys.* **2000**, *38*, 3247.
- (85) Singh, R.; Narula, A. K.; Tandon, R. P.; Rao, S. U. M.; Panwar, V. S.; Mansingh, A.; Chandra, S. *Synth. Met.* **1996**, *79*, 1.
- (86) Diaz, F. R.; Tagle, L. H.; Godoy, A.; Contreras, S. *Synth. Met.* **1995**, *73*, 95.
- (87) Uemura, S.; Teshima, K.; Tokuda, S.; Kobayashi, N.; Hirohashi, R. *Synth. Met.* **1999**, *101*, 701.
- (88) An, H.; Seki, M.; Yosomiya, R. *Makromol. Chem. Rapid Commun.* **1987**, *8*, 325.
- (89) Cotteville, D.; Le Mehaute, A.; Challioui, C.; Mirebeau, P.; Demay, J. N. *Synth. Met.* **1999**, *101*, 703.
- (90) Wood, A. S. *Mod. Plast.* **1991**, *68* (8), 47.
- (91) Wessling, B. *Synth. Met.* **1998**, *93*, 143.
- (92) Wei, Y.; Focke, W. W.; Wnek, G. E. *J. Phys. Chem.* **1989**, *93*, 495.
- (93) Leclerc, M.; Guay, J.; Dao, L. H. *Macromolecules* **1989**, *22*, 649.
- (94) Quint, P.; Knoll, W.; Hara, M. *Macromolecules* **1995**, *28*, 4029.
- (95) Macinnes, D.; Funt, B. L. *Synth. Met.* **1988**, *25*, 235.
- (96) Watanabe, A.; Mori, K.; Iwabuchi, Y. *Macromolecules* **1989**, *22*, 3521.
- (97) Chevalier, J. W.; Bergeron, J. Y.; Dao, L. H. *Macromolecules* **1992**, *25*, 5, 3325.
- (98) Manohar, S. K.; MacDiarmid, A. G.; Cromack, K. R. *Synth. Met.* **1989**, *29*, E349.
- (99) Wu, L. L.; Luo, J.; Lin, Z. H. *Chem. J. Chin. Univ.* (in Chinese) **1997**, *18*, 1657.
- (100) Wu, L. L.; Luo, J.; Lin, Z. H. *J. Electroanal. Chem.* **1996**, *417*, 53.
- (101) Piccard, J. *Ann.* **1911**, *381*, 351.
- (102) Piccard, J. *Ber.* **1926**, *59*, 1438.
- (103) Michaelis, L.; Granick, S. *J. Am. Chem. Soc.* **1943**, *65*, 1747.
- (104) Lord, S. S., Jr.; Rogers, L. B. *Anal. Chem.* **1954**, *26*, 284.
- (105) Porcher, R. E.; Adams, R. N. *Anal. Chem.* **1956**, *28*, 828.
- (106) Elving, P. J.; Krivis, A. F. *Anal. Chem.* **1958**, *30*, 1645.
- (107) Elving, P. J.; Krivis, A. F. *Anal. Chem.* **1958**, *30*, 1648.
- (108) Glicksman, R. *J. Electrochem. Soc.* **1961**, *108*, 1.
- (109) Mark, H. B., Jr.; Anson, F. C. *Anal. Chem.* **1963**, *35*, 722.
- (110) Prater, K. B. *J. Electrochem. Soc.* **1973**, *120*, 365.
- (111) Mark, H. B., Jr.; Koran, D.; Gierst, L. *J. Electroanal. Chem.* **2001**, *498*, 228.
- (112) Yacynych, A. M.; Mark, H. B., Jr. *J. Electrochem. Soc.* **1976**, *123*, 1346.
- (113) Yano, J.; Kitani, A.; Vasquez, R. E.; Sasaki, K. *Nippon Kagaku Kaishi* **1985**, 1124.
- (114) Bach, H. C. *Polym. Prepr.* **1966**, *7*, 576.
- (115) Wei, Y.; Jang, G. W.; Chan, C. C.; Hsueh, K. F.; Hariharan, R.; Whitecar, C. K. *J. Phys. Chem.* **1990**, *94*, 7716.
- (116) Rawat, B.; Kansara, S. S.; Rama, H. S. *Polym. Int.* **1991**, *26*, 233.
- (117) Kobayashi, S.; Kaneko, I.; Uyama, H. *Chem. Lett.* **1992**, *243*, 393.
- (118) Deshpande, M. V.; Amalnerkar, D. P. *Prog. Polym. Sci.* **1993**, *18*, 623.
- (119) Kang, E. T.; Neoh, K. G.; Tan, K. L. *Prog. Polym. Sci.* **1998**, *23*, 277.
- (120) Gospodinova, N.; Terlemezyan, L. *Prog. Polym. Sci.* **1998**, *23*, 1443.
- (121) Bhattacharya, A.; De, A. *J. Macromol. Sci. Rev. Macromol. Chem. Phys.* **1999**, *C39* (1), 17.
- (122) Malinauskas, A. *Polymer* **2001**, *42*, 3957.
- (123) Patil, A. O.; Heeger, A. J.; Wudl, F. *Chem. Rev.* **1988**, *88*, 183.
- (124) Inzelt, G.; Pinerib, M.; Schultze, J. W.; Vorotyntsevd, M. A. *Electrochim. Acta* **2000**, *45*, 2403.
- (125) Bykera, H. J. *Electrochim. Acta* **2001**, *46*, 2015.
- (126) Cosniera, S. *Biosens. Bioelectron.* **1999**, *14*, 443.
- (127) Lux, F. *Polymer* **1994**, *35*, 2915.
- (128) Wang, L. X.; Li, X.-G.; Yang, Y. L. *React. Funct. Polym.* **2001**, *47*, 125.
- (129) Sadki, S.; Schottland, P.; Brodie, N.; Sabouraud, G. *Chem. Soc. Rev.* **2000**, *29*, 283.
- (130) De Jesus, M. C.; Fu, Y.; Weiss, R. A. *Polym. Eng. Sci.* **1997**, *37*, 1936.
- (131) Tushima, N.; Hara, S. *Prog. Polym. Sci.* **1995**, *20*, 155.
- (132) Stenger-Smith, J. D. *Prog. Polym. Sci.* **1998**, *23*, 57.
- (133) Chan, H. S. O.; Ng, S. C. *Prog. Polym. Sci.* **1998**, *23*, 1167.
- (134) Potember, R. S.; Hoffman, R. C.; Hu, H. S.; Cocchiari, J. E.; Vinands, C. A.; Murphy, R. A.; Poehler, T. O. *Polymer* **1987**, *28*, 574.
- (135) Yamamoto, T. *Prog. Polym. Sci.* **1992**, *17*, 1153.
- (136) Choi, S. K.; Gal, Y. S.; Jin, S. H.; Kim, H. K. *Chem. Rev.* **2000**, *100*, 1645.
- (137) Anand, J.; Palaniappan, S.; Sathyanarayana, D. N. *Prog. Polym. Sci.* **1998**, *23*, 993.
- (138) Mederos, A.; Dominguez, S.; Hernandez-Molina, R.; Sanchiz, J.; Brito, F. *Coord. Chem. Rev.* **1999**, *193–195*, 913.
- (139) Oyama, N.; Sato, M.; Ohsaka, T. *Synth. Met.* **1989**, *29*, E501.
- (140) Karalemas, I. D.; Georgiou, C. A.; Papastathopoulos, D. S. *Talanta* **2000**, *53*, 391.
- (141) Elliott, J. M.; Cabuche, L. M.; Bartlett, P. N. *Anal. Chem.* **2001**, *73*, 2855.
- (142) Malitesta, C.; Palmisano, F.; Torsi, L.; Zamboni, P. G. *Anal. Chem.* **1990**, *62*, 2735.
- (143) Palmisano, F.; Centonze, D.; Malitesta, C.; Zamboni, P. G. *J. Electroanal. Chem.* **1995**, *381*, 235.
- (144) Davis, J.; Huw Vaughan, D.; Cardosi, M. F. *Electrochim. Acta* **1996**, *41*, 2375.
- (145) Volkov, A.; Tourillon, G.; Lacaze, P. C.; Dubois, J. E. *J. Electroanal. Chem.* **1980**, *115*, 279.
- (146) Malitesta, C.; Losoto, I.; Zamboni, P. G. *Anal. Chem.* **1999**, *71*, 1366.
- (147) Cheng, Z.; Wang, E.; Yang, X. *Biosens. Bioelectron.* **2001**, *16*, 179.
- (148) Peng, H.; Zhang, Y. Y.; Zhang, J. H.; Xie, Q. J.; Nie, L. H.; Yao, S. Z. *Analyst* **2001**, *126*, 189.
- (149) Myler, S.; Eaton, S.; Higson, S. P. *J. Anal. Chim. Acta* **1997**, *357*, 55.
- (150) Yano, J.; Kawakami, K.; Hata, C.; Yamasaki, S. *J. Solid State Electrochem.* **2000**, *4* (5), 279.
- (151) Martinusz, K.; Czirok, E.; Inzelt, G. *J. Electroanal. Chem.* **1994**, *379*, 437.
- (152) Wieck, H. J.; Yacynych, A. M. *Anal. Chem.* **1980**, *52*, 345.
- (153) Premkumar, J.; Ramaraj, R. *J. Appl. Electrochem.* **1996**, *26*, 763.
- (154) Losito, I.; De Giglio, E.; Cioffi, N.; Malitesta, C. *J. Mater. Chem.* **2001**, *11*, 1812.
- (155) Prasad, B. M.; Singh, D.; Misra, R. A. *J. Polym. Mater.* **1996**, *13* (2), 157.
- (156) Ujvari, M.; Lang, G.; Inzelt, G. *Electrochem. Commun.* **2000**, *2*, 497.
- (157) Xu, Q.; Xu, C.; Wang, Y.; Zhang, W.; Jin, L.; Tanaka, K.; Haraguchi, H.; Itoh, A. *Analyst* **2000**, *125*, 1453.
- (158) Wu, Q. H.; Xiao, X. Y.; Yang, Y. Y.; Cai, L. R.; Dai, H. P.; Sun, S. G. *Chin. J. Appl. Chem.* (in Chinese) **1999**, *16* (5), 5.
- (159) Yano, J.; Kai, S.; Ogura, K. *J. Mater. Sci. Lett.* **1993**, *12*, 1791.
- (160) Yano, J.; Terayama, K.; Yamasaki, S. *J. Mater. Sci.* **1996**, *31*, 4785.
- (161) Dai, H. P.; Wu, Q. H.; Sun, S. G.; Shiu, K. K. *J. Electroanal. Chem.* **1998**, *456*, 47.
- (162) Malinauskas, A.; Bron, M.; Holze, R. *Synth. Met.* **1998**, *92*, 127.
- (163) Ekinci, E.; Erdogdu, G.; Karagozler, A. E. *J. Appl. Polym. Sci.* **2001**, *79*, 327.
- (164) Yano, J. *J. Polym. Sci., Part A: Polym. Chem.* **1995**, *33*, 2435.
- (165) Curulli, A.; Carelli, I.; Trischitta, O.; Palleschi, G. *Biosens. Bioelectron.* **1997**, *12*, 1043.

- (166) Ekinci, E.; Erdogdu, G.; Karagozler, A. E. *Polym. Bull.* **2000**, *44*, 547.
- (167) Ekinci, E.; Ogunc, S. T.; Karagozler, A. E. *J. Appl. Polym. Sci.* **1998**, *68*, 145.
- (168) Si, S. H.; Xu, Y. J.; Nie, L. H.; Yao, S. Z. *Electrochim. Acta* **1995**, *40*, 2715.
- (169) Yang, C. H.; Wen, T. C. *J. Appl. Electrochem.* **1994**, *24*, 166.
- (170) Ekinci, E.; Karagozler, A. A.; Karagozler, A. E. *Synth. Met.* **1996**, *79*, 57.
- (171) Compton, R. G.; King, P. M.; Reynolds, C. A.; Richards, W. G.; Waller, A. M. *J. Electroanal. Chem.* **1989**, *258*, 79.
- (172) Jackowska, K.; Skompska, M.; Przulyska, E. *J. Electroanal. Chem.* **1996**, *418*, 35.
- (173) Azzem, M. A.; Yousef, U. S.; Limosin, D.; Pierre, G. *J. Electroanal. Chem.* **1996**, *417*, 163.
- (174) Jackowska, K.; Bukowska, J.; Jamkowski, M. *J. Electroanal. Chem.* **1995**, *388*, 101.
- (175) Azzem, A. M.; Yousef, U. S.; Limosin, D.; Pierre, G. *Synth. Met.* **1994**, *63*, 79.
- (176) Pham, M. C.; Oulahyane, M.; Mostefai, M.; Chehimi, M. M. *Synth. Met.* **1998**, *93*, 89.
- (177) Abdel-Azzem, M.; Yousef, U. S.; Pierre, G. *Eur. Polym. J.* **1998**, *34*, 819.
- (178) Jin, C. S.; Shim, Y. B.; Park, S. M. *Synth. Met.* **1995**, *69*, 561.
- (179) Meneguzzi, A.; Pham, M. C.; Ferreira, C. A.; Lacroix, J. C.; Aejyach, S.; Lacaze, P. C. *Polym. Mater. Sci. Eng.* **1989**, *61*, 905.
- (180) Skompska, M.; Hillman, A. R. *J. Chem. Soc., Faraday Trans.* **1996**, *92*, 4101.
- (181) Lee, J. W.; Park, D. S.; Shim, Y. B.; Park, S. M. *J. Electrochem. Soc.* **1992**, *139*, 3507.
- (182) Del Valle, M. A.; Silva, E. T.; Diaz, F. R.; Gargallo, L. *J. Polym. Sci., Part A: Polym. Chem.* **2000**, *38*, 1698.
- (183) Rehan, H. H. *J. Appl. Electrochem.* **2000**, *30*, 945.
- (184) Wei, Y.; Jang, G. W.; Hsueh, K. F.; Hariharan, R.; Patel, S. A.; Chan, C. C.; Whitecar, C. *Polym. Mater. Sci. Eng.* **1989**, *61*, 905.
- (185) Yang, C. H.; Wen, T. C. *J. Electrochem. Soc.* **1994**, *141*, 2624.
- (186) Alva, K. S.; Kumar, J.; Marx, K. A.; Tripathy, S. K. *Macromolecules* **1997**, *30*, 4024.
- (187) Morea, G.; Guerrieri, A.; Malitesta, C.; Torsi, L. *J. Chem. Soc., Faraday Trans.* **1991**, *87*, 3515.
- (188) Ohsaka, T.; Watanabe, T.; Kitamura, F.; Oyama, N.; Tokuda, K. *Chem. Commun.* **1991**, 487.
- (189) (a) D'Eramo, F.; Arevalo, A. H.; Silber, J. J.; Sereno, L. E. *J. Electroanal. Chem.* **1995**, *382*, 85. (b) Bagheri, A.; Nateghi, M. R.; Massoumi, A. *Synth. Met.* **1998**, *97*, 85.
- (190) Arevalo, A. H.; Fernandez, H.; Silber, J. J.; Sereno, L. *Electrochim. Acta* **1990**, *35*, 731.
- (191) Abd El-Rahman, H. A.; Hathoot, A. A.; El-Bagoury, M.; Addel-Azzem, M. *J. Electrochem. Soc.* **2000**, *147*, 242.
- (192) Kilmartin, P. A.; Wright, G. A. *Synth. Met.* **1999**, *104*, 145.
- (193) Cintra, E. P.; Cordoba de Torresi, S. I. *J. Electroanal. Chem.* **2002**, *518*, 33.
- (194) Prokes, J.; Stejskal, J.; Krivka, I.; Tobolkova, E. *Synth. Met.* **1999**, *102*, 1205.
- (195) Prokes, J.; Krivka, I.; Kuzel, R.; Stejskal, J.; Kratochvil, P. *Int. J. Electron.* **1996**, *81*, 407.
- (196) Stejskal, J.; Kratochvil, P.; Spirkova, M. *Polymer* **1995**, *36*, 4135.
- (197) Wu, J.; Liu, G.; Huang, S.; Yu, R. *Chin. J. Anal. Chem.* (in Chinese) **2001**, *29*, 1140.
- (198) Koketsu, J.; Kato, K.; Ando, F.; Fujimura, Y. *Synth. Met.* **1993**, *60*, 45.
- (199) Wang, Z.; Zhang, D.; Zhang, Y.; Zhou, S. *Chin. J. Anal. Chem.* (in Chinese) **2001**, *29*, 83.
- (200) Wei, Y.; Hsueh, K. F.; Jang, G. W. *Polymer* **1994**, *35*, 3572.
- (201) Prokes, J.; Krivka, I.; Stejskal, J. *Polym. Int.* **1997**, *43*, 117.
- (202) Wei, Y.; Jia, X.; Jin, D.; Mathai, M. W.; Yeh, J. M. *Polym. Prepr.* **1998**, *39* (1), 115.
- (203) Tang, H.; Kitani, A.; Maitani, S.; Munemura, H.; Shiotani, M. *Electrochim. Acta* **1995**, *40*, 849.
- (204) Beadle, P. M.; Nicolau, Y. F.; Banka, E.; Rannou, P.; Djurado, D. *Synth. Met.* **1998**, *95*, 29.
- (205) Shao, K.; Ma, Y.; Cao, Y.; Chen, Z.; Ji, X.; Yao, J. *Acta Phys.-Chim. Sin.* (in Chinese) **2000**, *16*, 865.
- (206) Kim, Y.; Fukai, S.; Kobayashi, N. *Synth. Met.* **2001**, *119*, 337.
- (207) Ohno, N.; Wang, H. J.; Yan, H.; Tushima, N. *Polym. J.* **2001**, *33*, 165.
- (208) Vijayashree, M. N.; Subramanyam, S. V.; Samuelson, A. G. *Macromolecules* **1992**, *25*, 2988.
- (209) Alagesan, K.; Samuelson, A. G. *Synth. Met.* **1997**, *87*, 37.
- (210) Qin, W.; Zhao, X.; Li, F. *Acta Polym. Sin.* (in Chinese) **1993**, *(4)*, 502.
- (211) Tsuchida, E.; Kaneko, M.; Kurimura, Y. *Makromol. Chem.* **1970**, *132*, 209.
- (212) Tsuchida, E.; Kaneko, M.; Kurimura, Y. *Makromol. Chem.* **1970**, *132*, 215.
- (213) Sulimenko, T.; Stejskal, J.; Prokes, J. *J. Colloid Interface Sci.* **2001**, *236*, 328.
- (214) Puzari, A.; Baruah, J. B. *React. Funct. Polym.* **2001**, *47*, 147.
- (215) Li, X.-G.; Huang, M.-R. Manuscript in preparation.
- (216) Tsuchida, E. *Asahi Garasu Kogyo Gijutsu Shoreikai Kenkyu Hokoku* **1969**, *15*, 537.
- (217) Stejskal, J.; Spirkova, M.; Riede, A.; Helmstedt, M.; Mokreva, P.; Prokes, J. *Polymer* **1999**, *40*, 2487.
- (218) Johannsen, I.; Torrance, J. B.; Nazzari, A. *Macromolecules* **1989**, *22*, 566.
- (219) Torrance, J. B.; Oostra, S.; Nazaal, A. *Synth. Met.* **1987**, *19*, 709.
- (220) Li, X.-G.; Huang, M.-R.; Yang, Y.-L. *Polymer* **2001**, *42*, 4099.
- (221) Huang, M.-R.; Li, X.-G.; Yang, Y.-L. *Polym. Degrad. Stabil.* **2001**, *71*, 31.
- (222) Ogura, K.; Shiigi, H.; Nakayama, M. *J. Electrochem. Soc.* **1996**, *143*, 2925.
- (223) Li, X.-G.; Duan, W.; Huang, M. R.; Yang, Y. L. *J. Polym. Sci., Part A: Polym. Chem.* **2001**, *39*, 3989.
- (224) Li, X.-G.; Huang, M.-R.; Chen, R.-F.; Jin, Y.; Yang, Y.-L. *J. Appl. Polym. Sci.* **2001**, *81*, 3107.
- (225) Shim, Y. B.; Park, J. H. *J. Electrochem. Soc.* **2000**, *147*, 381.
- (226) Palys, B. J.; Bukowska, J.; Jackowska, K. *J. Electroanal. Chem.* **1997**, *428*, 19.
- (227) Naoi, K.; Suematsu, S.; Manago, A. *J. Electrochem. Soc.* **2000**, *147*, 420.
- (228) Kunimura, S.; Ohsaka, T.; Oyama, N. *Macromolecules* **1988**, *21*, 894.
- (229) Li, X.-G.; Duan, W.; Huang, M.-R. Manuscript in preparation.
- (230) Chandrasekhar, P.; Gumbs, R. W. *J. Electrochem. Soc.* **1991**, *138*, 1337.
- (231) Naoi, K.; Suematsu, S.; Komiyama, M.; Ogihara, N. *Electrochim. Acta* **2002**, *47*, 1091.
- (232) Wen, T. C.; Huang, L. M.; Gopalan, A. *Synth. Met.* **2001**, *123*, 451. Wen, T. C.; Huang, L. M.; Gopalan, A. *J. Electrochem. Soc.* **2001**, *148*, D9.
- (233) Lu, G. Q.; Sun, S. G.; Cai, L. R.; Chen, S. P.; Tian, Z. W.; Shiu, K. K. *Langmuir* **2000**, *16*, 778.
- (234) Nishikitani, Y.; Kobayashi, M.; Uchida, S.; Kubo, T. *Electrochim. Acta* **2001**, *46*, 2035.
- (235) Kumar, M. N.; Nagabhooshanam, M.; Rao, M. A.; Rao, M. B. *Cryst. Res. Technol.* **2001**, *36*, 309.
- (236) Balasubramanian, Kim, J.; Kim, D. Y.; Kumar, J.; Tripathy, S. K. NTIS No: AD-A313 871/6/HDM, Contract No: N00014-95-1-1292, **1996**, Pages: 17p.
- (237) Abe, M.; Ohtani, A.; Higuchi, H.; Ezoe, M.; Akizuki, S.; Nakamoto, K.; Mochizuki, K.; Umemoto, Y.; Umeda, M. U.S. Patent 5,728,321, 1998.
- (238) Krivka, I.; Prokes, J.; Starykov, O.; Stejskal, J. *Synth. Met.* **2001**, *119*, 481.
- (239) Yue, J.; Epstein, A. J.; Zhong, Z.; Gallagher, P. K.; MacDiarmid, A. G. *Synth. Met.* **1991**, *41-43*, 765.
- (240) Moon, D. K.; Osakada, K.; Maruyama, T.; Yamamoto, T. *Makromol. Chem.* **1992**, *193*, 1723.
- (241) Chandrakanthi, N.; Careem, M. A. *Polym. Bull.* **2000**, *44*, 101.
- (242) Le, L. P.; Keren, A.; Luke, G. M.; Wu, W. D.; Uemura, Y. J.; Jenks, W. S.; Graff, A.; Breslow, R.; Dosanjh, P. *Hyperfine Interact.* **1994**, *85*, 287.
- (243) Ito, A.; Miyajima, H.; Yoshizawa, K.; Tanaka, K.; Yamabe, T. *Synth. Met.* **1997**, *85*, 1777.
- (244) Trlica, J.; Saha, P.; Quadrat, O.; Stejskal, J. *Physica A* **2000**, *283*, 337.
- (245) Trlica, J.; Saha, P.; Quadrat, O.; Stejskal, J. *Eur. Polym. J.* **2000**, *36*, 2313.
- (246) Kobayashi, S.; Kaneko, I.; Kurioka, H.; Uyama, H. *J. Macromol. Sci. Pure Appl. Chem.* **1994**, *A31*, Suppl. No. 3-4, 421.
- (247) Shan, J.; Cao, S. *Polym. Adv. Technol.* **2000**, *11* (6), 288.
- (248) Aranda, F. J.; Cheng, C. F.; Rao, D. V. G. L. N.; Akkara, J. A.; Kaplan, D. L.; Roach, J. F. *Materials for Optical Limiting* Materials Research Society Symposium Proceedings; Materials Research Society: Pittsburgh, PA, 1995; Vol. 374, p 185.
- (249) Ono, T.; Kawakami, K.; Goto, M.; Furusaki, S. *J. Mol. Catal. B, Enzym.* **2001**, *11*, 955.
- (250) Zhu, Y.; Li, J.; Liu, Z.; Cheng, G.; Dong, S.; Wang, E. *J. Mol. Catal. B, Enzym.* **1998**, *4*, 33.
- (251) Jiao, K.; Sun, W.; Zhang, S. S.; Sun, G. *Anal. Chim. Acta* **2000**, *413*, 71.
- (252) Niu, S. Y.; Jiao, K. *Acta Chim. Sin.* (in Chinese) **2000**, *58*, 617.
- (253) Xu, H.; Xu, L. *Polym. Mater. Sci. Eng.* (in Chinese) **1995**, *11* (4), 124.
- (254) Ichinohe, D.; Akagi, K.; Kise, H. *Synth. Met.* **1997**, *85*, 1671.
- (255) Segawa, H.; Shimizu, T.; Honda, K. *Chem. Commun.* **1989**, 132.
- (256) Teshima, K.; Yamada, K.; Kobayashi, N.; Hirohashi, R. *Chem. Commun.* **1996**, 829.
- (257) Uemura, S.; Yoshie, M.; Kobayashi, N.; Nakahira, T. *Polym. J.* **2000**, *32*, 987.
- (258) Teshima, K.; Uemura, S.; Kobayashi, N.; Hirohashi, R. *Macromolecules* **1998**, *31*, 6783.
- (259) Zimmermann, A.; Kunzelmann, U.; Dunsch, L. *Synth. Met.* **1998**, *93*, 17.
- (260) Uemura, S.; Nakahira, T.; Kobayashi, N. *J. Mater. Chem.* **2001**, *11*, 1585.
- (261) Uemura, S.; Tokuda, S.; Nakahira, T.; Kobayashi, N. *Synth. Met.* **2001**, *119*, 89.

- (262) Uemura, S.; Shimakawa, T.; Kusabuka, K.; Nakahira, T.; Kobayashi, N. *J. Mater. Chem.* **2001**, *11*, 267.
- (263) Goyette, M. A.; Leclerc, M. *J. Electroanal. Chem.* **1995**, *382*, 17.
- (264) Yu, B. *Electrochemical Technology Group: Electrochemistry; Society of Chemical Industry: Loughborough*, 2001, Sept 17.
- (265) Nakaminami, T.; Ito, S. I.; Kuwabata, S.; Yoneyama, H. *Anal. Chem.* **1999**, *71*, 1928.
- (266) Suzuki, T.; Yoshikawa, M.; Kojima, A. U.S. Patent 4,874,481, -1989.
- (267) Krysinski, P.; Jackowska, K.; Mazur, M.; Tagowska, M. *Electrochim. Acta* **2001**, *46*, 231.
- (268) Desideri, P. G.; Heimler, D.; Lepri, L. *J. Electroanal. Chem.* **1978**, *88*, 407.
- (269) Ogura, K.; Kokura, M.; Yano, J.; Shiigi, H. *Electrochim. Acta* **1995**, *40*, 2707.
- (270) Naoi, K.; Kawase, K. I.; Mori, M.; Komiyama, M. *J. Electrochem. Soc.* **1997**, *144*, L173.
- (271) Yang, C. H.; Wen, T. C. *J. Electrochem. Soc.* **1997**, *144*, 2078.
- (272) Yano, J.; Shimoyama, A.; Ogura, K. *J. Electrochem. Soc.* **1992**, *139*, L52.
- (273) Chen, B. H.; Zhu, K.; Wu, H. H.; Zhang, Y. Z. *Chem. J. Chin. Univ.* (in Chinese) **1997**, *18*, 615.
- (274) Gao, J. S.; Cai, X. W.; Tian, Z. Q. *Chin. J. Appl. Chem.* (in Chinese) **1997**, *14* (2), 72.
- (275) Ogura, K.; Kokura, M.; Nakayama, M. *J. Electrochem. Soc.* **1995**, *142*, L152.
- (276) Ohsaka, T.; Watanabe, T.; Kitamura, F.; Oyama, N.; Tokuda, K. *Chem. Commun.* **1991**, 1072.
- (277) Zhang, H. P.; Luo, J.; Huang, H. G.; Wu, L. L.; Lin, Z. H. *Chem. Phys. Lett.* **2000**, *326*, 169.
- (278) Peng, H.; Liang, C.; Zhou, A.; Zhang, Y.; Xie, Q.; Yao, S. *Anal. Chim. Acta* **2000**, *423*, 221.
- (279) Jackowska, K.; Bukowska, J.; Jamkowski, M. *J. Electroanal. Chem.* **1995**, *388*, 101.
- (280) Mostefai, M.; Pham, M.-C.; Marsault, J.-P.; Aubard, J.; Lacaze, P.-C. *J. Electrochem. Soc.* **1996**, *143*, 2116.
- (281) Meneguzzi, A.; Ferreira, C. A.; Pham, M.-C.; Delamar, M.; Lacaze, P.-C. *Electrochim. Acta* **1999**, *44*, 2149.
- (282) Pham, M. C.; Oulahyane, M.; Mostefai, M.; Lacaze, P. C. *Synth. Met.* **1997**, *84*, 411.
- (283) Elliott, J. M.; Cabuche, L. M.; Bartlett, P. N. *Anal. Chem.* **2001**, *73*, 2855.
- (284) Mailhe-Randolph, C.; Desilvestro, J. *J. Electroanal. Chem.* **1989**, *262*, 289.
- (285) Mazeikiene, R.; Malinauskas, A. *Synth. Met.* **1998**, *92*, 259.
- (286) Mazeikiene, R.; Malinauskas, A. *React. Funct. Polym.* **2000**, *45*, 45.
- (287) Michaelson, J. C.; McEvoy, A. J.; Kuramoto, N. *J. Electroanal. Chem.* **1990**, *287*, 191.
- (288) Chen, W. C.; Wen, T. C.; Gopalan, A. *J. Electrochem. Soc.* **2001**, *148*, E427.
- (289) Murphy, L. *J. Anal. Chem.* **1998**, *70*, 2928.
- (290) Wei, D.; Wu, H. *Electrochemistry* (in Chinese) **1995**, *1*, 186.
- (291) Sabbatini, L.; De Giglio, E. *Curr. Trends Anal. Chem.* **1998**, *1*, 65.
- (292) Thomas, K. A.; Euler, W. B. *J. Electroanal. Chem.* **2001**, *501*, 235.
- (293) Cui, M.; Feng, J. K.; Zhang, H. X.; Ge, M. F.; Sun, C. C.; Zhang, J. P. *Synth. Met.* **1999**, *100*, 261.
- (294) Park, J. K.; Tran, P. H.; Chao, J. K. T.; Ghodadra, R.; Rangarajan, R.; Thakor, N. V. *Biosens. Bioelectron.* **1998**, *13*, 1187.
- (295) Lin, X. Q.; Zhang, H. Q. *Electrochim. Acta* **1996**, *41*, 2019.
- (296) Palys, B. J.; Skompska, M.; Jackowska, K. *J. Electroanal. Chem.* **1997**, *433*, 41.
- (297) Ye, B.; Xia, P.; Qi, C. *J. Zhengzhou Univ.* (in Chinese) **1999**, *31* (2), 78.
- (298) Chiba, K.; Ohsaka, T.; Ohnuki, Y.; Oyama, N. *J. Electroanal. Chem.* **1987**, *219*, 117.
- (299) He, W.; Wang, X.; Xiong, F. *J. Shandong Inst. Build. Mater.* (in Chinese) **1998**, *12*, 103.
- (300) Morioka, H.; Yamoato, M.; Kimura, T. *Synth. Met.* **1999**, *101*, 33.
- (301) Wu, L.-L.; Luo, J.; Lin, Z.-H. *J. Electroanal. Chem.* **1997**, *440*, 173.
- (302) Wen, T. C.; Huang, L. M.; Gopalan, A. *Electrochim. Acta* **2001**, *46*, 2463.
- (303) Brenneman, K. R.; Feng, J.; Zhou, Y.; MacDiarmid, A. G.; Kahol, P. K.; Epstein, A. J. *Synth. Met.* **1999**, *101*, 785.
- (304) Kudelski, A.; Bukowska, J.; Jackowska, K. *Synth. Met.* **1998**, *95*, 87.
- (305) Lang, G.; Inzelt, G. *Electrochim. Acta* **1999**, *44*, 2037.
- (306) Bagheri, A.; Nateghi, M. R. *Indian J. Chem., Sect. A: Inorg. Bio-Inorg. Phys. Theor. Anal. Chem.* **1998**, *3*, 606.
- (307) Martinusz, K.; Lang, G.; Inzelt, G. *J. Electroanal. Chem.* **1997**, *433*, 1.
- (308) Komura, T.; Yamaguti, T.; Takahashi, K. *Electrochim. Acta* **1996**, *41*, 2865.
- (309) Komura, T.; Funahashi, Y.; Yamaguti, T.; Takahashi, K. *J. Electroanal. Chem.* **1998**, *446*, 113.
- (310) Malinauskas, A.; Holze, R. *Ber. Bunsen-Ges.* **1997**, *101*, 1851.
- (311) Inoue, Y.; Yamato, M.; Kimura, T.; Ito, E. *Synth. Met.* **1997**, *84*, 435.
- (312) Suematsu, S.; Naoi, K. *J. Power Sources* **2001**, *97-98*, 816.
- (313) Rhemrev-Boom, M. M.; Jonker, M. A.; Venema, K.; Jobst, G.; Tiessen, R.; Korf, J. *Analyst* **2001**, *126*, 1073.
- (314) Wei, Y.; Jang, G. W.; Sun, Y.; Tang, X.; Chan, C. C. *Polym. Mater. Sci. Eng.* **1989**, *61*, 910.
- (315) Nyffenegger, R.; Gerber, C.; Siegenthaler, H. *Synth. Met.* **1993**, *55*, 402.
- (316) Alva, K. S.; Samuelson, L. A.; Kumar, J.; Marx, K. A.; Kaplan, D. L.; Tripathy, S. K. *Thin Films and Surfaces for Bioactivity and Biomedical Applications Materials Research Society Symposium Proceedings*; Materials Research Society: Pittsburgh, PA, 1996; Vol. 414, p 119.
- (317) Pham, M. C.; Mostefai, M.; Simon, M.; Lacaze, P. C. *Synth. Met.* **1994**, *63*, 7.
- (318) Jang, D. H.; Yoo, Y. S.; Oh, S. M. *Bull. Korean Chem. Soc.* **1995**, *16*, 392.
- (319) Zaki, A. B.; El-Sheikh, M. Y.; Evans, J.; El-Safty, S. A. *Polyhedron* **2000**, *19*, 1317.
- (320) Kamisuki, T.; Hirose, C. *Spectrochim. Acta, Part A* **2000**, *56*, 2141.
- (321) Kitani, A.; Yano, J.; Sasaki, K. *J. Electroanal. Chem.* **1986**, *209*, 227.
- (322) Madaras, M. B.; Buck, R. P. *Anal. Chem.* **1996**, *68*, 3832.
- (323) Popok, V. N.; Karpovich, I. A.; Odzhaev, V. B.; Sviridov, D. V. *Nucl. Instrum. Methods Phys. Res., Sect. B* **1999**, *148*, 1106.
- (324) Yano, J.; Yamasaki, S. *Synth. Met.* **1999**, *102*, 1157.
- (325) Watanabe, T.; Tokuda, K.; Ohsaka, T. *Denki Kagaku* **1992**, *60*, 455.
- (326) D'Elia, L. F.; Ortiz, R. L.; Marquez, O. P.; Marquez, J.; Martinez, Y. *J. Electrochem. Soc.* **2001**, *148*, C297.
- (327) Meneguzzi, A.; Pham, M. C.; Lacroix, J. C.; Piro, B.; Adenier, A.; Ferreira, C. A.; Lacaze, P. C. *J. Electrochem. Soc.* **2001**, *148*, B121.
- (328) Huang, M.-R.; Li, X.-G. *World Sci.* (in Chinese) **2001**, *275*, 23.
- (329) Posadas, D.; Rodriguez Presa, M. J.; Florit, M. I. *Electrochim. Acta* **2001**, *46*, 4075.
- (330) D'Eramo, F.; Silber, J. J.; Arevalo, A. H.; Sereno, L. E. *J. Electroanal. Chem.* **2000**, *494*, 60.
- (331) Bartlett, P. N.; Birkin, P. R.; Palmisano, F.; De Benedetto, G. *J. Chem. Soc., Faraday Trans.* **1996**, *92*, 3123.
- (332) Ganesan, V.; Ramaraj, R. *J. Appl. Electrochem.* **2000**, *30*, 757.
- (333) Ju, H.; Sun, H.; Chen, H. *Anal. Chim. Acta* **1996**, *327*, 125.
- (334) Newkome, G. R.; Narayanan, V. V.; Godinez, L. A.; Perez-Cordero, E.; Echegoyen, L. *Macromolecules* **1999**, *32*, 6782.
- (335) Szkurlat, A.; Palys, B.; Jackowska, K. *NATO Advanced Research Workshop on Electrochemistry of Electroactive Polymer Films, WEEPF-2000*.
- (336) Horwitz, C. P.; Dailey, G. C. *Chem. Mater.* **1990**, *2*, 344.
- (337) Yousef, U. S.; Abdel-Azzem, M. *Pol. J. Chem.* **1998**, *72*, 2583.
- (338) Liu, M.; Shuai, M.; Jiang, Y.; Qian, F. *J. Anal. Sci.* (in Chinese) **1999**, *15*, 390.
- (339) Yano, J.; Nagaoka, T. *J. Electroanal. Chem.* **1996**, *410*, 213.
- (340) Yano, J.; Nagaoka, T. *Synth. Met.* **1997**, *84*, 271.
- (341) Vidal, J. C.; Espuelas, J.; Garcia-Ruiz, E.; Castillo, J. R. *Anal. Lett.* **2002**, *35*, 837.
- (342) Ji, X.; Zhang, Y. *Chin. J. Appl. Chem.* (in Chinese) **1993**, *10* (2), 97.
- (343) Centonze, D.; Malitesta, C.; Palmisano, F.; Zambonin, P. G. *Electroanalysis* **1994**, *6*, 423.
- (344) Kobayashi, N.; Yano, T.; Teshima, K.; Hirohashi, R. *Electrochim. Acta* **1998**, *43*, 1645.
- (345) Wang, X.; Yang, Q.; Luo, X. *J. Shandong Inst. Build. Mater.* (in Chinese) **1996**, *10* (4), 19.
- (346) Yamasaki, S.; Terayama, K.; Yano, J. *J. Electrochem. Soc.* **1996**, *143*, L212.
- (347) Palmisano, F.; Centonze, D.; Zambonin, P. G. *Biosens. Bioelectron.* **1994**, *9*, 471.
- (348) Centonze, D.; Guerrieri, A.; Malitesta, C.; Palmisano, F.; Zambonin, P. G. *Ann. Chim. (Rome)* **1992**, *82*, 219.
- (349) Ryan, M. R.; Lowry, J. P.; O'Neill, R. D. *Analyst* **1997**, *122*, 1419.
- (350) Garjonyte, R.; Malinauskas, A. *Sens. Actuators* **1999**, *B56*, 85.
- (351) Cai, L. T.; Chen, H. Y. *Sens. Actuators* **1999**, *B55*, 14.
- (352) Vidal, J. C.; Mendez, S.; Castillo, J. R. *Anal. Chim. Acta* **1999**, *385*, 203.
- (353) Garjonyte, R.; Malinauskas, A. *Sens. Actuators* **2000**, *B63*, 122.
- (354) Yasuzawa, M.; Nieda, T.; Hirano, T.; Kunugi, A. *Sens. Actuators* **2000**, *B66*, 77.
- (355) Yasuzawa, M.; Matsuki, T.; Mitsui, H.; Kunugi, A.; Nakaya, T. *Sens. Actuators* **2000**, *B66*, 25.
- (356) Alvarez-Crespo, S. L.; Lobo-Castano, M. J.; Miranda-Ordieres, A. J.; Tunon-Blanco, P. *Biosens. Bioelectron.* **1997**, *12*, 739.
- (357) Yao, T.; Takashima, K. *Biosens. Bioelectron.* **1998**, *13*, 67.
- (358) Dempsey, E.; Wang, J.; Smyth, M. R. *Talanta* **1993**, *40*, 445.
- (359) Curulli, A.; Kelly, S.; Sullivan, C. O.; Guilbault, G. G.; Pallechi, G. *Biosens. Bioelectron.* **1998**, *13*, 1245.



- (359) Karalemas, I. D.; Georgiou, C. A.; Papastathopoulos, D. S. *Talanta* **2000**, *53*, 391.
- (360) Kelly, S. C.; O'Connell, P. J.; O'Sullivan, C. K.; Guilbault, G. G. *Anal. Chim. Acta* **2000**, *412*, 111.
- (361) Stred'ansky, M.; Pizzariello, A.; Stred'anska, S.; Miertus, S. *Anal. Chim. Acta* **2000**, *415*, 151.
- (362) Centonze, D.; Losito, I.; Malitesta, C. *J. Electroanal. Chem.* **1997**, *435*, 103.
- (363) Palmisano, F.; Centonze, D.; Malitesta, C.; Zambonin, P. G. *J. Electroanal. Chem.* **1995**, *381*, 235.
- (364) Bartlett, P. N.; Birkin, P. R. *Anal. Chem.* **1994**, *66*, 1552.
- (365) Dumont, J.; Fortier, G. *Biotechnol. Bioeng.* **1996**, *49*, 544.
- (366) Griffith, A.; Glidle, A.; Cooper, J. M. *Biosens. Bioelectron.* **1996**, *11*, 625.
- (367) Liu, T. Z.; Wang, Y.; Kounaves, S. P.; Brush, E. J. *Anal. Chem.* **1995**, *67*, 1679.
- (368) Geise, R. J.; Rao, S. Y.; Yacynych, A. M. *Anal. Chim. Acta* **1993**, *281*, 467.
- (369) Li, Q.; Zhang, S.; Yu, J. *Anal. Lett.* **1995**, *28*, 2161.
- (370) Yang, Q.; Atanasov, P.; Wilkins, E. *Biosens. Bioelectron.* **1999**, *14*, 203.
- (371) Abdel-Hamid, I.; Atanasov, P.; Wilkins, E. *Anal. Chim. Acta* **1995**, *313*, 45.
- (372) Sasso, S. V.; Pierce, R. J.; Wella, R. *Anal. Chem.* **1990**, *62*, 1111.
- (373) Xu, J. J.; Chen, H. Y. *Anal. Biochem.* **2000**, *280*, 221.
- (374) Ju, H. X.; Zhou, D. M.; Xiao, Y.; Chen, H. Y. *Electroanalysis* **1998**, *10*, 541.
- (375) Lenigk, R.; Zhu, H.; Lo, T. C.; Renneberg, R. *Fresenius' J. Anal. Chem.* **1999**, *364*, 66.
- (376) Wang, J.; Chen, L.; Hocevar, S. B.; Ogorevc, B. *Analyst* **2000**, *125*, 1431.
- (377) Reynolds, E. R.; Yacynych, A. M. *Electroanalysis* **1993**, *5*, 405.
- (378) Reynolds, E. R.; Yacynych, A. M. *Biosens. Bioelectron.* **1994**, *9*, 283.
- (379) Centonze, D.; Guerrieri, A.; Palmisano, F.; Torsi, L.; Zambonin, P. G. *Fresenius' J. Anal. Chem.* **1994**, *349*, 497.
- (380) Nguyen, A. L.; Luong, J. H. T. *Appl. Biochem. Biotechnol.* **1993**, *43* (2), 117.
- (381) Mulchandani, A.; Pan, S. *Anal. Biochem.* **1999**, *267* (1), 141.
- (382) Bartlett, P. N.; Birkin, P. R.; Wang, J. H.; Palmisano, F.; De Benedetto, G. *Anal. Chem.* **1998**, *70*, 3685.
- (383) Yasuzawa, M.; Fujii, S.; Kunugi, A.; Nakaya, T. *Electrochemistry* **2000**, *68*, 920.
- (384) Moussy, F.; Harrison, D. J.; O'Brien, D. W.; Rajotte, R. V. *Anal. Chem.* **1993**, *65*, 2072.
- (385) Moussy, F.; Jakeway, S.; Harrison, D. J.; Rajotte, R. V. *Anal. Chem.* **1994**, *66*, 3882.
- (386) Yegnaraman, V.; Yacynych, A. M. *Bull. Electrochem.* **2000**, *16*, 21.
- (387) Zambonin, C. G.; Losito, I. *Anal. Chem.* **1997**, *69*, 4113.
- (388) Emre, F. B. M.Sc. Thesis, Graduate School of Natural and Applied Sciences, Department of Chemistry, 2000.
- (389) Lowry, J. P.; McAteer, K.; El Atrash, S. S.; Duff, A.; O'Neill, R. D. *Anal. Chem.* **1994**, *66*, 1754.
- (390) Lowry, J. P.; Miele, M.; O'Neill, R. D.; Boutelle, M. G.; Fillenz, M. J. *Neurosci. Methods* **1998**, *79*, 65.
- (391) Lowry, J. P.; Fillenz, M. *Bioelectrochemistry* **2001**, *54*, 39–47.
- (392) Netchiporouk, L. I.; Shram, N. F.; Jaaffrezic-Renault, N.; Martelet, C.; Cespuoglio, R. *Anal. Chem.* **1996**, *68*, 4358.
- (393) Trojanowicz, M.; Geschke, O.; Krawczycki vel Krawczyk, T.; Cammann, K. *Sens. Actuators B* **1995**, *28*, 191.
- (394) Warrington, R. J.; Higson, S. P. *Biomed. Sci. Instrum.* **2001**, *37*, 75.
- (395) Dalton, M.; Lowry, J. P. *Electrochemical Technology Group: Electrochemistry*; Society of Chemical Industry: Loughborough, 2001, Sept 17.
- (396) Krawczyk, T. K. V.; Trojanowicz, M.; Lewenstam, A.; Moszczynska, A. *Biosens. Bioelectron.* **1996**, *11*, 1155.
- (397) Palmisano, F.; Zambonin, P. G. *Anal. Chem.* **1993**, *65*, 2690.
- (398) Palmisano, F.; Centonze, D.; Quinto, M.; Zambonin, P. G. *Biosens. Bioelectron.* **1996**, *11*, 419.
- (399) Palmisano, F.; Guerrieri, A.; Quinto, M.; Zambonin, P. G. *Anal. Chem.* **1995**, *67*, 1005.
- (400) Shu, H. C.; Gorton, L.; Persson, B.; Mattiasson, B. *Biotechnol. Bioeng.* **1995**, *46*, 280.
- (401) Lobo-Castanon, M. J.; Miranda-Ordieres, A. J.; Tunon-Blanco, P. *Anal. Chim. Acta* **1997**, *346*, 165.
- (402) Zilkha, E.; Obrenovitch, T. P.; Koshy, A.; Kusakabe, H.; Ben-netto, H. P. *J. Neurosci. Methods* **1995**, *60*, 1.
- (403) Cooper, J. M.; Pritchard, D. J. *J. Mater. Sci. Mater. Electron.* **1994**, *5* (2), 111.
- (404) Cooper, J. M.; Foreman, P. L.; Glidle, A.; Ling, T. W.; Pritchard, D. J. *J. Electroanal. Chem.* **1995**, *388*, 143.
- (405) Matsumoto, K.; Asada, W.; Murai, R. *Anal. Chim. Acta* **1998**, *358*, 127.
- (406) Nguyen, A. L.; Luong, J. H. T.; Yacynych, A. M. *Biotechnol. Bioeng.* **1991**, *37*, 729.
- (407) Manowitz, P.; Stoecker, P. W.; Yacynych, A. M. *Biosensors Bioelectron.* **1995**, *10*, 359.
- (408) Stoecker, P. W.; Yacynych, A. M.; Manowitz, P. *Polym. Mater. Sci. Eng.* **1997**, *76*, 509.
- (409) Saidman, S. B.; Lobo-Castañón, M. J.; Miranda-Ordieres, A. J.; Tuñón-Blanco, P. *Anal. Chim. Acta* **2000**, *424*, 45.
- (410) Lobo Castanon, M. J.; Miranda Ordieres, A. J.; Tunon Blanco, P. *Biosens. Bioelectron.* **1997**, *12*, 511.
- (411) Mo, J. W.; Dgorevc, B. *Anal. Chem.* **2001**, *73*, 1196.
- (412) Jin, L. T.; Zhao, G. Z.; Fang, Y. Z. *Chem. J. Chin. Univ.* (in Chinese) **1994**, *15*, 189.
- (413) Friedmann, M. N.; Robinson, S. W.; Gerhardt, G. A. *Anal. Chem.* **1996**, *68*, 2621.
- (414) Pontie, M.; Gobin, C.; Pauporte, T.; Bedioui, F.; Devynck, J. *Anal. Chim. Acta* **2000**, *411*, 175.
- (415) Pontie, M.; Bedioui, F.; Devynck, J. *Electroanalysis* **1999**, *11*, 845.
- (416) Wu, W. C.; Wang, Y.; Su, C. K.; Chai, C. Y. *Neurosci. Lett.* **2001**, *310*, 121.
- (417) Badea, M.; Amine, A.; Palleschi, G.; Moscone, D.; Volpe, G.; Curulli, A. *J. Electroanal. Chem.* **2001**, *509*, 66.
- (418) Moretto L. M.; Ugo, P.; Zanata, M.; Guerriero, P.; Martin, C. R. *Anal. Chem.* **1998**, *70*, 2163.
- (419) Chen, R.; Lu, F.; Li, D.; Wan, Z. *Anal. Instrum.* (in Chinese) **1998**, *(2)*, 18.
- (420) Chen, R.; Lu, F.; Li, D.; Zhang, C. *Chin. J. Appl. Chem.* (in Chinese) **1998**, *15* (6), 25.
- (421) Wang, Y.; Zhou, D.; Chen, H. J. *Wuxi Univ. Light Ind.* (in Chinese) **1998**, *17* (1), 69.
- (422) Reynolds, E. R.; Geise, R. J.; Yacynych, A. M. *ACS Symp. Ser.* **1992**, *487*, 186.
- (423) Curulli, A.; Carelli, I.; Trischitta, O.; Palleschi, G. *Talanta* **1997**, *44*, 1659.
- (424) Dong, S. J. *Anal. Sci.* **1994**, *10*, 175.
- (425) Nakabayashi, Y.; Yoshikawa, H. *Anal. Sci.* **2000**, *16*, 609.
- (426) Yao, T.; Satomura, M.; Nakahara, T. *Anal. Chim. Acta* **1994**, *296*, 271.
- (427) Yao, T.; Satomura, M.; Nakahara, T. *Electroanalysis* **1995**, *7*, 395.
- (428) Yao, T.; Suzuki, S.; Nishino, H.; Nakahara, T. *Anal. Sci.* **1997**, *13*, 665.
- (429) Marzouk, S. A. M.; Sayour, H. E. M.; Ragab, A. M.; Cascio, W. E.; Hassan, S. S. M. *Electroanalysis* **2000**, *12*, 1304.
- (430) Si, S.; Ren, F.; Cheng, W.; Yao, S. *Fresenius' J. Anal. Chem.* **1997**, *357*, 1101.
- (431) Martinusz, K.; Inzelt, G.; Horanyi, G. *J. Electroanal. Chem.* **1996**, *404*, 143.
- (432) Martinusz, K.; Inzelt, G.; Horanyi, G. *J. Electroanal. Chem.* **1995**, *395*, 293.
- (433) Binag, C. A.; Bartolome, A. J.; Tongol, B. J. V.; Santiago, K. S. *Philippine J. Sci.* **1999**, *128*, 3.
- (434) Ogura, K.; Tonosaki, T.; Shiigi, H. *J. Electrochem. Soc.* **2001**, *148*, H21.
- (435) Ogura, K.; Shiigi, H.; Nakayama, M.; Fujii, A. *J. Electrochem. Soc.* **1998**, *145*, 3351.
- (436) Tonosaki, T.; Oho, T.; Isomura, K.; Ogura, K. *J. Electroanal. Chem.* **2002**, *520*, 89.
- (437) Ogura, K.; Fujii, A.; Shiigi, H.; Nakayama, M.; Tonosaki, T. *J. Electrochem. Soc.* **2000**, *147*, 1105.
- (438) Janasek, D.; Spohn, U. *Sens. Actuators, B: Chem.* **1997**, *B39*, 291.
- (439) Li, Y.; Lenigk, R.; Wu, X.; Gruendig, B.; Dong, S.; Renneberg, R. *Electroanalysis* **1998**, *10*, 671.
- (440) Bartlett, P. N.; Pletcher, D.; Zeng, J. *J. Electrochem. Soc.* **1997**, *144*, 3705.
- (441) Wei, D.; Wu, H. H. *Chem. J. Chin. Univ.* (in Chinese) **1995**, *16*, 1761.
- (442) Chen, B.; Wu, H.; Zhu, K. *J. Xiamen Univ.* (in Chinese) **1997**, *36*, 728.
- (443) Zhu, Q. W.; Yu, Q. C.; Zhang, C. G.; Wu, Y. H. *Bull. Sci. Technol.* (in Chinese) **1999**, *15*, 363.
- (444) He, W.; Wang, X.; Xu, Y. J. *Shandong Inst. Build. Mater.* (in Chinese) **1999**, *13* (1), 16.
- (445) Jackowska, K.; Kudelski, A.; Bukowska, J. *Mater. Sci. Forum* **1995**, *191*, 247.
- (446) Naoi, K.; Suematsu, S. *Mater. Res. Soc. Symp.—Proc.* **2000**, *575*, 395.
- (447) Sotomura, T.; Uemachi, H.; Takeyama, K.; Naoi, K.; Oyama, N. *Electrochim. Acta* **1992**, *37*, 1851.
- (448) White, H. S.; Abruna, H. D.; Bard, A. J. *J. Electrochem. Soc.* **1982**, *129*, 265.
- (449) Kido, H. Spring Meeting of Electrochemical Society of Japan, March 31–April 2, 1999, Yokohama, Japan.
- (450) Na, J.-J.; Park, S.-G.; Lee, H.-K.; Lee, J.-S. *Proc. Jt. Conf. 1996 Asian Int. Conf. Dielectr. Electron. Insul. Diagnos 96 AICDEI 4 JCCEID 1996*; Xi'an Jiaotong University 459.
- (451) Park, S.-G.; Kim, J.-J.; Park, J.-E.; Cho, S.-R.; Lim, K.-J.; Ruy, B.-H.; Lee, J.-S. *Proc. IEEE Intern. Conf. on Properties and Applications of Dielectric Materials*, IEEE, Piscataway, NJ, 97CH35794, **1997**, *2*, 609.

- (452) Epstein, A. J.; Smallfield, J. A. O.; Guan, H.; Fahlman, M. *Synth. Met.* **1999**, *102*, 1374.
- (453) Nguyen, T. D.; Camalet, J. L.; Lacroix, J. C.; Aeiych, S.; Pham, M. C.; Lacaze, P. C. *Synth. Met.* **1999**, *102*, 1388.
- (454) Spellane, P. J.; Via, F. A.; Weil, E. D. U.S. Patent 5,853,462, 1998.
- (455) Wei, Y.; Jamasbi, H.; Li, S.; Cheng, S.; Jansen, S. A.; Sein, L. T., Jr. *Polym. Prepr.* **2000**, *41* (2), 1778.
- (456) Kim, Y.; Kobayashi, N.; Teshima, K.; Hirohashi, R. *Synth. Met.* **1999**, *101*, 699.
- (457) Kim, Y.; Teshima, K.; Kobayashi, N. *Electrochim. Acta* **2000**, *45*, 1549.
- (458) Zhao, Y.; Zhao, Q.; Zhou, J.; Zhang, Z. *J. Henan Univ. Natural Sci.* (in Chinese) **1999**, *29* (1), 24.
- (459) Mekler, V. M.; Belonogova, O. V. *Peroxidase Biotechnology and Application*; Oral abstracts II: Moscow, 1995.
- (460) Mekler, V. M.; Bystryak, S. M. *Anal. Chim. Acta* **1992**, *264*, 359.
- (461) He, Y. N.; Chen, H. Y.; Zheng, J. J.; Zhang, G. Y.; Chen, Z. L. *Talanta* **1997**, *44*, 823.
- (462) Zhang, K.; Cai, R.; Chen, D.; Mao, L. *Anal. Chim. Acta* **2000**, *413*, 109.
- (463) Huang, H.; Cai, R.; Du, Y.; Zeng, Y. *Lab. Rob. Autom.* **1996**, *8*, 231.
- (464) Huang, Z.; Liu, Z.; Cai, R.; Zeng, Y. *Wuhan Univ. J. Nat. Sci.* (in Chinese) **1998**, *3* (1), 123.
- (465) Zhang, K.; Mao, L.; Cai, R. *Talanta* **2000**, *51*, 179.
- (466) Shekhovtsova, T. N.; Muginova, S. V.; Bagirova, N. A. *Anal. Chim. Acta* **1997**, *344*, 145.
- (467) Shekhovtsova, T. N.; Chernetskaja, S. V.; Dolmanova, I. F.; Gazarian, I. G. *Peroxidase Biotechnology and Application*; Oral abstracts II: Moscow, 1995.
- (468) Li, Z.; Cui, M.; Zheng, Y. *Chin. J. Anal. Chem.* (in Chinese), **2000**, *28*, 1049.
- (469) Shekhovtsova, T. N.; Muginova, S. V.; Dolmanova, I. F. *Intern. J. Environ. Anal. Chem.* **1998**, *69*, 191.
- (470) Nickel, U.; Liu, C.; Chen, Y. *Colloids Surf., A: Physicochem. Eng. Aspects* **2001**, 183–185, 575.
- (471) Fuhrmann, B.; Spohn, U. *Biosens. Bioelectron.* **1998**, *13*, 895.
- (472) Capellmann, M.; Bolt, H. M. *Fresenius J. Anal. Chem.* **1992**, *342*, 462.

CR010423Z